

LATE TRANSITION METAL COMPLEXES FOR E-H BOND ACTIVATION AND
ADDITIONS TO MULTIPLE BONDS

by

Kevin D. Hesp

Submitted in partial fulfilment of the requirements
for the degree of Doctor of Philosophy

at

Dalhousie University
Halifax, Nova Scotia
September 2010

© Copyright by Kevin D. Hesp, 2010

DALHOUSIE UNIVERSITY

Department of Chemistry

The undersigned hereby certify that they have read and recommend to the Faculty of Graduate Studies for acceptance a thesis entitled "LATE TRANSITION METAL COMPLEXES FOR E-H BOND ACTIVATION AND ADDITIONS TO MULTIPLE BONDS" by Kevin D. Hesp in partial fulfilment of the requirements for the degree of Doctor of Philosophy.

Dated: September 23, 2010

Supervisor: _____

Readers: _____

Departmental Representative: _____

DALHOUSIE UNIVERSITY

DATE: September 23, 2010

AUTHOR: Kevin D. Hesp

TITLE: LATE TRANSITION METAL COMPLEXES FOR E-H BOND ACTIVATION AND
ADDITIONS TO MULTIPLE BONDS

DEPARTMENT OR SCHOOL: Department of Chemistry

DEGREE: PhD CONVOCATION: May YEAR: 2011

Permission is herewith granted to Dalhousie University to circulate and to have copied for non-commercial purposes, at its discretion, the above title upon the request of individuals or institutions.

Signature of Author

The author reserves other publication rights, and neither the thesis nor extensive extracts from it may be printed or otherwise reproduced without the author's written permission.

The author attests that permission has been obtained for the use of any copyrighted material appearing in the thesis (other than the brief excerpts requiring only proper acknowledgement in scholarly writing), and that all such use is clearly acknowledged.

Table of Contents

List of Figures.....	viii
List of Schemes	x
List of Tables	xiii
Abstract.....	xiv
List of Abbreviations and Symbols Used.....	xv
Acknowledgements	xviii
Chapter 1 - Introduction	1
1.1 Organometallic Complexes in Bond Activation and Catalysis	1
1.2 Design of Complexes for E-H Bond Activation	2
1.3 Research in the Stradiotto Laboratory: Overview	4
1.4 Overview of Thesis.....	6
Chapter 2 – Cationic and Zwitterionic Cp* <i>M</i> (κ^2 - <i>P,S</i>) Complexes (<i>M</i> = Rh, Ir): Divergent Reactivity Pathways Arising from Alternative Modes of Ancillary Ligand Participation in Substrate Activation	9
2.1 Introduction.....	9
2.2 Results and Discussion.....	13
2.2.1 Synthesis and L-donor Reactivity of the Coordinatively Unsaturated Cations 2-2 and 2-3	14
2.2.2 Pursuit of the Coordinatively Unsaturated Zwitterion 2-6	15
2.2.3 Probing the Reactivity of 2-7 with CO and PMe ₃	17
2.2.4 Net M-X Cooperative H-Si Bond activation by 2-3 and Stoichiometric Silane Transfer to Acetophenone	18
2.2.5 Formation of Rh Complexes and Ketone Hydrosilylation Catalysis.....	21

2.2.6 Net M ^X Cooperative H-Si Bond Activation Employing 2-7	23
2.3 Summary and Conclusions	26
2.4 Experimental Section	27
2.4.1 General Considerations	27
2.4.2 Synthetic Details and Characterization Data	28
2.4.3 Crystallographic Solution and Refinement Details.....	42
Chapter 3 – Platinum Benzyl Complexes Derived from 1/3-PiPr₂-2-StBu-Indene: Synthesis of Carbanion- and Borate-Containing Zwitterions	46
3.1 Introduction	46
3.2 Results and Discussion	47
3.2.1 Preparation of Neutral Precursor 3-1	47
3.2.2 Isolation of Carbanion-Based Zwitterion 3-2 and its Reaction with DMAP	49
3.2.3 Synthesis of Cationic and Borato-Zwitterionic Relatives of 3-2	50
3.2.4 Reactivity of 3-2 , 3-4 , and 3-5 with E-H bond Containing Substrates	53
3.3 Summary and Conclusions	54
3.4 Experimental Section	55
3.4.1 General Considerations	55
3.4.2 Synthetic Details and Characterization Data	56
3.4.3 Crystallographic Solution and Refinement Details.....	60
Chapter 4 – Iridium-Catalyzed Intramolecular Hydroamination of Aminoalkenes: Scope and Mechanistic Studies	64
4.1 Introduction	64
4.2 Results and Discussion	66

4.2.1 Catalyst Identification and Optimization	66
4.2.2 Intramolecular Hydroamination of Secondary Alkylamines	71
4.2.3 Intramolecular Hydroamination of Secondary Arylamines	74
4.2.4 Intramolecular Hydroamination of Primary Amines	76
4.2.5 Kinetic Studies	77
4.2.6 Summary of Kinetic Studies	82
4.3 Summary and Conclusions.....	84
4.4 Experimental Section.....	85
4.4.1 General Considerations	85
4.4.2 Synthetic Details and Characterization Data	87
Chapter 5 – Gold-Catalyzed Intermolecular Hydroamination of Internal Alkynes with Dialkylamines: Scope and Mechanistic Studies.....	100
5.1 Introduction.....	100
5.2 Results and Discussion.....	102
5.2.1 Catalyst Optimization Studies: Ligand, Solvent, and Salt Effects.....	102
5.2.2 Substrate Scope for the Au-Catalyzed Addition of Dialkylamines to Internal Alkynes.....	105
5.2.3 Mechanistic Studies	109
5.2.3.1 Stoichiometric reactions of 5-1 / $\text{AgB}(\text{C}_6\text{F}_5)_4$ with 3-hexyne and morpholine	110
5.2.3.2 Kinetic Investigations.....	112
5.2.3.3 Mechanistic Discussion	115
5.3 Conclusions.....	119
5.4 Experimental Section.....	120
5.4.1 General Considerations	120

5.4.2 Synthetic Details and Characterization Data	121
5.4.3 Crystallographic Solution and Refinement Details.....	135
Chapter 6 – Conclusions.....	137
6.1 Chapter 2	137
6.1.1 Summary	137
6.1.2 Future Directions	138
6.2 Chapter 3	139
6.2.1 Summary	139
6.2.2 Future Directions	139
6.3 Chapter 4	140
6.3.1 Summary	140
6.3.2 Future Directions	141
6.4 Chapter 5	142
6.4.1 Summary	142
6.4.2 Future Directions	143
References.....	145

List of Figures

Figure 2-1. ORTEP diagram for 2-1 .	14
Figure 2-2. ORTEP diagram for 2-4 .	15
Figure 2-3. ORTEP diagram for 2-7 .	17
Figure 2-4. ORTEP diagram for 2-12 .	20
Figure 2-5. ORTEP diagram for one diastereomer of 2-16 .	26
Figure 3-1. ORTEP diagram for 3-1 .	48
Figure 3-2. ORTEP diagram for 3-3 .	50
Figure 3-3. ORTEP diagram for 3-4 (left) and 3-5 (right).	51
Figure 4-1. Conversion of 4-2a to 4-3a as a function of time employing 2.5 mol% 4-1 in 1,4-dioxane at 110 °C.	67
Figure 4-2. Salt effects on the [Ir(COD)Cl] ₂ -catalyzed hydroamination of 4-2a to 4-3a .	69
Figure 4-3. Relationship between k_{obs} and [4-L2].	71
Figure 4-4. (a) Representative plot for the conversion of 4-2a to 4-3a catalyzed by [Ir(COD)Cl] ₂ . (b) Relationship between k_{obs} and [Ir]. (c) Relationship between k_{obs} and [4-2a].	79
Figure 4-5. Hammett plot for the [Ir(COD)Cl] ₂ catalyzed hydroamination of arylamines 4-4a – 4-4e .	80
Figure 4-6. H/D kinetic isotope effect for the [Ir(COD)Cl] ₂ catalyzed hydroamination of 4-2a .	81
Figure 4-7. (a) Eyring plot for the hydroamination of 4-2a catalyzed by [Ir(COD)Cl] ₂ . (b) Arrhenius plot for the hydroamination of 4-2a catalyzed by [Ir(COD)Cl] ₂ .	82
Figure 5-1. Ligand screen for the Au-catalyzed hydroamination of diphenylacetylene with morpholine.	103
Figure 5-2. Salt effects for the Au-catalyzed hydroamination of diphenylacetylene with morpholine.	104

Figure 5-3. Comparison of the initial rates of reaction for the Au-catalyzed hydroamination of diphenylacetylene with morpholine using 5-1 (top), 5-2 (middle), and 5-3 (bottom).	105
Figure 5-4. Representative example for determining regioselectivity by relative integration of enamine signals against an internal standard by ¹ H NMR.	107
Figure 5-5. ORTEP diagram for 5-1 (left) and 5-22 (right).	112
Figure 5-6. (a) Relationship between k_{obs} and the [5-11]. (b) Relationship between k_{obs} and the [diphenylacetylene (5-4)]. (c) Relationship between k_{obs} and the [morpholine (5-5a)].	113
Figure 5-7. (a) Eyring plot for the hydroamination of diphenylacetylene with morpholine catalyzed by 5-1 /AgB(C ₆ F ₅) ₄ . (b) Arrhenius plot for the hydroamination of diphenylacetylene with morpholine catalyzed by 5-1 /AgB(C ₆ F ₅) ₄ .	114
Figure 5-8. H/D kinetic isotope effect for the 5-1 /AgB(C ₆ F ₅) ₄ -catalyzed hydroamination of diphenylacetylene with morpholine.	115

List of Schemes

Scheme 1-1. A simplified representation of two mechanisms for PGM-mediated E-H additions to unsaturated C-C bonds.	2
Scheme 1-2. Generic neutral, cationic, and zwitterionic PGM complexes employing P,N- indene and indenide ligation strategies.	5
Scheme 1-3. Pd-catalyzed amination of aryl chlorides with ammonia.	6
Scheme 1-4. Cationic and zwitterionic complexes discussed in Chapters 2 (left) and 3 (right).	8
Scheme 1-5. Generic examples of hydroamination reactions discussed in Chapters 4 (top) and 5 (bottom).	8
Scheme 2-1. Ru-catalyzed transfer hydrogenation of ketones involving M-X cooperative addition of H ⁺ and H ⁻ via a proposed six-membered transition state.	10
Scheme 2-2. (κ^3 -P,N,P)Ru-mediated N-H bond activation of ammonia via M ⁺ X ⁻ metal- ligand cooperation involving a dearomatization-aromatization process.	11
Scheme 2-3. Cationic (left) and zwitterionic (right) Ru complexes as pre-catalysts in the transfer hydrogenation of ketones.	11
Scheme 2-4. Generic example of M-X versus M ⁺ X ⁻ E-H bond activation using monoanionic, heterobidentate P,S-substituted indene and indenide ligands.	12
Scheme 2-5. Synthesis of P,S-indene ligand and the neutral Cp*Ir(Cl)(η^2 -P,S) complex 2-1 .	13
Scheme 2-6. Synthesis of coordinatively unsaturated cationic complexes 2-2 and 2-3 and the L-donor stabilized adducts 2-4 and 2-5 .	15
Scheme 2-7. Attempted syntheses of coordinatively unsaturated zwitterion 2-6 and formation of 2-7 .	16
Scheme 2-8. Loss of CH ₃ CN and 1,2,3,4-tetramethylfulvene from 2-7 upon treatment with CO (1 atm) to generate 2-8 .	18
Scheme 2-9. Reactivity of 2-2 and 2-3 with organosilanes.	19

Scheme 2-10. Proposed mechanism for the reaction of 2-10 with diethyl ether to form 2-12 .	20
Scheme 2-11. Stoichiometric transfer of Ph ₂ SiH ₂ from 2-10 to acetophenone to generate the corresponding silyl ether and 2-3 .	21
Scheme 2-12. Synthesis of Cp*Rh(² - <i>P,S</i>) complexes 2-13 , 2-14 , and 2-15 .	22
Scheme 2-13. Reactivity of 2-7 with organosilanes.	25
Scheme 3-1. Representative examples of group 10 organoborate-based zwitterions.	47
Scheme 3-2. Synthesis of neutral (² - <i>P,S</i>)Pt(¹ -benzyl)Cl complex 3-1 .	48
Scheme 3-3. Synthesis of zwitterion 3-2 and DMAP-stabilized zwitterion 3-3 .	50
Scheme 3-4. Synthesis of borato-zwitterion 3-4 and cation 3-5 .	51
Scheme 3-5. Potential pathway for the formation of 3-6 from 3-4 and Ph ₂ SiH ₂ .	54
Scheme 4-1. Synthesis of (+)-xenovenine using a lanthanide hydroamination catalyst.	65
Scheme 4-2. PGM catalyst systems capable of the cyclohydroamination of alkylaminoalkenes.	65
Scheme 4-3. Cyclohydroamination of 4-2a to 4-3a catalyzed by Ir-phosphino-phenolate complex 4-1 .	67
Scheme 4-4. ¹ H NMR of the competition reaction for the cyclohydroamination of benzyl- and Boc-protected aminoalkenes 4-2a and 4-2f .	73
Scheme 4-5. Competing mechanistic pathways involving initial alkene activation (left) and N-H bond activation (right).	78
Scheme 4-6. Proposed mechanism for the [Ir(COD)Cl] ₂ -mediated intramolecular hydroamination of aminoalkenes.	84
Scheme 5-1. A representative example of the Zr-mediated hydroamination of terminal alkynes with primary amines proceeding through a Zr-imido intermediate.	100

Scheme 5-2. TpRh/PPh ₃ -mediated hydroamination of terminal alkynes with primary and secondary alkylamines proceeding through a proposed rhodium-vinylidene intermediate.	101
Scheme 5-3. Au-mediated synthesis of allenes by intermediate hydroamination of internal alkynes with secondary alkylamines.	102
Scheme 5-4. Competing mechanistic pathways for the Au-catalyzed hydroamination of internal alkynes with dialkylamines based on (a) nucleophilic attack and (b) alkyne insertion mechanisms.	109
Scheme 5-5. Synthesis of 5-1 .	110
Scheme 5-6. Stoichiometric reactions of 5-1 with morpholine and 3-hexyne.	111
Scheme 5-7. Proposed mechanism for the 5-11 -mediated hydroamination of diphenylacetylene with morpholine.	116
Scheme 5-8. Proposed series of transformations leading up to turnover-limiting alkyne insertion.	117
Scheme 5-9. Comparison of reaction rates (k_{obs}) for amines with varied $\text{p}K_{\text{a}}$ values in the hydroamination of diphenylacetylene catalyzed by 5-1 /AgB(C ₆ F ₅) ₄ .	118
Scheme 5-10. Two potential rationales for the regioselectivity observed in the hydroamination of unsymmetrical alkynes based on the two competing mechanisms of (a) alkyne insertion and (b) amine nucleophilic attack.	119
Scheme 6-1. Postulated application of a fluorinated Cp*M(² - <i>P,S</i> -indene-F ₄) (M=Ir, Rh) complex in the M ⁺ X ⁻ derived organosilane activation with transfer to ketone substrates.	138
Scheme 6-2. Proposed development of cationic and zwitterionic (² - <i>P,P</i>)Pt(³ -benzyl) complexes for E-H σ -bond activation studies.	140
Scheme 6-3. Alternative ligands that may enhance catalyst performance by either adjusting the Lewis acidity of the metal center (top) or promoting C-H reductive elimination (bottom).	142
Scheme 6-4. (a) Second generation ligands for Au-mediated hydroamination. (b) Proposed development of ammonia hydroamination reactions for the synthesis of pyrroles and isoquinolines.	144

List of Tables

Table 2-1. Rh-Catalyzed Hydrosilylation of Ketones.	24
Table 2-2. Crystallographic Data for 2-1 , 2-4 , and 2-7 .	44
Table 2-3. Crystallographic Data for 2-12 and 2-16 .	45
Table 3-1. Selected Interatomic Distances (Å) for 3-1 , 3-3 , 3-4 , and 3-5 .	52
Table 3-2. Crystallographic Data for 3-1 and 3-3 .	62
Table 3-3. Crystallographic Data for 3-4 and 3-5 .	63
Table 4-1. Screening of Group 9 Catalyst Precursors for the Cyclohydroamination of 4-2a to Give 4-3a .	68
Table 4-2. Effect of Added Ligands on the Hydroamination of 4-2a Using $[\text{Ir}(\text{COD})\text{Cl}]_2$.	70
Table 4-3. Intramolecular Hydroamination of Unactivated Alkenes by Secondary Alkylamines Employing $[\text{Ir}(\text{COD})\text{Cl}]_2$ as a Pre-Catalyst.	72
Table 4-4. Intramolecular Hydroamination of Unactivated Alkenes by Secondary Arylamines Employing $[\text{Ir}(\text{COD})\text{Cl}]_2$ as a Pre-Catalyst.	75
Table 4-5. Intramolecular Hydroamination of Unactivated Alkenes by Primary Alkylamines Employing $[\text{Ir}(\text{COD})\text{Cl}]_2$ and HNEt_3Cl (1:2) as a Pre-Catalyst Mixture.	77
Table 5-1. Gold-Catalyzed Hydroamination of Diphenylacetylene (5-4) with Primary and Secondary Amines.	106
Table 5-2. Gold-Catalyzed Hydroamination of Internal Alkynes with Morpholine (5-5a).	108
Table 5-3. Crystallographic Data for 5-1 and 5-11 .	136

Abstract

The study of organometallic chemistry in the context of catalysis can be approached from a stoichiometric perspective, in which PGM complexes are examined in the context of understanding fundamental reactions to provide insight into established catalytic transformations. Alternatively, a catalytic perspective can be adopted, in which an unknown or underdeveloped transformation is identified and PGM catalysis is employed to assist in the further development of this area. In this regard, two general goals of this thesis are: 1) to explore alternative ligation strategies based on P,S-functionalized indene ligands, with a particular focus of studying divergent stoichiometric reactivity between related cationic and zwitterionic PGM complexes; and 2) to identify general PGM catalysts for the cyclohydroamination of alkylaminoalkenes and the hydroamination of internal alkynes with secondary alkylamines.

The preparation and divergent reactivity of a previously unreported class of coordinatively unsaturated cationic and zwitterionic Cp*Ir(*P,S*) complexes that feature structurally analogous P,S-indene and mono-deprotonated P,S-indenide ancillary ligands, respectively, are discussed. The cationic complex was observed to activate organosilanes via the first well-documented H-Si addition across an M-SR linkage. In contrast, the unusual stoichiometric reactivity of the putative zwitterion with CH₃CN or Ph₂SiH₂ can be viewed as resulting from the dual action of the Lewis acidic Cp*Ir fragment and the Lewis basic 10π-electron indenide unit within this formally charge-separated zwitterion. Building on these initial studies, the synthesis of structurally related (benzyl)Pt(*P,S*) borato- and carbanion-based zwitterions and cationic complexes featuring the P,S-indene and indenide ligand framework are also presented.

In the context of hydroamination studies, [Ir(COD)Cl]₂ was identified as an effective pre-catalyst for the efficient synthesis of pyrrolidine and piperidine heterocycles via the cyclohydroamination of tethered aminoalkenes. Following optimization studies of this catalyst system, a broad substrate scope that included the cyclization of primary and secondary alkyl- or arylamines was established. A kinetic and mechanistic evaluation of this reaction suggested the operative pathway as involving olefin activation in a manner that had not previously been documented for Ir-catalyzed alkene hydroamination. In the pursuit of a general catalyst for the alkyne hydroamination reaction, an effective gold pre-catalyst featuring a P,N-ligand was identified and was used in the addition of a variety of functionalized dialkylamines to internal alkynes. In particular, the first examples of the regioselective addition of dialkylamines to unsymmetrically substituted alkynes are discussed. A preliminary mechanistic survey, consisting of kinetic and stoichiometric experiments, has provided empirical evidence to support a mechanism comprised of turnover-limiting alkyne insertion into a Au–N bond followed by proto-deauration.

List of Abbreviations and Symbols Used

Å	angstrom
δ	chemical shift <i>or</i> partial charge
η	hapticity (contiguous donor atoms)
κ	hapticity (non-contiguous donor atoms)
σ_p	substituent parameter for <i>para</i> -substitution
ρ	reaction constant <i>or</i> sensitivity constant
ΔH^\ddagger	enthalpy of activation
ΔS^\ddagger	entropy of activation
E_a	activation energy
Anal. Calcd.	analysis calculated
BF ₂₀	tetrakis(pentafluorophenyl)borate
Bn	benzyl
Boc	tert-butoxycarbonyl
br	broad
cat	catalyst
COD	1,5-cyclooctadiene
COSY	homonuclear shift correlation spectroscopy
Cp*	pentamethylcyclopentadienyl, η^5 -C ₅ Me ₅
d	doublet(s) <i>or</i> days(s)
DCE	1,2-dichloroethane
dd	doublet of doublets
dt	doublet of triplets
DEPT	distortionless enhancement by polarization transfer
DMAP	4-dimethylaminopyridine
DPEphos	bis(2-diphenylphosphinophenyl)ether
DPPB	1,2-bis(diphenylphosphino)butane
DPPE	1,2-bis(diphenylphosphino)ethane
DPPF	1,1'-bis(diphenylphosphino)ferrocene
DiPPF	1,1'-bis(diisopropylphosphino)ferrocene

E	main group element
ESI	electrospray ionization
GC	gas chromatography
h	hour(s)
HMBC	heteronuclear multiple bond correlation
HSQC	heteronuclear single quantum correlation
HRMS	high-resolution mass spectrometry
IPr	1,3-Bis(2,6-Diisopropylphenyl)imidazol-2-ylidene
IR	infrared
${}^nJ_{XX'}$	n bond coupling constant between atom X and atom X'
KIE	H/D kinetic isotope effect
k_{obs}	observed rate constant
L	neutral 2-electron donor ligand
L_n	generic ligand set
NHC	N-heterocyclic carbene
m	multiplet
M	generic transition metal <i>or</i> mol/litre <i>or</i> molecular ion
m/z	mass-to-charge ratio
max.	maximum
min	minute(s)
mol	mole(s)
NMR	nuclear magnetic resonance
ORTEP	Oak Ridge thermal ellipsoid plot
OTf	triflate (trifluoromethanesulfonate)
<i>o</i>	ortho
<i>p</i>	para
PGM	platinum group metal
ppm	parts per million
PTFE	poly(tetrafluoroethylene)
py	pyridine
q	quartet

s	singlet
T	temperature
t	triplet
THF	tetrahydrofuran
Tp	tris(pyrazolyl)borate
Ts	<i>p</i> -toluenesulfonyl
X	generic anion <i>or</i> anionic ligand
Xantphos	4,5-bis(diphenylphosphino)-9,9-dimethylxanthene

Acknowledgements

This thesis would not have been possible without the guidance and support of many people. First off, I would like to thank my thesis advisor Mark Stradiotto. Since my arrival at Dalhousie, his approach as my research supervisor has been ideal; his chemical insight, unwavering enthusiasm, patience, and humor have been essential to my success. He has always supported projects that fascinated me, and I am grateful for all his encouragement. Mark has fostered an environment in which to develop my own scientific independence, while at the same time providing direction when I was unsure which way to turn next. Outside of the lab, he has taught me many practical skills that I know will benefit me throughout my career.

During my time in the Stradiotto research group I have had the opportunity to interact with some outstanding people. The members of my supervisory committee, Profs. Neil Burford, Jean Burnell and Norm Schepp, are acknowledged for their support and advice during the course of my studies at Dalhousie. Furthermore, Prof. Laura Turculet has provided meaningful insight into my thesis research during group meeting presentations. I would also like to thank Prof. Heather Andreas for her assistance in conducting solution conductivity measurements, and Prof. Sven Tobisch (University of St. Andrews) for completing a thorough computational investigation that served to complement my experimental findings in Chapter 4. Thank you to the members of the support staff from the Department of Chemistry for all of their hard work. In particular, Mike Lumsden and Kathy Robertson have been tremendously helpful for NMR spectroscopy assistance relating to the characterization of many compounds discussed in this thesis. Bob MacDonald and Mike Ferguson (University of Alberta), as well as Gabrielle Schatte (University of Saskatchewan), are thanked for their expertise and assistance in X-ray crystallography related studies.

My time at Dalhousie has given me the opportunity to interact with a diverse group of people, and form great friendships. I am grateful to all my colleagues in the Stradiotto and Turculet research groups, past and present, for providing a constant source of camaraderie and making my experience in the lab enjoyable. In particular, I would like to thank Matt Rankin and Rylan Lundgren. They were always ready to bounce ideas around or rationalize an unexpected result, whether it was over coffee or after last call at

the GradHouse. Without a doubt, their suggestions and criticisms have taken my research to the next level and inspired me to become a better chemist.

I am grateful to Profs. Kathryn Preuss and Richard Manderville (University of Guelph) for doing an excellent job in preparing me for graduate school. Furthermore, Dr. Nigel Hearn, a former graduate student in the Preuss group, was an excellent mentor and friend during my honours project.

The unwavering support of family has been unsurpassed. My parents have always believed in me, even when I didn't; they have been reassuring when things went poorly, and thrilled for me when things went well. Without their guidance and morals I would not be where I am today. Lastly, I am indebted to my wife, Maria, who has tolerated many long days and late nights in the lab, as well as the highs and lows that are associated with graduate research. Whether it was carving a thesis writing 'nook' into our tiny apartment or delivering homemade muffins and coffee to me at the lab, her unparalleled support and dedication has made my time at Dalhousie as stress-free and fun as I could ever have imagined.

Chapter 1 - Introduction

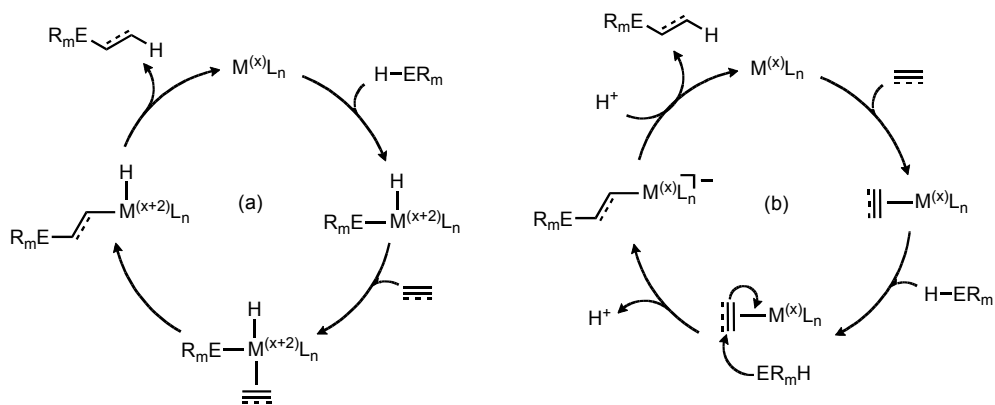
1.1 Organometallic Complexes in Bond Activation and Catalysis

With a firm foundation in both the physical and biological sciences, catalysis has emerged as an indispensable tool in modern synthetic chemistry. In this context, the development of new and/or improved catalytic routes to bulk and fine chemicals is not only an important and worthy scientific pursuit, but also has significant economic and environmental ramifications.^[1] One appealing, yet challenging, approach in the development of new chemical transformations is to exploit abundant and inexpensive reagents (e.g. olefins, NH₃, H₂, CO, alkanes, etc.) in the preparation of useful chemical products.^[2] The use of transition metal coordination complexes has proven instrumental in the pursuit of this goal. In particular, the ability of organometallic complexes comprised of late second and third row transition metals (i.e. platinum group metals, PGMs) to access several stable oxidation states with diverse structural geometries, coupled with their heightened tolerance to functional groups and the ability to mediate substrate transformations under mild conditions, has contributed to their application as catalysts for a diversity of chemical synthesis.^[3]

The development of catalytic methods that utilize E-H containing molecules (where E = main group element) in the making and breaking of σ -bonds represents a persistent goal of organometallic chemists. In particular, reactions based on E-H additions, rather than substitutions, are appealing for the bulk synthesis of chemicals, as such reactions allow for the construction of new σ -bonds while minimizing waste by-products. In this context, the development of appropriately designed organometallic complexes for use in promoting E-H additions to unsaturated bonds is an attractive target of inquiry. However, the identification of such complexes as successful catalysts for a given chemical transformation is not a trivial process. Importantly, reactivity trends observed through stoichiometric reactions between organometallic complexes and E-H containing substrate molecules have played a pivotal role in the development of increasingly effective catalysts.^[4] These studies have provided considerable insight into the underlying structural and electronic effects that control both catalyst performance and

selectivity. Furthermore, an appreciation of how the substrate molecules interact with the metal center can lead to more informed catalyst modifications.

The reactivity of organometallic complexes is governed not only by the choice of the transition metal, but is also highly influenced by the coordination environment in the proximity of the metal.^[5] As such, the judicious choice of ligands has a direct influence on late metal-mediated E-H addition reactions, which consist of catalytic cycles involving a series of discrete elementary steps. For electron-rich metal centers, catalytic pathways often consist of steps such as oxidative addition, substrate coordination, bond insertion, and reductive elimination processes (Scheme 1-1a).^[6] In contrast, when the metal is more electrophilic in nature, alternative mechanistic pathways involving nucleophilic attack by an E-H containing species on a metal coordinated unsaturated substrate followed by protonolysis are commonly invoked (Scheme 1-1b).^[7] Regardless of the operative mechanism, ligand selection plays a crucial role in the fine-tuning of the electronic and steric profile of an organometallic complex.



Scheme 1-1. A simplified representation of two mechanisms for PGM-mediated E-H additions to unsaturated C-C bonds.

1.2 Design of Complexes for E-H Bond Activation

The landmark research conducted by the recipients of the 2001 and 2005 Nobel Prizes in Chemistry has exemplified the systematic approach to developing highly active catalysts, including for PGM-mediated hydrogenation^[8] and olefin metathesis^[9] reactions, respectively. Meticulous ligand design and organometallic synthesis, coupled with careful mechanistic investigations, have enabled remarkable achievements in catalyst

performance and selectivity to be realized. Using this approach to catalyst design, significant progress has been made in the development of alternative catalysts for a breadth of chemical transformations.

As identified in Scheme 1-1a, the oxidative addition of an E-H bond to an organometallic complex is concomitant with an increase in both the coordination number and oxidation state of the metal by two. Typically, complexes that possess strong σ -donating ligands, such as tertiary alkylphosphine and *N*-heterocyclic carbene (NHC) ligands, promote the formation of coordinatively unsaturated, electron-rich PGM complexes, which represent ideal candidates for facilitating these oxidative processes.^[5] Following insertion of an unsaturated substrate into the metal-element bond, the large steric profile of these ligands can be optimized further to encourage C-H reductive elimination and regenerate a low-coordinate metal species for re-entry into the catalytic cycle (Scheme 1-1a).^[10] Alternatively, for pathways involving nucleophilic attack on a metal coordinated substrate, a more Lewis acidic metal center is preferred to facilitate coordination with the Lewis basic substrate and render the alkene (or alkyne) more electrophilic and thus more susceptible to nucleophilic attack (Scheme 1-1b).^[11] In principle, the subtle balance between a Lewis acidic and Lewis basic metal center could be moderated by the careful selection of ancillary ligands. In this sense, the development of innovative ligand scaffolds for coordination to transition metal centers with the objective of engendering unique reactivity towards E-H and unsaturated substrates represents a current area of interest.

The enhanced stability of chelate complexes,^[5b] coupled with the modular approach of ligand synthesis, has attracted considerable interest in the use of multidentate, mixed-donor ligands in the context of E-H bond activation processes.^[12] The pairing of mixed hard and soft donor atoms in a multidentate ligand has been particularly effective for promoting remarkable catalytic and stoichiometric reactivity of organometallic complexes.^[13] In general, the soft metal center will form a stronger bond with the soft donor atom, whereas the harder donor atom will engender a more labile interaction. In the most extreme case, the weaker of the donor atoms can be completely displaced from the metal coordination sphere to create a transient coordinatively unsaturated species with an open coordination site for subsequent substrate binding; this process is commonly

referred to as ligand hemi-lability.^[14] From a ligand design perspective, the ability of multidentate, hemi-labile ancillary ligands to actively participate in substrate activation processes represents an attractive area of current organometallic research.

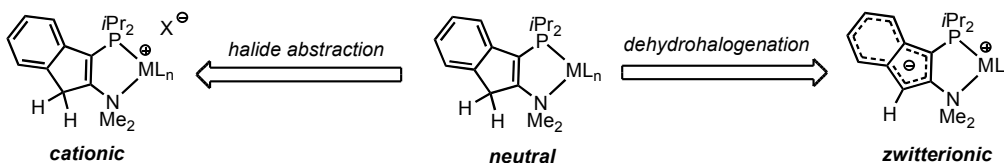
The development of cationic relatives of neutral PGM complexes has been extensively studied in the pursuit of enhanced catalytic activity.^[5] These complexes have figured prominently in the early development of organometallic chemistry, and continue to attract attention due to the ability of such species to mediate myriad substrate transformations involving the breaking and forming of E-H σ -bonds, often in a manner that cannot be achieved by use of simple neutral complexes. For example, PGM cations have made significant contributions to the field of catalytic hydrogenation,^[8b, 15] and the ongoing examination of such complexes in this field continues to yield important reactivity breakthroughs.^[16] Nonetheless, the inherently polar nature of such discrete salts can limit the range of conditions under which they can be employed, whereby cationic complexes commonly exhibit poor solubility in low-polarity media, and can be rendered inactive in strongly coordinating solvents.^[15] Furthermore, the systematic design of cationic species is complicated by the fact that the accompanying outer-sphere counteranion can influence the reactivity properties of the complex via ion pairing^[17] in a manner that cannot be predicted easily.^[18] As an attractive alternative to cationic species, zwitterionic complexes that feature formal charge separation between a cationic metal fragment and a negatively charged ancillary ligand moiety within an overall neutral molecular framework have been studied in the context of stoichiometric and catalytic σ -bond activations.^[19] The allure of these complexes is rooted in the favorable combination of the appealing reactivity properties of more conventional cationic PGM complexes with the desirable solubility profile and solvent tolerance associated with neutral species.

1.3 Research in the Stradiotto Laboratory: Overview

Research objectives in the Stradiotto laboratory target the preparation of PGM complexes that may facilitate new or improved substrate transformations involving E-H bond activation processes. Using some of the design principles outlined in Sections 1-1 and 1-2, initial efforts have led to the development of a family of P,N-functionalized

indene and phenylene ligands and their corresponding coordination complexes with PGMs.

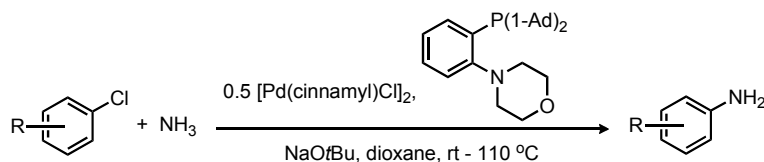
Using a donor-substituted indene framework, the ligand 3-*i*Pr₂-2-NMe₂-indene has provided access to a class of structurally related neutral, cationic, and zwitterionic PGM complexes (Scheme 1-2). The convenience of employing a single indene-based ligand precursor in the synthesis of cationic and zwitterionic species offers advantages over alternative strategies that require the preparation of distinct ligands for supporting cationic and zwitterionic complexes. These zwitterions can be viewed as comprising a formally cationic PGM fragment whose charge is counterbalanced by a sequestered, uncoordinated 10 π -electron indenide unit that is built into the backbone of a bidentate ancillary ligand. Despite the comparable metal coordination spheres featured in these structurally related PGM cation/zwitterion pairs, catalytic studies examining (transfer) hydrogenation,^[20] hydrosilylation,^[20c, 21] and hydroboration^[22] have highlighted the important reactivity differences between these classes of complexes. Moreover, stoichiometric studies of cationic and zwitterionic (κ^2 -*P,N*)Ru indene and indenide complexes, respectively, with E-H containing substrates have illustrated divergent reactivity pathways that can be traversed, in particular with regards to indenide participation in substrate activation processes.^[23]



Scheme 1-2. Generic neutral, cationic, and zwitterionic PGM complexes employing P,N-indene and indenide ligation strategies.

More recently, a research program in the Stradiotto group has been initiated to explore the utility of simple P,N-substituted phenylene ligands in PGM-mediated catalysis. In this context, it has been observed that ligands possessing an electron-rich and sterically demanding phosphine donor in addition to a weakly coordinating amino donor give rise to highly effective catalysts for Pd-mediated C-N coupling reactions^[24] and Ir-catalyzed transfer hydrogenations.^[20a] In particular, the combination of

[Pd(cinnamyl)Cl]₂ with a P,N-phenylene ligand featuring a di(1-adamantyl)phosphino and an *ortho*-morpholino group in the presence of NaOtBu as a base functions as the state-of-the-art catalyst for the chemoselective amination of aryl chloride substrates with ammonia (Scheme 1-3).^[24b] Progress towards alternative PGM-mediated catalysis employing this and other P,N-phenylene ligands is currently underway in the Stradiotto group and holds promise for further breakthrough reactivity.



Scheme 1-3. Pd-catalyzed amination of aryl chlorides with ammonia.

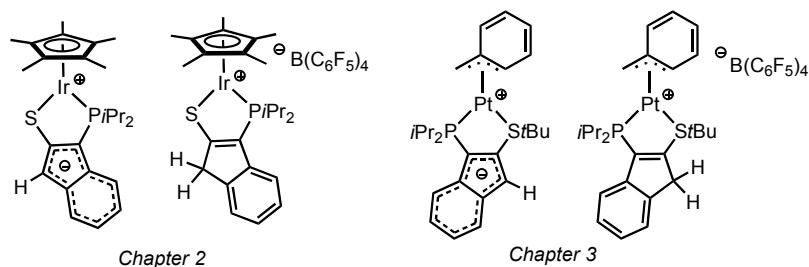
1.4 Overview of Thesis

As discussed in Sections 1.1-1.3, the rational design of organometallic complexes as catalysts for E-H addition reactions relies on a delicate balance between electronic and steric factors. The study of organometallic chemistry in the context of catalysis can be approached from a stoichiometric perspective, in which PGM complexes are examined in the context of understanding fundamental reactions to provide insight into established catalytic transformations. Alternatively, a catalytic perspective can be adopted, in which an unknown or underdeveloped transformation is identified and PGM catalysis is employed to assist in the further development of this area. In this regard, two general goals of this thesis are: 1) to explore alternative ligation strategies based on donor-functionalized indene ligands, with a particular focus of studying divergent stoichiometric reactivity between related cationic and zwitterionic PGM complexes (Chapters 2 and 3); and 2) to identify general PGM catalysts for the cyclohydroamination of alkylaminoalkenes and the hydroamination of internal alkynes with secondary alkylamines (Chapters 4 and 5).

A major research theme over the past several years in the Stradiotto group has been the synthesis of structurally related cationic and zwitterionic PGM complexes employing the 3-*Pi*Pr₂-2-NMe₂-indene ligand (see Section 1.3). Using these complexes, comparative catalytic and stoichiometric reactivity surveys have been conducted to

provide insight into how the electronic nature of the structurally analogous metal complexes can influence reactivity. Inspired by these studies and the prospect of studying divergent reactivity between cation/zwitterion pairs, an alternative version of the P,N-indene ligand was pursued. In order to construct a more robust chelating ligand, the NMe₂ group of the C2 position of indene was substituted with a -*S*tBu group. The corresponding P,S-indene ligand, 3-*Pi*Pr₂-2-*S*tBu-indene, featuring two different soft donor atoms, was envisioned to afford a more electron-rich metal center (versus the analogous P,N-complex), which should facilitate metal-mediated E-H bond activation reactions.

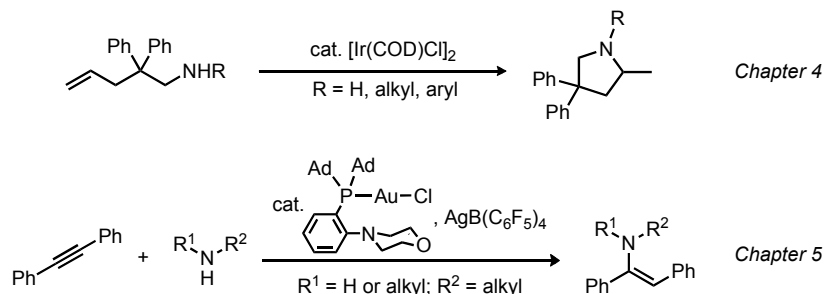
The utility of 3-*Pi*Pr₂-2-*S*tBu-indene as a bidentate ligand precursor for the Cp*M (M = Rh, Ir) frameworks, and in particular, the pursuit of structurally related coordinatively unsaturated cationic and zwitterionic species is discussed in Chapter 2 (Scheme 1-4). Treatment of [Cp*MCl₂]₂ with 3-*Pi*Pr₂-2-*S*tBu-indene resulted in the net loss of the *t*Bu fragment from the sulfide linkage to afford phosphino-thiolate complexes of iridium and rhodium. The cationic complex was observed to activate organosilanes via the first well-documented H-Si addition across an M-SR linkage. In contrast, the unusual stoichiometric reactivity of the putative zwitterion with CH₃CN or Ph₂SiH₂ can be viewed as resulting from the dual action of the Lewis acidic Cp*Ir fragment and the Lewis basic 10π-electron indenide unit within this formally charge-separated zwitterion. Collectively, the results demonstrate the versatility of this P,S-functionalized indene ancillary ligand to promote divergent metal-ligand cooperativity pathways in the activation of organosilanes and simple two-electron donor molecules such as carbon monoxide and acetonitrile. The versatility of 3-*Pi*Pr₂-2-*S*tBu-indene as a ligand precursor is further discussed in Chapter 3, where it is employed in the preparation of neutral and cationic (κ²-*P,S*)Pt(benzyl) complexes, as well as structurally related zwitterions in which the formally cationic metal fragment is counterbalanced by an uncoordinated indenide or borate fragment that is contained within the ancillary ligand backbone (Scheme 1-4).



Scheme 1-4. Cationic and zwitterionic complexes discussed in Chapters 2 (left) and 3 (right).

The cyclohydroamination of alkylaminoalkenes represents a direct and atom-economical method for the synthesis of pyrrolidine and piperidine heterocycles. Although several catalysts are active for variations of this transformation, the identification of a general catalyst capable of the cyclization of a broad range of aminoalkenes has yet to be reported. In this regard, the focus of Chapter 4 is on the identification, substrate scope, and mechanistic analysis of the $[\text{Ir}(\text{COD})\text{Cl}]_2$ -mediated cyclohydroamination of a wide range of primary and secondary alkyl- or aryl-substituted amines with pendant alkenes (Scheme 1-5).

In Chapter 5 the pursuit of a general catalyst for the intermolecular hydroamination of alkynes with primary and secondary alkylamines is discussed. In this context, a $(\kappa^1\text{-P,N})\text{Au}$ complex was identified as a very effective catalyst for this transformation, whereby the addition of a breadth of functionalized amines to symmetrical and unsymmetrical alkynes was observed. Preliminary mechanistic findings are discussed with respect to the rate-accelerating effects of employing a P,N ligand architecture (Scheme 1-5). In the final chapter (Chapter 6), the key findings of Chapters 2-5 are summarized.

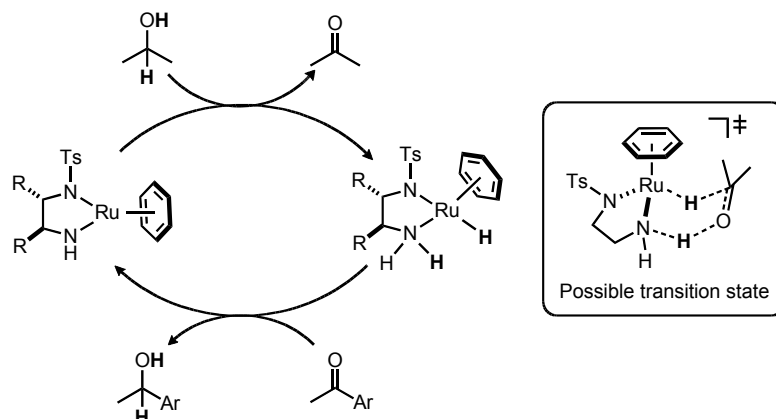


Scheme 1-5. Generic examples of hydroamination reactions discussed in Chapters 4 (top) and 5 (bottom).

Chapter 2 – Cationic and Zwitterionic Cp*M(κ^2 -P,S) Complexes (M = Rh, Ir): Divergent Reactivity Pathways Arising from Alternative Modes of Ancillary Ligand Participation in Substrate Activation

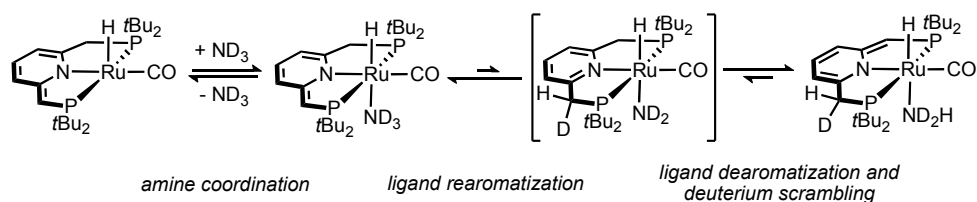
2.1 Introduction

Coordinatively unsaturated platinum-group metal (PGM) complexes have long represented intriguing targets of inquiry owing to their extraordinary propensity for stoichiometric and catalytic substrate activation.^[5] In an effort to control metal-centered reactivity, the coordination of strategically constructed ancillary ligands principally intended to tune the steric and electronic properties of the metal coordination sphere has been exploited widely.^[5] In moving beyond these more traditional design approaches, important reactivity breakthroughs have been achieved through the development of PGM complexes that can mediate challenging substrate transformations via cooperative metal-ligand interactions in which the ancillary ligand is a participant, rather than a spectator, in the substrate activation process.^[25] The most widely studied class of PGM complexes that exhibit such cooperative reactivity behavior are those pairing a Lewis acidic metal fragment with a directly coordinated nucleophilic/basic, non-dative X-type ligand (X = OR, NR₂, or other heteroatom-based fragment).^[25-26] It has been demonstrated that the dual action of adjacent Lewis acidic (M) and Lewis basic (X) fragments in such M-X systems can enable the cooperative activation of a range of polar and non-polar substrates.^[26] Such PGM-amido species typify the mechanistically novel catalytic reactivity that can be accessed via M-X cooperativity; appropriately designed complexes of this type have been shown to mediate the catalytic hydrogenation and/or transfer hydrogenation of polar bonds via outer-sphere mechanisms involving the heterolytic splitting of H₂ (or the net extrusion of H₂ from a donor-solvent) across an M-NHR unit to give an (*H*)M-NH₂R intermediate, which in turn can deliver H₂ to the substrate in a cooperative fashion (Scheme 2-1).^[27]



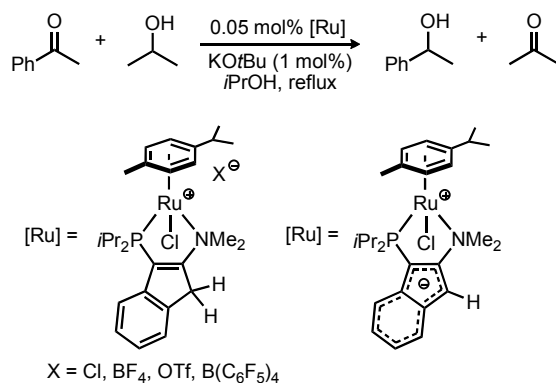
Scheme 2-1. Ru-catalyzed transfer hydrogenation of ketones involving M-X cooperative addition of H⁺ and H⁻ via a proposed six-membered transition state.

By comparison, alternative modes of net metal-ligand cooperative substrate activation involving a reactive PGM center and a non-coordinating anionic portion of a bound ancillary ligand (referred to herein as M^{^X'} cooperativity) are rare. Nonetheless, the examples documented thus far in the literature exemplify the way in which M^{^X'} cooperativity can provide access to unusual stoichiometric and catalytic substrate activation pathways.^[28] In particular, Milstein and co-workers^[28a, 28c-e] have made considerable progress in the development of new reactions through the stoichiometric and catalytic study of PGM complexes bearing pincer ligands capable of facile dearomatization-aromatization processes. A recent report has documented the ability of a (κ^3 -*P,N,P*)Ru complex to achieve reversible N-H bond cleavage of alkylamines and ammonia under ambient conditions via M^{^X'} cooperative activation.^[28a] Although the rearomatized, Ru-amido species could only be isolated for less basic aniline substrates, a deuterium-labeling study using ND₃ unequivocally confirmed the reversible transfer of a deuterium atom to the unsaturated ligand arm, followed by deuterium scrambling of the ligand methylene hydrogens (Scheme 2-2). In the quest to uncover novel modes of PGM-mediated substrate activation with potential applications in catalysis, the development of versatile new classes of ancillary ligands that can be modified easily so as to enable M-X and/or M^{^X'} cooperativity represents an important challenge.



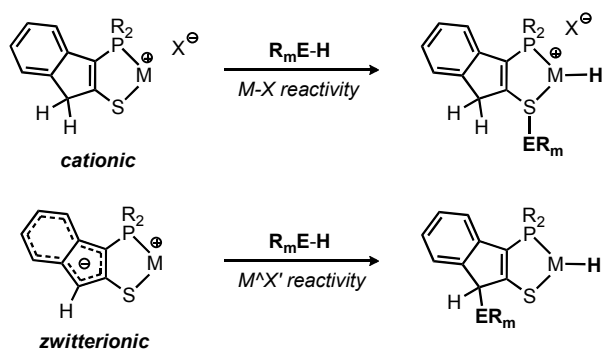
Scheme 2-2. (κ^3 -*P,N,P*)Ru-mediated N-H bond activation of ammonia via $M^{\wedge}X^{\vee}$ metal-ligand cooperation involving a dearomatization-aromatization process.

In this context, comparative reactivity studies of metal complexes featuring structurally analogous cationic and formally zwitterionic PGM complexes supported by 3- PR_2 -2- NR'_2 -indene and related mono-deprotonated indenide ancillary ligands, respectively, have been reported previously in the Stradiotto group (Scheme 1-2).^[19] The focus of these studies was to explore unusual modes of substrate activation that might arise from net $M^{\wedge}X^{\vee}$ cooperativity involving a cationic PGM fragment and the 10π -electron indenide unit within the ancillary ligand backbone of such formally charge-separated zwitterions. While definitive experimental evidence to support net $M^{\wedge}X^{\vee}$ cooperativity of these zwitterionic (κ^2 -*P,N*)-PGM complexes has yet to be obtained, such behavior may underpin the remarkable catalytic activity exhibited by a zwitterionic (κ^2 -*P,N*-indenide)Ru complex in the transfer hydrogenation of ketones.^[20b] Whereas cationic (κ^2 -*P,N*-indene)Ru⁺X⁻ pre-catalysts exhibited only modest activity, with final conversions to 1-phenylethanol ranging between 4-23%, the structurally analogous (κ^2 -*P,N*-indenide)Ru zwitterion afforded 99% conversion to 1-phenylethanol after only 5 minutes (Scheme 2-3).



Scheme 2-3. Cationic (left) and zwitterionic (right) Ru complexes as pre-catalysts in the transfer hydrogenation of ketones.

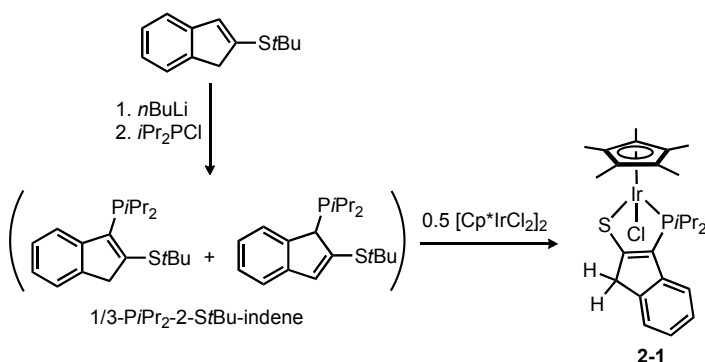
Building on these results, and motivated by the remarkable reactivity exhibited by $[\text{Cp}^*\text{Ir}(\text{LX})]^+$ ($\text{Cp}^* = \eta^5\text{-C}_5\text{Me}_5$) intermediates in both stoichiometric C-H and Si-H bond activation^[29] as well as catalytic^[27c, 30] substrate transformations, the identification of coordinatively unsaturated Cp^*Ir complexes supported by new chelating LX-type indene and indenide ancillary ligands represented a worthwhile target of inquiry. Given that the reactivity properties of Ir-SR fragments within mononuclear complexes are significantly less well-documented than those of Ir-OR and Ir-NR₂ linkages,^[31] the development of synthetic routes to new cationic and zwitterionic species featuring bidentate ligands that pair neutral dialkylphosphino and anionic thiolate pendant donor groups was undertaken as part of this thesis research (Scheme 2-4). Whereas cationic complexes of this type featuring $\kappa^2\text{-PR}_2\text{,S}$ -indene ligation may be well-suited to activate substrates via M-X cooperativity, the presence of a tethered anionic backbone within structurally related zwitterionic complexes featuring $\kappa^2\text{-PR}_2\text{,S}$ -indenide ligation could provide access to alternative reaction manifolds arising from less-conventional M⁺X⁻ cooperative reactivity. The content of Chapter 2 focuses on the strikingly divergent substrate activation pathways (i.e. M-X versus M⁺X⁻) that are traversed by such coordinatively unsaturated cationic and zwitterionic $\text{Cp}^*\text{Ir}(\kappa^2\text{-P,S})$ complexes in reactions with acetonitrile and other L-donor ligands, as well as with organosilanes. Furthermore, the synthetic and reactivity investigations of related Rh complexes, including the application of cationic $\text{Cp}^*\text{Rh}(\kappa^2\text{-P,S})$ species in the catalytic hydrosilylation of ketones are also discussed.



Scheme 2-4. Generic example of M-X versus M⁺X⁻ E-H bond activation using monoanionic, heterobidentate P,S-substituted indene and indenide ligands.

2.2 Results and Discussion

Lithiation of 2-*St*Bu-indene followed by quenching with *i*Pr₂P_iCl provided an isomeric mixture of 1/3-*Pi*Pr₂-2-*St*Bu-indene in 87% isolated yield (Scheme 2-5). Attempts to drive the rearrangement of the ligand to a single isomer in the presence of weak bases or protic solvents under ambient or thermal conditions had no effect on the ratios of the observed isomers. Nonetheless, the precursor compound Cp*Ir(Cl)(κ²-3-*Pi*Pr₂-2-*S*-indene) **2-1** was prepared in 95% isolated yield from an isomeric mixture of 1/3-*Pi*Pr₂-2-*St*Bu-indene and 0.5 equiv [Cp*IrCl₂]₂ (Scheme 2-5). During the course of this reaction the *t*Bu group on the sulfur atom was removed. A putative mechanism to account for this observation might involve elimination of 1-butene/HCl; however, radical mechanisms cannot be unambiguously discounted. The structure of **2-1** was determined initially on the basis of NMR spectroscopic data, and subsequently was confirmed by use of single-crystal X-ray diffraction techniques. An ORTEP^[32] diagram of **2-1** is provided in Figure 2-1, while X-ray experimental data and refinement details for each of the crystallographically characterized complexes reported in this Chapter are collected in Section 2.4.3 (Tables 2-2 and 2-3). The structural features in **2-1** are not unusual and can be compared with those found in a related Cp*Ir(κ²-*P,S*)Cl complex.^[33]



Scheme 2.5. Synthesis of P,S-indene ligand and the neutral Cp*Ir(Cl)(κ²-*P,S*) complex **2-1**.

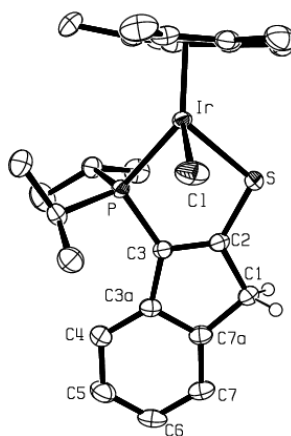
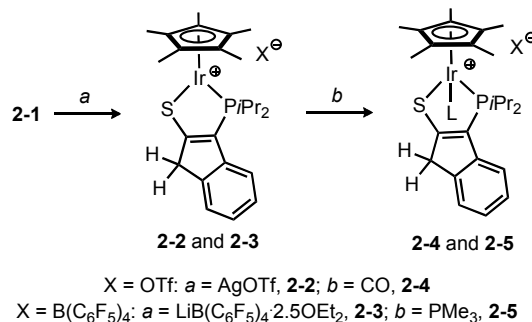


Figure 2-1. ORTEP diagram for **2-1**, shown with 50% displacement ellipsoids and with the atomic numbering scheme depicted; selected hydrogen atoms have been omitted for clarity. Selected bond lengths (Å) for **2-1**: Ir-C1 2.4021(9); Ir-P 2.3220(8); Ir-S 2.3566(9); S-C2 1.718(3); P-C3 1.797(3); C1-C2 1.516(4); C2-C3 1.358(4).

2.2.1 Synthesis and L-donor Reactivity of the Coordinatively Unsaturated Cations **2-2** and **2-3**

Treatment of an orange solution of **2-1** in CH_2Cl_2 with AgOTf or $\text{LiB}(\text{C}_6\text{F}_5)_4 \cdot 2.5\text{OEt}_2$ in each case resulted in the quantitative conversion to a single phosphorus-containing product (^{31}P NMR) accompanied by an immediate color change to dark blue (Scheme 2-6). The assignment of these products as the targeted coordinatively unsaturated, C_s -symmetric **2-2** (78%) and **2-3** (82%) complexes is entirely consistent with ^1H and ^{13}C NMR spectra obtained for these species, in which resonances attributable to chemically equivalent isopropyl fragments within the PiPr_2 group are observed. Combustion analysis data obtained for **2-2** and **2-3** precludes the presence of an additional co-ligand, as does the dark blue coloration of these complexes.^[31b, 34] As anticipated for such unsaturated species, exposure of a blue solution of **2-2** to an atmosphere of CO afforded cleanly an orange solution of the C_1 -symmetric adduct **2-4** ($\nu_{\text{CO}} = 2053 \text{ cm}^{-1}$) from which the product was isolated as an analytically pure, bright orange solid in 91% yield. Similarly, treatment of **2-3** with PMe_3 afforded the 18-electron complex **2-5** in 94% isolated yield. The connectivity in **2-4** and **2-5** is supported by NMR spectroscopic data, as well as X-ray diffraction data in the case of **2-4** (Figure 2-2). While efforts to prepare the corresponding acetonitrile adducts by treatment of **2-2** or **2-3** with excess CH_3CN resulted in the partial bleaching of the dark blue solution along with the consumption of

2-2 and **2-3** (^{31}P NMR), an intractable mixture of phosphorus-containing products was generated.



Scheme 2-6. Synthesis of coordinatively unsaturated cationic complexes **2-2** and **2-3** and the L-donor stabilized adducts **2-4** and **2-5**.

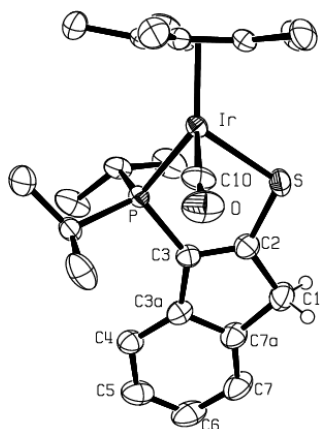
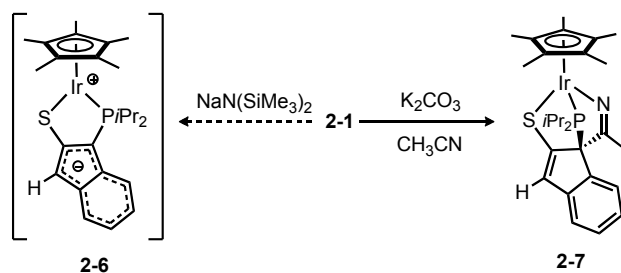


Figure 2-2 ORTEP diagram for **2-4**, shown with 50% displacement ellipsoids and with the atomic numbering scheme depicted; selected hydrogen atoms and the SO_3CF_3 anion have been omitted for clarity. Selected bond lengths (\AA) for **2-4**: Ir–P 2.3497(10); Ir–S 2.3776(12); Ir–C 1.887(5); C–O 1.119(5); S–C2 1.734(5); P–C3 1.792(4); C1–C2 1.519(6); C2–C3 1.351(6).

2.2.2 Pursuit of the Coordinatively Unsaturated Zwitterion 2-6

Having successfully prepared the new coordinatively unsaturated cationic Ir complexes **2-2** and **2-3**, the synthesis of the structurally related zwitterion **2-6** was then targeted (Scheme 2-7). Efforts to prepare **2-6** via HX extrusion from the neutral **2-1** or cationic species **2-2** and **2-3** employing $\text{NaN}(\text{SiMe}_3)_2$ afforded a green solid that exhibited broad ^1H and ^{31}P NMR features (223–333 K; $\delta^{31}\text{P}$ ca. 44), and which has thus far resisted crystallization. Alternatively, treatment of **2-1** with K_2CO_3 in CH_3CN led to the consumption of **2-1** along with the formation of one major product (**2-7**, > 90% on the

basis of ^{31}P NMR data). Upon workup, **2-7** was obtained as analytically pure, brown crystals in 41% isolated yield. Combustion analysis, NMR, and X-ray diffraction data (Figure 2-3) all support the identification of this product as the unusual tripodal $\kappa^3\text{-P,S,N}$ Ir-iminato species **2-7**, in which the CH_3CN can be described as bridging the Lewis acidic Cp^*Ir and Lewis basic indenide fragments of zwitterionic **2-6** (i.e. net M^+X^- cooperative reactivity). In keeping with such a formulation, the normally linear acetonitrile moiety adopts a bent structure ($\text{N-C27-C28} = 121.6(2)^\circ$) in **2-7**, with the sum of the angles at C27 (359.9°) being consistent with a trigonal planar geometry. Such crystallographically characterized Ir-iminato complexes are rare,^[35] and there is scant precedent for net metal-ligand cooperative activation of nitriles involving a mononuclear Cp^*Ir complex.^[36] While the aforementioned green solid that is formed upon treatment of **2-1** or **2-2/2-3** with $\text{NaN}(\text{SiMe}_3)_2$ behaves as a source of **2-6** in generating **2-7** or **2-16** (see Section 2.2.6) as the major product (^{31}P NMR) upon addition of CH_3CN or Ph_2SiH_2 (respectively), the identity of this green solid as being the desired zwitterionic species **2-6** has yet to be unequivocally confirmed.



Scheme 2-7. Attempted syntheses of coordinatively unsaturated zwitterion **2-6** and formation of **2-7**.

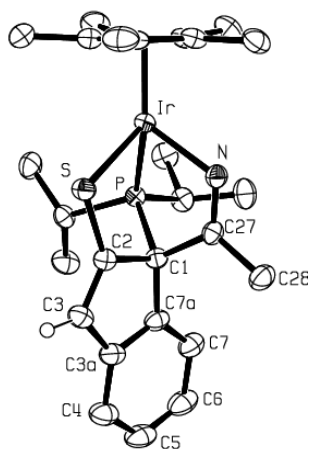
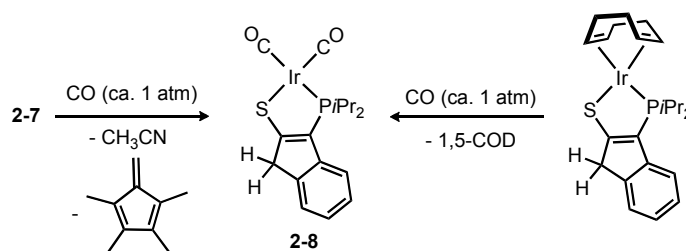


Figure 2-3. ORTEP diagram for **2-7** shown with 50% displacement ellipsoids and with the atomic numbering scheme depicted; selected hydrogen atoms have been omitted for clarity. Selected bond lengths (Å) for **2-7**: Ir–P 2.2752(6); Ir–S 2.3787(6); Ir–N 2.053(2); N–C27 1.270(3); C27–C28 1.509(4); S–C2 1.730(3); P–C1 1.875(3); C1–C2 1.531(3); C2–C3 1.359(4).

2.2.3 Probing the Reactivity of **2-7** with CO and PMe₃

The rapid formation of **2-7-d₃** and an equivalent of free CH₃CN upon addition of CD₃CN (5 equivalents, 15 minutes) to a solution of **2-7** in C₆D₆ confirmed the lability of the coordinated acetonitrile ligand in **2-7** (¹H NMR). In viewing **2-7** as a potentially reactive source of the zwitterion **2-6**, the L-donor substrate activation chemistry of **2-7** was further explored to allow for comparisons to be made with the related cations **2-2** and **2-3**. Unexpected reactivity was observed between **2-7** and CO (Scheme 2-8). Unlike the clean formation of the adduct **2-4** that occurred upon treatment of **2-2** with CO (see Section 2.2.1), exposure of **2-7** to an atmosphere of CO did not afford the anticipated adduct; rather, NMR analysis of the reaction mixture revealed the clean formation of (κ²-3-*P*Pr₂-2-*S*-indene)Ir(CO)₂ **2-8** and 1,2,3,4-tetramethylfulvene (1:1).^[37] To confirm this structural assignment, compound **2-8** was prepared independently from (κ²-3-*Pi*Pr₂-2-*S*-indene)Ir(COD) and CO. The formation of **2-8** in the reaction of **2-7** with CO can be viewed as arising from net deprotonation of (η⁵-C₅Me₅)Ir^[38] by the indenide unit in **2-6** (or possibly a CO adduct of **2-6**), followed by substitution of the coordinated 1,2,3,4-tetramethylfulvene by CO ligands. In contrast to the quantitative conversion of **2-7** into **2-8**, treatment of **2-1** or **2-4** with NaN(SiMe₃)₂ followed by the introduction of an

atmosphere of CO gave rise to a mixture of phosphorus-containing products in which **2-8** represented less than 50% of the reaction mixture (on the basis of ^{31}P NMR data). Whereas addition of PMe_3 to **2-3** afforded the isolable adduct **2-5** (see Section 2.2.1), under similar conditions **2-7** gave rise to a first-formed bis(phosphine)Ir product (ca. 75%, possibly corresponding to a PMe_3 adduct of **2-6**; $^{31}\text{P}\{^1\text{H}\}$ NMR (CDCl_3): δ 25.0 (d, $^2J_{\text{PP}} = 27.9$ Hz), -37.7 (d, $^2J_{\text{PP}} = 27.9$ Hz)) that was observed to decompose to a mixture of phosphorus-containing products upon standing in solution, or upon workup. Notably, treatment of **2-5** with $\text{NaN}(\text{SiMe}_3)_2$ affords an as-yet-unidentified bis(phosphine)Ir product ($^{31}\text{P}\{^1\text{H}\}$ NMR (CD_2Cl_2): 34.1 (δ , $^2J_{\text{PP}} = 28.8$ Hz), -40.8 (d, $^2J_{\text{PP}} = 28.0$ Hz)) that differs from the first-formed product generated upon addition of PMe_3 to **2-7**, and which has yet to be isolated in pure form.

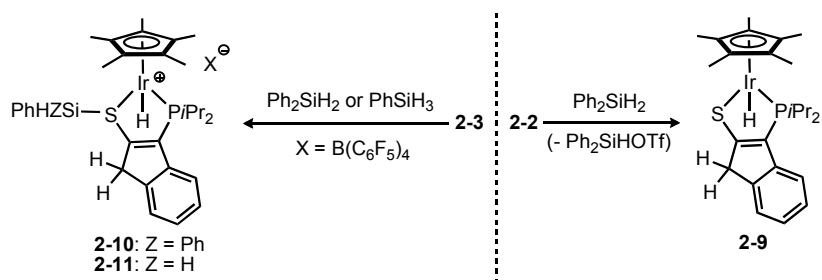


Scheme 2-8. Loss of CH_3CN and 1,2,3,4-tetramethylfulvene from **2-7** upon treatment with CO (1 atm) to generate **2-8**.

2.2.4 Net M-X Cooperative H-Si Bond activation by **2-3** and Stoichiometric Silane Transfer to Acetophenone

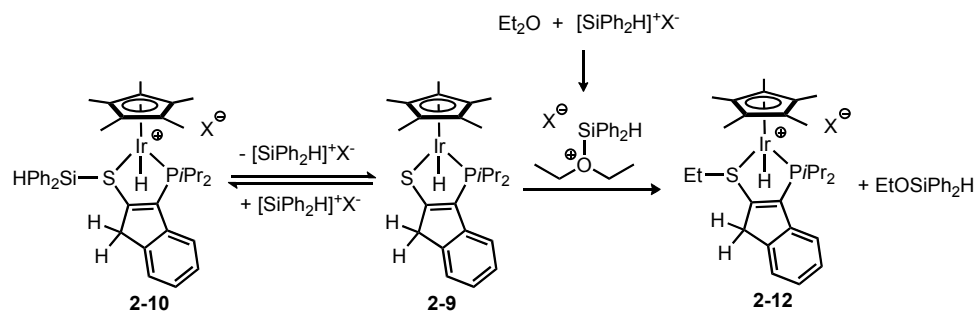
Intrigued by the differing L-donor substrate activation pathways exhibited by cationic complexes **2-2** and **2-3** and the putative zwitterion **2-6**, the study of E-H bond activation chemistry mediated by these structurally related complexes was explored. Given the propensity of coordinatively unsaturated Cp^*Ir complexes to mediate unusual transformations of organosilanes, such as double geminal Si-H bond activation to form Ir-Si multiple bonds,^[29a, 29b] the activation of H-Si containing substrates was selected as an entry point for these investigations. Treatment of **2-2** with Ph_2SiH_2 resulted in the net loss of $\text{Ph}_2\text{Si}(\text{OTf})\text{H}$ to give **2-9** in 44% isolated yield (Scheme 2-9). In contrast, the analogous reaction involving **2-3** proceeded via H-Si addition across the Ir-S linkage (i.e. net M-X cooperative reactivity) to give the cationic hydrido species **2-10** (68% isolated yield),

which features a newly established S-SiHPh₂ linkage. Although under similar conditions employing PhSiH₃ the related addition product **2-11** was obtained in 77% isolated yield, an intractable mixture of products was generated upon addition of Ph₃SiH to **2-3**. Whereas net H-Si addition across an M-SR linkage to give an isolable mononuclear addition product has not been reported previously in the literature, the related activation of H₂ by dinuclear complexes featuring an M₂S₂ core (e.g. M = Rh,^[39] Ir^[40]) is known. No reaction was observed (¹H and ³¹P NMR) upon exposure of either **2-2** or **2-3** to H₂ (ca. 1 atm) at ambient temperature over the course of five days.



Scheme 2-9. Reactivity of **2-2** and **2-3** with organosilanes.

While both **2-2** and **2-3** proved unreactive towards diethyl ether, the H-Si addition product **2-10** effected net C-O bond cleavage in this substrate with net loss of Ph₂Si(OEt)H over the course of 24 h at ambient temperature (in the absence of spectroscopically observable intermediates), thereby affording the cationic Ir-S-Et complex **2-12** in 77% isolated yield (Scheme 2-10). An ORTEP^[32] diagram for **2-12** is presented in Figure 2-4. The structural features of **2-12** can be compared with those of Cp*(H)Ir(PMe₃)(*St*Bu), the only closely related Cp*Ir complex for which crystallographic data have been reported.^[31a] While definitive evidence regarding mechanistic details of the conversion of **2-10** into **2-12** remain elusive, a likely mechanism might involve a reaction pathway where silylium ion could be transiently generated upon loss of [Ph₂SiH]⁺BAR₄⁻ from **2-10**, followed by coordination to diethyl ether and nucleophilic displacement of EtOSi(H)Ph₂ by the Ir-thiolate (Scheme 2-10).^[41] Notably, the mixture of Ph₂Si(OTf)H and **2-9** that is apparently formed upon treatment of **2-2** with Ph₂SiH₂ (Scheme 2-9) was not observed to react with diethyl ether under similar conditions (¹H and ³¹P NMR).



Scheme 2-10. Proposed mechanism for the reaction of **2-10** with diethyl ether to form **2-12** ($X = \text{B}(\text{C}_6\text{F}_5)_4$).

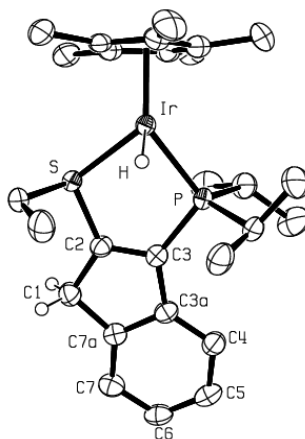
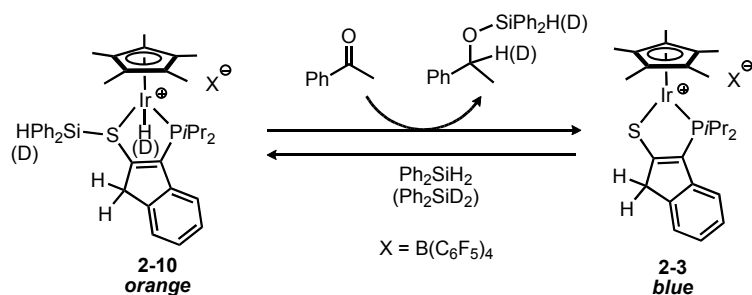


Figure 2-4. ORTEP diagram for **2-12**, shown with 50% displacement ellipsoids and with the atomic numbering scheme depicted; selected hydrogen atoms and the $\text{B}(\text{C}_6\text{F}_5)_4$ anion have been omitted for clarity. Selected bond lengths (\AA) for **2-12**: Ir–P 2.2787(9); Ir–S 2.2912(8); Ir–H 1.69(1); S–C2 1.759(4); P–C3 1.817(4); C1–C2 1.496(5); C2–C3 1.350(5).

Toste and co-workers^[42] have reported that $(\text{PPh}_3)_2\text{Re}(\text{O})_2\text{I}$ catalyzes the hydrosilylation of carbonyl compounds by way of a previously unprecedented mechanism involving net H-Si addition across a $\text{Re}=\text{O}$ linkage. Given the conceptual relationship between this elementary reaction step and the stoichiometric H-Si addition of Ph_2SiH_2 to **2-3** giving **2-10**, and in light of the apparent ability of **2-10** to effect the silylation of diethyl ether (see Section 2.2.4), the ability of **2-10** to transfer the bound fragments of the activated silane to unsaturated substrates was assessed. While no reaction was observed visually or by use of NMR methods upon exposure of **2-10** to excess styrene (10 equiv), treatment of an initially orange solution of **2-10** (ca. 0.05 mmol) in CH_2Cl_2 (2 mL) with excess acetophenone (0.26 mmol) resulted in a color change of the solution to dark blue

over the course of several minutes at ambient temperature, in keeping with the formation of **2-3** (Scheme 2-11). This qualitative assessment was substantiated on the basis of ^{31}P NMR data obtained after a total reaction time of 0.25 h, which confirmed the consumption of **2-10** with concomitant formation of **2-3** as the major product ($> 85\%$ on the basis of ^{31}P NMR). Subsequent addition of Ph_2SiH_2 to this reaction mixture led to the complete transformation of **2-3** back into **2-10** (^{31}P NMR). In an effort to monitor the fate of the H-Si fragment in these reactions, **2-3** was treated with Ph_2SiD_2 , affording **2-10-d₂**, in which deuterium incorporation was observed only at the Si-H and Ir-H positions. In keeping with a process involving net transfer of Ir-D and S-SiDPh₂ fragments, the addition of acetophenone to **2-10-d₂** produced exclusively $\text{PhMeC(D)(OSiPh}_2\text{D)}$ on the basis of NMR data. While these experiments unequivocally confirm the ability of **2-10** to transfer the activated Ph_2SiH_2 to acetophenone in a stoichiometric fashion, it is worthy of mention that an *in situ* generated mixture of $\text{Ph}_2\text{Si(OTf)H}$ and **2-9** (Scheme 2-9) is also transformed cleanly into $\text{PhMeC(H)(OSiPh}_2\text{H)}$ and **2-2** upon treatment with acetophenone (^1H and ^{31}P NMR). On the basis of these observations, and in the absence of further mechanistic data, the role of sulfur atom participation in acetophenone hydrosilylation reactions involving **2-10** and/or mixtures of $\text{Ph}_2\text{Si(OTf)H}$ and **2-9** has yet to be unambiguously determined.

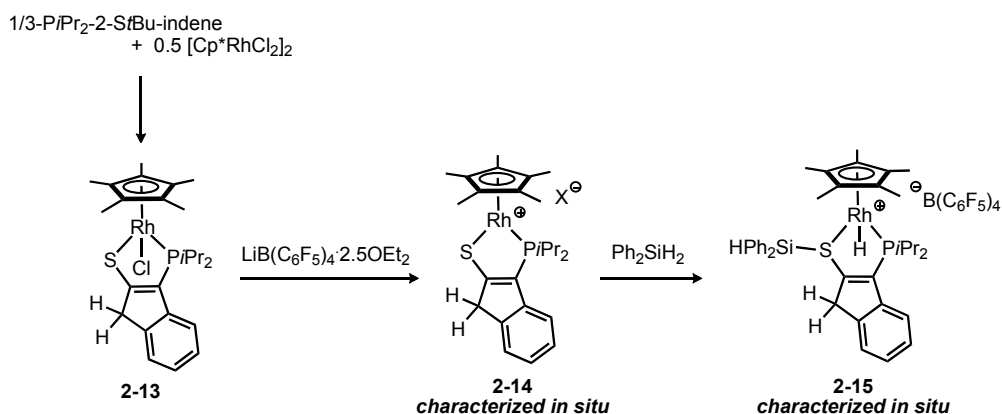


Scheme 2-11. Stoichiometric transfer of Ph_2SiH_2 from **2-10** to acetophenone to generate the corresponding silyl ether and **2-3**.

2.2.5 Formation of Rh Complexes and Ketone Hydrosilylation Catalysis

Having established that Ph_2SiH_2 adds cleanly to the Ir-S linkage in **2-3**, and that the resulting adduct **2-10** can transfer stoichiometrically the activated silane to acetophenone, the ability of **2-3** to catalyze the hydrosilylation of acetophenone with

Ph₂SiH₂ was examined. However, only modest conversions (< 20%, on the basis of GC data) were achieved under a variety of conditions employing 2.0 mol% **2-3** (prepared *in situ* from 2.0 mol% **2-1** and 2.0 mol% LiB(C₆F₅)₄·2.5Et₂O). In the pursuit of an analogous system that might offer improved catalytic activity, the preparation of Cp*Rh derivatives of 1/3-PiPr₂-2-StBu-indene was targeted (Scheme 2-12). Treatment of 1/3-PiPr₂-2-StBu-indene with 0.5 equiv [Cp*RhCl₂]₂ afforded Cp*Rh(Cl)(κ²-3-PiPr₂-2-S-indene) **2-13** as an analytically pure, light brown solid in 94% isolated yield. In keeping with the stoichiometric reactions observed in the Ir system, combination of **2-13** and LiB(C₆F₅)₄·2.5Et₂O resulted in the consumption of **2-13** along with the formation of a dark green solution of the desired coordinatively unsaturated cation **2-14** (ca. 75% on the basis of ³¹P NMR data), which in turn was transformed into an orange solution of **2-15** (ca. 80% on the basis of ³¹P NMR data) upon addition of Ph₂SiH₂ to the reaction mixture. Due to their heightened reactivity, the isolation **2-14** or **2-15** in analytically pure form has proven difficult, and efforts to explore the ability of **2-15** to transfer silane to acetophenone in a stoichiometric fashion (as was observed for the Ir analogue **2-10**; Scheme 2-9) have been thwarted by the apparent instability of **2-15**. Furthermore, attempts to prepare Rh analogues of **2-6** or **2-7** by using similar protocols employed successfully for the Ir congeners generated complex reaction mixtures from which no pure materials could be isolated.



Scheme 2-12. Synthesis of Cp*Rh(κ²-P,S) complexes **2-13**, **2-14**, and **2-15**.

In a preliminary catalytic survey of the ambient temperature hydrosilylation of acetophenone employing 2.0 mol% **2-14** (prepared *in situ* from a mixture of 2.0 mol% **2-13** and 2.0 mol% LiB(C₆F₅)₄·2.5Et₂O), efficient conversion (¹H NMR) to the corresponding silyl ether was achieved by using either Ph₂SiH₂ (85%) or PhSiH₃ (98%); by comparison, negligible conversion (< 5%) was noted for analogous reactions employing Ph₃SiH. The inability of **2-14** to catalyze the reduction of acetophenone employing Ph₃SiH may correlate with the complex stoichiometric reactivity observed between the Ir analogue **2-14** and this tertiary silane. Consistent with the stoichiometric reactivity observed for **2-10-d₂** (see Section 2.2.4), the catalytic reduction of acetophenone mediated by **2-14** and employing Ph₂SiD₂ produced exclusively PhMeC(D)(OSiPh₂D). Encouraged by these preliminary results, the ability of *in situ* prepared **2-14** to catalyze the hydrosilylation of various ketone substrates using PhSiH₃ was examined (Table 2-1); for convenience, the progress of each hydrosilylation reaction was monitored through analysis of the product mixture obtained following hydrolytic workup. In keeping with the preliminary catalytic survey, the reduction of acetophenone proceeded with near quantitative conversion (98%, entry 1) on the basis of GC data, thereby enabling the isolation of PhMeC(H)(OH) in 89% yield. Furthermore, *in situ* prepared **2-14** proved effective in reducing a range of other aryl alkyl ketones (entries 2-5), functionalized acetophenones (entries 6-8), and diaryl ketones (entries 9 and 10).

2.2.6 Net M^X Cooperative H-Si Bond Activation Employing 2-7

Having documented the addition of H-Si fragments to M-S linkages in **2-3** and **2-14**, investigation into the potential of the indenide fragment in the structurally related Ir zwitterion **2-6** to provide access to alternative net M^X cooperative reaction pathways in σ-bond activation chemistry was carried out. Whereas no reaction was observed upon exposure of either **2-2** or **2-3** to H₂ (ca. 1 atm) at ambient temperature, reactions conducted under similar conditions employing **2-7** (as a source of **2-6**) produced a complex mixture of phosphorus-containing products (³¹P NMR). Conversely, treatment of **2-7** with Ph₂SiH₂ resulted in the liberation of CH₃CN (¹H NMR) along with the

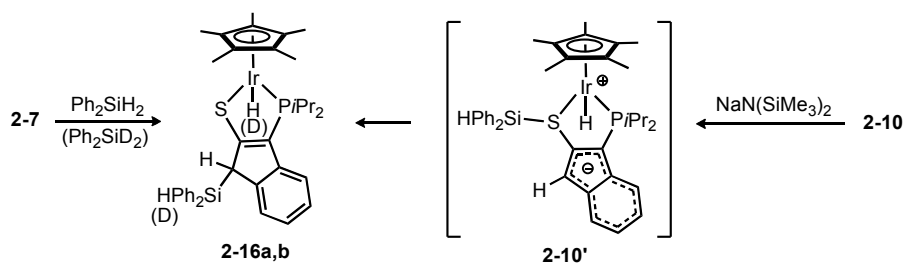
Table 2-1. Rh-Catalyzed Hydrosilylation of Ketones.^[a]

entry	substrate	conversion (%) ^[b]	entry	substrate	conversion (%) ^[b]
1		98 (89) ^[c]	6		99
2		98	7		98
3		98	8		95
4		96	9		93
5		83	10		95

^[a] Reaction conditions: 0.2 mmol ketone, 0.3 mmol PhSiH₃, 2.0 mol% **2-13**, 2.0 mol% LiB(C₆F₅)₄·2.5Et₂O in 2 mL of THF at ambient temperature for 5 h. ^[b] Conversion to the secondary alcohol determined on the basis of GC data. ^[c] Isolated yield (> 95% purity on the basis of ¹H NMR data) when the reaction was conducted on a 0.8 mmol ketone scale.

quantitative formation of **2-16** (64% isolated yield; Scheme 2-13). Notably, the formation of **2-16** corresponds to heterolytic H-Si bond activation, involving net addition of H⁻ and Ph₂HSi⁺ fragments to Ir and indenide (respectively) in the unobserved zwitterion **2-6**. Compound **2-16** is formed as a mixture of two diastereomers (**2-16a,b**, ca. 3:1) that arise from the stereogenic nature of C1 and Ir, and a similar **2-16a,b** mixture can be prepared via addition of NaN(SiMe₃)₂ to a solution of **2-1** and Ph₂SiH₂ (79% isolated yield). Both diastereomers of **2-16** are detected early on in each synthesis in the absence of other phosphorus-containing products (³¹P NMR), and their relative proportions in the final reaction mixture do not change substantially, even upon heating. While the connectivity in **2-16a,b** was determined initially on the basis of NMR data, single crystals obtained from the reaction mixture that were subjected to X-ray diffraction analysis correspond to the diastereomer of **2-16** whereby the Ir-H and C1-SiHPh₂ groups adopt an *anti*-relationship with regard to the plane defined by the indene backbone of **2-16** (Figure 2-5).

Reactions employing Ph_2SiD_2 afforded **2-16-d₂**, in which exclusive deuterium incorporation at the Si-*H* and Ir-*H* positions of both diastereomers was noted, thereby precluding more complex mechanistic pathways that would lead to scrambling of the isotopic label (e.g. C-H/Si-D exchange). Upon treatment of the cationic H-Si addition product **2-10** with $\text{NaN}(\text{SiMe}_3)_2$, **2-16a,b** is generated as the major phosphorus-containing species (ca. 75%, ^{31}P NMR). This result supports the possible intermediacy of **2-10'** (the conjugate base of **2-10**; Scheme 2-13) as an unobserved first-formed addition product in the reaction of Ph_2SiH_2 with putative **2-6**, which in turn could rearrange to **2-16a,b** via net transfer of Ph_2HSi^+ from sulfur to the indenide backbone. On the basis of these observations, further mechanistic experimentation will be required to ascertain if the H-Si bond cleavage process leading to **2-16a,b** involves the net addition of silane across a single molecule of **2-6**. Unlike **2-10**, no reaction was observed between **2-16a,b** and acetophenone, suggesting that the newly formed Si-C_{indenide} linkage in such complexes must be rendered more labile (via ancillary ligand modification) in order to allow for the incorporation of such net $\text{M}^{\wedge}\text{X}'$ cooperative H-Si activation steps into productive catalytic cycles.



Scheme 2-13. Reactivity of **2-7** with organosilanes.

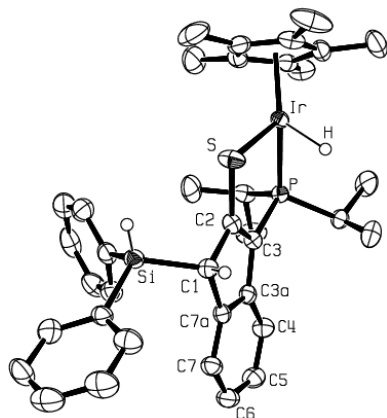


Figure 2-5. ORTEP diagram for one diastereomer of **2-16**, shown with 50% displacement ellipsoids and with the atomic numbering scheme depicted; selected hydrogen atoms have been omitted for clarity. Selected bond lengths (Å) for **2-16**: Ir–P 2.2668(10); Ir–S 2.3447(11); Ir–H 1.574(19); S–C2 1.729(4); P–C3 1.797(4); C1–C2 1.503(6); C2–C3 1.367(5); Si–C1 1.900(4).

2.3 Summary and Conclusions

In summary, efforts to prepare and characterize a previously unreported class of coordinatively unsaturated cationic (**2-2** and **2-3**) and formally zwitterionic (**2-6**) Cp*Ir(κ^2 -*P,S*) complexes that feature structurally analogous monoanionic κ^2 -*PiPr*₂,*S*-indene and dianionic κ^2 -*PiPr*₂,*S*-indenide ancillary ligands, respectively, have been described. The versatility of donor-functionalized indene ancillary ligands in allowing for the selection of divergent metal-ligand cooperativity pathways (simply by ancillary ligand deprotonation) in the activation of small molecule substrates was demonstrated in comparative reactivity studies involving **2-2/2-3** and putative **2-6**. In this regard, the cationic complex **2-3** was observed to activate organosilanes via the first well-documented H-Si addition across an M-SR linkage (i.e. net M-X cooperative reactivity); the resulting adduct proved capable of effecting the stoichiometric silylation of diethyl ether via C-O bond cleavage, and of selectively transferring the bound fragments of the activated silane to acetophenone. Related cationic Cp*Rh complexes exhibited similar stoichiometric H-Si bond activation chemistry, and in turn proved capable of mediating the catalytic hydrosilylation of various ketone substrates. The possible involvement of H-Si addition to M-SR as an elementary step in this catalysis is intriguing, in that such a transformation is without precedent in metal-mediated hydrosilylation chemistry.

Conversely, the unusual stoichiometric reactivity of putative **2-6** with CH₃CN or Ph₂SiH₂ can be viewed as resulting from the dual action of the Lewis acidic Cp*Ir fragment and the Lewis basic 10π-electron indenide unit within this formally charge-separated zwitterion (i.e. net M⁺X⁻ cooperative reactivity). Building on these and other encouraging observations, work in the Stradiotto group is directed towards examining in greater detail the utility of donor-functionalized indene and indenide ancillary ligands in the development of selective new stoichiometric and catalytic substrate activation chemistry that is enabled by novel metal-ligand cooperative behavior. In this vein, the focus of Chapter 3 is on the coordination chemistry of Pt with 1/3-PiPr₂-2-StBu-indene with particular emphasis on the development of synthetic pathways to cationic complexes and structurally similar carbon- or boron-based zwitterions.

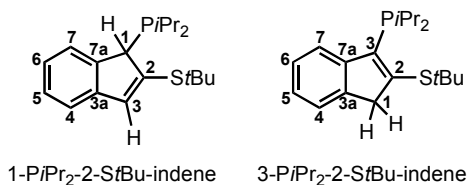
2.4 Experimental Section

2.4.1 General Considerations

All manipulations were conducted in the absence of oxygen and water under an atmosphere of dinitrogen, either by use of standard Schlenk methods or within an mBraun glovebox apparatus, utilizing glassware that was oven-dried (130 °C) and evacuated while hot prior to use. Celite (Aldrich) was oven-dried for 5 d and then evacuated for 24 h prior to use. The non-deuterated solvents dichloromethane, diethyl ether, tetrahydrofuran, benzene, toluene, and pentane were deoxygenated and dried by sparging with dinitrogen gas, followed by passage through a double-column solvent purification system purchased from mBraun Inc. Dichloromethane, tetrahydrofuran, and diethyl ether were purified over two alumina-packed columns, while benzene, toluene, and pentane were purified over one alumina-packed column and one column packed with copper-Q5 reactant. Purification of CH₃CN was achieved by refluxing over CaH₂ for 4 d under dinitrogen, followed by distillation. CDCl₃ (Aldrich) was degassed by using three repeated freeze-pump-thaw cycles, dried over CaH₂ for 7 days, distilled *in vacuo*, and stored over 4 Å molecular sieves for 24 h prior to use. Benzene-*d*₆, tetrahydrofuran-*d*₈, and dichloromethane-*d*₂ (Cambridge Isotopes) were degassed by using three repeated freeze-pump-thaw cycles and then dried over 4 Å molecular sieves for 24 h prior to use. All solvents used within

the glovebox were stored over activated 4 Å molecular sieves. $\text{NaN}(\text{SiMe}_3)_2$ (Aldrich), anhydrous K_2CO_3 (Aldrich), $[(\text{COD})\text{IrCl}]_2$ (Strem), $[\text{Cp}^*\text{IrCl}_2]_2$ (Strem), $[\text{Cp}^*\text{RhCl}_2]_2$ (Strem), and $\text{LiB}(\text{C}_6\text{F}_5)_4 \cdot 2.5\text{Et}_2\text{O}$ (Boulder Scientific) were dried *in vacuo* for 24 h prior to use. Ph_3SiH , Ph_2SiH_2 , and PhSiH_3 (Gelest, shipped under argon) were dried over 4 Å molecular sieves for 24 h prior to use; Ph_2SiD_2 was prepared via reduction of Ph_2SiCl_2 with LiAlD_4 and was dried over 4 Å molecular sieves for 24 h prior to use. All ketones were obtained from commercial sources in high purity; solid ketones were dried *in vacuo* for a minimum of 12 h prior to use, while liquid ketones were degassed by use of three repeated freeze-pump-thaw cycles. All other reagents were used as received. ^1H , ^{13}C , ^{29}Si and ^{31}P NMR characterization data were collected at 300K on a Bruker AV-500 spectrometer operating at 500.1, 125.8, 99.4, and 202.5 MHz (respectively) with chemical shifts reported in parts per million downfield of SiMe_4 (for ^1H , ^{13}C , and ^{29}Si) or 85% H_3PO_4 in D_2O (for ^{31}P). ^1H and ^{13}C NMR chemical shift assignments are made on the basis of data obtained from ^{13}C -DEPT, ^1H - ^1H COSY, ^1H - ^{13}C HSQC, and ^1H - ^{13}C HMBC NMR experiments, and ^{13}C resonances associated with $\text{B}(\text{C}_6\text{F}_5)_4^-$ and SO_3CF_3^- (OTf) were not assigned. ^{29}Si NMR chemical shift assignments are given on the basis of data obtained from ^1H - ^{29}Si HMQC NMR experiments. UV-Vis data were obtained using a Varian Cary 100 Bio spectrometer within a 10 mm cell. IR data were collected on a Bruker VECTOR 22 FT-IR instrument using neat CH_2Cl_2 solutions of the target compound that were evaporated on NaCl plates. Elemental analyses were performed by Canadian Microanalytical Service Ltd., Delta, British Columbia, Canada.

2.4.2 Synthetic Details and Characterization Data



Synthesis of 1/3- $\text{PiPr}_2\text{-2-StBu-indene}$. A Schlenk tube containing 2-*tert*-butylthioindene^[43] (6.10 g, 29.9 mmol) in diethyl ether (10 mL) was cooled to $-78\text{ }^\circ\text{C}$, followed by initiation of magnetic stirring and dropwise addition of a 2.9 M solution of

*n*BuLi in hexanes (10.3 mL, 29.9 mmol). The resulting solution was left to stir and warm to ambient temperature. After 3 h, the reaction mixture was cooled to -78 °C with subsequent addition of *i*Pr₂PCl (4.70 mL, 29.9 mmol), which effected the precipitation of a white solid. The reaction mixture was left to stir and warm to ambient temperature over 16 h, followed by filtration by use of a Schlenk filter stick to remove the white precipitate. The solvent and other volatile materials were removed *in vacuo*, affording 1/3-*PiPr*₂-2-*StBu*-indene (the isomeric ratio can vary from 1:10 to 10:1 on the basis of NMR data) as an analytically pure, light brown oil (8.33 g, 26.0 mmol, 87%). Anal. Calcd for C₁₉H₂₉PS: C 71.21; H 9.12; N 0.00. Found: C 71.09; H 9.15; N <0.3. **3-*PiPr*₂-2-*StBu*-indene**: ¹H NMR (C₆D₆): δ 7.72 (d, ³*J*_{HH} = 7.5 Hz, 1H, C4-H or C7-H), 7.26-7.19 (m, 2H, Ar-CH), 7.11 (t, ³*J*_{HH} = 7.5 Hz, 1H, C5-H or C6-H), 3.58 (s, 2H, C1(H)₂), 2.62 (m, 2H, P(CHMe_aMe_b)), 1.20 (s, 9H, C(CH₃)₃), 1.22 (dd, ³*J*_{PH} = 18.5 Hz, ³*J*_{HH} = 7.0 Hz, 6H, P(CHMe_aMe_b)), 1.01 (dd, ³*J*_{PH} = 12.0 Hz, ³*J*_{HH} = 7.0 Hz, 6H, P(CHMe_aMe_b)); ¹³C{¹H} NMR (C₆D₆): δ 154.1 (d, ²*J*_{PC} = 24.5 Hz, C2), 147.1 (C3a or C7a), 143.7 (d, *J*_{PC} = 2.0 Hz, C3a or C7a), 143.2 (d, ¹*J*_{PC} = 25.5 Hz, C3), 126.7 (Ar-CH), 124.7 (Ar-CH), 123.5 (Ar-CH), 121.8 (d, *J*_{PC} = 3.8 Hz, C4 or C7), 46.7 (d, ³*J*_{PC} = 3.1 Hz, C1), 46.5 (C(CH₃)₃), 32.2 (C(CH₃)₃), 24.3 (d, ¹*J*_{PC} = 12.1 Hz, P(CHMe_aMe_b)), 22.2 (d, ²*J*_{PC} = 25.4 Hz, P(CHMe_aMe_b)), 21.3 (d, ²*J*_{PC} = 11.8 Hz, P(CHMe_aMe_b)); ³¹P{¹H} NMR (C₆D₆): δ -4.8. **1-*PiPr*₂-2-*StBu*-indene**: ¹H NMR (C₆D₆): δ 7.29 (d, ³*J*_{HH} = 7.5 Hz, 1H, C4-H or C7-H), 7.23 (d, ³*J*_{HH} = 7.5 Hz, 1H, C7-H or C4-H), 7.17 (t, ³*J*_{HH} = 7.0 Hz, 1H, C5-H or C6-H), 7.08 (t, ³*J*_{HH} = 7.5 Hz, 1H, C6-H or C5-H), 6.86 (s, 1H, C3-H), 4.03 (s, 1H, C1-H), 2.00 (m, 1H, P(CHMe_aMe_b)), 1.87 (m, 1H, P(CHMe_cMe_d)), 1.30 (s, 9H, C(CH₃)₃), 1.11-0.96 (m, 9H, P(CHMe_aMe_b) and P(CHMe_cMe_d)), 0.79 (dd, ³*J*_{PH} = 11.5 Hz, ³*J*_{HH} = 7.0 Hz, 3H, P(CHMe_aMe_b)); ¹³C{¹H} NMR (C₆D₆): δ 145.5 (C3a or C7a), 144.1 (d, ²*J*_{PC} = 21.0 Hz, C2), 143.2 (C3a or C7a), 132.6 (C3), 125.5 (C5 or C6), 123.4 (C5 or C6), 122.8 (d, *J*_{PC} = 5.3 Hz, C4 or C7), 119.8 (C4 or C7), 64.8 (C(CH₃)₃), 51.7 (d, ¹*J*_{PC} = 32.2 Hz, C1), 30.3 (C(CH₃)₃), 21.1-19.9 (m, P(CHMe_aMe_b) and P(CHMe_cMe_d)), 19.3 (d, ²*J*_{PC} = 13.5 Hz, P(CHMe_aMe_b)); ³¹P{¹H} NMR (C₆D₆): δ 21.4.

Synthesis of 2-1. To a magnetically stirred mixture of [Cp*IrCl₂]₂ (0.25 g, 0.32 mmol) and CH₂Cl₂ (5 mL) was added a solution of 1/3-*PiPr*₂-2-*StBu*-indene (0.20 g, 0.64 mmol) in CH₂Cl₂ (1 mL). After 20 h of magnetic stirring at ambient temperature, ³¹P

NMR analysis of the reaction mixture confirmed the consumption of the starting material and the presence of a single new phosphorus-containing product (**2-1**). The solvent and other volatiles were removed *in vacuo* affording an orange solid that was washed with pentane (2 x 2 mL). Removal of the solvent from the residual solid afforded **2-1** as an analytically pure, orange solid (0.38 g, 0.62 mmol, 97%). Anal. Calcd for C₂₅H₃₅ClIrPS: C 47.95; H 5.63; N 0.00. Found: C 47.91; H 5.49; N < 0.3. ¹H NMR (CDCl₃): δ 7.18 (d, ³J_{HH} = 7.5 Hz, 1H, C4 or C7), 7.14 (d, ³J_{HH} = 7.0 Hz, 1H, C4 or C7), 7.12 (t, ³J_{HH} = 7.0 Hz, 1H, C5 or C6), 6.97 (d of t, ³J_{HH} = 7.0 Hz, J = 1.0 Hz, C5 or C6), 3.67-3.51 (m, 2H, C1(H)₂), 3.46 (m, 1H, P(CHMe_aMe_b)), 2.18 (m, 1H, P(CHMe_cMe_d)), 1.82 (d, J = 2.0 Hz, 15H, C₅Me₅), 1.51 (dd, ³J_{PH} = 15.0 Hz, ³J_{HH} = 7.0 Hz, 3H, P(CHMe_aMe_b)), 1.38 (dd, ³J_{PH} = 12.5 Hz, ³J_{HH} = 7.0 Hz, 3H, P(CHMe_cMe_d)), 1.36 (dd, ³J_{PH} = 11.5 Hz, ³J_{HH} = 7.0 Hz, 3H, P(CHMe_aMe_b)), 1.00 (dd, ³J_{PH} = 16.0 Hz, ³J_{HH} = 7.0 Hz, 3H, P(CHMe_cMe_d)); ¹³C{¹H} NMR (CDCl₃): δ 179.4 (d, ²J_{PC} = 22.8 Hz, C2), 148.6 (d, J_{PC} = 7.5 Hz, C3a or C7a), 145.1 (d, J_{PC} = 4.2 Hz, C7a or C3a), 128.0 (d, ¹J_{PC} = 60.1 Hz, C3), 126.2 (C5 or C6), 124.2 (C6 or C5), 121.7 (C4 or C7), 117.6 (C7 or C4), 92.5 (d, ²J_{PC} = 2.8 Hz, C₅Me₅), 41.9 (d, ³J_{PC} = 10.6 Hz, C1), 30.7 (d, ¹J_{PC} = 28.8 Hz, P(CHMe_cMe_d)), 25.6 (d, ¹J_{PC} = 35.6 Hz, P(CHMe_aMe_b)), 20.3 (d, ²J_{PC} = 1.4 Hz, P(CHMe_aMe_b)), 20.1 (d, ²J_{PC} = 6.4 Hz, P(CHMe_cMe_d)), 19.8 (d, ²J_{PC} = 5.7 Hz, P(CHMe_aMe_b)), 18.1 (d, ²J_{PC} = 1.6 Hz, P(CHMe_cMe_d)), 9.1 (C₅Me₅); ³¹P{¹H} NMR (CDCl₃): δ 32.9. Crystals suitable for X-ray crystallographic analysis were grown by vapor diffusion of pentane into a concentrated solution of **2-1** in benzene at ambient temperature.

Synthesis of 2-2. To a magnetically stirred solution of **2-1** (0.029 g, 0.047 mmol) in CH₂Cl₂ (2 mL) was added solid AgOTf (0.012 g, 0.047 mmol) which effected an immediate color change from orange to dark blue, accompanied by the formation of precipitate. The blue solution was magnetically stirred for 0.5 h; ³¹P NMR analysis of the reaction mixture showed complete consumption of **2-1** and the presence of a single new phosphorus-containing product (**2-2**). The precipitate was then removed by filtration through Celite. Removal of the solvent and other volatiles afforded a dark blue solid that was triturated with pentane (2 x 2 mL) followed by removal of the pentane layer by use of a Pasteur pipette. Residual pentane and other volatiles were removed *in vacuo* affording **2-2** as an analytically pure, dark blue solid (0.028 g, 0.037 mmol, 78%). Anal. Calcd for

C₂₆H₃₅F₃IrO₃PS₂: C 42.20; H 4.77; N 0.00. Found: C 42.12; H 4.69; N < 0.3. ¹H NMR (CD₂Cl₂): δ 7.44 (d, ³J_{HH} = 7.5 Hz, 1H, C4-H or C7-H), 7.39 (d, ³J_{HH} = 7.5 Hz, 1H, C4-H or C7-H), 7.33 (t, ³J_{HH} = 7.5 Hz, 1H, C5-H or C6-H), 7.28 (t, ³J_{HH} = 7.5 Hz, 1H, C5-H or C6-H), 3.92 (s, 2H, C1(H)₂), 3.12 (br. m, 2H, P(CHMe_aMe_b)), 1.95 (s, 15H, C₅Me₅), 1.29 (dd, ³J_{PH} = 18.5 Hz, ³J_{HH} = 7.0 Hz, 6H, P(CHMe_aMe_b)), 1.22 (dd, ³J_{PH} = 17.0 Hz, ³J_{HH} = 7.0 Hz, 6H, P(CHMe_aMe_b)); ¹³C{¹H} NMR (CD₂Cl₂): δ 177.8 (C2), 150.2 (C3a or C7a), 140.3 (C7a or C3a), 126.5 (C3), 126.8 (C5 or C6), 125.3 (C5 or C6), 124.8 (C4 or C7), 119.2 (C4 or C7), 96.7 (C₅Me₅), 40.9 (d, J_{PC} = 11.4 Hz, C1), 23.8 (br m, P(CHMe_aMe_b)), 18.2 (P(CHMe_aMe_b)), 17.8 (d, ²J_{PC} = 2.8 Hz, P(CHMe_aMe_b)), 10.4 (C₅Me₅); ³¹P{¹H} NMR (CD₂Cl₂): δ 64.9 (br s).

Synthesis of 2-3. A protocol similar to that described for the synthesis of **2-2** was employed, using **2-1** (0.039 g, 0.062 mmol) and solid LiB(C₆F₅)₄·2.5Et₂O (0.054 g, 0.062 mmol; in place of AgOTf), thereby affording **2-3** as an analytically pure, dark blue solid (0.065 g, 0.051 mmol, 82%). Anal. Calc for C₄₉H₃₅BF₂₀IrPS: C 46.32; H 2.78; N 0.00. Found: C 46.19; H 3.00; N < 0.3. ¹H NMR (CD₂Cl₂): δ 7.47 (m, 1H, C4 or C7), 7.41 (m, 1H, C4 or C7), 7.36-7.30 (m, 2H, C5 and C6), 3.96 (d, J = 2.5 Hz, 2H, C1(H)₂), 3.11 (m, 2H, P(CHMe_aMe_b)), 1.94 (d, ⁴J_{PH} = 1.5 Hz, 15H, C₅Me₅), 1.30 (dd, ³J_{PH} = 18.5 Hz, ³J_{HH} = 7.0 Hz, 6H, P(CHMe_aMe_b)), 1.20 (dd, ³J_{PH} = 18.0 Hz, ³J_{HH} = 7.0 Hz, 6H, P(CHMe_aMe_b)); ¹³C{¹H} NMR (CD₂Cl₂): δ 177.8 (d, ²J_{PC} = 25.2 Hz, C2), 150.2 (d, J_{PC} = 10.1 Hz, C3a or C7a), 140.1 (d, J_{PC} = 37.7 Hz, C3a or C7a), 134.7 (d, ¹J_{PC} = 62.9 Hz, C3), 127.2 (C5 or C6), 125.8 (C4 or C7), 125.7 (C5 or C6), 120.5 (C4 or C7), 96.9 (C₅Me₅), 41.1 (d, ³J_{PC} = 11.4 Hz, C1), 23.9 (d, ¹J_{PC} = 31.1 Hz, P(CHMe_aMe_b)), 18.3 (P(CHMe_aMe_b)), 18.0 (d, ²J_{PC} = 1.8 Hz, P(CHMe_aMe_b)), 10.7 (C₅Me₅); ³¹P{¹H} NMR (CD₂Cl₂): δ 65.2; UV-Vis (THF): λ_{max} 569 (ε = 1.49 x 10³), 673 (ε = 1.40 x 10³).

Synthesis of 2-4. Compound **2-2** was prepared *in situ* by treatment of a solution of **2-1** (0.068 g, 0.11 mmol) in CH₂Cl₂ (2 mL) with solid AgOTf (0.028 g, 0.11 mmol), causing an immediate color change to dark blue accompanied by the formation of a precipitate. The reaction mixture was stirred at ambient temperature for 0.5 h followed by filtration through Celite to remove the precipitate. The resulting dark blue CH₂Cl₂ solution containing **2-2** was transferred to a re-sealable flask and was degassed by use of three consecutive freeze-pump-thaw cycles, followed by backfilling with CO (ca. 1 atm)

which effected an immediate color change to bright orange. After 1 h of periodic shaking of the reaction flask, the solvent and other volatiles were removed *in vacuo*, affording an oily orange solid that was triturated with pentane (3 mL). Subsequent drying *in vacuo* afforded **2-4** as an analytically pure, bright orange powder (0.081 g, 0.10 mmol, 91%). Anal. Calcd for C₂₇H₃₅F₃IrO₄PS₂: C 42.23; H 4.59; N 0.00. Found: C 42.12; H 4.28; N < 0.3. ¹H NMR (CD₂Cl₂): δ 7.26 (d, ³J_{HH} = 7.5 Hz, 1H, C4-H or C7-H), 7.22 (t, ³J_{HH} = 7.5 Hz, 1H, C5-H or C6-H), 7.13 (d, ³J_{HH} = 7.5 Hz, 1H, C4-H or C7-H), 7.10 (t, ³J_{HH} = 7.5 Hz, 1H, C5-H or C6-H), 3.61 (m, 2H, C1(H)₂), 3.31 (m, 1H, P(CHMe_aMe_b)), 2.28 (m, 1H, P(CHMe_cMe_d)), 2.15 (d, ⁴J_{PH} = 1.5 Hz, 15H, C₅Me₅), 1.37 (dd, ³J_{PH} = 19.5 Hz, ³J_{HH} = 7.0 Hz, 3H, P(CHMe_cMe_d)), 1.24 (dd, ³J_{PH} = 19.5 Hz, ³J_{HH} = 7.0 Hz, 3H, P(CHMe_aMe_b)), 1.15 (dd, ³J_{PH} = 18.5 Hz, ³J_{HH} = 7.0 Hz, 3H, P(CHMe_aMe_b)), 0.95 (dd, ³J_{PH} = 18.5 Hz, ³J_{HH} = 7.0 Hz, 3H, P(CHMe_cMe_d)); ¹³C{¹H} NMR (CD₂Cl₂): δ 178.0 (d, ²J_{PC} = 18.5 Hz, CO), 166.6 (d, ²J_{PC} = 13.6 Hz, C2), 147.8 (d, J_{PC} = 8.3 Hz, C3a or C7a), 142.7 (d, J_{PC} = 6.0 Hz, C3a or C7a), 130.0 (d, ¹J_{PC} = 62.3 Hz, C3), 127.2 (C5 or C6), 125.0 (C4 or C7), 124.2 (C4 or C7), 118.3 (C5 or C6), 104.5 (C₅Me₅), 41.6 (d, ³J_{PC} = 10.9 Hz, C1), 29.6 (d, ¹J_{PC} = 27.8 Hz, P(CHMe_cMe_d)), 25.4 (d, ¹J_{PC} = 37.7 Hz, P(CHMe_aMe_b)), 19.1 (d, ²J_{PC} = 6.5 Hz, P(CHMe_cMe_d)), 18.6 (P(CHMe_aMe_b)), 18.5 (P(CHMe_aMe_b)), 17.3 (P(CHMe_cMe_d)), 9.7 (C₅Me₅). ³¹P{¹H} NMR (CD₂Cl₂): δ 42.6; FT-IR (NaCl; cm⁻¹) ν(CO): 2053. Crystals suitable for X-ray crystallographic analysis were grown by vapor diffusion of diethyl ether into a concentrated CH₂Cl₂ solution of **2-4** at ambient temperature.

Synthesis of 2-5. Compound **2-3** was prepared *in situ* by treatment of a solution of **2-1** (0.10 g, 0.17 mmol) in CH₂Cl₂ (2 mL) with solid LiB(C₆F₅)₄·2.5Et₂O (0.14 g, 0.17 mmol), causing an immediate color change to dark blue accompanied by the formation of a precipitate. The reaction mixture was stirred at ambient temperature for 0.5 h followed by filtration through Celite to remove the precipitate. To the dark blue supernatant solution containing **2-3** was added a 1.0 M solution of PMe₃ in toluene (0.20 mL, 0.20 mmol) which effected an immediate color change to bright orange. After 1 h of magnetic stirring, the solvent and other volatiles were removed *in vacuo*, affording an oily orange solid that was triturated with pentane (3 mL). Subsequent drying *in vacuo* afforded **2-5** as an analytically pure, bright orange powder (0.22 g, 0.16 mmol, 94%). Anal. Calcd for

C₅₂H₄₄BF₂₀IrP₂S: C 46.40; H 3.30; N 0.00. Found: C 46.79; H 3.43; N < 0.3. ¹H NMR (CDCl₃): δ 7.29-7.19 (m, 2H, Ar-H), 7.17 (d, ³J_{HH} = 8.0 Hz, 1H, C4-H or C7-H), 7.13 (t, ³J_{HH} = 7.5 Hz, 1H, C5-H or C6-H), 3.62 (m, 1H, C1(H_a)(H_b)), 3.52 (m, 1H, C1(H_a)(H_b)), 3.24 (m, 1H, P(CHMe_aMe_b)), 2.34 (m, 1H, P(CHMe_cMe_d)), 1.92 (m, 15H, C₅Me₅), 1.65 (br m, 9H, PMe₃), 1.35 (dd, ³J_{PH} = 13.5 Hz, ³J_{HH} = 7.0 Hz, 3H, P(CHMe_cMe_d)), 1.27 (dd, ³J_{PH} = 13.0 Hz, ³J_{HH} = 7.0 Hz, 3H, P(CHMe_aMe_b)), 1.23 (dd, ³J_{PH} = 11.0 Hz, ³J_{HH} = 7.5 Hz, 3H, P(CHMe_aMe_b)), 0.91 (dd, ³J_{PH} = 15.0 Hz, ³J_{HH} = 7.0 Hz, 3H, P(CHMe_cMe_d)); ¹³C{¹H} NMR (CDCl₃): δ 176.6 (d, ²J_{PC} = 21.3 Hz, C2), 147.8 (d, J_{PC} = 7.8 Hz, C3a or C7a), 142.5 (d, J_{PC} = 5.4 Hz, C3a or C7a), 129.7 (C3), 127.1 (Ar-CH), 124.9 (Ar-CH), 123.8 (C5 or C6), 118.6 (C4 or C7), 99.6 (C₅Me₅), 40.8 (d, ³J_{PC} = 10.4 Hz, C1), 30.7 (d, ¹J_{PC} = 28.4 Hz, P(CHMe_cMe_d)), 25.8 (d, ¹J_{PC} = 34.5 Hz, P(CHMe_aMe_b)), 20.2 (d, ²J_{PC} = 6.8 Hz, P(CHMe_cMe_d)), 20.1 (P(CHMe_aMe_b)), 19.5 (d, ²J_{PC} = 3.4 Hz, P(CHMe_aMe_b)), 18.0 (P(CHMe_cMe_d)), 17.2 (d, ¹J_{PC} = 40.6 Hz, PMe₃), 9.8 (C₅Me₅); ³¹P{¹H} NMR (CDCl₃): δ 33.6 (d, ²J_{PP} = 28.3 Hz, ⁱPr₂PInd), -41.5 (d, ²J_{PP} = 28.3 Hz, PMe₃).

Synthesis of 2-7. To a magnetically stirred suspension of **2-1** (0.17 g, 0.27 mmol) in CH₃CN (2 mL) was added solid anhydrous K₂CO₃ (0.077 g, 0.55 mmol) followed by stirring at ambient temperature for 48 h; the suspension darkened from orange to brown during the reaction time. The reaction mixture was filtered through Celite followed by removal of solvent and other volatiles *in vacuo*, affording a mixture of **2-7** and another phosphorus-containing product (ca. 92:8 on the basis of ³¹P NMR data). Analytically pure **2-7** was subsequently isolated by crystallization from a concentrated CH₃CN solution of the aforementioned mixture stored at -35 °C (0.069 g, 0.11 mmol, 41%). From these brown crystals was selected a sample that proved suitable for X-ray diffraction analysis. Anal. Calcd for C₂₇H₃₇IrNPS: C 51.39; H 5.92; N 2.22. Found C 51.37; H 5.94; N 2.39. ¹H NMR (C₆D₆): δ 7.22-7.16 (m, 2H, C5 or C6 and C4 or C7), 7.05 (d, ³J_{HH} = 7.5 Hz, 1H, C4 or C7), 6.95 (t, ³J_{HH} = 7.5 Hz, 1H, C5 or C6), 6.81 (s, 1H, C3-H), 2.40 (m, 1H, P(CHMe_aMe_b)), 2.21 (m, 1H, P(CHMe_cMe_d)), 1.83 (s, 3H, N=C-CH₃), 1.77 (d, ⁴J_{PH} = 2.0 Hz, 15H, C₅Me₅), 1.11 (dd, ³J_{PH} = 14.0 Hz, ³J_{HH} = 7.0 Hz, 3H, P(CHMe_aMe_b)), 0.91 (dd, ³J_{PH} = 16.5 Hz, ³J_{HH} = 7.0 Hz, 3H, P(CHMe_cMe_d)), 0.71 (dd, ³J_{PH} = 15.5 Hz, ³J_{HH} = 7.0 Hz, 3H, P(CHMe_aMe_b)), 0.49 (dd, ³J_{PH} = 12.0 Hz, ³J_{HH} = 7.5 Hz, 3H, P(CHMe_cMe_d)); ¹³C{¹H} NMR (C₆D₆): δ 160.0 (d, ²J_{PC} = 7.4 Hz, N=C-CH₃), 158.8 (d, ²J_{PC} = 9.2 Hz, C2),

151.7 (d, $J_{PC} = 4.3$ Hz, C3a or C7a), 140.6 (d, $J_{PC} = 4.9$ Hz, C3a or C7a), 126.6 (C5 or C6), 122.4 (d, $J_{PC} = 1.9$ Hz, C4 or C7), 119.7 (d, $J_{PC} = 1.5$ Hz, C5 or C6), 117.9 (C4 or C7), 115.6 (d, $^3J_{PC} = 3.5$ Hz, C3), 92.2 (d, $J = 3.1$ Hz, C₅Me₅), 24.1 (N=C-CH₃), 22.1 (d, $^1J_{PC} = 26.3$ Hz, P(CHMe_cMe_d)), 21.2 (d, $^2J_{PC} = 3.3$ Hz, P(CHMe_cMe_d)), 21.1 (d, $^1J_{PC} = 10.3$ Hz, P(CHMe_aMe_b)), 19.6 (d, $^2J_{PC} = 1.3$ Hz, P(CHMe_aMe_b)), 17.6 (d, $^2J_{PC} = 3.0$ Hz, P(CHMe_aMe_b)), 15.9 (d, $^2J_{PC} = 4.5$ Hz, P(CHMe_cMe_d)), 8.8 (C₅Me₅); $^{31}\text{P}\{^1\text{H}\}$ NMR (C₆D₆): δ 91.6.

Synthesis of (κ^2 -3-*PiPr*₂-2-*S*-indene)Ir(COD). A solution of 1/3-*PiPr*₂-2-*S*tBu-indene (0.12 g, 0.38 mmol) in CH₂Cl₂ (1 mL) was added dropwise to a magnetically stirred mixture of [(COD)IrCl]₂ (0.13 g, 0.19 mmol) and CH₂Cl₂ (2 mL), causing an immediate darkening of the solution to dark red. The reaction mixture was magnetically stirred at ambient temperature for 0.25 h, followed by treatment with NaN(SiMe₃)₂ (0.070 g, 0.38 mmol), and continued magnetic stirring for 20 h. Subsequent removal of the solvent and other volatiles *in vacuo* afforded a dark red solid that was extracted into benzene followed by filtration through Celite and removal of the solvent and volatiles *in vacuo*. The residual solid was then washed with pentane (3 x 2 mL) and dried *in vacuo* affording (κ^2 -3-*PiPr*₂-2-*S*-indene)Ir(COD) as an analytically pure, red solid (0.13 g, 0.23 mmol, 61%). Anal. Calcd for C₂₃H₃₂IrPS: C 49.00; H 5.72; N 0.00. Found: C 49.11; H 5.62; N <0.3. ^1H NMR (CDCl₃): δ 7.27 (d, $^3J_{\text{HH}} = 7.0$ Hz, 1H, C4-H or C7-H), 7.22 (d, $^3J_{\text{HH}} = 8.0$ Hz, 1H, C4-H or C7-H), 7.17 (t, $^3J_{\text{HH}} = 8.0$ Hz, 1H, C5-H or C6-H), 7.03 (t, $^3J_{\text{HH}} = 7.5$ Hz, 1H, C5-H or C6-H), 4.81 (m, 2H, COD), 3.93 (m, 2H, COD), 3.67 (s, 2H, C1(H)₂), 3.01 (m, 2H, P(CHMe_aMe_b)), 2.31 (m, 2H, COD), 2.14 (m, 2H, COD), 1.97 (m, 2H, COD), 1.82 (m, 2H, COD), 1.34 (dd, $^3J_{\text{PH}} = 16.0$ Hz, $^3J_{\text{HH}} = 7.5$ Hz, 6H, P(CHMe_aMe_b)), 1.27 (dd, $^3J_{\text{PH}} = 15.5$ Hz, $^3J_{\text{HH}} = 7.0$ Hz, 6H, P(CHMe_aMe_b)); $^{13}\text{C}\{^1\text{H}\}$ NMR (CDCl₃): δ 182.5 (quat.), 149.5 (quat.), 143.7 (quat.), 129.9 (quat.), 126.0 (C5 or C6), 124.5 (C4 or C7), 122.2 (C5 or C6), 118.4 (C4 or C7), 83.8 (d, $^2J_{PC} = 12.5$ Hz, COD-CH), 59.7 (COD-CH), 42.2 (d, $^3J_{PC} = 13.1$ Hz, C1), 33.8 (COD-CH₂), 29.5 (COD-CH₂), 25.8 (d, $^1J_{PC} = 28.8$ Hz, P(CHMe_aMe_b)), 19.6 (P(CHMe_aMe_b)), 18.3 (d, $^2J_{PC} = 3.0$ Hz, P(CHMe_aMe_b)); $^{31}\text{P}\{^1\text{H}\}$ NMR (CDCl₃): δ 45.9.

Synthesis of 2-8. A solution of (κ^2 -3-*PiPr*₂-2-*S*-indene)Ir(COD) (0.11 g, 0.20 mmol) in CH₂Cl₂ (4 mL) was degassed by use of three freeze-pump-thaw cycles, and

subsequently exposed to an atmosphere of CO, which caused a gradual color change from dark red to orange. After 0.75 h, ^{31}P NMR data collected on an aliquot of the reaction mixture confirmed the quantitative formation of **2-8**. Removal of the solvent caused a darkening of the solution to dark brown, ultimately affording a brown solid that was extracted into pentane (3 x 2 mL) and filtered through Celite. Removal of the solvent and other volatiles afforded **2-8** as an analytically pure, orange solid (0.041 g, 0.079 mmol, 39%). Anal. Calcd for $\text{C}_{17}\text{H}_{20}\text{IrO}_2\text{PS}$: C 39.91; H 3.94; N 0.00. Found: C 40.03; H 4.25; N <0.3. ^1H NMR (C_6D_6): δ 7.10 (t, $^3J_{\text{HH}} = 8.0$ Hz, 1H, C5-H or C6-H), 6.96-6.86 (m, 3H, Ar-H), 3.40 (d, $^4J_{\text{PC}} = 2.0$ Hz, 2H, C1(H) $_2$), 2.40 (m, 2H, P(CHMe $_a$ Me $_b$)), 1.15 (dd, $^3J_{\text{PH}} = 17.5$ Hz, $^3J_{\text{HH}} = 7.0$ Hz, 6H, P(CHMe $_a$ Me $_b$)), 0.89 (dd, $^3J_{\text{PH}} = 16.5$ Hz, $^3J_{\text{HH}} = 7.0$ Hz, 6H, P(CHMe $_a$ Me $_b$)); $^{13}\text{C}\{^1\text{H}\}$ NMR (C_6D_6): δ 181.6 (d, $^2J_{\text{PC}} = 88.8$ Hz, CO trans to P), 180.4 (d, $^2J_{\text{PC}} = 30.7$ Hz, C2), 178.5 (d, $^2J_{\text{PC}} = 10.8$ Hz, CO cis to P), 149.1 (d, $J_{\text{PC}} = 6.8$ Hz, C3a or C7a), 141.8 (d, $J_{\text{PC}} = 5.5$ Hz, C3a or C7a), 126.4 (C3), 126.6 (Ar-CH), 124.3 (Ar-CH), 122.5 (Ar-CH), 117.0 (Ar-CH), 42.2 (d, $^3J_{\text{PC}} = 14.1$ Hz, C1), 26.1 (d, $^1J_{\text{PC}} = 33.0$ Hz, P(CHMe $_a$ Me $_b$)), 19.2 (d, $^2J_{\text{PC}} = 2.6$ Hz, P(CHMe $_a$ Me $_b$)), 18.1 (P(CHMe $_a$ Me $_b$)); $^{31}\text{P}\{^1\text{H}\}$ NMR (C_6D_6): δ 62.2; FT-IR (NaCl; cm^{-1}) $\nu(\text{CO})$: 2059, 1983.

Reaction of 2-7 with CO to give 2-8. A benzene- d_6 solution (2 mL) of **2-7** (0.019 g, 0.030 mmol) was transferred to a J. Young NMR tube, degassed by use of three freeze-pump-thaw cycles, and subsequently exposed to an atmosphere of CO, which caused an immediate color change from brown to orange. ^{31}P NMR analysis of the reaction mixture after 0.75 h confirmed the quantitative consumption of **2-7** along with the clean formation of **2-8**. ^1H and ^{13}C NMR analysis of the reaction mixture also confirmed the formation of **2-8**, along with a stoichiometric equivalent amount of 1,2,3,4-tetramethylfulvene.

Synthesis of 2-9. Compound **2-2** was prepared *in situ* by treatment of a solution of **2-1** (0.098 g, 0.16 mmol) in CH_2Cl_2 (2 mL) with solid AgOTf (0.040 g, 0.16 mmol), followed by magnetic stirring at ambient temperature, during which time the solution turned dark blue with the concomitant formation of a precipitate. After 0.5 h of stirring, the precipitate was removed by filtration through Celite. To the dark blue supernatant solution was added Ph_2SiH_2 (29 μL , 0.16 mmol) which caused an immediate color change to orange. After 1 h of magnetic stirring the solvent and other volatiles were removed *in vacuo* followed by washing with pentane (2 mL). Subsequent drying *in vacuo* afforded an

orange solid that was extracted into pentane (2 x 2 mL). Concentration of the pentane solution and storage at -35 °C afforded **2-9** as analytically pure, orange crystals (0.041 g, 0.068 mmol, 44%). Anal. Calcd for C₂₅H₃₆IrPS: C 50.74; H 6.13; N 0.00. Found: C 50.53; H 5.94; N <0.3. ¹H NMR (C₆D₆): δ 7.19-7.12 (m, 2H, Ar-H), 6.94-6.87 (m, 2H, Ar-H), 3.50 (d, ²J_{HH} = 22.0 Hz, 1H, C1(H_a)(H_b)), 3.42 (d, ²J_{HH} = 22.0 Hz, 1H, C1(H_a)(H_b)), 2.63 (m, 1H, P(CHMe_aMe_b)), 2.00 (m, 1H, P(CHMe_cMe_d)), 1.82 (s, 15H, C₅Me₅), 1.21 (dd, ³J_{PH} = 12.5 Hz, ³J_{HH} = 7.0 Hz, 3H, P(CHMe_cMe_d)), 1.03 (dd, ³J_{PH} = 16.5 Hz, ³J_{HH} = 7.0 Hz, 3H, P(CHMe_cMe_d)), 0.95 (dd, ³J_{PH} = 16.5 Hz, ³J_{HH} = 7.0 Hz, 3H, P(CHMe_aMe_b)), 0.87 (dd, ³J_{PH} = 14.5 Hz, ³J_{HH} = 7.0 Hz, 3H, P(CHMe_aMe_b)), -15.74 (d, ²J_{PH} = 37.5 Hz, 1H, Ir-H); ¹³C{¹H} NMR (C₆D₆): δ 182.4 (d, ²J_{PC} = 24.5 Hz, C2), 147.9 (d, J_{PC} = 7.0 Hz, C3a or C7a), 144.9 (d, J_{PC} = 4.4 Hz, C3a or C7a), 128.6 (d, ¹J_{PC} = 62.1 Hz, C3), 125.9 (Ar-CH), 123.7 (Ar-CH), 120.6 (Ar-CH), 116.2 (Ar-CH), 91.4 (C₅Me₅), 40.4 (d, ³J_{PC} = 10.6 Hz, C1), 28.7 (d, ¹J_{PC} = 25.4 Hz, P(CHMe_cMe_d)), 22.6 (d, ¹J_{PC} = 42.8 Hz, P(CHMe_aMe_b)), 18.4 (P(CHMe_aMe_b)), 18.2 (d, ²J_{PC} = 5.7 Hz, P(CHMe_cMe_d)), 17.9 (d, ²J_{PC} = 4.7 Hz, P(CHMe_aMe_b)), 17.3 (d, ²J_{PC} = 3.6 Hz, P(CHMe_cMe_d)), 9.4 (C₅Me₅); ³¹P{¹H} NMR (C₆D₆): δ 43.8.

Synthesis of 2-10. A magnetically stirred solution of **2-3** (0.12 g, 0.098 mmol) in CH₂Cl₂ (2 mL) was treated with Ph₂SiH₂ (18 μL, 0.098 mmol) which caused an immediate color change from dark blue to orange; ³¹P NMR analysis of the reaction mixture revealed the quantitative formation of **2-10**. After 0.5 h of magnetic stirring, the CH₂Cl₂ was removed *in vacuo* followed by the addition of benzene (2 mL) which caused the separation of a red oil that was isolated by removal of the benzene supernatant by use of a Pasteur pipette. The red oil was washed with benzene (3 x 2 mL) followed by drying *in vacuo* to afford **2-10** as an analytically pure, orange solid (0.097 g, 0.067 mmol, 68%). Anal. Calcd for C₆₁H₄₇BF₂₀IrPSSi: C 50.36; H 3.26; N 0.00. Found: C 50.11; H 3.45; N < 0.3. ¹H NMR (CD₂Cl₂): δ 7.67-7.15 (m, 14H, Ar-CH), 5.52 (s, 1H, Si-H), 3.28 (d, ²J_{HH} = 23.5 Hz, 1H, C1(H_a)(H_b)), 3.12 (d, ²J_{HH} = 24.0 Hz, 1H, C1(H_a)(H_b)), 2.75 (m, 1H, P(CHMe_aMe_b)), 2.22 (m, 1H, P(CHMe_cMe_d)), 2.00 (s, 15H, C₅Me₅), 1.35 (dd, ³J_{PH} = 14.0 Hz, ³J_{HH} = 7.5 Hz, 3H, P(CHMe_cMe_d)), 0.94 (dd, ³J_{PH} = 19.5 Hz, ³J_{HH} = 7.0 Hz, 3H, P(CHMe_aMe_b)), 0.77 (dd, ³J_{PH} = 18.0 Hz, ³J_{HH} = 7.5 Hz, 3H, P(CHMe_cMe_d)), 0.076 (dd, ³J_{PH} = 18.0 Hz, ³J_{HH} = 6.5 Hz, 3H, P(CHMe_aMe_b)), -15.12 (d, ²J_{PH} = 50.0 Hz, 1H, Ir-H);

$^{13}\text{C}\{^1\text{H}\}$ NMR (CD_2Cl_2): δ 152.4 (quat.), 148.9 (quat.), 148.4 (quat.), 148.0 (quat.), 139.3 (quat.), 135.9 (Ar-CH), 135.4 (quat.), 132.4 (Ar-CH), 128.9 (Ar-CH), 128.1 (Ar-CH), 127.0 (Ar-CH), 126.3 (Ar-CH), 125.4 (Ar-CH), 121.4 (Ar-CH), 96.0 (C_5Me_5), 39.9 (d, $^3J_{\text{PC}} = 8.9$ Hz, C1), 27.1 (d, $^1J_{\text{PC}} = 28.3$ Hz, P(CHMe_cMe_d)), 23.4 (d, $^1J_{\text{PC}} = 40.0$ Hz, P(CHMe_aMe_b)), 18.1 (d, $^2J_{\text{PC}} = 6.3$ Hz, P(CHMe_cMe_d)), 17.6 (d, $^2J_{\text{PC}} = 3.8$ Hz, P(CHMe_aMe_b)), 17.4 (P(CHMe_aMe_b) and P(CHMe_cMe_d)), 9.9 (C_5Me_5); $^{31}\text{P}\{^1\text{H}\}$ NMR (CD_2Cl_2): δ 49.3; ^{29}Si NMR (CD_2Cl_2): δ 3.6.

Synthesis of 2-11. A protocol analogous to that described for the synthesis of **2-10** was employed, using PhSiH_3 (12 μL , 0.098 mmol) in place of Ph_2SiH_2 with similar qualitative observations. Compound **2-11** was isolated as an analytically pure, orange solid (0.10 g, 0.075 mmol, 77%). Anal. Calcd for $\text{C}_{55}\text{H}_{43}\text{BF}_{20}\text{IrPSSi}$: C 47.94; H 3.15; N 0.00. Found: C 47.81; H 3.18; N < 0.3. ^1H NMR (CD_2Cl_2): δ 7.66-7.57 (m, 3H, Ar-CH), 7.56-7.46 (m, 3H, Ar-CH), 7.42-7.32 (m, 3H, Ar-CH), 5.40 (m, 1H, Si(H_a)(H_b)), 4.99 (m, 1H, Si(H_a)(H_b)), 3.51 (s, 2H, C1(H)₂), 2.93 (m, 1H, P(CHMe_aMe_b)), 2.34 (m, 1H, P(CHMe_cMe_d)), 2.07 (m, 15H, C_5Me_5), 1.47 (dd, $^3J_{\text{PH}} = 13.5$ Hz, $^3J_{\text{HH}} = 7.0$ Hz, 3H, P(CHMe_cMe_d)), 1.09 (dd, $^3J_{\text{PH}} = 19.5$ Hz, $^3J_{\text{HH}} = 6.5$ Hz, 3H, P(CHMe_aMe_b)), 0.86 (dd, $^3J_{\text{PH}} = 17.5$ Hz, $^3J_{\text{HH}} = 7.0$ Hz, 3H, P(CHMe_cMe_d)), 0.57 (dd, $^3J_{\text{PH}} = 17.5$ Hz, $^3J_{\text{HH}} = 7.0$ Hz, 3H, P(CHMe_aMe_b)), -15.02 (d, $^2J_{\text{PH}} = 34.0$ Hz, Ir-H); $^{13}\text{C}\{^1\text{H}\}$ NMR (CD_2Cl_2): δ 153.4 (quat.), 149.4 (quat.), 149.0 (quat.), 139.4 (quat.), 135.7 (Ar-CH), 132.8 (Ar-CH), 129.1 (Ar-CH), 127.3 (Ar-CH), 126.7 (Ar-CH), 125.7 (Ar-CH), 121.8 (Ar-CH), 96.4 (C_5Me_5), 39.3 (d, $^3J_{\text{PC}} = 9.1$ Hz, C1), 27.1 (d, $^1J_{\text{PC}} = 28.4$ Hz, P(CHMe_cMe_d)), 23.8 (d, $^1J_{\text{PC}} = 39.9$ Hz, P(CHMe_aMe_b)), 18.3 (d, $^2J_{\text{PC}} = 6.2$ Hz, P(CHMe_cMe_d)), 18.2 (P(CHMe_aMe_b)), 17.9 (d, $^2J_{\text{PC}} = 4.5$ Hz, P(CHMe_aMe_b)), 17.8 (P(CHMe_cMe_d)), 10.1 (C_5Me_5); $^{31}\text{P}\{^1\text{H}\}$ NMR (CD_2Cl_2): δ 49.5; ^{29}Si NMR (CD_2Cl_2): δ 94.1.

Synthesis of 2-12. Compound **2-10** (prepared *in situ* employing the protocols described above using **2-1** (0.098 g, 0.16 mmol), $\text{LiB}(\text{C}_6\text{F}_5)_4 \cdot 2.5\text{Et}_2\text{O}$ (0.14 g, 0.16 mmol), and Ph_2SiH_2 (29 μL , 0.16 mmol)) was dissolved in diethyl ether (2 mL) and the resulting solution was stored at ambient temperature for 24 h, during which time **2-12** precipitated from the solution as an analytically pure, orange crystalline solid (0.12 g, 0.092 mmol, 58% based on **2-1**). Anal. Calcd for $\text{C}_{51}\text{H}_{41}\text{BF}_{20}\text{IrPS}$: C 47.10; H 3.18; N 0.00. Found: C 47.08; H 3.24; N < 0.3. ^1H NMR (CD_2Cl_2): δ 7.60 (d, $^3J_{\text{HH}} = 7.5$ Hz, 1H, C5-H or C6-H),

7.50 (d, $^3J_{\text{HH}} = 7.5$ Hz, 1H, C5-H or C6-H), 7.46-7.36 (m, 2H, C4-H and C7-H), 3.65 (m, 2H, C1(H)₂), 3.09-2.93 (m, 2H, P(CHMe_aMe_b) and S(CH_aH_b)CH₃), 2.59 (m, 1H, S(CH_aH_b)CH₃), 2.35 (m, 1H, P(CHMe_cMe_d)), 2.11 (s, 15H, C₅Me₅), 1.49 (dd, $^3J_{\text{PH}} = 14.0$ Hz, $^3J_{\text{HH}} = 7.0$ Hz, 3H, P(CHMe_cMe_d)), 1.16 (dd, $^3J_{\text{PH}} = 19.5$ Hz, $^3J_{\text{HH}} = 7.0$ Hz, 3H, P(CHMe_aMe_b)), 1.02 (t, $^3J_{\text{HH}} = 7.5$ Hz, 3H, SCH₂CH₃), 0.90 (dd, $^3J_{\text{PH}} = 14.0$ Hz, $^3J_{\text{HH}} = 7.0$ Hz, 3H, P(CHMe_cMe_d)), 0.86 (dd, $^3J_{\text{PH}} = 13.5$ Hz, $^3J_{\text{HH}} = 7.0$ Hz, 3H, P(CHMe_aMe_b)), -15.36 (d, $^2J_{\text{PH}} = 32.5$ Hz, 1H, Ir-H); $^{13}\text{C}\{^1\text{H}\}$ NMR (CD₂Cl₂): δ 157.9 (d, $^2J_{\text{PC}} = 18.9$ Hz, C2), 149.5 (d, $J_{\text{PC}} = 6.0$ Hz, C3a or C7a), 138.9 (C3a or C7a), 127.6 (C5 or C6), 127.2 (C5 or C6), 126.0 (C4 or C7), 125.8 (C3), 122.3 (C4 or C7), 96.8 (C₅Me₅), 37.7 (d, $^3J_{\text{PC}} = 6.2$ Hz, C1), 37.6 (SCH₂CH₃), 26.9 (d, $^1J_{\text{PC}} = 29.4$ Hz, P(CHMe_cMe_d)), 24.2 (d, $^1J_{\text{PC}} = 39.2$ Hz, P(CHMe_aMe_b)), 18.6 (P(CHMe_aMe_b)), 18.3 (d, $^2J_{\text{PC}} = 6.2$ Hz, P(CHMe_cMe_d)), 18.0 (d, $^2J_{\text{PC}} = 4.4$ Hz, P(CHMe_aMe_b)), 17.9 (P(CHMe_cMe_d)), 11.6 (SCH₂CH₃), 10.1 (C₅Me₅); $^{31}\text{P}\{^1\text{H}\}$ NMR (CD₂Cl₂): δ 48.6. Crystals suitable for X-ray crystallographic analysis were grown from a concentrated diethyl ether solution of **2-12** at ambient temperature.

Synthesis of 2-13. A solution of 1/3-PiPr₂-2-StBu-indene (0.10 g, 0.32 mmol) in CH₂Cl₂ (2 mL) was added dropwise to a suspension of [Cp**Rh*Cl₂]₂ (0.097 g, 0.16 mmol) in CH₂Cl₂ (2 mL) resulting in an immediate darkening of the solution. The reaction mixture was magnetically stirred at ambient temperature for 16 h prior to removal of the solvent and other volatiles *in vacuo*. The residual solid was washed with pentane (3 x 2 mL) and dried *in vacuo* to afford **2-13** as an analytically pure, light brown solid (0.16 g, 0.30 mmol, 94%). Anal. Calcd for C₂₅H₃₅ClRhPS: C 55.92; H 6.57; N 0.00. Found: C 55.88; H 6.52; N < 0.3. ^1H NMR (CDCl₃): δ 7.19 (d, $^3J_{\text{HH}} = 7.5$ Hz, 1H, C4-H or C7-H), 7.13 (t, $^3J_{\text{HH}} = 8.0$ Hz, 1H, C5-H or C6-H), 7.06 (d, $^3J_{\text{HH}} = 7.5$ Hz, 1H, C4-H or C7-H), 6.96 (t, $^3J_{\text{HH}} = 7.5$ Hz, 1H, C5-H or C6-H), 3.63 (m, 1H, C1(H_a)(H_b)), 3.54 (m, 1H, C1(H_a)(H_b)), 3.19 (m, 1H, P(CHMe_aMe_b)), 2.30 (m, 1H, P(CHMe_cMe_d)), 1.77 (d, $J_{\text{PC}} = 3.0$ Hz, 15H, C₅Me₅), 1.51 (dd, $^3J_{\text{PH}} = 15.0$ Hz, $^3J_{\text{HH}} = 7.0$ Hz, 3H, P(CHMe_aMe_b)), 1.45-1.37 (m, 6H, P(CHMe_aMe_b) and P(CHMe_cMe_d)), 1.10 (dd, $^3J_{\text{PH}} = 16.0$ Hz, $^3J_{\text{HH}} = 7.0$ Hz, 3H, P(CHMe_cMe_d)); $^{13}\text{C}\{^1\text{H}\}$ NMR (CDCl₃): δ 179.5 (d, $^2J_{\text{PC}} = 24.3$ Hz, C2), 147.7 (d, $J_{\text{PC}} = 6.9$ Hz, C3a or C7a), 145.8 (C3a or C7a), 126.2 (C5 or C6), 123.5 (C4 or C7), 121.9 (C5 or C6), 117.6 (C4 or C7), 98.8 (dd, $^1J_{\text{RhC}} = 5.9$ Hz, $^2J_{\text{PC}} = 3.0$ Hz, C₅Me₅), 43.1 (dd,

$^3J_{PC} = 11.8$ Hz, $^3J_{RhC} = 1.4$ Hz, C1), 29.4 (dd, $^1J_{PC} = 19.6$ Hz, $^2J_{RhC} = 1.4$ Hz, P(CHMe_cMe_d)), 26.4 (d, $^1J_{PC} = 28.9$ Hz, P(CHMe_aMe_b)), 20.5 (P(CHMe_aMe_b)), 20.2 (d, $^2J_{PC} = 7.5$ Hz, P(CHMe_aMe_b)), 19.7 (d, $^2J_{PC} = 6.8$ Hz, P(CHMe_cMe_d)), 18.7 (d, $^2J_{PC} = 2.1$ Hz, P(CHMe_cMe_d)), 9.6 (C₅Me₅); $^{31}P\{^1H\}$ NMR (CDCl₃): δ 65.7 (d, $^1J_{RhP} = 141.7$ Hz).

Synthesis of 2-14. To a magnetically stirred solution of **2-13** (0.023 g, 0.042 mmol) in CD₂Cl₂ (2 mL) was added solid LiB(C₆F₅)₄·2.5Et₂O (0.037 g, 0.042 mmol) which caused an immediate color change of the reaction mixture to dark green. After 0.25 h, ^{31}P NMR analysis of the reaction mixture revealed the complete consumption of **2-13** and the presence of a major phosphorus-containing product (ca. 75% of mixture, ^{31}P NMR) that we assign as **2-14**. Although we have thus far not been able to isolate **2-14** in analytically pure form due to the apparent instability of this complex in solution and upon workup, 1H and ^{13}C NMR characterization data obtained *in situ* are consistent with the C_S-symmetric nature of the target complex. Alternative reactions conducted in THF-*d*₈ afforded red reaction mixtures in which the transformation of **2-13** into **2-14** in a similar fashion was observed by use of NMR methods. 1H NMR (CD₂Cl₂): δ 7.47 (d, $^3J_{HH} = 7.5$ Hz, 1H, C4-H or C7-H), 7.36-7.29 (m, 2H, Ar-CH), 7.25 (d of t, $^3J_{HH} = 7.0$ Hz, $^4J_{HH} = 1.5$ Hz, 1H, C5-H or C6-H), 3.89 (d, $^4J_{PH} = 2.0$ Hz, 2H, C1(H)₂), 2.96 (m, 2H, P(CHMe_aMe_b)₂), 1.86 (d, $^4J_{PH} = 2.0$ Hz, 15H, C₅Me₅), 1.32 (dd, $^3J_{PH} = 18.5$ Hz, $^3J_{HH} = 7.0$ Hz, P(CHMe_aMe_b)₂), 1.22 (dd, $^3J_{PH} = 16.5$ Hz, $^3J_{HH} = 7.0$ Hz, P(CHMe_aMe_b)₂); $^{13}C\{^1H\}$ NMR (CD₂Cl₂): δ 175.0 (C2), 149.5 (C3a or C7a), 141.4 (C3a or C7a), 131.7 (C3), 127.2 (Ar-CH), 125.3 (C5 or C6), 125.1 (C4 or C7), 120.4 (Ar-CH), 102.6 (d, $^1J_{RhC} = 5.2$ Hz, C₅Me₅), 42.3 (d, $^3J_{PC} = 12.8$ Hz, C1), 24.9 (d, $^1J_{PC} = 24.0$ Hz, P(CHMe_aMe_b)₂), 18.6 (P(CHMe_aMe_b)₂), 18.4 (d, $^2J_{PC} = 4.0$ Hz, P(CHMe_aMe_b)₂), 10.9 (C₅Me₅). $^{31}P\{^1H\}$ NMR (CD₂Cl₂): δ 69.3 (d, $^1J_{RhP} = 172.0$ Hz).

Synthesis of 2-15. Treatment of a magnetically stirred THF-*d*₈ solution of **2-14** (0.042 mmol scale; prepared *in situ* as outlined above) with Ph₂SiH₂ (7.8 μ L, 0.042 mmol) caused an immediate color change to dark orange. After 0.25 h, ^{31}P NMR analysis of the reaction mixture revealed the complete consumption of **2-14** and the presence of a major phosphorus-containing product (ca. 80% of mixture, ^{31}P NMR) that we assign as **2-15**. Although we have thus far not been able to isolate **2-15** in analytically pure form due to the apparent instability of this complex in solution and upon workup, NMR

characterization data obtained *in situ* are consistent with the identity of **2-15** as being the Rh analogue of the isolable Ir complex **2-10**. ^1H NMR (THF- d_8): δ 7.78-7.73 (m, Ar-CH), 7.60-7.55 (m, 2H, Ar-CH), 7.54-7.49 (m, Ar-CH), 7.16-7.10 (m, 2H, C4-H and C7-H), 7.08 (t, $^3J_{\text{HH}} = 7.0$ Hz, 1H, C5-H or C6-H), 6.87 (t, $^3J_{\text{HH}} = 7.5$ Hz, 1H, C5-H or C6-H), 5.79 (s, 1H, Si-H), 3.42 (m, 1H, C1(H_a)(H_b)), 3.33 (m, 1H, C1(H_a)(H_b)), 2.99 (m, 1H, P(CHMe $_2$)), 2.43 (m, 1H, P(CHMe $_2$)), 1.99 (m, 15H, C $_5$ Me $_5$), 1.41 (dd, $^3J_{\text{PH}} = 12.0$ Hz, $^3J_{\text{HH}} = 7.0$ Hz, P(CHMeMe)), 1.20 (dd, $^3J_{\text{PH}} = 14.5$ Hz, $^3J_{\text{HH}} = 7.5$ Hz, P(CHMeMe)), 1.17 (dd, $^3J_{\text{PH}} = 11.5$ Hz, $^3J_{\text{HH}} = 7.0$ Hz, P(CHMeMe)), 1.02 (dd, $^3J_{\text{PH}} = 16.5$ Hz, $^3J_{\text{HH}} = 7.0$ Hz, P(CHMeMe)), -12.81 (dd, $^1J_{\text{RhP}} = 45.0$ Hz, $^2J_{\text{PH}} = 20.0$ Hz, 1H, Rh-H; ^{13}C NMR data on the basis of ^1H - ^{13}C HMBC/HSQC experiments (THF- d_8): δ 135.0 (Ar-C), 134.7 (Ar-C), 131.7 (Ar-C), 129.1 (Ar-C), 129.0 (Ar-C), 128.8 (Ar-C), 126.5 (C5 or C6), 123.9 (C4 or C7), 121.6 (C5 or C6), 117.5 (C4 or C7), 42.8 (C1), 29.1 (P(CHMe $_2$)), 23.9 (P(CHMe $_2$)), 19.3 (P(CHMeMe)), 19.2 (P(CHMeMe)), 18.8 (P(CHMeMe)), 18.6 (P(CHMeMe)), 10.5 (C $_5$ Me $_5$); $^{31}\text{P}\{^1\text{H}\}$ NMR (THF- d_8): δ 77.4 (d, $^1J_{\text{RhP}} = 143.7$ Hz).

Synthesis of 2-16. Method A: To a magnetically stirred solution of **2-7** (0.066 g, 0.10 mmol) in THF (2 mL) was added Ph $_2$ SiH $_2$ (19 μL , 0.10 mmol) which effected an immediate color change from dark red to orange. The reaction mixture was magnetically stirred at ambient temperature for 2 h at which time ^{31}P NMR data collected on an aliquot of the reaction mixture indicated the complete consumption of **2-7** and the appearance of two new phosphorus-containing products (**2-16a,b**). The solvent was removed *in vacuo* affording an orange residue that was extracted into pentane (3 mL). Removal of the pentane afforded **2-16** as a mixture of diastereomers (**2-16a,b**) in a 3:1 ratio (0.049 g, 0.064 mmol, 64%). **Method B:** A mixture of **1** (0.053 g, 0.085 mmol) and Ph $_2$ SiH $_2$ (16 μL , 0.085 mmol) in THF (2 mL) was cooled to -35 $^\circ\text{C}$ followed by the dropwise addition of a solution of NaN(SiMe $_3$) $_2$ (0.016 g, 0.085 mmol) in THF (1 mL) which caused a rapid color change from orange to dark brown followed by immediate return to orange. The reaction mixture was magnetically stirred and allowed to warm to ambient temperature followed by magnetic stirring for 3 h, at which time ^{31}P NMR data collected on an aliquot of the reaction mixture indicated complete consumption of **2-1** and the formation of **2-16a,b**. The solvent was removed *in vacuo* affording an orange residue that was extracted into pentane (3 mL). Removal of the pentane afforded **2-16** as a mixture of diastereomers

(2-16a,b; similar to that observed by use of Method A) in a 4:1 ratio (0.052 g, 0.067 mmol, 79%). Anal. Calcd for $C_{37}H_{46}IrPSSi$: C 57.41; H 5.99; N 0.00. Found: C 57.09; H 6.20; N < 0.3. **Diastereomer 2-16a:** 1H NMR (C_6D_6): δ 7.55 (m, 2H, Ar-CH), 7.38 (m, 2H, Ar-CH), 7.21-6.99 (m, 8H, Ar-CH), 6.88 (m, 1H, Ar-CH), 6.82 (m, 1H, Ar-CH), 5.66 (d, $^3J_{HH} = 1.0$ Hz, 1H, Si-H), 4.18 (m, 1H, C1-H), 2.60 (m, 1H, P(CHMe_aMe_b)), 1.86-1.79 (m, 16H, C₅Me₅ and P(CHMe_cMe_d)), 1.06 (dd, $^3J_{PH} = 12.5$ Hz, $^3J_{HH} = 7.0$ Hz, 3H, P(CHMe_cMe_d)), 0.91 (dd, $^3J_{PH} = 16.0$ Hz, $^3J_{HH} = 6.5$ Hz, 3H, P(CHMe_aMe_b)), 0.84 (dd, $^3J_{PH} = 17.5$ Hz, $^3J_{HH} = 6.5$ Hz, 3H, P(CHMe_aMe_b)), 0.37 (dd, $^3J_{PH} = 17.0$ Hz, $^3J_{HH} = 7.0$ Hz, 3H, P(CHMe_cMe_d)), -15.81 (d, $^2J_{PH} = 37.0$ Hz, 1H, Ir-H); $^{13}C\{^1H\}$ NMR (C_6D_6): δ 182.8 (d, $^2J_{PC} = 25.5$ Hz, C2), 148.5 (d, $^2J_{PC} = 7.5$ Hz, C3a or C7a), 144.5 (d, $^2J_{PC} = 4.9$ Hz, C3a or C7a), 135.7 (Ar-CH), 135.2 (Ar-CH), 132.9 (SiPh₂-quat.), 130.8 (SiPh₂-quat.), 129.0 (Ar-CH), 128.7 (Ar-CH), 127.1 (Ar-CH), 127.0 (d, $^1J_{PC} = 23.3$ Hz, C3), 126.9 (Ar-CH), 124.8 (Ar-CH), 123.8 (Ar-CH), 119.7 (Ar-CH), 116.2 (Ar-CH), 91.4 (d, $^2J_{PC} = 3.0$ Hz, C₅Me₅), 44.2 (d, $^3J_{PC} = 9.8$ Hz, C1), 27.8 (d, $^1J_{PC} = 26.3$ Hz, P(CHMe_cMe_d)), 22.4 (d, $^1J_{PC} = 42.8$ Hz, P(CHMe_aMe_b)), 18.3 (P(CHMe_aMe_b)), 17.9 (d, $^2J_{PC} = 5.9$ Hz, P(CHMe_cMe_d)), 17.8 (d, $^2J_{PC} = 4.8$ Hz, P(CHMe_aMe_b)), 16.6 (d, $^2J_{PC} = 4.3$ Hz, P(CHMe_cMe_d)), 9.3 (C₅Me₅); $^{31}P\{^1H\}$ NMR (C_6D_6): δ 42.3; ^{29}Si NMR (C_6D_6): δ 89.1. **Diastereomer 2-16b:** 1H NMR (C_6D_6): δ 7.59-7.57 (m, 2H, Ar-CH), 7.37-7.35 (m, 2H, Ar-CH), 7.13-6.99 (m, 9H, Ar-CH), 6.84-6.81 (m, 1H, Ar-CH), 5.72 (d, $^3J_{HH} = 1.0$ Hz, 1H, Si-H), 4.21 (m, 1H, C1-H), 2.48 (m, 1H, P(CHMe_aMe_b)), 1.99 (m, 1H, P(CHMe_cMe_d)), 1.79 (s, 15H, C₅Me₅), 1.19 (dd, $^3J_{PH} = 12.5$ Hz, $^3J_{HH} = 7.0$ Hz, 3H, P(CHMe_cMe_d)), 0.99 (dd, $^3J_{PH} = 16.0$ Hz, $^3J_{HH} = 7.0$ Hz, 3H, P(CHMe_cMe_d)), 0.86 (dd, $^3J_{PH} = 13.0$ Hz, $^3J_{HH} = 6.5$ Hz, 3H, P(CHMe_aMe_b)), 0.41 (dd, $^3J_{PH} = 16.0$ Hz, $^3J_{HH} = 7.0$ Hz, 3H, P(CHMe_aMe_b)), -16.04 (d, $^2J_{PH} = 37.5$ Hz, 1H, Ir-H); $^{13}C\{^1H\}$ NMR (C_6D_6): δ 181.4 (d, $^2J_{PC} = 25.2$ Hz, C2), 148.3 (d, $J_{PC} = 7.5$ Hz, C3a or C7a), 144.0 (d, $J_{PC} = 4.7$ Hz, C3a or C7a), 135.6 (Ar-CH), 135.2 (Ar-CH), 132.5 (SiPh₂-quat.), 130.3 (SiPh₂-quat.), 128.8 (Ar-CH), 128.7 (Ar-CH), 127.3 (d, $^1J_{PC} = 25.9$ Hz, C3), 127.0 (Ar-CH), 126.6 (Ar-CH), 124.6 (Ar-CH), 123.5 (Ar-CH), 119.8 (Ar-CH), 116.4 (Ar-CH), 91.4 (d, $^2J_{PC} = 3.0$ Hz, C₅Me₅), 43.9 (d, $^3J_{PC} = 9.7$ Hz, C1), 28.8 (d, $^1J_{PC} = 25.4$ Hz, P(CHMe_cMe_d)), 22.8 (d, $^1J_{PC} = 42.8$ Hz, P(CHMe_aMe_b)), 18.4 (d, $^2J_{PC} = 5.7$ Hz, P(CHMe_cMe_d)), 18.0 (d, $^2J_{PC} = 4.8$ Hz, P(CHMe_aMe_b)), 17.9 (P(CHMe_aMe_b)), 17.2 (d, $^2J_{PC} = 3.8$ Hz, P(CHMe_cMe_d)), 9.4

(C_5Me_5); $^{31}P\{^1H\}$ NMR (C_6D_6) δ 43.2; ^{29}Si NMR δ 89.1. A crystal of one of the diastereomers of **2-16** suitable for X-ray crystallographic analysis was grown by evaporation of a concentrated diethyl ether solution of **2-16a,b** at ambient temperature.

General Protocol for Ketone Hydrosilylation Experiments. Representative protocols for reactions involving acetophenone and $PhSiH_3$ are presented. Within a glovebox, a glass vial was charged with a stir-bar, **2-13** (2.1 mg, 0.0040 mmol), $LiB(C_6F_5)_4 \cdot 2.5Et_2O$ (3.5 mg, 0.0040 mmol), THF (2 mL), and acetophenone (23 μ L, 0.20 mmol). The resulting solution was stirred for 10 minutes followed by the addition of $PhSiH_3$ (37 μ L, 0.30 mmol). The resulting mixture was magnetically stirred for 5 h at ambient temperature at which time the contents of the vial were cooled to 0 °C followed by the addition of acetone (5 mL) and 1M HCl (aq) (ca. 5 mL). The mixture was stirred for 2 h at 0 °C followed by 0.5 h at ambient temperature. An aqueous solution of saturated sodium bicarbonate was added (ca. 5 mL), and the reaction mixture was stirred until no more gas evolution was observed (ca. 0.25 h). The reaction mixture was extracted with Et_2O (2 x 5 mL). The combined organic layers were dried over Na_2SO_4 , filtered through a plug of silica, and concentrated *in vacuo*. This solution was transferred to a GC vial and sealed. Products were identified by comparison to the 1H NMR of authentic samples, while quantitative data (average of at least two independent experiments) were obtained from GC analysis using a Supelco BETA-DEX 120 column (30m, 0.25 mm, I.D. column).

2.4.3 Crystallographic Solution and Refinement Details

Crystallographic data collection, solution, and refinement for **2-1**, **2-4**, **2-7**, **2-12**, and **2-16** were conducted by Drs. Robert McDonald and Michael Ferguson, X-Ray Crystallography Laboratory, University of Alberta. Selected crystallographic data are located in tabulated form at the end of this chapter; the ORTEP diagrams featured in the text were prepared by use of ORTEP-3 for Windows version 1.074.^[32]

Crystallographic Characterization of 2-1, 2-4, 2-7, 2-12, and 2-16. For each of the crystallographically characterized compounds reported herein, single-crystal X-ray diffraction data were obtained at 193(\pm 2) K on a Bruker PLATFORM/SMART 1000 CCD diffractometer using graphite-monochromated Mo $K\alpha$ ($\lambda = 0.71073 \text{ \AA}$) radiation,

employing a sample that was mounted in inert oil and transferred to a cold gas stream on the diffractometer. Programs for diffractometer operation, data collection, and data reduction were supplied by Bruker. Gaussian integration (for **2-1** and **2-16**), TWINABS (for **2-4**), or SADABS (for **2-7** and **2-12**) was employed as the absorption correction method, and the structure was solved by use of a Patterson search/structure expansion (for **2-1** and **2-7**) or direct methods (for **2-4**, **2-12**, and **2-16**). The crystal of **2-4** used for data collection was found to display non-merohedral twinning, and both components of the twin were indexed by use of the program CELL_NOW (Bruker AXS Inc., Madison, WI, 2004). The second twin component can be related to the first component by 180° rotation about the $[-0.390 \ -0.180 \ 1]$ axis in real space and about the $[-0.002 \ 0 \ 1]$ axis in reciprocal space. Integrated intensities for the reflections from the two components were written into a SHELXL-93 HKLF 5 reflection file by use of the data integration program SAINT (version 7.06A), employing all reflection data (exactly overlapped, partially overlapped and non-overlapped). Each structure was refined by use of full-matrix least-squares procedures (on F^2) with R_1 based on $F_o^2 \geq 2\sigma(F_o^2)$ and wR_2 based on $F_o^2 \geq -3\sigma(F_o^2)$. Anisotropic displacement parameters were employed throughout for the non-H atoms, and all H-atoms were added at calculated positions (with the exception of Si-*H* and Ir-*H*, which were located in the difference map) and refined by use of a riding model employing isotropic displacement parameters based on the isotropic displacement parameter of the attached atom. For each of **2-12** and **2-16**, the near-zero final refined value of the Flack^[44] absolute structure parameter (-0.005(3) for **2-12**; 0.002(5) for **2-16**) supported that the correct absolute structure had been chosen.

Table 2-2. Crystallographic Data for **2-1**, **2-4**, and **2-7**.

	2-1	2-4	2-7
empirical formula	C ₂₅ H ₃₅ ClIrPS	C ₂₇ H ₃₅ F ₃ IrO ₄ PS ₂	C ₂₇ H ₃₇ NIrPS
formula weight	626.21	767.84	630.81
crystal dimensions	0.64 x 0.57 x 0.33	0.34 x 0.22 x 0.07	0.40 x 0.40 x 0.23
crystal system	monoclinic	triclinic	monoclinic
space group	<i>P2₁/c</i>	<i>P(-1)</i>	<i>P2₁/c</i>
<i>a</i> (Å)	8.4287(9)	9.1759(8)	8.0173(5)
<i>b</i> (Å)	18.747(2)	10.9655(8)	19.3970(13)
<i>c</i> (Å)	15.3597(17)	15.4658(9)	16.3635(11)
α (deg)	90	80.643(2)	90
β (deg)	91.1555(15)	75.359(2)	95.6603(9)
γ (deg)	90	80.987(2)	90
<i>V</i> (Å ³)	2426.5(5)	1474.66(19)	2532.3(3)
<i>Z</i>	4	2	4
ρ_{calcd} (g cm ⁻³)	1.714	1.729	1.655
μ (mm ⁻¹)	5.774	4.773	5.433
range of transmission	0.2516–0.1194	0.7165–0.2878	0.3680–0.2199
2 θ limit (deg)	54.90	55.06	54.98
index ranges	$-10 \leq h \leq 10$ $-24 \leq k \leq 24$ $-19 \leq l \leq 19$	$-11 \leq h \leq 11$ $-13 \leq k \leq 14$ $-0 \leq l \leq 20$	$-10 \leq h \leq 10$ $-25 \leq k \leq 25$ $-21 \leq l \leq 21$
total data collected	21057	12226	21919
ind reflections	5539	12226	5811
<i>R</i> _{int}	0.0261	na	0.0188
obd reflections	5311	11389	5416
data/restraints/params	5539/0/267	12226/0/349	5811/0/286
goodness-of-fit	1.169	1.027	1.097
<i>R</i> ₁ [<i>F</i> _o ² ≥ 2σ(<i>F</i> _o ²)]	0.0245	0.0378	0.0203
<i>wR</i> ₂ [<i>F</i> _o ² ≥ 3σ(<i>F</i> _o ²)]	0.0617	0.0945	0.0512

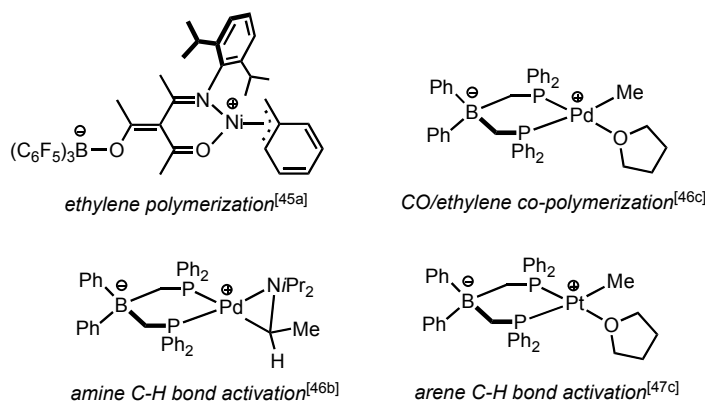
Table 2-3. Crystallographic Data for **2-12** and **2-16**.

	2-12	2-16
empirical formula	C ₅₁ H ₄₁ BF ₂₀ IrPS	C ₃₇ H ₄₆ IrPSSi
formula weight	1299.88	774.06
crystal dimensions	0.33 x 0.23 x 0.11	0.24 x 0.20 x 0.18
crystal system	monoclinic	orthorhombic
space group	<i>P2</i> ₁	<i>Pna2</i> ₁
<i>a</i> (Å)	11.2171(9)	16.2760(12)
<i>b</i> (Å)	12.4867(10)	9.3991(7)
<i>c</i> (Å)	18.0424(14)	22.3078(16)
α (deg)	90	90
β (deg)	103.9330(10)	90
γ (deg)	90	90
<i>V</i> (Å ³)	2452.7(3)	34.12.6(4)
<i>Z</i>	2	4
ρ_{calcd} (g cm ⁻³)	1.760	1.507
μ (mm ⁻¹)	2.910	4.080
range of transmission	0.7402–0.4468	0.571–0.4410
2 θ limit (deg)	54.98	54.96
index ranges	$-14 \leq h \leq 14$ $-16 \leq k \leq 16$ $-23 \leq l \leq 23$	$-21 \leq h \leq 21$ $-12 \leq k \leq 12$ $-28 \leq l \leq 28$
total data collected	20942	28450
ind reflections	11110	7816
<i>R</i> _{int}	0.0221	0.0331
obd reflections	10394	7138
data/restraints/params	11110/0/685	7816/1/379
goodness-of-fit	0.921	1.028
<i>R</i> ₁ [<i>F</i> _o ² ≥ 2σ(<i>F</i> _o ²)]	0.0244	0.0274
<i>wR</i> ₂ [<i>F</i> _o ² ≥ -3σ(<i>F</i> _o ²)]	0.0548	0.0657

Chapter 3 – Platinum Benzyl Complexes Derived from 1/3-*PiPr*₂-2-*SfBu*-Indene: Synthesis of Carbanion- and Borate-Containing Zwitterions

3.1 Introduction

Zwitterionic late transition metal complexes featuring enforced formal charge separation between a cationic metal fragment and an anionic moiety sequestered within a coordinated ancillary ligand have emerged as attractive alternatives to related cationic complexes in reactivity applications, owing to their heightened solubility in low-polarity media, increased tolerance to polar coordinating solvents, and avoidance of counteranion effects.^[19] Indeed, such zwitterions can offer a useful intermediate range of electrophilicity relative to more traditional neutral and cationic species. Although significantly less well-explored than their group 9 relatives, zwitterionic Ni,^[45] Pd,^[46] and Pt^[47] complexes have proven useful in a range of substrate transformations, including: Ni-catalyzed ethylene polymerization,^[45a, 45d-f] Pd-catalyzed CO/ethylene copolymerization^[46c] and aldol condensation,^[46d] and metal-mediated stoichiometric C-H bond activation of amines (Pd),^[46b] as well as hydrocarbons (Pt) (Scheme 3-1).^[47b-d] Notwithstanding these advances, further diversification in this field is limited by a lack of ligation strategies for supporting group 10 zwitterionic complexes. Nearly all such zwitterionic species reported thus far feature borate-based ligation; in fact, non-borate group 10 zwitterions are restricted to a limited class of Pd pincer complexes that contain tethered sulfate groups.^[46a, 46d] In this regard, the identification of alternative ligation strategies that allow for the preparation of neutral, cationic, and zwitterionic group 10 complexes represents an important goal in the pursuit of further control in tuning the reactivity of group 10 metal species.



Scheme 3-1. Representative examples of Group 10 organoborate-based zwitterions.

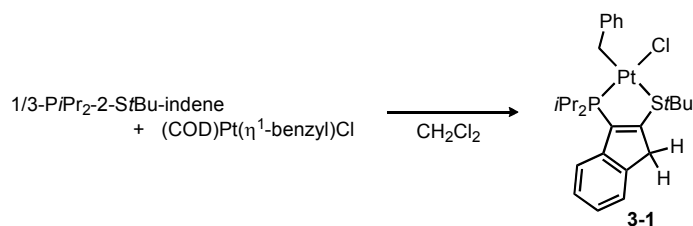
Research in the Stradiotto group has dealt with investigations of cationic and formally zwitterionic complexes of Ru, Rh, and Ir, supported by 3- PR_2 -2- NR'_2 -indene and mono-deprotonated indenide ligands, respectively.^[19, 20b, 20c, 23d, 48] These zwitterions are unusual in that the 10π -electron indenide unit functions as an uncoordinated anionic charge reservoir to counterbalance the cationic κ^2 - P,N - ML_n fragment, rather than as a site for metal binding. Zwitterions of this type are viewed as particularly attractive candidates for multiple E-H activation, since the anionic backbone is poised to accept a proton from a cationic metal center following an initial E-H bond activation step, thereby re-establishing coordinative unsaturation at the reactive metal center and enabling subsequent E-H activation processes. Encouraged by the divergent reactivity exhibited by cations and related zwitterions in the previously described $\text{Cp}^*\text{Ir}(\kappa^2\text{-}P,S)$ chemistry (see Chapter 2), this chapter focuses on the use of 1/3- PiPr_2 -2- $\text{Si}t\text{Bu}$ -indene as a ligand precursor for the construction of new neutral, cationic, and zwitterionic (κ^2 - P,S) $\text{Pt}(\text{benzyl})$ complexes, with the intent of studying these structurally related species in substrate transformations involving multiple E-H bond activations.

3.2 Results and Discussion

3.2.1 Preparation of Neutral Precursor 3-1

In targeting Pt-benzyl derivatives due to their ability to adopt η^1 , η^3 , and other coordination modes, 1/3- PiPr_2 -2- $\text{Si}t\text{Bu}$ -indene was added to $(\text{COD})\text{Pt}(\eta^1\text{-benzyl})\text{Cl}$,

affording (κ^2 -3-*PiPr*₂-2-*StBu*-indene)Pt(η^1 -benzyl)Cl **3-1** in 68% isolated yield (Scheme 3-2). In contrast to the observations in Chapter 2, the ligand S-*t*Bu linkage is retained upon coordination to the Pt(η^1 -benzyl)Cl fragment. Monitoring of this reaction by use of ¹H and ³¹P NMR methods confirmed that **3-1** is formed quantitatively as a single diastereomer, the identity of which was ascertained on the basis of X-ray crystallographic data (Figure 3-1); selected metrical parameters for **3-1** and the other crystallographically characterized compounds in this chapter are collected in Table 3-1. While crystallographically characterized (κ^2 -*P,S*)Pt(benzyl) species have not been reported previously, the *trans*-disposition of chloride and phosphorus ligands in **3-1** mirrors that observed in a related (κ^2 -*P,N*)Pt(η^1 -benzyl)Cl complex,^[49] in keeping with the greater *trans*-directing ability of phosphorus relative to sulfur.^[50]



Scheme 3-2. Synthesis of neutral (κ^2 -*P,S*)Pt(η^1 -benzyl)Cl complex **3-1**.

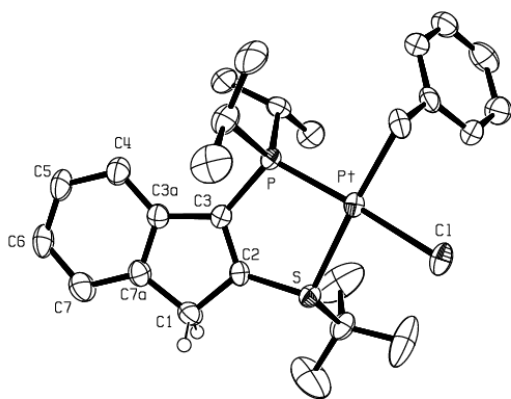
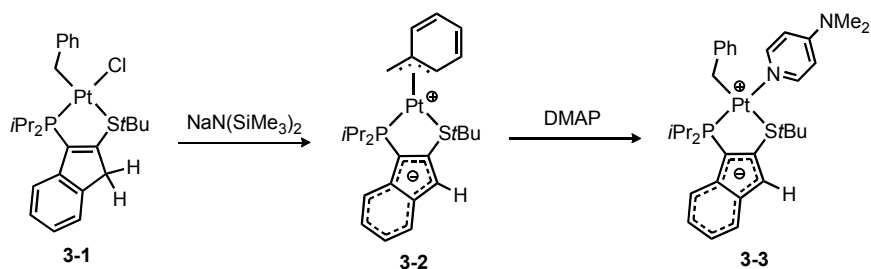


Figure 3-1. ORTEP diagram for **3-1**, shown with 50% displacement ellipsoids and with the atomic numbering scheme depicted; selected hydrogen atoms have been omitted for clarity.

3.2.2 Isolation of Carbanion-Based Zwitterion **3-2** and its Reaction with DMAP

Dehydrohalogenation of **3-1** employing $\text{NaN}(\text{SiMe}_3)_2$ produced the κ^2 -*P,S*-indenide complex **3-2**, which was isolated as an analytically pure solid in 67% yield (Scheme 3-3). Notably, **3-2** represents the first isolable Pt zwitterion to feature non-borate ancillary ligation. In contrast to the relatively sharp NMR signals observed for **3-1** at 300 K, the ^1H NMR spectrum of **3-2** at this temperature exhibited very broad features, possibly attributable to slow inversion at sulfur, and/or η^1 - η^3 dynamics of the coordinated benzyl ligand.^[51] While upon cooling to 273 K some diagnostic ^1H NMR signals associated with **3-2** could be assigned qualitatively, further cooling to 185 K provided no gains in spectral resolution. Conversely, the $^{31}\text{P}\{^1\text{H}\}$ NMR resonance for **3-2** remained sharp between 273-300 K, apparently precluding an observable temperature-dependent equilibrium involving **3-2** and other phosphorus-containing species. Exposure of **3-2** to 4-dimethylaminopyridine (DMAP) afforded the adduct **3-3** as an analytically pure solid in 82% isolated yield (Scheme 3.2). As with **3-2**, this adduct exhibited broad ^1H NMR features (and a single sharp $^{31}\text{P}\{^1\text{H}\}$ NMR resonance) in the range of 185-300 K. While X-ray quality crystals of **3-2** have yet to be obtained, the identification of **3-3** (and indirectly **3-2**) as a κ^2 -*P,S*-indenide complex was confirmed by use of diffraction methods (Figure 3-2). The assignment of **3-3** as a formally zwitterionic species is supported by the observation of C–C distances within the carbocyclic backbone that are intermediate between C–C and C=C bonds and are consistent with a delocalized 10π -electron indenide framework. However, as noted for κ^2 -*P,N*-indenide complexes of groups 8 and 9,^[20b, 20c, 23d] the relatively short P–C3 distance in **3-3** suggests that a non-zwitterionic $\text{R}_2\text{P}=\text{C}3$ resonance contributor featuring a formal negative charge on phosphorus^[52] should be considered in describing the electronic structure of this adduct.



Scheme 3-3. Synthesis of zwitterion **3-2** and DMAP-stabilized zwitterion **3-3**.

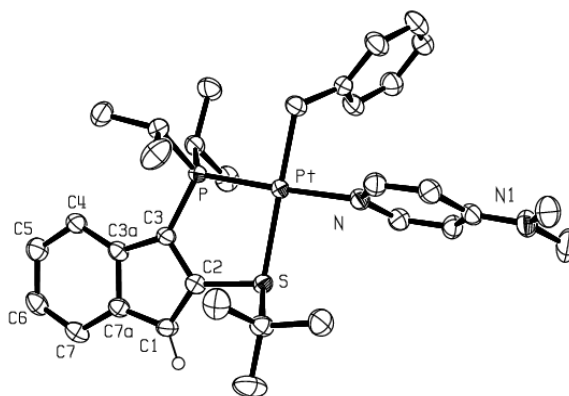
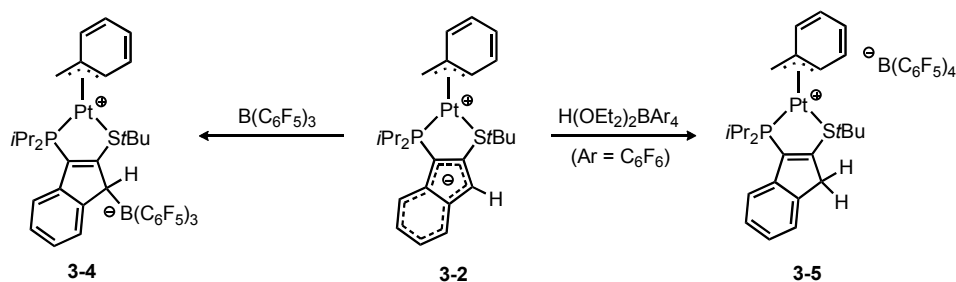


Figure 3-2. ORTEP diagram for **3-3**, shown with 50% displacement ellipsoids and with the atomic numbering scheme depicted; selected hydrogen atoms have been omitted for clarity.

3.2.3 Synthesis of Cationic and Borato-Zwitterionic Relatives of **3-2**

The indenide-based zwitterion **3-2** serves as a convenient synthon in the preparation of alternative cationic and zwitterionic (κ^2 -*P,S*)Pt(η^3 -benzyl) complexes. Treatment of **3-2** with $\text{B}(\text{C}_6\text{F}_5)_3$ afforded the borate-based zwitterion **3-4** in 68% isolated yield, while addition of $\text{H}(\text{OEt}_2)_2\text{B}(\text{C}_6\text{F}_5)_4$ to **3-2** produced the cationic complex **3-5** in 88% isolated yield (Scheme 3-4). The ability of **3-2** to serve as a precursor to **3-5** is of particular significance, since efforts to prepare **3-5** from **3-1** by use of $\text{LiB}(\text{C}_6\text{F}_5)_4 \cdot 2.5\text{OEt}_2$ were unsuccessful. In contrast to the broad NMR spectral features that were noted for **3-2** and **3-3** at 300 K (see Section 3.2.2), under similar conditions the ^1H and $^{13}\text{C}\{^1\text{H}\}$ NMR spectra for each of **3-4** and **3-5** are consistent with a C_1 -symmetric structure, with only modest line-broadening observed in the case of **3-4**.



Scheme 3-4. Synthesis of borato-zwitterion **3-4** and cation **3-5**.

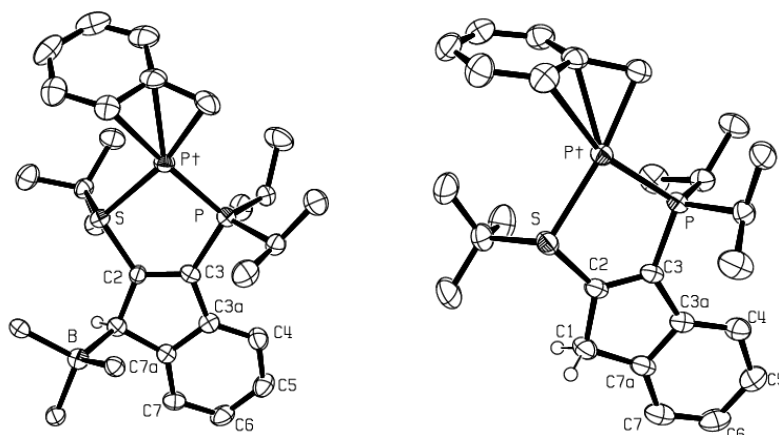


Figure 3-3. ORTEP diagram for **3-4** (left) and **3-5** (right), shown with 50% displacement ellipsoids and with the atomic numbering scheme depicted; selected hydrogen atoms and portions of the C_6F_5 groups in **3-4**, as well as the $B(C_6F_5)_4$ anion in **3-5**, have been omitted for clarity.

Data obtained from X-ray diffraction studies involving **3-4** and **3-5** also revealed C_1 -symmetric connectivity for these complexes (Figure 3-3), and enabled further structural comparisons.^[53] In contrast to the C–C bond delocalization and somewhat short P–C3 distance that are found in the κ^2 -*P,S*-indenide complex **3-3** (see Section 3.2.2), more localized single (e.g. C1–C2) and double (e.g. C2–C3) bonds, along with typical P–C3 distances, are observed in both **3-4** and **3-5** (Table 3-1). In this regard, **3-4** and **3-5** can be viewed as $(\kappa^2$ -*P,S*-indenene)Pt(η^3 -benzyl) complexes, in keeping with the line drawing representations in Scheme 3-4; whereas in **3-5** the formally cationic Pt fragment is counterbalanced by an outer-sphere $B(C_6F_5)_4^-$ counteranion, the indenylborate ligation featured in **3-4** gives rise to a structurally analogous zwitterionic complex.^[54] Despite these apparent similarities, some structural variations within the coordinated η^3 -benzyl ligands of **3-4** and **3-5** were observed. Progressive lengthening of the Pt–C linkage is

noted for both complexes on going from Pt-CH₂ to Pt-C_{ipso} to Pt-C_{ortho} (Table 3-1), in keeping with structural trends commonly observed in L_nM(η³-benzyl) complexes.^[53, 55] However, while the first two of these distances are statistically equivalent in **3-4** and **3-5**, the elongation of the Pt-C_{ortho} distance in **3-5** (2.566(4) Å) is significantly more pronounced than in **3-4** (2.354(5) Å). While the potential influence of crystal packing as a source of such structural differences cannot be discounted, it is worthy of mention that the observed structural trend also matches the ¹J_{Pt} values measured for **3-2** (5012 Hz), **3-4** (5264 Hz), and **3-5** (5317 Hz), with the increasing ¹J_{Pt} value signaling a progressively weaker interaction between Pt and the η²-(C11=C12) moiety that occupies a position *trans* to phosphorus in **3-4** and **3-5** (and presumably **3-2**).^[51c] When considered collectively, the solid state structural variations noted within the η³-benzyl fragments of **3-4** and **3-5**, as well as the differing solution dynamic behavior observed for **3-2**, **3-4**, and **3-5**, may presage divergent reactivity for these complexes, attributable in part to the unique electronic characteristics of the ancillary ligand backbone.

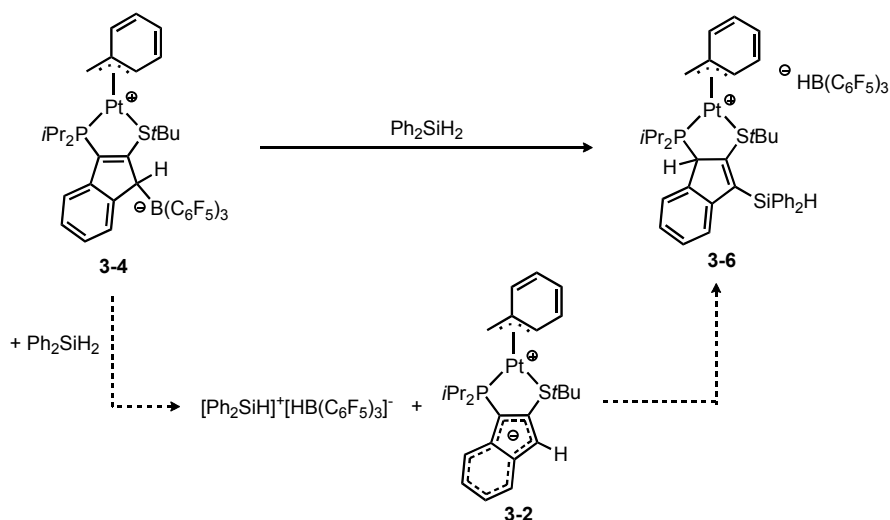
Table 3-1. Selected Interatomic Distances (Å) for **3-1**, **3-3**, **3-4**, and **3-5**.

	3-1 ^[a]	3-3 ^[b]	3-4 ^[c]	3-5
Pt-S	2.3637(14)	2.4005(7)	2.3658(12)	2.3608(10)
Pt-P	2.2135(14)	2.2342(7)	2.2254(13)	2.2116(10)
Pt-CH ₂	2.096(5)	2.075(3)	2.085(5)	2.061(4)
Pt-C _{ipso}	na	na	2.255(5)	2.269(4)
Pt-C _{ortho}	na	na	2.354(5)	2.566(4)
P-C3	1.814(6)	1.767(3)	1.817(5)	1.800(4)
S-C2	1.757(5)	1.775(3)	1.785(5)	1.775(4)
C1-C2	1.502(7)	1.399(4)	1.513(6)	1.505(5)
C1-C7a	1.498(8)	1.411(4)	1.517(6)	1.515(6)
C2-C3	1.368(7)	1.420(4)	1.354(6)	1.347(5)
C3-C3a	1.479(8)	1.433(4)	1.458(6)	1.480(5)
C3a-C4	1.394(8)	1.412(4)	1.392(7)	1.382(6)
C4-C5	1.399(9)	1.374(4)	1.370(7)	1.387(6)
C5-C6	1.368(9)	1.405(4)	1.383(7)	1.384(6)
C6-C7	1.405(9)	1.373(4)	1.381(7)	1.381(7)
C7-C7a	1.393(8)	1.405(4)	1.390(7)	1.373(6)
C7a-C3a	1.388(8)	1.441(4)	1.402(7)	1.411(5)

^[a] Pt-Cl = 2.3695(14). ^[b] Pt-N = 2.102(2). ^[c] B-Cl = 1.701(7).

3.2.4 Reactivity of **3-2**, **3-4**, and **3-5** with E-H bond Containing Substrates

Having established the synthetic feasibility of heterobidentate indenide ligation in group 10 chemistry, a comparative reactivity survey involving **3-2**, **3-4**, and **3-5**, was initiated to document the influence of the indenide, indenylborate, and indene ligand backbone (respectively) in tuning the reactivity of these structurally related Pt complexes with E-H bond containing substrates. Although complete consumption of **3-2** and **3-5** (^{31}P NMR) was observed upon treatment with a range of organosilane (PhSiH_3 , Ph_2SiH_2 , and Ph_3SiH), organoborane (HBPin and H_2BMes), amine (PhNH_2 , pyrrole, and morpholine), and phosphine (PhPH_2 and Ph_2PH) substrates, multiple phosphorus containing products were generated in each case, regardless of the substrate equivalents (1-10 equiv) or the temperature employed (22-100 °C) and to date these products have yet to unambiguously characterized. In monitoring these reactions by use of ^1H NMR techniques, no Pt-H species were detected and the Pt-benzyl resonances persisted throughout the course of each reaction. In contrast to these results, treatment of **3-4** with Ph_2SiH_2 afforded **3-6** – a cationic Pt-complex featuring a $-\text{SiPh}_2\text{H}$ fragment bonded to the indene backbone that is counterbalanced by an $\text{HB}(\text{C}_6\text{F}_5)_3$ counteranion (Scheme 3-5). In light of the established ability of electrophilic boranes to abstract hydride from silanes,^[41] a plausible mechanism for the generation of **3-6** could involve initial dissociation of the indenyl-coordinated $\text{B}(\text{C}_6\text{F}_5)_3$ to generate **3-2** and free $\text{B}(\text{C}_6\text{F}_5)_3$. Subsequent reaction of $\text{B}(\text{C}_6\text{F}_5)_3$ with Ph_2SiH_2 could transiently generate the salt $[\text{HSiPh}_2]^+[\text{HB}(\text{C}_6\text{F}_5)_3]^-$ which could then react with **3-2** to form the proposed Si- C_{indene} linkage in **3-6**.



Scheme 3-5. Potential pathway for the formation of **3-6** from **3-4** and Ph_2SiH_2 .

3.3 Summary and Conclusions

In summary, this work demonstrates that 1/3-*PiPr*₂-2-*StBu*-indene functions as a versatile ligand precursor in the synthesis of cationic $[(\kappa^2\text{-}P,S)\text{Pt}(\eta^3\text{-benzyl})]^+X^-$ species (**3-5**), as well as analogous zwitterionic complexes in which the formally cationic metal fragment is counterbalanced by an uncoordinated indenide (**3-2**) or borate (**3-4**) fragment within the ancillary ligand backbone. In addition to offering a new and complementary approach for the assembly of structurally related cationic and zwitterionic group 10 complexes, the convenience of employing a single ligand precursor in these syntheses may offer advantages over alternative strategies that require the preparation of distinct ligands for supporting cations and zwitterions. In contrast to the divergent reactivity observed in Chapter 2 involving cationic and zwitterionic $\text{Cp}^*\text{Ir}(\kappa^2\text{-}P,S)$ complexes, reactivity studies involving the cationic and zwitterionic $(\kappa^2\text{-}P,S)\text{Pt}$ system were unfruitful, in that complex reactivity was observed throughout. In order to address the limitations of this system, current research in the Stradiotto group is focused on the synthesis of structurally related cationic and zwitterionic Pt complexes derived from alternative donor-substituted indene ligands. The identification and discussion of an alternative class donor-substituted indene ligands for coordination to Pt that may provide

access to enhanced reactivity towards E-H bonds is discussed in Chapter 6 (see Section 6.2).

3.4 Experimental Section

3.4.1 General Considerations

All manipulations were conducted in the absence of oxygen and water under an atmosphere of dinitrogen, either by use of standard Schlenk methods or within an mBraun glovebox apparatus, utilizing glassware that was oven-dried (130 °C) and evacuated while hot prior to use. Celite (Aldrich) was oven-dried for 5 d and then evacuated for 24 h prior to use. The non-deuterated solvents tetrahydrofuran, diethyl ether, dichloromethane, benzene, and pentane were deoxygenated and dried by sparging with dinitrogen gas, followed by passage through a double-column solvent purification system purchased from mBraun Inc. Tetrahydrofuran, diethyl ether and dichloromethane were purified over two alumina-packed columns, while benzene and pentane were purified over one alumina-packed column and one column packed with copper-Q5 reactant. CDCl_3 (Aldrich) was degassed by using three repeated freeze-pump-thaw cycles, dried over CaH_2 for 7 days, distilled in vacuo, and stored over 4 Å molecular sieves for 24 h prior to use. Benzene- d_6 , methylene chloride- d_2 and toluene- d_8 (Cambridge Isotopes) were degassed by using three repeated freeze-pump-thaw cycles and then dried over 4 Å molecular sieves for 24 h prior to use. All solvents used within the glovebox were stored over activated 4 Å molecular sieves. $(\text{COD})\text{Pt}(\eta^1\text{-benzyl})\text{Cl}$ ^[56] and $\text{H}(\text{OEt})_2\text{B}(\text{C}_6\text{F}_5)_4$ ^[57] were prepared by using literature procedures, and were dried *in vacuo* for 24 h prior to use. $\text{NaN}(\text{SiMe}_3)_2$ (Aldrich) and $\text{B}(\text{C}_6\text{F}_5)_3$ (Boulder Scientific) were dried in vacuo for 24 h prior to use. All other reagents were obtained from Aldrich and were used as received. Variable-temperature NMR experiments were conducted on a Bruker AC-250 spectrometer. Otherwise, ^1H , ^{13}C , ^{29}Si , ^{11}B and ^{31}P NMR characterization data were collected at 300 K on a Bruker AV-500 spectrometer operating at 500.1, 125.8, 99.4, 160.5 and 202.5 MHz (respectively) with chemical shifts reported in parts per million downfield of SiMe_4 (for ^1H , ^{13}C , and ^{29}Si), 85% H_3PO_4 in D_2O (for ^{31}P), or BF_3 in diethyl ether (for ^{11}B). ^1H and ^{13}C NMR chemical shift assignments are given on the basis of data obtained from ^{13}C -DEPT, ^1H - ^1H COSY, ^1H - ^{13}C HSQC, and ^1H - ^{13}C HMBC NMR experiments. In some

cases slightly fewer than expected independent ^1H or ^{13}C NMR resonances were observed (despite prolonged data acquisition times), and ^{13}C NMR resonances associated with $\text{B}(\text{C}_6\text{F}_5)_4^-$ were not assigned. ^{29}Si NMR chemical shift assignments are given on the basis of data obtained from ^1H - ^{29}Si HMQC NMR experiments. Elemental analyses were performed by Canadian Microanalytical Service Ltd., Delta, British Columbia, Canada.

3.4.2 Synthetic Details and Characterization Data

Synthesis of 3-1. A solution of 1/3- PtPr_2 -2- StBu -indene (0.60 g, 1.9 mmol) in CH_2Cl_2 (2 mL) was added dropwise to a suspension of $(\text{COD})\text{Pt}(\eta^1\text{-benzyl})\text{Cl}$ (0.82 g, 1.9 mmol) in CH_2Cl_2 (2 mL) followed by magnetic stirring for 16 h at ambient temperature. ^{31}P NMR analysis of the reaction mixture indicated the quantitative formation of **3-1**. The CH_2Cl_2 and other volatiles were removed *in vacuo* and the resulting solid was washed with diethyl ether (3 x 5 mL). Removal of the residual solvent afforded **3-1** as an analytically pure, pale yellow solid (0.83 g, 1.3 mmol, 68 %). Anal. Calcd for $\text{C}_{26}\text{H}_{36}\text{ClPPtS}$: C 48.62; H 5.65; N 0.00. Found: C 48.57; H 5.42; N < 0.3. ^1H NMR (CDCl_3): δ 7.45 (m, 1H, C4 or C7), 7.43 (m, 2H, Ar-CH), 7.32 (m, 1H, C7 or C4), 7.21 (m, 2H, C5 or C6 and Ar-CH), 7.04 (m, 2H, Ar-CH), 6.91 (m, 1H, C6 or C5), 4.04 (s, 2H, $\text{C1}(\text{H})_2$), 3.69 (d, $^3J_{\text{PH}} = 3.0$ Hz with ^{195}Pt satellites $^2J_{\text{PtH}} = 70.0$ Hz, 2H, benzyl- CH_2), 3.14 (m, 2H, $\text{P}(\text{CHMe}_a\text{Me}_b)_2$), 2.11 (s, 9H, $\text{C}(\text{CH}_3)_3$), 1.73 (dd, $^3J_{\text{PH}} = 14.5$ Hz, $^3J_{\text{HH}} = 6.0$ Hz, 6H, $\text{P}(\text{CHMe}_a\text{Me}_b)_2$), 1.69 (dd, $^3J_{\text{PH}} = 15.5$ Hz, $^3J_{\text{HH}} = 8.0$ Hz, 6H, $\text{P}(\text{CHMe}_a\text{Me}_b)_2$); $^{13}\text{C}\{^1\text{H}\}$ NMR (CDCl_3): δ 157.9 (d, $^2J_{\text{PC}} = 13.1$ Hz, C2), 149.1 (d, $J_{\text{PC}} = 6.0$ Hz, C3a or C7a), 148.5 (d, $^1J_{\text{PC}} = 44.9$ Hz, C3), 147.1 (Ar-quat.), 139.2 (d, $J_{\text{PC}} = 3.8$ Hz, C7a or C3a), 130.1 (Ar-CH), 127.3 (Ar-CH), 126.9 (C5 or C6), 126.6 (Ar-CH), 125.0 (C7 or C4), 123.5 (C6 or C5), 122.6 (C4 or C7), 57.8 (d, $J_{\text{PC}} = 0.8$ Hz, $\text{C}(\text{CH}_3)_3$), 43.1 (d, $^3J_{\text{PC}} = 9.8$ Hz, C1), 32.4 ($\text{C}(\text{CH}_3)_3$), 24.8 (d, $^1J_{\text{PC}} = 35.3$ Hz, $\text{P}(\text{CHMe}_a\text{Me}_b)$), 19.6 (d, $^2J_{\text{PC}} = 1.4$ Hz, $\text{P}(\text{CHMe}_a\text{Me}_b)$), 19.0 (d, $^2J_{\text{PC}} = 1.9$ Hz, $\text{P}(\text{CHMe}_a\text{Me}_b)$), 14.2 (d, $^2J_{\text{PC}} = 5.3$ Hz, benzyl- CH_2); $^{31}\text{P}\{^1\text{H}\}$ NMR (CDCl_3): δ 38.3 (s, with ^{195}Pt satellites $^1J_{\text{PtP}} = 3848$ Hz). Crystals suitable for X-ray crystallographic analysis were grown by vapor diffusion of pentane into a concentrated solution of **3-1** in benzene at ambient temperature.

Synthesis of 3-2. To a magnetically stirred suspension of **3-1** (0.51 g, 0.78 mmol) in benzene (5 mL) was added solid $\text{NaN}(\text{SiMe}_3)_2$ (0.16 g, 0.85 mmol). The resulting solution turned deep red and an orange precipitate formed. The mixture was magnetically stirred at ambient temperature for 16 h followed by removal of all volatiles *in vacuo*. The resulting orange solid was extracted into CH_2Cl_2 (5 mL) followed by filtration through Celite, which afforded a deep red supernatant solution. The supernatant was evaporated to dryness *in vacuo* and the resulting solid was washed with pentane (3 x 3 mL) followed by drying *in vacuo* to afford **3-2** as an analytically pure, orange solid (0.32 g, 0.52 mmol, 67 %). Anal Calcd. for $\text{C}_{26}\text{H}_{35}\text{PPtS}$: C 51.54; H 5.83; N 0.00. Found: C 51.67; H 6.01; N < 0.3. The ^1H NMR spectrum of **3-2** at 300 K exhibited very broad features, possibly attributable to dynamic behavior arising due to slow inversion at sulfur as well as η^1 - η^3 dynamics of the coordinated benzyl ligand.^[51] Upon cooling to 273 K some diagnostic ^1H NMR signals associated with **3-2** could be assigned qualitatively; however, further cooling provided no gains in spectral resolution. ^1H NMR (toluene- d_8): δ 6.23 (s, C1-H), 2.69 (m, $\text{P}(\text{CHMe}_2)_2$), 2.52 (s, benzyl- CH_2), 1.02-1.26 (m, $\text{P}(\text{CHMe}_2)_2$), 0.88 (s, $\text{C}(\text{CH}_3)_3$). The $^{31}\text{P}\{^1\text{H}\}$ NMR resonance for **3-2** remained sharp between 273-300 K; $^{31}\text{P}\{^1\text{H}\}$ NMR (toluene- d_8): δ 55.5 (s, with ^{195}Pt satellites $^1J_{\text{PPt}} = 5012$ Hz).

Synthesis of 3-3. A magnetically stirred suspension of **3-2** (0.22 g, 0.36 mmol) in THF (5 mL) was treated with solid 4-dimethylaminopyridine (DMAP; 0.044 g, 0.36 mmol). The homogeneous solution was magnetically stirred at ambient temperature for 16 h during which time an off-white precipitate formed. All solvent and other volatiles were removed *in vacuo* and the resulting off-white solid was washed with diethyl ether (4 x 2 mL). The remaining off-white solid (**3-3**) was dried *in vacuo* and isolated (0.22 g, 0.30 mmol, 82 %). Anal Calcd. for $\text{C}_{33}\text{H}_{45}\text{N}_2\text{PPtS}$: C 54.44; H 6.24; N 3.85. Found: C 54.40; H 6.49; N 3.59. The ^1H NMR spectrum of **3-3** over the temperature range of 185-300 K exhibited very broad features, possibly attributable in part to dynamic processes associated with slow inversion at sulfur. Although NMR line-shape changes were noted over this temperature range, definitive chemical shift assignments for **3-3** could not be made unequivocally. The $^{31}\text{P}\{^1\text{H}\}$ NMR resonance for **3-3** remained sharp over this temperature range; $^{31}\text{P}\{^1\text{H}\}$ NMR (CD_2Cl_2): δ 24.1 (s, with ^{195}Pt satellites $^1J_{\text{PPt}} = 3755$

Hz). Crystals suitable for X-ray crystallographic analysis were grown by vapor diffusion of diethyl ether into a concentrated solution of **3-3** in CH₂Cl₂ at ambient temperature.

Synthesis of 3-4. To a vial containing solid B(C₆F₅)₃ (0.089 g, 0.17 mmol) was added a solution of **3-2** (0.11 g, 0.17 mmol) in benzene (2 mL). The vial was manually shaken for several minutes, affording initially a darkly colored homogeneous solution, followed by the precipitation of an off-white solid. The vial was left at ambient temperature without stirring for 1 h upon which time the supernatant was removed by using a Pasteur pipette and the precipitate was washed with pentane (4 x 1 mL). Drying of the solid *in vacuo* afforded **3-4** as an analytically pure, orange solid (0.13 g, 0.12 mmol, 68 %). Anal. Calcd for C₄₄H₃₅BF₁₅PPtS: C 47.26; H 3.16; N 0.00. Found: C 47.64; H 3.40; N < 0.3. Resonances observed in the ¹H and ¹³C{¹H} NMR spectra of **3-4** at 300 K were broadened modestly, thereby precluding the definitive assignment of peak multiplicities. Such broadness may possibly be attributable to the dynamic features associated with slow inversion at sulfur as well as η¹-η³ dynamics of the coordinated benzyl ligand.^[51] ¹H NMR (CD₂Cl₂): δ 7.83-7.52 (br m, 3H, Ar-CH), 7.44-7.28 (br m, 2H, Ar-CH), 7.21-7.07 (br m, 2H, Ar-CH), 7.04-6.58 (br m, 2H, Ar-CH), 5.53 (br s, 1H, C1-H), 3.48 (br s, 1H, benzyl-CH_aH_b), 3.10 (m, 1H, P(CHMe_aMe_b)), 2.79 (br s, 1H, benzyl-CH_aH_b), 2.61 (m, 1H, P(CHMe_cMe_d)), 1.48 (dd, ³J_{PH} = 16.5 Hz, ³J_{HH} = 7.0 Hz, 3H, P(CHMe_cMe_d)), 1.37 (dd, ³J_{PH} = 17.5 Hz, ³J_{HH} = 6.5 Hz, 3H, P(CHMe_aMe_b)), 1.26 (dd, ³J_{PH} = 18.5 Hz, ³J_{HH} = 7.5 Hz, 3H, P(CHMe_cMe_d)), 1.07 (s, 9H, C(CH₃)₃), 0.99 (dd, ³J_{PH} = 19.5 Hz, ³J_{HH} = 7.0 Hz, 3H, P(CHMe_aMe_b)); ¹³C{¹H} NMR (CD₂Cl₂): δ 158.0 (Ar-quat.), 156.9 (Ar-quat.), 148.7 (Ar-quat.), 137.3 (Ar-quat.), 134.3 (Ar-CH), 128.3 (Ar-CH), 127.1 (Ar-CH), 125.5 (Ar-CH), 124.1 (Ar-CH), 121.2 (Ar-CH), 119.3 (Ar-CH), 115.4 (Ar-quat.), 61.2 (C(CH₃)₃), 53.4 (C1-H), 31.2 (C(CH₃)₃), 29.8 (P(CHMe_cMe_d)), 29.5 (benzyl-CH₂), 24.9 (P(CHMe_aMe_b)), 20.6 (P(CHMe_cMe_d)), 19.3 (P(CHMe_cMe_d)), 18.5 (P(CHMe_aMe_b)), 18.3 (P(CHMe_aMe_b)); ³¹P{¹H} NMR (CD₂Cl₂): δ 59.6 (s, with ¹⁹⁵Pt satellites ¹J_{PtP} = 5264 Hz); ¹¹B NMR (CD₂Cl₂): δ -11.2. Crystals of **3-4**(C₇H₈) suitable for X-ray crystallographic analysis were grown by vapor diffusion of pentane into a concentrated solution of **3-4** in toluene at ambient temperature.

Synthesis of 3-5. To a magnetically stirred solution of **3-2** (0.065 g, 0.11 mmol) in benzene (2 mL) was added solid H(OEt)₂B(C₆F₅)₄ (0.18 g, 0.21 mmol) which effected

the separation of a red oil. After 2 h of magnetic stirring the benzene layer was removed by using a pipette, followed by washing of the remaining red oil with benzene (3 x 1 mL). Subsequent removal of the solvent and other volatiles *in vacuo* afforded **3-5** as an analytically pure, off-white solid (0.12 g, 0.093 mmol, 88 %). Anal. Calcd for C₅₀H₃₆BF₂₀PPtS: C 46.68; H 2.82; N 0.00. Found: C 46.55; H 3.06; N < 0.3. ¹H NMR (CDCl₃): δ 7.78-7.68 (m, 2H, Ar-CH), 7.60-7.48 (m, 3H, Ar-CH), 7.46-7.41 (m, 2H, Ar-CH), 6.98-6.89 (m, 2H, Ar-CH), 3.87 (s, 2H, C1(H)₂), 3.15-2.84 (m, 4H, P(CHMe_aMe_b)₂ and benzyl-CH₂), 1.40 (dd, ³J_{PH} = 19.5 Hz, ³J_{HH} = 7.0 Hz, 6H, P(CHMe_aMe_b)₂), 1.18-1.10 (m, 15H, P(CHMe_aMe_b)₂ and C(CH₃)₃); ¹³C{¹H} NMR (CDCl₃): δ 156.6 (Ar-quat.), 149.1 (Ar-quat.), 148.6 (Ar-quat.), 143.4 (Ar-quat.), 137.3 (Ar-quat.), 134.9 (Ar-CH), 132.6 (Ar-CH), 128.3 (Ar-CH), 128.1 (Ar-CH), 127.9 (Ar-CH), 125.8 (Ar-CH), 121.7 (Ar-CH), 60.7 (C(CH₃)₃), 42.2 (d, ³J_{PC} = 9.2 Hz, C1), 31.6 (benzyl-CH₂), 28.2 (d, ¹J_{PC} = 36.0 Hz, P(CHMe_aMe_b)₂), 20.0 (P(CHMe_aMe_b)₂), 19.5 (P(CHMe_aMe_b)₂), 14.3 (C(CH₃)₃); ³¹P{¹H} NMR (CDCl₃): δ 62.7 (s, with ¹⁹⁵Pt satellites ¹J_{Pt} = 5317 Hz). Crystals suitable for X-ray crystallographic analysis were grown from slow evaporation of a concentrated diethyl ether solution of **3-5** at ambient temperature.

Synthesis of 3-6. To a vial containing a suspension of **3-4** (prepared in situ from **3-2** (0.11 g, 0.20 mmol) and B(C₆F₅)₃ (0.10 g, 0.20 mmol)) in benzene (2 mL) was added Ph₂SiH₂ (37 μL, 0.20 mmol), which caused the solution to turn orange in color. After 1 h of periodic shaking, a dark oil settled to the bottom of the vial. The green supernatant was removed with a Pasteur pipette and the remaining oil was washed with benzene (2 x 1 mL). The oil was dried in vacuo affording **3-6** as an analytically pure off-white solid (0.12 g, 0.090 mmol, 45 %). Anal. Calcd for C₅₇H₄₆BF₁₅PPtSSi: C 51.64; H 3.64; N 0.00. Found: C 51.92; H 3.69; N < 0.3. ¹H NMR (CDCl₃): δ 7.71 (br m, 2H, Ar-CH), 7.58 (t, ³J_{HH} = 7.5 Hz, 4H, Ar-CH), 7.53-7.49 (m, 5H, Ar-CH and C4 or C7), 7.43 (t, ³J_{HH} = 1H, C5 or C6), 7.35 (t, ³J_{HH} = 7.5 Hz, 1H, Ar-CH), 7.30 (t, ³J_{HH} = 7.5 Hz, C5 or C6), 7.15 (t, ³J_{HH} = 7.5 Hz, 2H, Ar-CH), 6.94 (d, ³J_{HH} = 7.5 Hz, 1H, C4 or C7), 6.81 (d, ³J_{HH} = 6.5 Hz, 2H, Ar-H), 5.43 (s, 1H, Si-H), 4.63 (s, 1H, C3-H), 3.33 (d, ²J_{HH} = 5.5 Hz, 1H, Benzyl-CH_aH_b), 2.98 (m, 1H, P(CHMe_aMe_b)), 2.62 (m, 1H, P(CHMe_cMe_d)), 2.43 (d, ²J_{HH} = 5.5 Hz, 1H, Benzyl-CH_aH_b), 1.37 (dd, ³J_{PH} = 19.5, ³J_{HH} = 7.0 Hz, 3H, P(CHMe_aMe_b)), 1.17 (s, 9H, C(CH₃)₃), 1.05 (dd, ³J_{PH} = 19.0, ³J_{HH} = 7.0 Hz, 3H, P(CHMe_aMe_b)), 0.77 (dd, ³J_{PH}

= 14.0 Hz, $^3J_{\text{HH}} = 7.0$ Hz, 3H, P(CHMe_cMe_d)), 0.49 (dd, $^3J_{\text{PH}} = 18.5$ Hz, $^3J_{\text{HH}} = 6.5$ Hz, 3H, P(CHMe_cMe_d)); $^{13}\text{C}\{^1\text{H}\}$ NMR (CDCl₃): δ 157.2 (d, $^2J_{\text{PC}} = 16.9$ Hz, C2), 150.1 (d, $^3J_{\text{PC}} = 7.3$ Hz, C1), 137.6 (d, $J_{\text{PC}} = 4.9$ Hz, C3a or C7a), 135.4 (C3a or C7a), 135.2 (Benzyl-quat.), 135.6 (Ar-CH), 135.3 (Ar-CH), 134.7 (br s, Ar-CH), 131.5 (Ar-CH), 131.1 (C4 or C7), 130.2 (Ar-quat.), 128.7 (Ar-CH), 128.3 (Ar-CH), 126.9 (C5 or C6), 126.8 (C5 or C6), 126.3 (Ar-quat.), 125.0 (C4 or C7), 61.7 (C(CH₃)₃), 47.9 (d, $^1J_{\text{PC}} = 8.4$ Hz, C3), 31.0 (C(CH₃)₃), 30.9 (Benzyl-CH₂), 27.9 (d, $^1J_{\text{PC}} = 47.5$ Hz, P(CHMe_cMe_d)), 27.6 (d, $^1J_{\text{PC}} = 45.7$ Hz, P(CHMe_aMe_b)), 20.0 (P(CHMe_aMe_b)), 19.6 (d, $^2J_{\text{PC}} = 2.1$ Hz, P(CHMe_aMe_b)), 18.6 (P(CHMe_cMe_d)), 18.3 (d, $^2J_{\text{PC}} = 1.9$ Hz, P(CHMe_cMe_d)); $^{31}\text{P}\{^1\text{H}\}$ NMR (CDCl₃): δ 61.5 (s, with ^{195}Pt satellites $^1J_{\text{PtP}} = 5281.7$ Hz); ^{11}B NMR (CDCl₃): δ -25.3 (d, $^1J_{\text{BH}} = 87.6$ Hz, HBAr₃); ^{29}Si NMR (CDCl₃): δ 89.5 (Si-H).

3.4.3 Crystallographic Solution and Refinement Details

Crystallographic data collection, solution, and refinement for **3-3**, **3-4**, and **3-5** were conducted by Drs. Robert McDonald and Michael Ferguson, X-Ray Crystallography Laboratory, University of Alberta. Crystallographic data collection, solution, and refinement for **3-1** were conducted by Dr. Gabriele Schatte, Saskatchewan Structural Sciences Centre, University of Saskatchewan. Selected crystallographic data are located in tabulated form at the end of this chapter; the ORTEP diagrams featured in the text were prepared by use of ORTEP-3 for Windows version 1.074.^[32]

Crystallographic Characterization of 3-1. Crystallographic data for **3-1** was obtained at 173(±2) K on a Nonius KappaCCD 4-Circle Kappa FR540C diffractometer using graphite-monochromated Mo K α ($\lambda = 0.71073$ Å) radiation, employing a sample that was mounted in inert oil and transferred to a cold gas stream on the diffractometer. Cell parameters were initially retrieved by using the COLLECT software (Nonius), and refined with the HKL DENZO and SCALEPACK software. Data reduction and absorption correction (multi-scan) were also performed with the HKL DENZO and SCALEPACK software. The structures were solved by using the direct methods package in SIR-97, and refined by use of the SHELXL97-2 program, employing full-matrix least-squares procedures (on F^2) with R_1 based on $F_o^2 \geq 2\sigma(F_o^2)$ and wR_2 based on $F_o^2 \geq -$

$3\sigma(F_o^2)$. Anisotropic displacement parameters were employed throughout for the non-hydrogen atoms. Otherwise, all hydrogen atoms were added at calculated positions and refined by using a riding model employing isotropic displacement parameters based on the isotropic displacement parameter of the attached atom. Additional crystallographic information for **3-1** is provided in the deposited CIF (CCDC 687093).

Crystallographic Characterization of 3-3, 3-4(C₇H₈), and 3-5. In each case, crystallographic data were obtained at 193(±2) K on a Bruker PLATFORM/SMART 1000 CCD diffractometer using graphite-monochromated Mo K α ($\lambda = 0.71073$ Å) radiation, employing a sample that was mounted in inert oil and transferred to a cold gas stream on the diffractometer. Programs for diffractometer operation, data collection, data reduction, and absorption correction (including SAINT and SADABS) were supplied by Bruker. The structures of **3-3** and **3-4**(C₇H₈) were solved by using a Patterson search/structure expansion, while **3-5** was solved by use of the direct methods package in SIR-97. The structures were refined by use of the SHELXL97-2 program, employing full-matrix least-squares procedures (on F^2) with R_1 based on $F_o^2 \geq 2\sigma(F_o^2)$ and wR_2 based on $F_o^2 \geq -3\sigma(F_o^2)$. Anisotropic displacement parameters were employed throughout for the non-hydrogen atoms. All hydrogen atoms were added at calculated positions and refined by use of a riding model employing isotropic displacement parameters based on the isotropic displacement parameter of the attached atom. Additional crystallographic information is provided in the deposited CIFs (CCDC 687090 for **3-3**; CCDC 687091 for **3-4**(C₇H₈); and CCDC 687092 for **3-5**).

Table 3-2. Crystallographic Data for **3-1** and **3-3**.

	3-1	3-3
empirical formula	C ₂₆ H ₃₆ ClPPtS	C ₃₃ H ₄₅ N ₂ PPtS
formula weight	642.12	727.83
crystal dimensions	0.13 x 0.13 x 0.13	0.38 x 0.25 x 0.24
crystal system	monoclinic	monoclinic
space group	<i>P</i> 2 ₁ / <i>c</i>	<i>P</i> 2 ₁ / <i>c</i>
<i>a</i> (Å)	13.1479(3)	10.6807(9)
<i>b</i> (Å)	12.5326(4)	14.1937(11)
<i>c</i> (Å)	15.8100(5)	20.6273(17)
α (deg)	90	90
β (deg)	98.1364(17)	97.7681(9)
γ (deg)	90	90
<i>V</i> (Å ³)	2578.91(13)	3098.4(4)
<i>Z</i>	4	4
ρ_{calcd} (g cm ⁻³)	1.654	1.560
μ (mm ⁻¹)	5.699	4.672
range of transmission	0.5245-0.5245	0.4002-0.2698
2 θ limit (deg)	52.74	55.00
index ranges	-16 $\leq h \leq$ 16 -15 $\leq k \leq$ 15 -19 $\leq l \leq$ 19	-13 $\leq h \leq$ 13 -18 $\leq k \leq$ 18 -26 $\leq l \leq$ 26
total data collected	10055	23093
ind reflections	5271	7060
<i>R</i> _{int}	0.0389	0.0264
obd reflections	4253	6143
data/restraints/params	5271/0/279	7060/0/345
goodness-of-fit	1.081	1.059
<i>R</i> ₁ [<i>F</i> _o ² \geq 2 σ (<i>F</i> _o ²)]	0.0335	0.0235
<i>wR</i> ₂ [<i>F</i> _o ² \geq -3 σ (<i>F</i> _o ²)]	0.0810	0.0573

Table 3-3. Crystallographic Data for **3-4** and **3-5**.

	3-4	3-5
empirical formula	C ₅₁ H ₄₃ BF ₁₅ PPtS	C ₅₀ H ₃₆ BF ₂₀ PPtS
formula weight	1209.78	1285.72
crystal dimensions	0.31 x 0.30 x 0.07	0.33 x 0.29 x 0.13
crystal system	orthorhombic	monoclinic
space group	<i>Pbca</i>	<i>P2₁/c</i>
<i>a</i> (Å)	21.679(2)	17.6907(18)
<i>b</i> (Å)	18.6294(17)	17.3368(18)
<i>c</i> (Å)	23.275(2)	17.7636(18)
α (deg)	90	90
β (deg)	90	117.9280(10)
γ (deg)	90	90
<i>V</i> (Å ³)	9400.0(15)	4813.6
<i>Z</i>	8	4
ρ_{calcd} (g cm ⁻³)	1.710	1.774
μ (mm ⁻¹)	3.160	3.106
range of transmission	0.8091-0.4408	0.6883-0.4272
2 θ limit (deg)	54.00	55.06
index ranges	-27 $\leq h \leq$ 27 -23 $\leq k \leq$ 23 -29 $\leq l \leq$ 29	-22 $\leq h \leq$ 13 -22 $\leq k \leq$ 18 -23 $\leq l \leq$ 26
total data collected	69138	39940
ind reflections	10253	11034
R_{int}	0.1001	0.0431
obd reflections	6580	9086
data/restraints/params	10253/0/632	11034/0/667
goodness-of-fit	1.060	1.058
$R_1 [F_o^2 \geq 2\sigma(F_o^2)]$	0.0379	0.0367
$wR_2 [F_o^2 \geq -3\sigma(F_o^2)]$	0.0892	0.0934

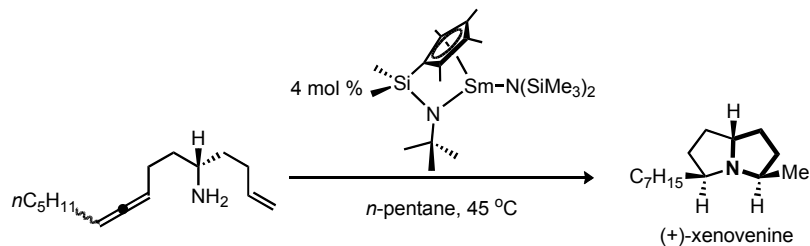
Chapter 4 – Iridium-Catalyzed Intramolecular Hydroamination of Aminoalkenes: Scope and Mechanistic Studies

4.1 Introduction

The hydroamination of alkenes represents an attractive strategy for the construction of nitrogen-containing compounds that circumvents the formation of by-products in the creation of a C-N linkage.^[58] Although the direct addition of amines to alkenes is thermodynamically feasible, the high activation barrier associated with the combination of these two electron-rich substrates has made the use of catalysts essential.^[58o, 59] Despite extensive research, most alkene hydroamination catalyst systems are limited to certain substrate classes. For example, the most common limitation of hydroamination catalysis is that activated alkenes, such as those featuring ring strain (e.g. norbornene), conjugation (e.g. styrenes, dienes), or substitution with electron-withdrawing groups (e.g. Michael acceptors), are often required to facilitate amine addition. Aside from a recent report of the gold-catalyzed hydroamination of α -olefins with cyclic ureas,^[60] the intermolecular hydroamination of unactivated alkenes possessing synthetically useful functional groups remains an otherwise unmet challenge within the field of hydroamination.

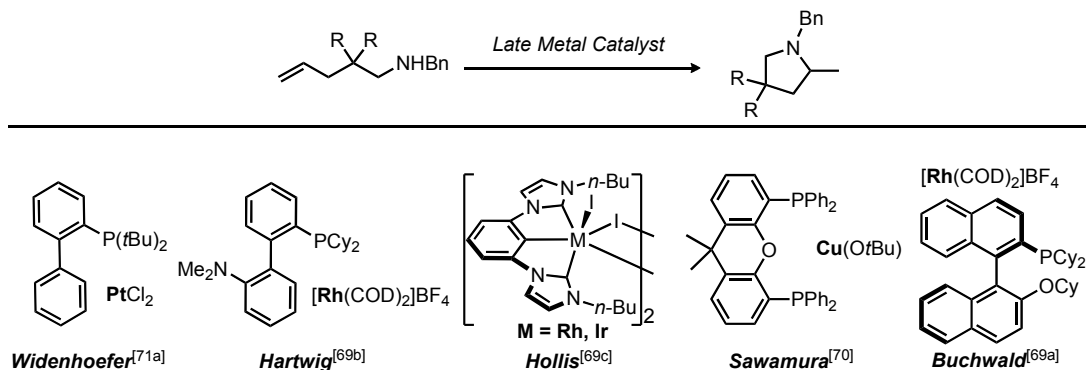
One method that has been employed successfully in promoting the addition of nitrogen nucleophiles to unactivated alkenes involves tethering the olefin and the amine by a linker chain. In addition to reducing the entropic penalty associated with intermolecular hydroaminations, these cyclohydroamination reactions are also appealing as atom-economical routes to nitrogen-containing heterocycles that are prevalent in naturally occurring and/or biologically active molecules; an example of such reactivity is presented in Scheme 4-1.^[61] Although the synthetic potential of cyclohydroamination is significant, general methods for promoting the intramolecular hydroamination of unactivated aminoalkenes under mild conditions and with broad substrate scope are still lacking. A diverse number of catalyst systems are known to effect such cyclizations,^[58a] including those based on rare earth elements and actinides,^[62] alkali and alkaline earth metals,^[63] Group 4 metals,^[64] and Brønsted acids;^[65] nonetheless, the pursuit of increased

substrate scope and functional group tolerance has prompted the development of alternative catalysts based on metals from Groups 8-11.



Scheme 4-1. Synthesis of (+)-xenovenine using a lanthanide hydroamination catalyst.

While progress has been made in the use of Fe,^[66] Pd,^[67] and Au^[60, 68] catalysts for the intramolecular addition of weakly basic secondary amides, carbamates, or ureas to unactivated olefins, the identification of late metal catalysts for analogous transformations involving secondary alkyl- or arylamines, as well as primary amines, has proven more elusive. The difficulty associated with the addition of these more basic amine substrates to olefins is most likely a result of catalyst inhibition by unproductive amine binding to the metal center. Though several catalysts based on Rh/Ir,^[69] Cu,^[70] and Pt^[71] have recently been described (Scheme 4-2), the identification of a general catalyst for use in promoting the cyclohydroamination of these amine partners to both terminal and internal olefins remains an important and significant challenge. Furthermore, with the exception of the NMR spectroscopic characterization of catalytic intermediates in the breakthrough Pt catalyst system disclosed by Bender and Widenhoefer,^[71b] no kinetic or mechanistic data pertaining to the cyclohydroamination of alkylaminoalkenes have been reported.



Scheme 4-2. PGM catalyst systems capable of the cyclohydroamination of alkylaminoalkenes.

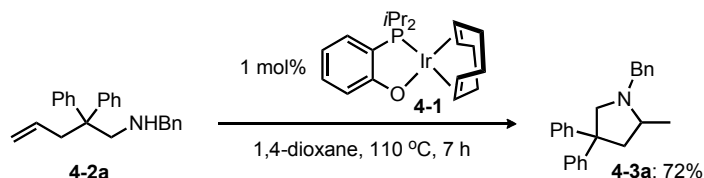
The use of Ir-based catalysts has figured prominently in the development of various forms of the hydroamination reaction. Milstein, Calabrese, and Casalnuovo^[4c] initially pioneered the Ir-catalyzed intermolecular addition of anilines to norbornene; however, recent progress has expanded the scope of this reaction to include the enantioselective addition of arylamines to activated bicyclic alkene frameworks, which provides access to chiral amine products poised for further synthetic manipulation.^[72] While progress has been made in the field of Ir-catalyzed alkyne cyclohydroamination,^[72a, 73] the extension of these methods to the corresponding alkene cyclizations has proved to be more challenging. These advances have provided motivation to investigate Ir-based species in the quest to identify a general catalyst that exhibits useful activity and broad substrate scope in the intramolecular hydroamination of unactivated olefins. In this vein, Chapter 4 features a complete account of catalyst optimization, substrate scope, and mechanistic investigations using phosphino-phenolate complexes of Ir, as well as simple phosphine-free Ir precursors, for the cyclohydroamination of aminoalkenes.

4.2 Results and Discussion

4.2.1 Catalyst Identification and Optimization

Encouraged by previous studies employing phosphino-phenolate complex (κ^2 -2-*i*Pr₂PC₆H₄O)IrCOD **4-1** as a highly active catalyst for the hydrogenation of substituted olefins under mild conditions,^[74] its efficacy as a catalyst for the cyclohydroamination of the benzyl-protected aminoalkene **4-2a** to the pyrrolidine **4-3a** was assessed. In a preliminary experiment, conversion to **4-3a** proceeded in a 72% yield (¹H NMR) in the presence of 1.0 mol% **4-1** in 1,4-dioxane at 110 °C over the course of 7 h with the balance corresponding to unreacted **4-2a** (Scheme 4-3). When the progress of the reaction was monitored as a function of time under identical reaction conditions a pronounced induction period of approximately 3 h was observed (Figure 4-1). Variable-temperature ¹H and ³¹P NMR studies (25 – 100 °C) of an equimolar mixture of **4-1** and **4-2a** conducted either with or without pre-conditioning under catalytic conditions for 3 h at 110 °C revealed the presence of only **4-1** and **4-2a**, as well as small quantities of **4-3a**.

Collectively, these spectroscopic observations seem to preclude slow dissociation of the P,O-ligand from Ir as the source of the induction period; however, conclusive evidence to unambiguously support this hypothesis has yet to be acquired.



Scheme 4-3. Cyclohydroamination of **4-2a** to **4-3a** catalyzed by Ir-phosphino-phenolate complex **4-1**.

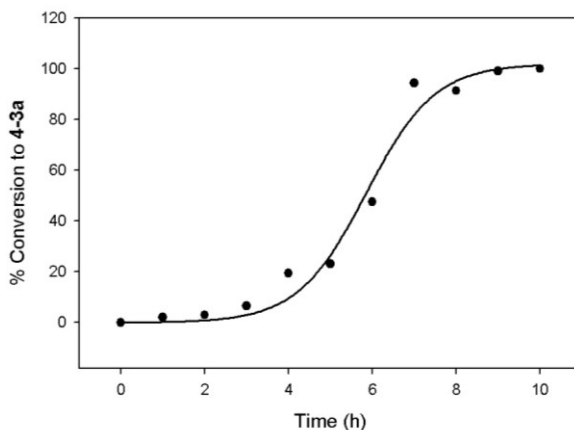


Figure 4-1. Conversion of **4-2a** to **4-3a** as a function of time employing 2.5 mol% **4-1** in 1,4-dioxane at 110 °C.

The potential of **4-1** to decompose thermally to an alternative catalyst formulation independent of the P,O-ligand featured in **4-1** was assessed through the survey of a range of simple Ir precursors for the cyclization of the secondary alkylamine **4-2a** to the corresponding pyrrolidine **4-3a** (Table 4-1). Under these conditions, the use of $[\text{Ir}(\text{COD})\text{Cl}]_2$ as a pre-catalyst provided clean conversion to **4-3a** (^1H NMR) and, in contrast to the previous observations when employing **4-1** as a catalyst, monitoring of the reaction as a function of time revealed the transformation to be complete after 1 h without the presence of an induction period. The observation that $[\text{Ir}(\text{COD})\text{Cl}]_2$ performed as a competent catalyst for this transformation was surprising, given that increased catalytic activity is often observed for late metal hydroamination catalysts when electron-rich phosphine ligands are employed in place of the diene ligand. By comparison, other

commercially available neutral Group 9 pre-catalysts performed poorly under these test conditions, including $[\text{Ir}(\eta^2\text{-cyclooctene})_2\text{Cl}]_2$, $[\text{Ir}(\text{COD})(\text{OMe})_2]$, $[\text{Cp}^*\text{IrCl}_2]_2$, and $[\text{Rh}(\text{COD})\text{Cl}]_2$ (entries 2 to 5, respectively); inferior performance was also observed for the cationic Ir pre-catalysts $[\text{Ir}(\text{COD})_2]\text{BF}_4$, $[\text{Ir}(\text{MeCN})_2(\text{COD})]\text{BF}_4$, and $[\text{Ir}(\text{COD})\text{PCy}_3(\text{pyridine})]\text{PF}_6$ (Crabtree's catalyst) (entries 6 to 8, respectively). Further investigations revealed that the quantitative conversion of **4-2a** into **4-3a** can also be achieved by use of only 0.125 mol % $[\text{Ir}(\text{COD})\text{Cl}]_2$ in 1,4-dioxane (3 h, 110 °C), or by employing higher Ir loadings at lower temperatures (2.5 mol % Ir; 7 h, 80 °C). While this reaction was also shown to proceed in 1,2-dichloroethane, 1,2-dimethoxyethane, or toluene, 1,4-dioxane proved to be the optimal solvent among those surveyed and was used for all subsequent catalytic studies.

Table 4-1. Screening of Group 9 Catalyst Precursors for the Cyclohydroamination of **4-2a** to Give **4-3a**^[a]

entry	catalyst precursor	conversion to 4-3a ^[b]
1	$[\text{Ir}(\text{COD})\text{Cl}]_2$	>95
2	$[\text{Ir}(\text{COE})\text{Cl}]_2$	10
3	$[\text{Ir}(\text{COD})\text{OMe}]_2$	7
4	$[\text{Cp}^*\text{IrCl}_2]_2$	<5
5	$[\text{Rh}(\text{COD})\text{Cl}]_2$	<5
6	$[\text{Ir}(\text{COD})_2]\text{BF}_4$	<5
7	$[\text{Ir}(\text{MeCN})_2(\text{COD})]\text{BF}_4$	28 ^[c]
8	$[\text{Ir}(\text{COD})\text{PCy}_3(\text{py})]\text{PF}_6$	10 ^[c]
9	none	<5

^[a] Reaction Conditions: 0.25 mmol **4-2a** and 1.0 mol% Ir or Rh in 0.5 mL 1,4-dioxane at 110 °C for 3 h. ^[b] On the basis of ¹H NMR data; unless otherwise noted **4-3a** was observed as the only reaction product. ^[c] Formation of **4-3a** was accompanied by other unknown byproducts.

In keeping with the observation that the hydroamination of **4-2a** catalyzed by $[\text{Ir}(\text{COD})\text{Cl}]_2$ exhibits an inverse-order rate dependence on the concentrations of each of **4-2a** and **4-3a** (see Section 4.2.5), the conversion of **4-2a** to **4-3a** was found to be completely inhibited when employing 0.5 mol % $[\text{Ir}(\text{COD})\text{Cl}]_2$ at 110 °C in 1,4-dioxane in the presence of an equivalent of K_2CO_3 (relative to **4-2a**) or 1.0 mol % 1,8-diazabicyclo(5.4.0)undec-7-ene (DBU). While efforts to definitively characterize

intermediates formed during the $[\text{Ir}(\text{COD})\text{Cl}]_2$ -mediated transformation of **4-2a** into **4-3a** ($\text{Ir}:\text{4-2a} = 1:1$) were thwarted by the relative complexity of the ^1H NMR spectra obtained under catalytically relevant conditions, it is worth noting that neither Ir–*H* nor Ir–*D* (when using **4-2a-d**₁ – the N-D isotopomer of **4-2a**) resonances were observed over a range of temperatures (25 - 80 °C) and throughout no free COD was detected (^1H and ^2H NMR).

In an effort to further enhance the catalytic performance of $[\text{Ir}(\text{COD})\text{Cl}]_2$, the effect of added salts, as well as added phosphine co-ligands, was evaluated. In monitoring the transformation of **4-2a** to **4-3a**, the use of 0.25 mol% $[\text{Ir}(\text{COD})\text{Cl}]_2$ as a pre-catalyst alone (110 °C) provided higher rates of conversion to **4-3a** than were achieved under analogous conditions when using 0.25 mol% $[\text{Ir}(\text{COD})\text{Cl}]_2$ in the presence of 0.5 mol% $n\text{Bu}_4\text{Cl}$, LiOTf , AgBF_4 , or $\text{LiB}(\text{C}_6\text{F}_5)_4 \cdot 2.5\text{OEt}_2$ (Figure 4-2); these results are surprising, given that increased catalytic activity is often observed for cationic late metal hydroamination catalysts when large, less-coordinating anions are employed in place of chloride.^[58a] In keeping with these observations, conductivity measurements of 1,4-dioxane solutions of $[\text{Ir}(\text{COD})\text{Cl}]_2$ carried out under various conditions, including in the presence or absence of **4-2a**, as well as at room temperature or following pre-conditioning under catalytic conditions, provided no evidence for heterolytic Ir-Cl bond cleavage.

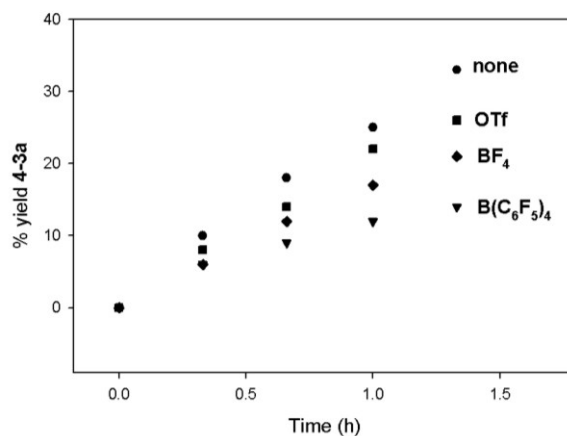
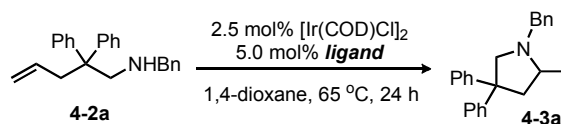
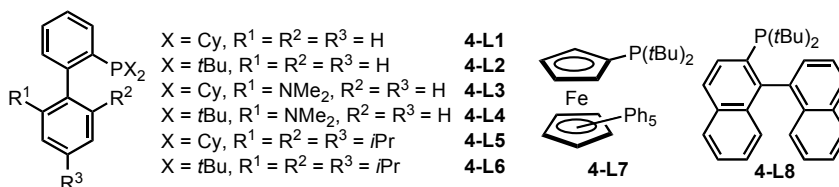


Figure 4-2. Salt effects on the $[\text{Ir}(\text{COD})\text{Cl}]_2$ -catalyzed hydroamination of **4-2a** to **4-3a**. The reactions were conducted at the following concentrations: $[\text{4-2a}] = 5.0 \times 10^{-1}$ M, $[\text{Ir}] = 2.5 \times 10^{-3}$ M, $[\text{MX}] = 2.5 \times 10^{-3}$ M, where X = OTf, BF_4 , $\text{B}(\text{C}_6\text{F}_5)_4 \cdot 2.5\text{OEt}_2$.

Table 4-2. Effect of Added Ligands on the Hydroamination of **4-2a** Using $[\text{Ir}(\text{COD})\text{Cl}]_2$.^[a]



entry	ligand	% yield 4-3a ^[b]	entry	ligand	% yield 4-3a ^[b]
1	none	60	11	DPPF ^[h]	<5 (>95) ^[d]
2	2,2'-bipyridine	<5	12	DiPPF ^[i]	<5 (45) ^[d]
3	terpyridine	<5	13	4-L1	<5
4	PPh ₃	<5	14	4-L2	>95
5	PCy ₃	34	15	4-L3	7
6	P(<i>t</i> Bu) ₃	62	16	4-L4	>95
7	DPPE ^[c]	<5 (>95) ^[d]	17	4-L5	6
8	DPPB ^[e]	<5	18	4-L6	58
9	Xantphos ^[f]	<5	19	4-L7	>95
10	DPEphos ^[g]	<5	20	4-L8	>95



^[a] Reaction Conditions: 0.125 mmol **4-2a**, 2.5 mol % $[\text{Ir}(\text{COD})\text{Cl}]_2$ and 5 mol % ligand in 0.25 mL 1,4-dioxane at 65 °C for 24 h. ^[b] On the basis of ¹H NMR data; **4-3a** was observed as the only reaction product unless noted. ^[c] 1,2-Bis(diphenylphosphino)ethane. ^[d] Total conversion of **4-2a** (¹H NMR). ^[e] 1,4-Bis(diphenylphosphino)butane. ^[f] 4,5-Bis(diphenylphosphino)-9,9-dimethylxanthene. ^[g] Bis(2-diphenylphosphinophenyl)ether. ^[h] 1,1'-Bis(diphenylphosphino)ferrocene. ^[i] 1,1'-Bis(diisopropylphosphino)ferrocene.

Given that the use of added phosphines has proven effective in promoting the intramolecular addition of secondary alkylamines to unactivated alkenes in reactions mediated by Rh,^[69a, 69b] Pt,^[71] and Cu^[70] pre-catalysts, the influence of such co-ligands on the catalytic performance of $[\text{Ir}(\text{COD})\text{Cl}]_2$ in the cyclization of **4-2a** was surveyed. While no reactivity benefits were derived from the addition of phosphines in reactions conducted at 110 °C, the use of bulky $\text{RP}t\text{Bu}_2$ phosphines (R = biaryl or ferrocenyl; Table 4-2) did prove useful in promoting the formation of **4-3a** under more mild conditions than could be achieved by use of $[\text{Ir}(\text{COD})\text{Cl}]_2$ alone. For example, while the use of 2.5 mol% $[\text{Ir}(\text{COD})\text{Cl}]_2$ at 65 °C afforded 60% conversion to **4-3a** in the absence of by-products over the course of 24 h, the incorporation of 5 mol% 2-(di-*t*-butylphosphino)biphenyl (**4-L2**, Table 4-2) as a co-ligand in this reaction afforded **4-3a** quantitatively (¹H NMR)

under similar reaction conditions. Upon further investigation, it was observed that the rate of **4-2a** cyclization employing $[\text{Ir}(\text{COD})\text{Cl}]_2/4\text{-L2}$ catalyst mixtures exhibits an inverse-order dependence on **4-L2** at 65 °C and a zero-order rate dependence on **4-L2** at 110 °C (Figure 4-3). On the basis of these data, it is unlikely that species featuring an Ir-P linkage represent important catalytic intermediates in the observed hydroamination of **4-2a**. Rather, the reactivity benefits of employing **4-L2** and related bulky phosphines at 65 °C may be attributable to the ability of such co-ligands to discourage the decomposition of catalytically inactive Ir intermediates, which in turn can serve as a source of catalytically active and phosphine-free Ir species. As such, $[\text{Ir}(\text{COD})\text{Cl}]_2$ was employed for all subsequent catalytic studies without added co-ligands.

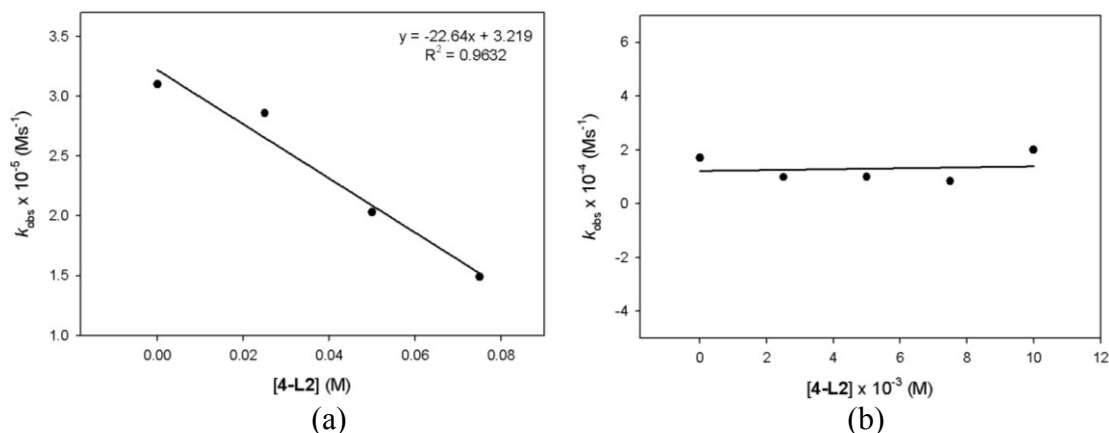


Figure 4-3. Relationship between k_{obs} and **[4-L2]**. (a) The reactions were conducted in 1,4-dioxane at 65 °C at the following concentrations: $[\text{4-2a}] = 5.0 \times 10^{-1} \text{ M}$, $[\text{Ir}] = 2.5 \times 10^{-2} \text{ M}$ and **[4-L2]** was varied from 0 M to $7.5 \times 10^{-2} \text{ M}$. (b) The reactions were conducted in 1,4-dioxane at 110 °C at the following concentrations: $[\text{4-2a}] = 5.0 \times 10^{-1} \text{ M}$, $[\text{Ir}] = 5.0 \times 10^{-3} \text{ M}$ and **[4-L2]** was varied from 0 M to $1.0 \times 10^{-2} \text{ M}$.

4.2.2 Intramolecular Hydroamination of Secondary Alkylamines

Encouraged by the ability of $[\text{Ir}(\text{COD})\text{Cl}]_2$ to mediate the cyclization of **4-2a**, the hydroamination of alternative secondary alkylamine substrates, including those featuring polar groups, was examined (Table 4-3). The presence of halide (entry 2), ester (entry 3), or alkoxy (entry 4) substituents within the benzylamines **4-2b** – **4-2d** did not significantly influence the progress of the reaction, and the bulky *N*-methylcyclohexyl aminoalkene **4-**

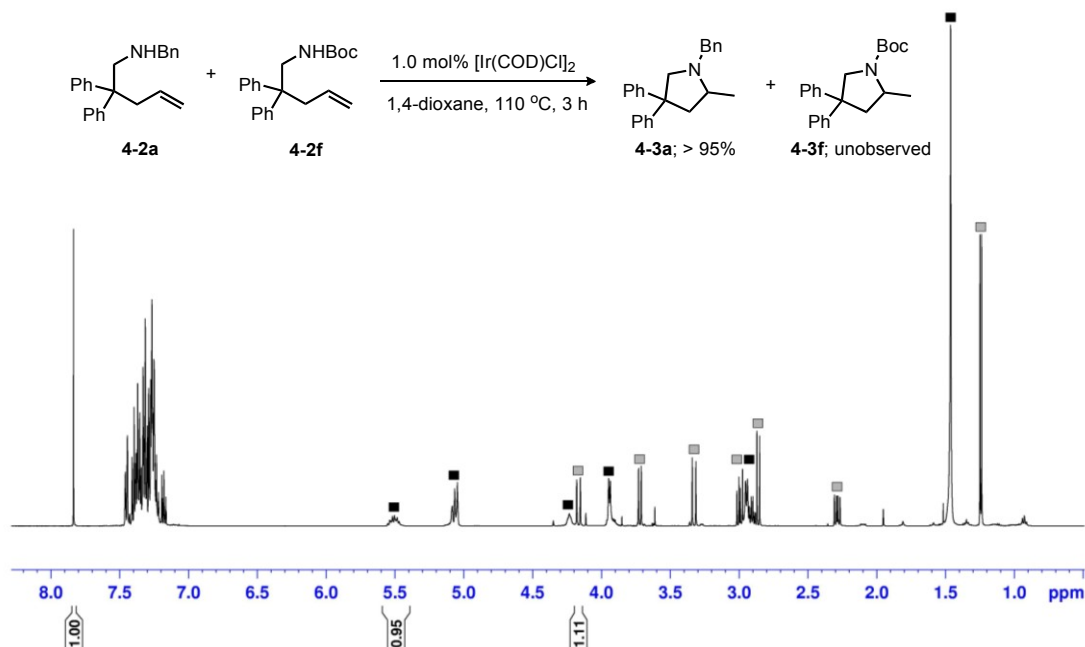
2e was also cyclized (entry 5); in all cases, high isolated yields were obtained (85-89%) despite the use of relatively low catalyst loading (1-2.5 mol% Ir).

Table 4-3 Intramolecular Hydroamination of Unactivated Alkenes by Secondary Alkylamines Employing $[\text{Ir}(\text{COD})\text{Cl}]_2$ as a Pre-Catalyst^[a]

entry	aminoalkene	product	mol% Ir (time, h)	yield ^[b]
1	R = Ph (4-2a)		0.25 (3)	88
2	R = C ₆ H ₄ Cl (4-2b)		1.0 (3)	85
3	R = C ₆ H ₄ CO ₂ Me (4-2c)		1.0 (3)	87
4	R = C ₆ H ₄ OMe (4-2d)		2.5 (3)	89
5	R = Cy (4-2e)		1.0 (7)	88
6			2.5 (7)	86
7			5.0 (24)	84
8			2.5 (16)	92 (1.3:1) ^[d]
9			5.0 (24)	81 ^[c] (1.5:1) ^[d]
10			5.0 (24)	72 ^[e]
11			2.5 (16)	88
12			5.0 (48)	74
13			10 (48)	88 (>20:1) ^[d]
14			10 (48)	52 ^[c]

^[a] Conditions: 0.25 mmol aminoalkene in 0.5 mL 1,4-dioxane at 110 °C; conversion to product > 95% (¹H NMR) unless stated. ^[b] Isolated percent yield unless stated (average of two runs). ^[c] ¹H NMR percent yield. ^[d] Diastereomeric ratio (dr, ¹H NMR). ^[e] Reaction run at 80 °C; conversion to the piperidine was 75% (¹H NMR) with the balance corresponding to an alkene isomerization product.

Alternative *gem*-disubstituted relatives of **4-2a** also proved to be suitable hydroamination substrates (entries 6 to 8), as did the monosubstituted isopropyl-containing species featured in entry 9. The hexenylamine substrate featured in entry 10 was also efficiently cyclized in the presence of $[\text{Ir}(\text{COD})\text{Cl}]_2$ to afford the corresponding piperidine derivative. The cyclohydroamination of more difficult substrates featuring unactivated disubstituted alkenes was then targeted. While the use of $[\text{Ir}(\text{COD})\text{Cl}]_2$ proved effective in promoting the cyclization of *gem*-disubstituted olefins (entries 11 and 12), hydroamination of the internal olefinic substrates featured in entries 13 and 14 presented a more significant challenge. Notably, throughout the course of these and the other $[\text{Ir}(\text{COD})\text{Cl}]_2$ -mediated cyclohydroamination reactions reported herein, no unsaturated hydroamination products arising from β -hydride elimination were detected.



Scheme 4-4. ^1H NMR of the competition reaction for the cyclohydroamination of benzyl- and Boc-protected aminoalkenes **4-2a** and **4-2f**. (δ 7.85 ppm = 1,4-bis(trifluoromethyl)benzene; grey square = **4-3a**; black square = **4-2f**)

In keeping with the $\text{Cu}(\text{O}t\text{Bu})/\text{Xantphos}$ catalyst system,^[70] but in contrast to the $\text{PtCl}_2/\text{biarylphosphine}$ ^[71a] and $[\text{Rh}(\text{COD})_2]\text{BF}_4/\text{biarylphosphine}$ ^[69b] catalyst systems, the use of $[\text{Ir}(\text{COD})\text{Cl}]_2$ under our typical conditions (e.g. Table 4-2) proved ineffective in promoting the hydroamination of aminoalkene substrates lacking backbone substituents

that promote cyclization. Furthermore, the *N*-Boc relative of **4-2a** (i.e. **4-2f**) proved unreactive (^1H NMR) in the presence of $[\text{Ir}(\text{COD})\text{Cl}]_2$ (Boc = *t*-butoxycarbonyl; 1.0 mol % Ir; 3 h, 110 °C). However, the observation that the cyclization of **4-2a** proceeds unhampered (^1H NMR) when using a 1:1 mixture of **4-2a** and **4-2f** confirms that the latter does not poison the active catalyst derived from $[\text{Ir}(\text{COD})\text{Cl}]_2$ (^1H NMR; Scheme 4-4). In this regard, $[\text{Ir}(\text{COD})\text{Cl}]_2$ appears to be well-suited as a pre-catalyst for conducting chemoselective hydroaminations involving more complex organic molecules.

4.2.3 Intramolecular Hydroamination of Secondary Arylamines

The late metal-mediated cyclohydroamination of unactivated alkenes by secondary arylamines is limited to a single report featuring the cyclization of two simple *N*-Ph substrates.^[69c] The use of $[\text{Ir}(\text{COD})\text{Cl}]_2$ as a pre-catalyst established expanded scope for this class of transformations (Table 4-4) in enabling the cyclization of the parent *N*-Ph substrate **4-4a** (entry 1), as well as arylamine substrates featuring *para* electron-donating (**4-4b** and **4-4c**; entries 5 and 6) and *para* electron-withdrawing (**4-4d** and **4-4e**; entries 7 and 8) substituents. While high isolated yields of **4-5a** – **4-5d** were obtained for reactions conducted over the course of 7 h at 110 °C, the amount of catalyst needed to achieve quantitative conversion to **4-5** under these conditions varied significantly. Whereas only 0.25 mol% $[\text{Ir}(\text{COD})\text{Cl}]_2$ was required to effect the clean hydroamination of the anisole derivative **4-4c** (entry 6), the use of 2.5 mol% $[\text{Ir}(\text{COD})\text{Cl}]_2$ afforded only partial conversion of the trifluoromethyl species **4-4e** to **4-5e**, even after 24 h (entry 8); a more detailed kinetic analysis of these reactivity trends is provided (see Section 4.2.5). The observation that the intramolecular hydroamination of **4-4** is significantly enhanced by *para* electron-donating substituents is divergent from trends documented by Zhou and Hartwig,^[72b] who reported that both electron-rich and electron-poor anilines were less reactive than electron-neutral anilines toward the intermolecular hydroamination of activated bicyclic alkenes catalyzed by (bisphosphine)Ir species, which was shown to proceed by way of N-H bond activation/alkene insertion reaction pathway.^[72b] While an alternative backbone substitution pattern was tolerated (entry 9), the hydroamination of a 5-hexenyl substrate proceeded in low yield (entry 10), and efforts to promote the cyclization of the disubstituted olefinic substrate featured in entry 11 by use of $[\text{Ir}(\text{COD})\text{Cl}]_2$ were unsuccessful. One might predict arylamine substrates to be inherently

Table 4-4 Intramolecular Hydroamination of Unactivated Alkenes by Secondary Arylamines Employing [Ir(COD)Cl]₂ as a Pre-Catalyst^[a]

entry	aminoalkene	product	mol% Ir (time, h)	yield ^[b]
1	R = Ph (4-4a)		2.5 (7)	95
2	R = Ph (4-4a)		2.5 (7)	>95 ^[c,d]
3	R = Ph (4-4a)		2.5 (7)	<5 ^[c,e]
4	R = Ph (4-4a)		5.0 (7)	<5 ^[c,f]
5	R = 4-C ₆ H ₄ Me (4-4b)		1.0 (7)	96
6	R = 4-C ₆ H ₄ OMe (4-4c)		0.5 (7)	94
7	R = 4-C ₆ H ₄ F (4-4d)		2.5 (7)	95
8	R = 4-C ₆ H ₄ CF ₃ (4-4e)		5.0 (24)	67 ^[c]
9			5.0 (16)	95
10			5.0 (16)	20 ^[c,g]
11			5.0 (24)	n.r. ^[h]

^[a] Conditions: 0.25 mmol aminoalkene in 0.5 mL 1,4-dioxane at 110 °C; conversion to product > 95% (¹H NMR) unless stated. ^[b] Isolated percent yield unless stated (average of two runs). ^[c] ¹H NMR percent yield. ^[d] Using 2.5 mol% PtCl₂ and 2.5 mol% *t*Bu-DavePhos in place of [Ir(COD)Cl]₂. ^[e] Using 2.5 mol% [Rh(COD)₂]BF₄ and 3 mol% Cy-DavePhos in place of [Ir(COD)Cl]₂. ^[f] Using 5 mol% Au(*o*-*t*Bu₂P-biphenyl)Cl and 5 mol% AgOTf in place of [Ir(COD)Cl]₂. ^[g] Conversion to the piperidine was 20% (¹H NMR) with the balance corresponding to an alkene isomerization product. ^[h] No reaction of the aminoalkene was observed.

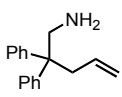
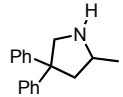
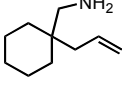
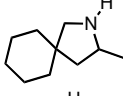
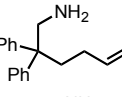
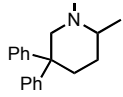
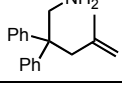
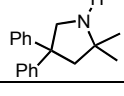
more susceptible to late metal-mediated hydroamination than alkylamines; the lower basicity of the former should reduce catalyst inhibition arising from unproductive substrate and/or product binding, and should also serve to promote N-H bond cleavage in hydroamination reactions involving net proton transfer from nitrogen. However, a comparative reactivity survey revealed that some of the most effective late metal catalysts

known for the intramolecular hydroamination of unactivated alkenes fail to promote the cyclization of arylamines such as **4-4a** (entries 2 to 4).

4.2.4 Intramolecular Hydroamination of Primary Amines

The cyclohydroamination of unactivated alkenes with primary amines provides an atom-economical synthetic route to N-H containing cyclic secondary amines, which, unlike alternative protocols, circumvents the installation and removal of nitrogen protecting groups. Although transformations of this type are well established for several classes of hydroamination catalysts,^[58a] the late metal-mediated cyclization of such substrates has been achieved only recently by use of [Rh(COD)₂]BF₄/biarylphosphine^[69b] or Cu(O*t*Bu)/Xantphos.^[70] Initial efforts to effect the cyclization of the primary aminoalkenes featured in Table 4-5 by using [Ir(COD)Cl]₂ as a pre-catalyst under a variety of experimental conditions were unsuccessful. However, the knowledge that Brønsted acids can act as catalysts^[65] or co-catalysts^[75] in promoting the intramolecular hydroamination of unactivated alkenes and alkynes provided the motivation to examine the use of [Ir(COD)Cl]₂/Brønsted acid catalyst mixtures. The Brønsted acid-mediated intramolecular hydroamination of unactivated alkenes with primary amines is limited to a single example by Ackermann and co-workers,^[65a] in which the cyclization of the substrate featured in entry 1 (Table 4-5) was achieved in 83% yield by use of 20 mol% [PhMe₂NH]B(C₆F₅)₄ (18 h, 120 °C). In the pursuit of a more convenient and cost-effective co-catalyst, HNEt₃Cl and CF₃SO₃H^[65b] were each evaluated. While none of 2.5 mol% [Ir(COD)Cl]₂, 10 mol% HNEt₃Cl, and 10 mol% CF₃SO₃H individually proved capable of promoting the hydroamination of the primary aminoalkene substrates featured in Table 4.5 (24 h, 110 °C), the use of 2.5 mol% [Ir(COD)Cl]₂/5 mol% HNEt₃Cl as a pre-catalyst mixture provided excellent conversions to the targeted N-H containing cyclic secondary amines. Inferior results were obtained, including the formation of undesired by-products, when 5 mol% CF₃SO₃H was used as a co-catalyst under similar conditions. Control experiments confirmed that neither 10 mol% *Nn*Bu₄Cl nor mixtures comprised of 2.5 mol% [Ir(COD)Cl]₂/5 mol% *Nn*Bu₄Cl are capable of promoting the cyclization of these substrates under these experimental conditions. The scope of the [Ir(COD)Cl]₂/HNEt₃Cl catalyzed cyclization of primary aminoalkene substrates is presented in Table 4-5.

Table 4-5 Intramolecular Hydroamination of Unactivated Alkenes by Primary Alkylamines Employing [Ir(COD)Cl]₂ and HNEt₃Cl (1:2) as a Pre-Catalyst Mixture^[a]

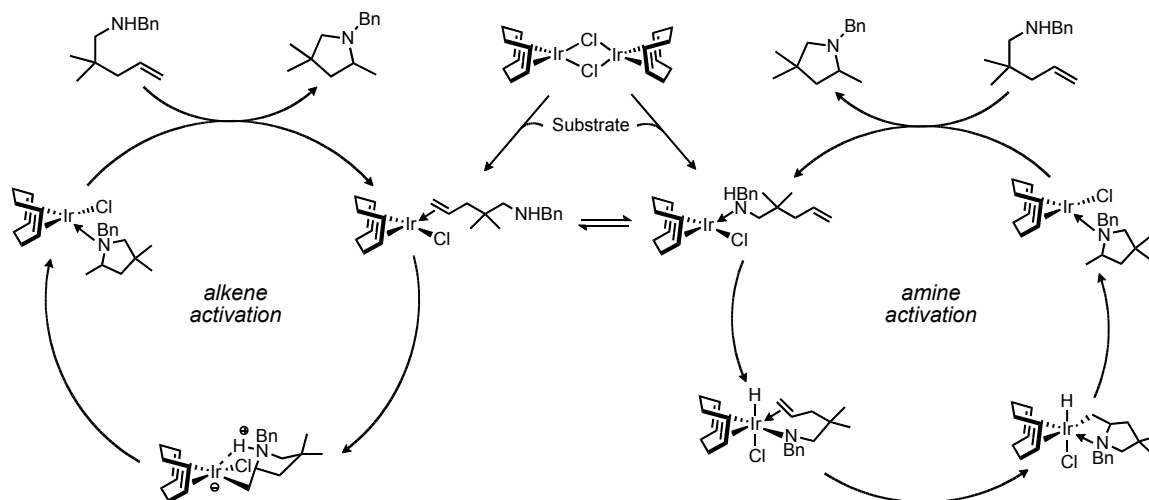
entry	aminoalkene	product	mol% Ir (time, h)	yield ^[b]
1			5.0 (24)	89
2			5.0 (24)	75 ^[c]
3			5.0 (24)	84
4			10 (48)	87

^[a] Conditions: 0.25 mmol aminoalkene in 0.5 mL 1,4-dioxane at 110 °C; conversion to product > 95% (¹H NMR) unless stated. ^[b] Isolated percent yield unless stated (average of two runs). ^[c] ¹H NMR percent yield; the remainder is attributed to an alkene isomerization product.

4.2.5 Kinetic Studies

A number of distinct mechanistic pathways have been uncovered for the hydroamination of alkenes.^[58] In the case of late metal-mediated transformations these include processes involving: nucleophilic attack of an amine on a metal-coordinated alkene,^[67a, 67b, 71, 76] an η^3 -allyl or related complex,^[7a, 77] or an η^6 -vinylarene complex;^[7b] N-H bond activation followed by alkene insertion into an M-NR₂ linkage;^[4c, 72b, 72c] amine coordination followed by proton-transfer to an activated alkene;^[78] and nucleophilic attack of a metal amido species on an activated alkene.^[79] While experimental evidence for Ir-mediated N-H bond activation/alkene insertion reaction sequences has been obtained for the intermolecular hydroamination of activated alkenes such as norbornene,^[4c, 72b, 72c] mechanistic experiments indicate that the Ir-catalyzed intramolecular hydroamination (and hydroalkoxylation) of alkynes can proceed via alternative reaction pathways involving alkyne activation/nucleophilic attack.^[73e, 80] Based on these reports, two competing mechanisms involving either initial N-H bond activation or alkene activation could be envisioned for the [Ir(COD)Cl]₂-catalyzed

cyclohydroamination of alkylaminoalkenes (Scheme 4-5). In an effort to gain insight into the mechanism of such transformations, so as to guide the development of increasingly effective catalysts, a kinetic examination of the $[\text{Ir}(\text{COD})\text{Cl}]_2$ -mediated hydroamination reactions featured herein was conducted.



Scheme 4-5. Competing mechanistic pathways involving initial alkene activation (left) and N-H bond activation (right).

Kinetic parameters were obtained for the hydroamination of **4-2a** catalyzed by $[\text{Ir}(\text{COD})\text{Cl}]_2$; pseudo-first order rate constants were determined by monitoring the disappearance and appearance of **4-2a** and **4-3a**, respectively, relative to an internal standard over the course of 2-3 half-lives (^1H NMR; Figure 4-4a). The order of reaction in $[\text{Ir}(\text{COD})\text{Cl}]_2$ was examined first by combining **4-2a** (0.5 M) with varied concentrations of $[\text{Ir}]$ (0.001 to 0.00475 M) in 1,4-dioxane at 110 °C. As shown in Figure 4-4b, a plot of k_{obs} versus $[\text{Ir}]$ was linear, indicating a first-order dependence on the catalyst concentration. This observation is consistent with a mechanism involving a monomeric Ir catalyst species, and would appear to preclude slow dissociation of a dimeric pre-catalyst to an active monomer.

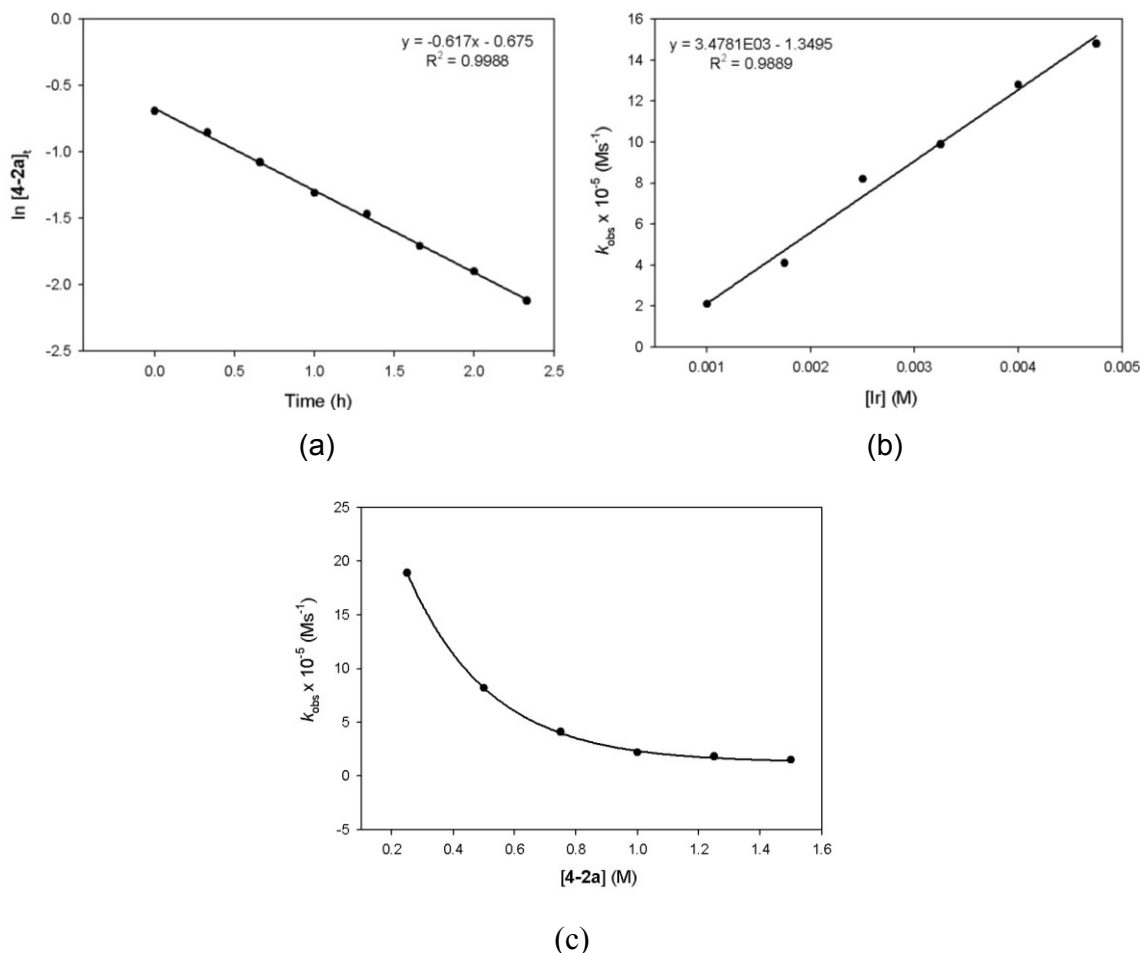


Figure 4-4. (a) Representative plot for the conversion of **4-2a** to **4-3a** catalyzed by $[\text{Ir}(\text{COD})\text{Cl}]_2$. The reactions were conducted in 1,4-dioxane at 110 °C at the following concentrations: $[\text{Ir}] = 5.0 \times 10^{-3} \text{ M}$ and $[\mathbf{4-2a}] = 5.0 \times 10^{-1} \text{ M}$. (b) Relationship between k_{obs} and $[\text{Ir}]$. The reactions were conducted in 1,4-dioxane at 110 °C at the following concentrations: $[\mathbf{4-2a}] = 5.0 \times 10^{-1} \text{ M}$ and $[\text{Ir}] = 1.0 \times 10^{-3} \text{ M}$ to $4.75 \times 10^{-3} \text{ M}$. (c) Relationship between k_{obs} and $[\mathbf{4-2a}]$. The reactions were conducted in 1,4-dioxane at 110 °C at the following concentrations: $[\text{Ir}] = 2.5 \times 10^{-3} \text{ M}$ and $[\mathbf{4-2a}] = 2.0 \times 10^{-1} \text{ M}$ to 1.5 M.

The reaction order in **4-2a** was investigated subsequently by using a constant $[\text{Ir}]$ (0.0025 M) along with a $[\mathbf{4-2a}]$ ranging from 0.25 to 1.5 M in 1,4-dioxane at 110 °C. In keeping with the findings of Cochran and Michael,^[67a, 67c] decreasing reaction rates were observed with increased initial concentrations of **4-2a**, which is consistent with an inverse order dependence of the rate of reaction on substrate concentration (Figure 4-4c). Furthermore, the rate of cyclization of **4-2a** was observed to decrease by approximately 50% when measured in the presence of an equivalent of added **4-3a**. These results

demonstrate both competitive substrate and product inhibition. While on the basis of these kinetic data alone definitive conclusions regarding the mode of catalyst inhibition by **4-2a** and **4-3a** cannot be made, possible scenarios that can be envisioned include unproductive binding of **4-2a** or **4-3a** to Ir, as well as deprotonation of an amine/ammonium intermediate^[67a] by **4-2a** or **4-3a**. However, computational studies support catalyst inhibition by **4-2a** and **4-3a** arising from the latter deprotonation pathway (see Section 4.2.6).

The rate of the [Ir(COD)Cl]₂-catalyzed hydroamination of **4-4a** – **4-4e** was examined as a function of the *para*-substituent on the arylamine. The cyclization of **4-4a** – **4-4e** (Table 4-4, entries 1 and 5 to 8) in the presence of 0.5 mol % [Ir(COD)Cl]₂ was monitored by use of ¹H NMR methods to obtain reaction rates. A Hammett plot of the resulting data provided a large, negative ρ-value of –2.4(2) (Figure 4-5), which is consistent with a build-up of positive charge before and/or during the turnover-limiting step as well as indicating that more electron-rich arylamines undergo hydroamination more rapidly.

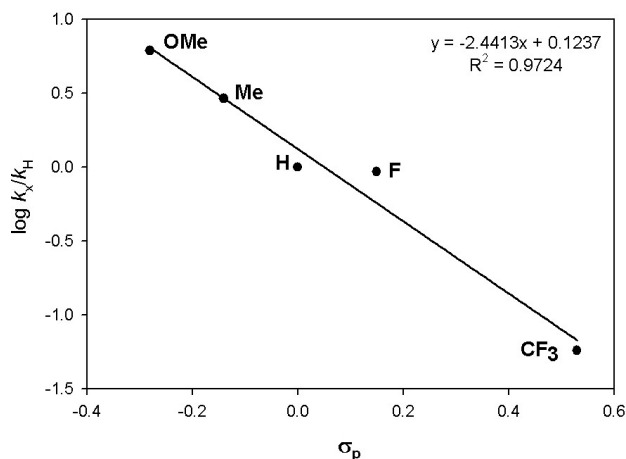


Figure 4-5. Hammett plot for the [Ir(COD)Cl]₂ catalyzed hydroamination of arylamines **4-4a** – **4-4e**. The reactions were conducted in 1,4-dioxane at 110 °C at the following concentrations: [**4-4a** – **4-4e**] = 5.0 x 10⁻¹ M and [Ir] = 5.0 x 10⁻³ M.

To provide some insight into the turnover-limiting step of the mechanism, the H/D kinetic isotope effect (KIE) for the [Ir(COD)Cl]₂-catalyzed hydroamination **4-2a** was measured under catalytic conditions. The first order plots (Figure 4-6) of the cyclization

of **4-2a** and **4-2a-d₁** in 1,4-dioxane at 110 °C provided $k_{\text{obs}} = 0.30(1) \text{ h}^{-1}$ and $k_{\text{obs}} = 0.089(2) \text{ h}^{-1}$, respectively, which translated to a primary KIE of 3.4(3). While these observations implicate the hydrogen derived from the N-H of **4-2a** in the rate-determining step, several competing reaction pathways (e.g. rate-limiting N-H oxidative addition or proton transfer following nucleophilic attack on a coordinated alkene) that account for these observations can be envisioned.

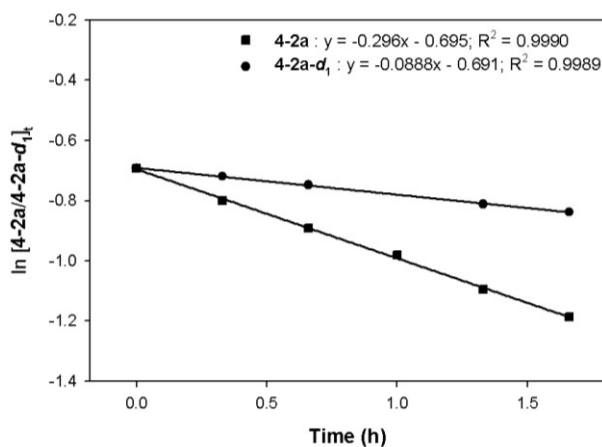


Figure 4-6. H/D kinetic isotope effect for the $[\text{Ir}(\text{COD})\text{Cl}]_2$ catalyzed hydroamination of **4-2a**. The reaction conditions were conducted at the following concentrations: $[\mathbf{4-2a}/\mathbf{4-2a-d}_1] = 5.0 \times 10^{-1} \text{ M}$ and $[\text{Ir}] = 2.5 \times 10^{-3} \text{ M}$.

In order to obtain activation parameters for the $[\text{Ir}(\text{COD})\text{Cl}]_2$ -catalyzed hydroamination of **4-2a**, a series of reactions were executed over a range of temperatures (90 – 130 °C); pseudo-first order rate constants were obtained from linear plots of $\ln[\mathbf{4-2a}]_t$ versus time over this temperature range. Eyring and Arrhenius analyses for the cyclization of **4-2a** to **4-3a** afforded $\Delta H^\ddagger = +20.9(3) \text{ kcal mol}^{-1}$, $\Delta S^\ddagger = -23.1(8) \text{ e.u.}$, and $E_a = +21.6(3) \text{ kcal mol}^{-1}$ (Figure 4-7). The observation of a large negative ΔS^\ddagger value in the cyclization **4-2a** mediated by $[\text{Ir}(\text{COD})\text{Cl}]_2$ is consistent with a highly ordered transition state.^[81]

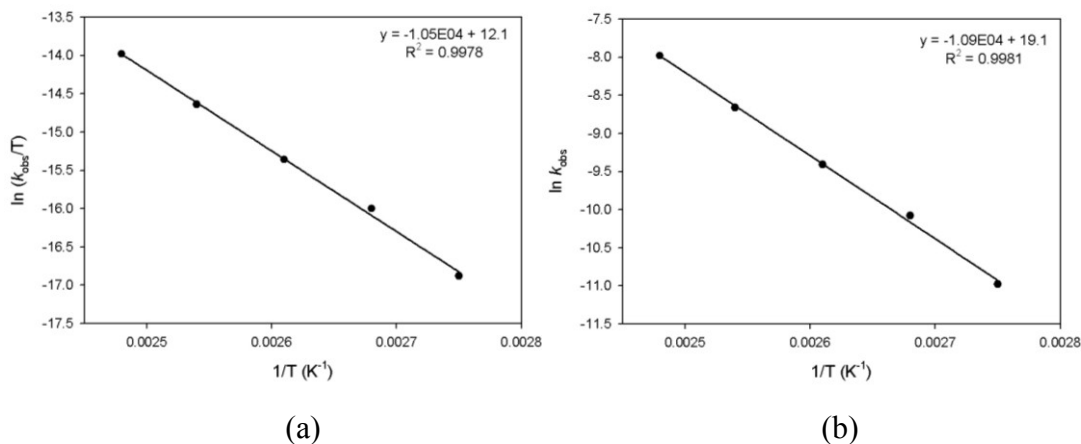


Figure 4-7. (a) Eyring plot for the hydroamination of **4-2a** catalyzed by $[\text{Ir}(\text{COD})\text{Cl}]_2$. The reactions were conducted in 1,4-dioxane over a temperature range of 90–130 °C at the following concentrations: $[\mathbf{4-2a}] = 5.0 \times 10^{-1}$ M and $[\text{Ir}] = 2.5 \times 10^{-3}$ M. (b) Arrhenius plot for the hydroamination of **4-2a** catalyzed by $[\text{Ir}(\text{COD})\text{Cl}]_2$. The reactions were conducted in 1,4-dioxane over a temperature range of 90–130 °C at the following concentrations: $[\mathbf{4-2a}] = 5.0 \times 10^{-1}$ M and $[\text{Ir}] = 2.5 \times 10^{-3}$ M.

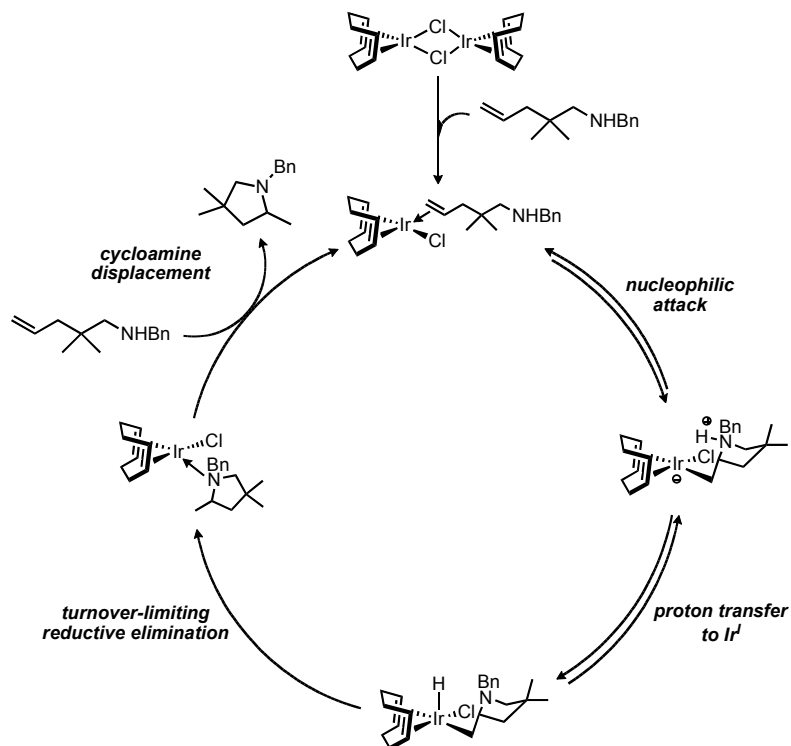
4.2.6 Summary of Kinetic Studies

Kinetic analyses of the $[\text{Ir}(\text{COD})\text{Cl}]_2$ -catalyzed hydroamination of **4-2a** have revealed that the reaction rate shows first order dependence on the concentration of Ir and inverse order dependence with respect to both substrate (**4-2a**) and product (**4-3a**) concentrations. While the observed primary kinetic isotope effect ($k_{\text{H}}/k_{\text{D}} = 3.4(3)$) and the observation that increased electron density at nitrogen in **4-4** promotes the cyclization of these arylamine substrates ($\rho = -2.4$) are in keeping with an alkene activation mechanism involving nucleophilic attack of a tethered amine on a metal-coordinated alkene followed by a rate-limiting protonolysis step, alternative mechanisms including those involving N–H oxidative addition cannot be ruled out on the basis of these empirical data alone.

Given the lack of spectroscopic evidence that would enable the definitive identification of catalytic intermediates in the present study (see Section 4.2.1), and in an effort to gain further insight into the elusive details of the mechanism of the $[\text{Ir}(\text{COD})\text{Cl}]_2$ -catalyzed cyclohydroamination of unactivated aminoalkenes, a collaboration was established in order to examine this process computationally. Computational investigations carried out by Prof. Sven Tobisch (University of St. Andrew's, Scotland) have provided significant insight into a range of intermediates

traversed along the putative amine and alkene activation reaction pathways (Scheme 4-5). The most compelling results identified the N-H oxidative addition step as imposing a significant activation barrier ($\Delta G^\ddagger = 38.2 \text{ kcal mol}^{-1}$) as well as being strongly endergonic ($\Delta G = 25.7 \text{ kcal mol}^{-1}$), thereby rendering the oxidative addition to be challenging from both kinetic and thermodynamic grounds. In contrast, backside attack of the pendant amine on an Ir-coordinated olefin emerged as the dominant pathway in a process that featured a moderate activation barrier ($\Delta G^\ddagger = 16.9 \text{ kcal mol}^{-1}$), in keeping with smooth and reversible ring closure.

Gratifyingly, the computationally assessed energy profile for the olefin activation pathway was consonant with the observed empirical data (Scheme 4-6). Turnover-limiting reductive elimination is consistent with the located highly organized transition state structure and rationalizes the negative activation entropy measured. The lack of spectroscopic evidence for the putative Ir^{III}-hydrido species is understandable on the basis of its identification as a metastable intermediate, and rate-limiting reductive elimination from this intermediate is in keeping with the measured primary kinetic isotope effect. β -Hydrogen elimination, as a potentially competitive event to productive hydroamination, proved not to be viable on the basis of computational data, thereby supporting the clean and efficient catalysis observed for several substrates (Tables 4-2 to 4-4). Finally, the assessed total barrier of $24.6 \text{ kcal mol}^{-1}$ for turnover-limiting reductive elimination agrees remarkably well with Eyring data for the cyclization of **4-2a** to **4-3a** ($\Delta G^\ddagger_{298} = 27.7 \text{ kcal mol}^{-1}$).



Scheme 4-6. Proposed mechanism for the $[\text{Ir}(\text{COD})\text{Cl}]_2$ -mediated intramolecular hydroamination of aminoalkenes.

4.3 Summary and Conclusions

Further investigation into the significant induction period observed for the **4-1**-catalyzed cyclohydroamination of **2-4a** has led to the identification of $[\text{Ir}(\text{COD})\text{Cl}]_2$ as a highly effective pre-catalyst for the intramolecular addition of primary as well as secondary alkyl- or arylamines to unactivated olefins at relatively low catalyst loading. With the exception of the hydroamination of primary aminoalkenes, for which HNEt_3Cl was required as a co-catalyst, no co-ligands or additives were required in order to promote the hydroamination of these challenging substrates. A comprehensive experimental investigation was conducted to provide insight into the mechanism of this transformation; these empirical results are supported by computational data. Collectively, the results of these studies reveal that these intramolecular hydroamination reactions commence from $[\text{Ir}(\text{COD})\text{Cl}(\text{substrate})]$ as the catalytically competent compound and proceed via initial electrophilic activation of the olefin unit by a relatively electron-poor metal center, in a manner that has previously not been documented for Ir-catalyzed alkene

hydroamination. An alternative mechanism involving activation of the amine functionality, which is firmly established for electron-rich Ir complexes, has proven inaccessible for the catalyst system under investigation. The operative mechanistic scenario involves: (1) smooth, reversible ring closure via nucleophilic attack of the amine on the metal coordinated, thus activated C=C bond; (2) stepwise cleavage of the Ir–C bond in the zwitterionic intermediate via proton transfer from the ammonium unit to Ir, with subsequent turnover-limiting C–H reductive elimination; and (3) associative displacement of the cycloamine by new substrate, thereby regenerating the active catalyst species. Turnover-limiting reductive elimination to involve a metastable, highly reactive Ir^{III}–hydride intermediate and traversing a highly ordered transition state structure is consistent with the measured primary H/D KIE and the observed negative activation entropy. Given the limited number of late metal catalysts that have proven capable of promoting the intramolecular addition of primary and/or secondary alkyl- and arylamines to unactivated olefins, as well as the paucity of mechanistic data pertaining to these transformations, the catalytic and mechanistic findings reported herein represent an important contribution toward the development of general late metal catalysts for use in mediating cyclohydroamination reactions. Potential strategies to modify further the electrophilicity of the Ir center, as well as to promote more facile turnover-limiting C–H reductive elimination, through ligand design are presented in Chapter 6 (see Section 6.3).

4.4 Experimental Section

4.4.1 General Considerations

All catalysis and kinetic studies were set up in the absence of oxygen and water under an atmosphere of dinitrogen, either by use of standard Schlenk methods or within an mBraun glovebox apparatus, utilizing glassware that was oven-dried (130 °C) and evacuated while hot prior to use, whereas workup of the catalytic and kinetic reactions was conducted in air on the benchtop. 1,4-Dioxane (Aldrich) was dried over Na/benzophenone followed by distillation under an atmosphere of dinitrogen. Toluene was deoxygenated by sparging with dinitrogen followed by passage through a double column solvent purification system purchased from mBraun Inc. 1,2-Dimethoxyethane

and 1,2-dichloroethane were deoxygenated by sparging with dinitrogen gas followed by storage over activated 4 Å molecular sieves for 48 h prior to use. Chloroform-*d*₁ (Cambridge Isotopes) was used as received. All solvents used within the glovebox were stored over activated 4 Å molecular sieves. With the exception of [Ir(COD)₂]⁺BF₄⁻^[82] and [Ir(MeCN)₂(COD)]⁺BF₄⁻^[82] as well as 2-(di-*tert*-butylphosphino)-*N,N*-dimethylaniline^[20a] and [Pd(cinnamyl)Cl]₂^[83] all of which were prepared using literature procedures, all other Rh and Ir complexes were purchased from Strem Chemicals and were evacuated under reduced pressure for 24 h prior to use. LiB(C₆F₅)₄·2.5OEt₂ (Boulder Scientific), LiOTf (Strem), and AgBF₄ (Strem) were evacuated under reduced pressure for 24 h prior to use. **4-1**,^[74] 2,2-Diphenylpent-4-en-1-amine,^[71b] (1-allylcyclohexyl)methanamine,^[71b] 2,2-diphenylhex-5-en-1-amine,^[69b] 4-methyl-2,2-diphenylpent-4-en-1-amine,^[71b] *N*-benzyl-2,2-diphenylpent-4-en-1-amine (**4-2a**),^[71b] *N*-(4-chlorobenzyl)-2,2-diphenylpent-4-en-1-amine (**4-2b**),^[65a] methyl 4-[(2,2-diphenylpent-4-enylamino)methyl]benzoate (**4-2c**),^[71b] *N*-(4-methoxybenzyl)-2,2-diphenylpent-4-en-1-amine (**4-2d**),^[65a] *N*-(cyclohexylmethyl)-2,2-diphenylpent-4-en-1-amine (**4-2e**),^[69b] (1-allylcyclohexyl)-*N*-benzylmethanamine,^[71b] *N*-benzyl-2,2-dimethylpent-4-en-1-amine,^[71b] 2-phenyl-2-(2-propenyl)-1-amino-4-pentene,^[64e] *N*-benzyl-2-isopropylpent-4-en-1-amine,^[71b] *N*-benzyl-2,2-diphenylhex-5-en-1-amine,^[69b] *N*-benzyl-4-methyl-2,2-diphenylpent-4-en-1-amine,^[84] benzyl[1-(2-methylallyl)-cyclohexylmethyl]amine,^{11a} *tert*-butyl-2,2-diphenylpent-4-enylcarbamate (**4-2f**),^[67a] (1-allylcyclohexyl)-*N*-phenylmethanamine,^[24a] *N*-phenyl-2,2-diphenylhex-5-en-1-amine,^[24a] and *N*-phenyl-4-methyl-2,2-diphenylpent-4-en-1-amine,^[24a] were synthesized according to literature procedures. All other reagents were used as received. ¹H and ¹³C NMR characterization data were collected at 300 K on a Bruker AV-500 spectrometer operating at 500.1 and 125.8 MHz (respectively) with chemical shifts reported in parts per million downfield of SiMe₄. Conductivity measurements were carried out on a VWR SympHony pH/Conductivity meter employing a VWR SympHony 4 carbon probe conductivity cell with 0.55 cm⁻¹ cell constant; calibrations were made with 1.12 microSeimens and 100,039 microSeimens Traceable conductivity solutions. The curve fittings were carried out using the program SigmaPlot for Windows v. 10.0 (Systat Software, San Jose, CA, USA). Mass

spectrometric data were acquired by Mr. Xiao Feng (Mass Spectrometry Laboratory, Dalhousie University).

4.4.2 Synthetic Details and Characterization Data

Preparation of *N*-Benzyl-2-Phenyl-2-(2-propenyl)-1-amino-4-pentene (Table 4-3, entry 8). The indicated compound was obtained in 80 % yield as a colorless oil by using the same procedure as was used for the preparation of *N*-benzyl-2,2-diphenylpent-4-en-1-amine.^[71b] The compound was purified by flash column chromatography on silica gel (hexane:EtOAc = 10:1). ¹H NMR (CDCl₃): δ 7.45-7.27 (m, 10H), 5.70 (m, 2H), 5.18-5.07 (m, 4H), 3.81 (s, 2H), 2.92 (s, 2H), 2.72-2.65 (m, 2H), 2.62-2.55 (m, 2H), 1.17 (s, 1H); ¹³C{¹H} NMR (CDCl₃): δ 144.9, 140.7, 134.6, 128.2, 128.1, 127.9, 126.8, 126.7, 125.9, 117.4, 55.9, 54.3, 44.9, 40.3. HRMS (ESI/[M+H]⁺) calcd. For C₂₁H₂₆N: 292.2060. Found: 292.2053.

Preparation of *N*-Benzyl-2,2-diphenyl-2-cyclohex-3-en-1-amine (Table 4-3, entry 13). The indicated compound was obtained in 95 % yield as a colorless oil by using the same procedure as was used for the preparation of *N*-benzyl-2,2-diphenylpent-4-en-1-amine.^[71b] The compound was purified by flash column chromatography on silica gel (hexane:EtOAc = 20:1). ¹H NMR (CDCl₃): δ 7.37-7.20 (m, 15H), 5.90 (m, 1H), 5.67 (m, 1H), 3.80-3.71 (m, 2H), 3.55 (m, 1H), 3.32 (m, 1H), 3.25 (m, 1H), 1.93 (m, 1H), 1.85-1.68 (m, 2H), 1.65-1.56 (m, 2H), 1.17-0.82 (m, 2H); ¹³C{¹H} NMR (CDCl₃): δ 145.2, 143.5, 140.6, 129.6, 129.5, 129.4, 128.5, 128.1, 127.8, 127.7, 127.0, 126.7, 125.9, 125.8, 56.2, 54.9, 54.0, 39.4, 25.0, 24.7, 22.4. HRMS (ESI/[M+H]⁺) calcd. For C₂₇H₂₉N: 368.2373. Found: 368.2380.

Preparation of (*E*)-*N*-Benzyl-2,2-diphenylhex-4-en-1-amine and (*Z*)-*N*-Benzyl-2,2-diphenylhex-4-en-1-amine (Table 4-3, entry 14). The indicated mixture of compounds was obtained in 94 % yield as a white solid by using the same procedure as was used for the preparation of *N*-benzyl-2,2-diphenylpent-4-en-1-amine.^[71b] The compound was purified by flash column chromatography on silica gel (hexane:EtOAc = 10:1). ¹H NMR (CDCl₃): δ 7.36-7.18 (m, 15H), 5.44 (m, 1H), 5.00 (m, 1H), 3.77 (s, 2H), 3.23 (s, 2H), 3.02-2.98 (m, 2H), 1.57-1.53 (m, 3H), 0.90 (br s, 1H); ¹³C{¹H} NMR

(CDCl₃): δ 147.1, 140.8, 128.1, 128.0, 127.9, 127.8, 126.9, 126.6, 125.8, 55.2, 54.2, 50.3, 40.3, 18.0. HRMS (ESI/[M+H]⁺) calcd. For C₂₅H₂₈N: 342.2216. Found: 342.2213.

General C-N coupling procedure for the preparation of N-(aryl)aminoalkenes. [Pd(cinnamyl)Cl]₂ (4.1 mg, 0.0080 mmol) and 2-(di-*tert*-butylphosphino)-*N,N*-dimethylaniline (8.3 mg, 0.031 mmol) were mixed in 4.200 mL toluene for 10 minutes. From this stock solution, 2.000 mL was added to a vial containing NaOtBu (173 mg, 1.8 mmol), followed by the addition of 2,2-diphenylpent-4-en-1-amine (380 mg, 1.58 mmol), 1.5 mmol of the corresponding aryl chloride or bromide and 1 mL of additional toluene. The vial was sealed with a cap containing a PTFE septum, heated at 110 °C and periodically monitored by TLC. Upon completion of the reaction, products were purified by column chromatography.

N-(4-methylphenyl)-2,2-diphenylpent-4-en-1-amine (Table 4-4, entry 5). From the corresponding aryl chloride, the product was isolated by flash column chromatography on silica gel (hexanes/EtOAc = 20:1) as a colorless solid in 82% yield. ¹H NMR (CDCl₃): δ 7.42-7.36 (m, 4H), 7.34-7.28 (m, 6H), 7.04 (d, ³J_{HH} = 8.0 Hz, 2H), 6.56 (d, ³J_{HH} = 8.5 Hz, 2H), 5.28 (m, 1H), 5.13-5.03 (m, 2H), 3.80 (s, 2H), 3.17 (br s, 1H), 3.10 (d, ³J_{HH} = 7.5 Hz, 2H), 2.30 (s, 3H); ¹³C{¹H} NMR (CDCl₃): δ 146.2, 145.8, 134.3, 128.6, 128.2, 128.0, 126.8, 126.4, 118.3, 113.3, 50.6, 50.0, 42.1, 20.3. HRMS (ESI/[M+H]⁺) calcd. For C₂₄H₂₆N: 328.2060. Found: 328.2040.

N-(4-methoxyphenyl)-2,2-diphenylpent-4-en-1-amine (Table 4-4, entry 6). From the corresponding aryl chloride, the product was isolated by flash column chromatography on silica gel (hexanes:EtOAc = 10:1 → 5:1) as a colorless solid in 68% yield. ¹H NMR (CDCl₃): δ 7.38-7.32 (m, 4H), 7.31-7.24 (m, 6H), 6.81-6.76 (m, 2H), 6.58-6.54 (m, 2H), 5.44 (m, 1H), 5.09-4.99 (m, 2H), 3.77 (s, 3H), 3.73 (s, 2H), 2.07 (d, ³J_{HH} = 7.0 Hz, 2H), 2.99 (br s, 1H); ¹³C{¹H} NMR (CDCl₃): δ 152.1, 145.9, 142.8, 134.6, 128.2, 128.0, 126.4, 118.3, 114.8, 114.5, 55.8, 51.4, 50.0, 42.1. HRMS (ESI/[M+H]⁺) calcd. For C₂₄H₂₆NO: 344.2009. Found: 344.1993.

N-(4-fluorophenyl)-2,2-diphenylpent-4-en-1-amine (Table 4-4, entry 7). From the corresponding aryl bromide, the product was isolated by flash column chromatography on silica gel (hexanes:EtOAc = 15:1) as a colorless oil that solidified as a white solid upon standing (60% yield). ¹H NMR (CDCl₃): δ 7.40-7.33 (m, 4H), 7.32-7.25

(m, 6H), 6.92-6.86 (m, 2H), 6.55-6.49 (m, 2H), 5.44 (m, 1H), 5.09-5.00 (m, 2H), 3.74 (d, $^3J_{\text{HH}} = 5.0$ Hz, 2H), 3.14 (br s, 1H), 3.06 (d, $J = 7.5$ Hz, 2H); $^{13}\text{C}\{^1\text{H}\}$ NMR (CDCl_3): δ 155.8 (d, $J = 234.6$ Hz), 145.7, 144.8, 134.2, 128.2, 128.0, 126.5, 118.4, 115.5 (d, $J = 22.8$ Hz), 113.9 (d, $J = 7.2$ Hz), 51.0, 50.0, 42.1. HRMS (ESI/[M+H] $^+$) calcd. For $\text{C}_{23}\text{H}_{23}\text{FN}$: 332.1809. Found: 332.1789.

Preparation of *N*-(4-Trifluoromethylphenyl)-2,2-diphenylpent-4-en-1-amine (Table 4-4, entry 8). From the corresponding aryl bromide, the product was isolated by flash column chromatography on silica gel (hexanes:EtOAc = 10:1 \rightarrow 5:1) as a colorless solid in 75% yield. ^1H NMR (CDCl_3): δ 7.44-7.35 (m, 6H), 7.34-7.26 (m, 6H), 6.59 (d, $^3J_{\text{HH}} = 10.0$ Hz, 2H), 5.43 (m, 1H), 5.09-5.02 (m, 2H), 3.82 (s, 2H), 3.63 (br s, 1H), 3.05 (d, $^3J_{\text{HH}} = 10.0$ Hz, 2H); $^{13}\text{C}\{^1\text{H}\}$ NMR (CDCl_3): δ 150.7, 145.3, 134.0, 128.4, 127.9, 126.6, 126.5, 126.4, 118.7, 112.1, 50.0, 49.6, 42.1. HRMS (ESI/[M+H] $^+$) calcd. For $\text{C}_{24}\text{H}_{23}\text{F}_3\text{N}$: 382.1777. Found: 382.1746.

Representative procedure for the intramolecular hydroamination of unactivated alkenes by secondary alkylamines (Table 4-3). To a screw-capped vial containing **4-2a** (82 mg, 0.25 mmol) and a stir-bar was added 0.125 mL of a stock solution of $[\text{Ir}(\text{COD})\text{Cl}]_2$ (2.6 mg, 0.0039 mmol) in 1.548 mL of 1,4-dioxane ($[\text{Ir}] = 0.005$ M) and 0.375 mL of dioxane (total reaction volume = 0.5 mL). The vial was sealed under N_2 with a cap containing a PTFE septum and, once all the material had dissolved, was removed from the glovebox and was placed in a temperature-controlled aluminum heating block set at 110 $^\circ\text{C}$. After 3 h of magnetic stirring the vial was removed from the temperature-controlled aluminum heating block, cooled to ambient temperature, diluted with CH_2Cl_2 (2 mL), and was washed with brine (2 x 5 mL). The organic extracts were combined, dried over Na_2SO_4 , and concentrated. The resulting residue was purified by flash column chromatography on silica gel (hexanes:EtOAc = 20:1) to yield **4-3a** as a white solid (72 mg, 0.22 mmol, 88 %) that afforded analytical data in agreement with data reported in the literature.^[71b]

1-Benzyl-2-methyl-4,4-diphenylpyrrolidine (entry 1). The indicated compound was purified by flash chromatography on silica gel (hexanes:EtOAc = 20:1) in a 88 % yield (72 mg) as a white solid.^[71b] ^1H NMR (CDCl_3): 7.53-7.19 (m, 15H), 4.21 (d, $^2J_{\text{HH}} = 13.5$ Hz, 1H), 3.77 (d, $^2J_{\text{HH}} = 9.5$ Hz, 1H), 3.38 (d, $^2J_{\text{HH}} = 13.5$ Hz, 1H), 3.07-2.89 (m,

3H), 2.34 (dd, $^2J_{\text{HH}} = 13.0$ Hz, $^3J_{\text{HH}} = 8.0$ Hz, 1H), 1.29 (d, $^3J_{\text{HH}} = 6.5$ Hz, 3H); $^{13}\text{C}\{^1\text{H}\}$ NMR (CDCl_3): 150.6, 148.7, 140.1, 128.6, 128.2, 128.1, 127.8, 127.4, 127.2, 126.7, 125.8, 125.4, 66.4, 59.6, 58.0, 52.5, 48.0, 19.5.

1-(4-Chlorobenzyl)-2-methyl-4,4-diphenylpyrrolidine (entry 2). The indicated compound was purified by flash chromatography on silica gel (pentane:Et₂O = 30:1) in an 85 % yield (77 mg) as a white solid.^[65a] ^1H NMR (CDCl_3): δ 7.43-7.17 (m, 14H), 4.12 (d, $^2J_{\text{HH}} = 13.5$ Hz, 1H), 3.71 (d, $^2J_{\text{HH}} = 10.0$ Hz, 1H), 3.33 (d, $^2J_{\text{HH}} = 13.5$ Hz, 1H), 3.05-2.89 (m, 2H), 2.87 (d, $^2J_{\text{HH}} = 9.5$ Hz, 1H), 2.33 (dd, $^2J_{\text{HH}} = 12.5$ Hz, $^3J_{\text{HH}} = 7.9$ Hz, 1H), 1.26 (d, $^3J_{\text{HH}} = 6.5$ Hz, 3H); $^{13}\text{C}\{^1\text{H}\}$ NMR (CDCl_3): δ 150.4, 148.6, 138.6, 132.4, 129.8, 128.3, 128.1, 127.8, 127.3, 127.1, 125.8, 125.5, 66.3, 59.6, 57.2, 52.5, 47.8, 19.5.

Methyl 4-(2-methyl-4,4-diphenylpyrrolidin-1-ylmethyl)-benzoate (entry 3). The indicated compound was purified by flash chromatography on silica gel (pentane:Et₂O = 8:1) in a 87 % yield (84 mg) as a colorless oil.^[71b] ^1H NMR (CDCl_3): δ 8.07 (d, $^3J_{\text{HH}} = 8.0$ Hz, 2H), 7.50 (d, $^3J_{\text{HH}} = 8.5$ Hz, 2H), 7.35-7.15 (m, 10H), 4.16 (d, $^2J_{\text{HH}} = 14.0$ Hz, 1H), 3.98 (s, 3H), 3.68 (d, $^2J_{\text{HH}} = 10.0$ Hz, 1H), 3.39 (d, $^2J_{\text{HH}} = 13.5$ Hz, 1H), 3.02-2.88 (m, 2H), 2.86 (d, $^2J_{\text{HH}} = 10.0$ Hz, 1H), 2.31 (dd, $^2J_{\text{HH}} = 13.0$ Hz, $^3J_{\text{HH}} = 7.5$ Hz, 1H), 1.23 (d, $^3J_{\text{HH}} = 5.5$ Hz, 3H); $^{13}\text{C}\{^1\text{H}\}$ NMR (CDCl_3): δ 167.1, 150.3, 148.5, 145.7, 129.6, 128.7, 128.4, 128.1, 127.8, 127.3, 127.1, 125.8, 125.5, 66.4, 59.7, 57.7, 52.6, 51.9, 47.8, 19.5.

1-(4-Methoxybenzyl)-2-methyl-4,4-diphenylpyrrolidine (entry 4). The indicated compound was purified by flash chromatography on silica gel (pentane:Et₂O = 15:1) in a 89 % yield (80 mg) as a colorless oil.^[65a] ^1H NMR (CDCl_3): δ 7.29 (m, 1H), 7.00-6.95 (m, 2H), 4.13 (d, $^2J_{\text{HH}} = 13.0$ Hz, 1H), 3.90 (s, 3H), 3.74 (d, $^2J_{\text{HH}} = 10.0$ Hz, 1H), 3.30 (d, $^2J_{\text{HH}} = 13.0$ Hz, 1H), 3.02 (dd, $^2J_{\text{HH}} = 13.0$ Hz, $^3J_{\text{HH}} = 7.5$ Hz, 1H), 2.96-2.85 (m, 2H), 2.30 (dd, $^2J_{\text{HH}} = 13.0$ Hz, $^3J_{\text{HH}} = 7.5$ Hz, 1H), 1.27 (d, $^3J_{\text{HH}} = 6.0$ Hz, 3H); $^{13}\text{C}\{^1\text{H}\}$ NMR (CDCl_3): δ 158.5, 150.6, 148.7, 132.0, 129.6, 128.1, 127.8, 127.4, 127.2, 125.7, 125.3, 113.5, 66.3, 59.5, 57.2, 55.2, 52.4, 48.0, 19.5.

1-Cyclohexylmethyl-2-methyl-4,4-diphenylpyrrolidine (entry 5). The indicated compound was purified by flash chromatography on silica gel (hexanes:EtOAc = 8:1) in a 88 % yield (73 mg) as a white solid.^[69b] ^1H NMR (CDCl_3): 7.38-7.21 (m, 9H), 7.16 (m, 1H), 3.87 (d, $^2J_{\text{HH}} = 9.5$ Hz, 1H), 2.87 (dd, $^2J_{\text{HH}} = 13.0$ Hz, $^3J_{\text{HH}} = 7.5$ Hz, 1H), 2.82 (d,

$^2J_{\text{HH}} = 10.0$ Hz, 1H), 2.66 (m, 1H), 2.56 (m, 1H), 2.18-2.03 (m, 3H), 1.82-1.63 (m, 4H), 1.53 (m, 1H), 1.36-1.15 (m, 3H), 1.10 (d, $^3J_{\text{HH}} = 6.0$ Hz, 3H), 1.02-0.87 (m, 2H); $^{13}\text{C}\{^1\text{H}\}$ NMR (CDCl_3): δ 151.3, 148.9, 128.1, 127.8, 127.6, 127.3, 125.7, 125.4, 67.6, 61.4, 60.3, 52.8, 48.1, 37.3, 32.2, 31.9, 26.9, 26.3, 26.1, 19.6.

2-Benzyl-3-methyl-2-aza-spiro[4,5]decane (entry 6). The indicated compound was purified by flash chromatography on silica gel (hexanes:EtOAc = 20:1) in a 86 % yield (52 mg) as a colorless oil. $^{[71b]}\text{H}$ NMR (CDCl_3): δ 7.40-7.24 (m, 5H), 4.06 (d, $^2J_{\text{HH}} = 13.0$ Hz, 1H), 3.14 (d, $^2J_{\text{HH}} = 13.5$ Hz, 1H), 2.82 (d, $^2J_{\text{HH}} = 9.5$ Hz, 1H), 2.54 (m, 1H), 1.91 (d, $^2J_{\text{HH}} = 9.5$ Hz, 1H), 1.80 (dd, $^2J_{\text{HH}} = 12.0$ Hz, $^3J_{\text{HH}} = 7.0$ Hz, 1H), 1.56-1.27 (m, 11H), 1.19 (d, $^3J_{\text{HH}} = 6.0$ Hz, 3H); $^{13}\text{C}\{^1\text{H}\}$ NMR (CDCl_3): δ 140.0, 128.6, 128.0, 126.5, 66.6, 59.0, 58.0, 47.0, 39.3, 39.2, 38.5, 26.1, 23.6, 23.5, 19.3.

1-Benzyl-2,4,4-trimethylpyrrolidine (entry 7). The indicated compound was purified by flash chromatography on silica gel (hexanes:EtOAc = 20:1) in a 84 % yield (42 mg) as a colorless oil. $^{[71b]}\text{H}$ NMR (CDCl_3): δ 7.39-7.23 (m, 5H), 4.05 (d, $^2J_{\text{HH}} = 14.5$ Hz, 1H), 3.15 (d, $^2J_{\text{HH}} = 13.5$ Hz, 1H), 2.67 (d, $^2J_{\text{HH}} = 9.0$ Hz, 1H), 2.59 (m, 1H), 1.98 (d, $^2J_{\text{HH}} = 9.0$ Hz, 1H), 1.76 (dd, $^2J_{\text{HH}} = 12.0$ Hz, $^3J_{\text{HH}} = 7.5$ Hz, 1H), 1.35 (dd, $^2J_{\text{HH}} = 12.5$ Hz, $^3J_{\text{HH}} = 9.0$ Hz, 1H), 1.19 (d, $^3J_{\text{HH}} = 6.0$ Hz, 3H), 1.11 (s, 3H), 1.01 (s, 3H); $^{13}\text{C}\{^1\text{H}\}$ NMR (CDCl_3): δ 140.1, 128.7, 128.0, 126.5, 68.4, 59.7, 58.0, 49.1, 35.4, 30.9, 29.2, 19.4.

1-Benzyl-4-allyl-2-methyl-4-phenyl-pyrrolidine (entry 8). The indicated compound was purified by flash chromatography on silica gel (hexanes:EtOAc = 10:1) in a 86 % yield (67 mg) as a colorless oil. The diastereomeric ratio was determined to be 1.7:1 on the basis of ^1H NMR integration of the crude product mixture prior to purification; the spectral data provided corresponds to the major diastereomer. ^1H NMR (CDCl_3): δ 7.51-7.38 (m, 4H), 7.36-7.30 (m, 3H), 7.26-7.15 (m, 3H), 5.48 (m, 1H), 5.02-4.94 (m, 2H), 4.17 (d, $^2J_{\text{HH}} = 13.4$ Hz, 1H), 3.25 (dd, $^2J_{\text{HH}} = 13.1$ Hz, $^3J_{\text{HH}} = 9.1$ Hz, 2H), 2.74-2.65 (m, 2H), 2.61-2.53 (m, 1H), 2.51-2.42 (m, 2H), 1.91 (dd, $^2J_{\text{HH}} = 12.5$ Hz, $^3J_{\text{HH}} = 7.7$ Hz, 1H), 1.34 (d, $^3J_{\text{HH}} = 6.0$ Hz, 3H); $^{13}\text{C}\{^1\text{H}\}$ NMR (CDCl_3): δ 148.0, 140.2, 135.5, 128.4, 128.1, 127.9, 126.8, 126.6, 125.5, 117.1, 63.9, 59.4, 57.8, 48.5, 47.4, 45.2, 20.2. HRMS (ESI/ $[\text{M}+\text{H}]^+$) calcd. For $\text{C}_{21}\text{H}_{26}\text{N}$: 292.2060. Found: 292.2046.

1-Benzyl-2-methyl-4-isopropylpyrrolidine (entry 9). The indicated compound was obtained in 81 % yield with a diastereomeric ratio of 1.5:1 on the basis of ^1H NMR using 1,4-bis(trifluoromethyl)benzene as an internal standard.^[71b]

1-Benzyl-2-methyl-5,5-diphenylpiperidine (entry 10). The indicated compound was purified by flash chromatography on silica gel (hexanes:EtOAc = 20:1) in a 72 % yield (62 mg) as a colorless oil.^[69b] ^1H NMR (CDCl_3): δ 7.46-7.14 (m, 15H), 4.13 (d, $^2J_{\text{HH}} = 13.5$ Hz, 1H), 3.43 (d, $^2J_{\text{HH}} = 12.5$ Hz, 1H), 3.21 (d, $^2J_{\text{HH}} = 13.5$ Hz, 1H), 3.60-2.50 (m, 3H), 2.25 (m, 1H), 1.70 (m, 1H), 1.45 (m, 1H), 1.21 (d, $^3J_{\text{HH}} = 6.0$ Hz, 3H); $^{13}\text{C}\{^1\text{H}\}$ NMR (CDCl_3): δ 148.6, 146.7, 139.4, 129.5, 128.4, 128.0, 127.9, 127.6, 127.0, 126.9, 125.6, 125.3, 61.0, 58.9, 56.1, 46.5, 34.2, 31.0, 18.6.

1-Benzyl-2,2-dimethyl-4,4-diphenylpyrrolidine (entry 11). The indicated compound was purified by flash chromatography on silica gel (hexanes:EtOAc = 20:1) in a 88 % yield (75 mg) as a white solid.^[84] ^1H NMR (CDCl_3): δ 7.52-7.20 (m, 15H), 3.73 (s, 2H), 3.41 (s, 2H), 2.74 (s, 2H), 1.26 (s, 6H); $^{13}\text{C}\{^1\text{H}\}$ NMR (CDCl_3): δ 149.7, 140.9, 128.5, 128.1, 127.8, 127.2, 126.7, 125.4, 6.1, 60.4, 54.4, 52.4, 51.6, 25.1.

2-benzyl-3,3-dimethyl-2-azaspiro[4.5]decane (entry 12). The indicated compound was purified by flash chromatography on silica gel (hexanes:EtOAc = 10:1) in a 74 % yield (48 mg) as a pale yellow oil.^[71b] ^1H NMR (CDCl_3): δ 7.47-7.20 (m, 5H), 3.56 (s, 2H), 2.46 (s, 2H), 1.60 (m, 10H), 1.14 (s, 6H); $^{13}\text{C}\{^1\text{H}\}$ NMR (CDCl_3): δ 141.6, 128.0, 127.9, 126.3, 62.7, 59.9, 53.7, 52.1, 39.1, 29.7, 26.0, 24.7, 23.7.

3,3-Diphenyl-1-benzyl-octahydro-indole (entry 13). The indicated compound was purified by flash column chromatography on silica gel (hexanes:EtOAc = 20:1) in a 88 % yield (81 mg) as a colorless oil. ^1H NMR (CDCl_3): δ 7.47-7.37 (m, 6H), 7.34-7.27 (m, 3H), 7.24-7.16 (m, 5H), 7.11 (m, 1H), 4.08-3.95 (m, 2H), 3.38 (d, $^2J_{\text{HH}} = 15.0$ Hz, 1H), 3.31 (d, $^2J_{\text{HH}} = 15.0$ Hz, 1H), 3.21 (m, 1H), 3.05 (m, 1H), 1.82 (m, 1H), 1.73-1.62 (m, 2H), 1.56 (m, 1H), 1.49-1.39 (m, 2H), 1.38-1.18 (m, 2H); $^{13}\text{C}\{^1\text{H}\}$ NMR (CDCl_3): δ 149.0, 146.0, 141.3, 128.3, 128.3, 128.2, 128.1, 127.7, 127.2, 126.6, 125.6, 125.3, 62.6, 62.1, 58.5, 57.1, 45.1, 27.2, 25.9, 25.0, 20.2. HRMS (ESI/[M+H]⁺) calcd. For $\text{C}_{27}\text{H}_{29}\text{N}$: 368.2373. Found: 368.2372.

2-Ethyl-1-benzyl-4,4-diphenylpyrrolidine (entry 14). The indicated compound was obtained in 52 % yield on the basis of ^1H NMR using 1,4-

bis(trifluoromethyl)benzene as an internal standard. The identity of the pyrrolidine was confirmed by use of GC-MS methods, as well as by comparison of ^1H NMR data for this product to data reported for an N-Me analog.^[69b]

Representative procedure for the intramolecular hydroamination of unactivated alkenes by arylamines (Table 4-4). To a screw-capped vial containing **4-4a** (78 mg, 0.25 mmol) and a stir-bar was added 0.5 mL of a stock solution of $[\text{Ir}(\text{COD})\text{Cl}]_2$ (5.7 mg, 0.0085 mmol) in 1.357 mL of 1,4-dioxane ($[\text{Ir}] = 0.0125 \text{ M}$). The vial was sealed under N_2 with a cap containing a PTFE septum and, once all the material had dissolved, was removed from the glovebox and was placed in a temperature-controlled aluminum heating block set at 110°C . After 7 h of magnetic stirring the vial was removed from the temperature-controlled aluminum heating block, cooled to ambient temperature, diluted with CH_2Cl_2 (2 mL), and was washed with brine (2 x 5 mL). The organic extracts were combined, dried over Na_2SO_4 , and concentrated. The resulting residue was purified by flash column chromatography on silica gel (hexanes:EtOAc = 10:1) to afford **4-5a** as a colorless oil that solidified to a white solid upon standing (74 mg, 0.22 mmol, 95 %), and for which obtained characterization data agreed with data reported in the literature.^[69c]

1-Phenyl-2-methyl-4,4-diphenylpyrrolidine (entry 1). The indicated compound was purified by flash chromatography on silica gel (hexanes:EtOAc) = 10:1) in a 95 % yield (74 mg) as a colorless oil that solidified to white solid upon standing.^[69c] ^1H NMR (CDCl_3): δ 7.45-7.36 (m, 6H), 7.35-7.26 (m, 3H), 7.25-7.15 (m, 3H), 6.85 (m, 1H), 6.82-6.78 (m, 2H), 4.21-4.14 (m, 2H), 3.88 (m, 1H), 2.91 (m, 1H), 2.61 (m, 1H), 1.32 (d, $^3J_{\text{HH}} = 6.0 \text{ Hz}$, 3H); $^{13}\text{C}\{^1\text{H}\}$ NMR (CDCl_3): δ 147.0, 146.9, 146.6, 129.1, 128.3, 128.2, 127.1, 126.7, 126.3, 126.0, 116.1, 113.0, 60.1, 52.8, 52.4, 46.8, 19.6.

1-(4-Methylphenyl)-2-methyl-4,4-diphenylpyrrolidine (entry 5). The indicated compound was purified by flash column chromatography on silica gel (hexanes:EtOAc = 10:1) in a 96 % yield (79 mg) as a white solid. ^1H NMR (CDCl_3): δ 7.40-7.35 (m, 4H), 7.31-7.22 (m, 3H), 7.20-7.10 (m, 5H), 6.70-6.66 (m, 2H), 4.12-4.07 (m, 2H), 3.80 (m, 1H), 2.84 (dd, $^2J_{\text{HH}} = 11.5 \text{ Hz}$, $^3J_{\text{HH}} = 7.0 \text{ Hz}$, 1H), 2.55 (dd, $^2J_{\text{HH}} = 12.0 \text{ Hz}$, $^3J_{\text{HH}} = 8.0 \text{ Hz}$, 1H), 2.36 (s, 3H), 1.25 (d, $^3J_{\text{HH}} = 5.5 \text{ Hz}$, 3H); $^{13}\text{C}\{^1\text{H}\}$ NMR (CDCl_3): δ 147.1, 146.8, 144.9, 129.6, 128.3, 128.2, 127.2, 126.8, 126.3, 126.0, 125.1, 113.0, 60.4, 52.8,

52.5, 46.9, 20.3, 19.6. HRMS (ESI/[M+H]⁺) calcd. For C₂₄H₂₆N: 328.2060. Found: 328.2052.

1-(4-Methoxyphenyl)-2-methyl-4,4-diphenylpyrrolidine (entry 6). The indicated compound was purified by flash column chromatography on silica gel (hexanes:EtOAc = 6:1) in a 94 % yield (81 mg) as a colorless oil. ¹H NMR (CDCl₃): δ 7.38-7.32 (m, 4H), 7.31-7.14 (m, 4H), 7.11-7.07 (m, 2H), 6.95-6.90 (m, 2H), 6.71-6.66 (m, 2H), 4.11-4.02 (m, 2H), 3.84 (s, 3H), 3.74 (m, 1H), 2.80 (dd, ²J_{HH} = 12.5 Hz, ³J_{HH} = 7.0 Hz, 1H), 2.53 (dd, ²J_{HH} = 12.0 Hz, ³J_{HH} = 8.0 Hz, 1H), 1.22 (d, ³J_{HH} = 6.0 Hz, 3H); ¹³C{¹H} NMR (CDCl₃): δ 151.1, 147.2, 146.8, 141.9, 128.3, 128.2, 127.2, 126.8, 126.3, 126.0, 114.9, 113.9, 61.0, 55.8, 52.9, 52.7, 46.9, 19.7. HRMS (ESI/[M+H]⁺) calcd. For C₂₄H₂₆NO: 344.2009. Found: 344.2003.

1-(4-Fluorophenyl)-2-methyl-4,4-diphenylpyrrolidine (entry 7). The indicated compound was purified by flash column chromatography on silica gel (hexanes:EtOAc = 10:1) in a 95 % yield (79 mg) as a colorless oil that solidified as a white solid upon standing. ¹H NMR (CDCl₃): δ 7.41-7.34 (m, 4H), 7.31-7.22 (m, 3H), 7.19 (m, 1H), 7.13-7.09 (m, 2H), 7.08-7.02 (m, 2H), 6.68-6.63 (m, 2H), 4.11-4.08 (m, 2H), 3.75 (m, 1H), 2.84 (dd, ²J_{HH} = 12.0 Hz, ³J_{HH} = 6.0 Hz, 1H), 2.57 (dd, ²J_{HH} = 12.0 Hz, ³J_{HH} = 8.0 Hz, 1H), 1.25 (d, ³J_{HH} = 6.0 Hz, 3H); ¹³C{¹H} NMR (CDCl₃): δ 155.1 (d, *J* = 234.0 Hz), 146.9, 146.5, 143.7, 128.4, 128.3, 127.1, 126.7, 126.4, 126.1, 115.5 (d, *J* = 21.6 Hz), 113.5 (d, *J* = 7.2 Hz), 60.8, 52.9, 52.7, 46.9, 19.5. HRMS (ESI/[M+H]⁺) calcd. For C₂₃H₂₃FN: 332.1809. Found: 332.1805.

1-(4-Trifluoromethyl)-2-methyl-4,4-diphenylpyrrolidine (entry 8). The indicated compound was obtained in 67 % yield on the basis of ¹H NMR using 1,4-bis(trifluoromethyl)benzene as an internal standard. The identity of the pyrrolidine was confirmed by comparison of ¹H NMR data for this product to data reported for an N-Ph analog.^[69c]

2-Phenyl-3-methyl-2-aza-spiro[4,5]decane (entry 9). The indicated compound was purified by flash column chromatography on silica gel (hexanes:EtOAc = 20:1) in a 95 % yield (54 mg) as a colorless oil. ¹H NMR (CDCl₃): δ 7.34-7.25 (m, 2H), 6.76-6.64 (m, 3H), 3.95 (m, 1H), 3.30 (m, 2H), 2.18 (dd, ²J_{HH} = 12.8 Hz, ³J_{HH} = 6.5 Hz, 1H), 1.72-1.37 (m, 11H), 1.32 (d, ³J_{HH} = 6.2 Hz, 3H); ¹³C{¹H} NMR (CDCl₃): δ 148.0, 128.9,

115.3, 112.6, 60.3, 52.4, 46.4, 41.1, 37.3, 36.2, 26.2, 23.9, 23.3, 20.3. HRMS (ESI/[M+H]⁺) calcd. For C₁₆H₂₄N: 230.1903. Found: 230.1902.

Representative procedure for the intramolecular hydroamination of unactivated alkenes by primary amines (Table 4-5). To a screw-capped vial containing 2,2-diphenylpent-4-en-1-amine (59 mg, 0.25 mmol), triethylammonium chloride (1.7 mg, 0.0125 mmol) and a stir-bar was added 0.5 mL of a stock solution of [Ir(COD)Cl]₂ (21 mg, 0.031 mmol) in 2.548 mL of 1,4-dioxane ([Ir] = 0.025 M). The vial was sealed under N₂ with a cap containing a PTFE septum and, once all the material had dissolved, was removed from the glovebox and was placed in a temperature-controlled aluminum heating block set at 110 °C. After 24 h of magnetic stirring the vial was removed from the temperature-controlled aluminum heating block, cooled to ambient temperature, diluted with CH₂Cl₂ (2 mL), and was washed with brine (2 x 5 mL). The organic extracts were combined, dried over Na₂SO₄, and concentrated. The resulting residue was purified by flash column chromatography on silica gel (CH₂Cl₂:MeOH = 10:1) to yield 2-methyl-4,4-diphenylpyrrolidine as a pale yellow oil (53 mg, 0.22 mmol, 89 %) that afforded analytical data in agreement with data reported in the literature.^[69b]

2-Methyl-4,4-diphenylpyrrolidine (entry 1). The indicated compound was purified by flash column chromatography on silica gel (CH₂Cl₂:MeOH = 10:1) in a 89 % yield (53 mg) as a colorless oil.^[69b] ¹H NMR (CDCl₃): δ 7.34-7.26 (m, 8H), 7.23-7.18 (m, 2H), 3.73 (d, ²J_{HH} = 11.0 Hz, 1H), 3.52 (d, ²J_{HH} = 11.0 Hz, 1H), 3.42 (m, 1H), 2.79 (dd, ²J_{HH} = 10.0 Hz, ³J_{HH} = 6.5 Hz, 1H), 2.19-2.03 (m, 2H), 1.26 (d, ³J_{HH} = 6.0 Hz, 3H); ¹³C{¹H} NMR (CDCl₃): δ 147.8, 147.1, 128.3, 128.2, 127.0, 126.9, 126.0, 125.9, 57.9, 57.3, 53.1, 47.1, 22.3.

2-Methyl-5,5-diphenylpiperidine (entry 2). The indicated compound was purified by flash column chromatography on silica gel (CH₂Cl₂:MeOH = 10:1) in a 84 % yield (53 mg) as a colorless oil.^[69b] ¹H NMR (CDCl₃): δ 7.50-7.44 (m, 2H), 7.43-7.36 (m, 2H), 7.33-7.13 (m, 6H), 3.97 (dd, ²J_{HH} = 13.7 Hz, ³J_{HH} = 3.1 Hz, 1H), 3.17 (d, ²J_{HH} = 13.7 Hz, 1H), 2.83 (m, 1H), 2.76 (m, 1H), 2.27 (dt, ²J_{HH} = 13.4 Hz, ³J_{HH} = 3.8 Hz, 1H), 1.69 (m, 1H), 1.38 (s, 1H), 1.21 (m, 1H), 1.07 (d, ³J_{HH} = 6.3 Hz, 3H); ¹³C{¹H} NMR (CDCl₃): δ 148.8, 144.7, 128.6, 128.2, 128.1, 126.4, 125.7, 125.6, 55.8, 52.3, 45.2, 35.4, 31.7, 22.4.

2,3-Dimethyl-2-aza-spiro[4,5]decane (entry 3). The indicated compound was obtained in 75 % yield on the basis of ^1H NMR using 1,4-bis(trifluoromethyl)benzene as an internal standard.^[69b]

2,2-Methyl-4,4-diphenylpyrrolidine (entry 4). The indicated compound was purified by flash column chromatography on silica gel ($\text{CH}_2\text{Cl}_2:\text{MeOH} = 10:1$) in a 84 % yield (53 mg) as a faint yellow oil.^[69b] ^1H NMR (CDCl_3): δ 7.37-7.28 (m, 8H), 7.22-7.16 (m, 2H), 3.69 (s, 2H), 2.59 (s, 2H), 1.95 (br s, 1H), 1.20 (s, 6H); $^{13}\text{C}\{^1\text{H}\}$ NMR (CDCl_3): δ 147.5, 128.4, 126.9, 125.9, 59.3, 58.3, 57.2, 52.0, 30.7.

Representative procedure for determining the effect of added salts (Figure 4-2). To five screw-capped vials containing **4-2a** (41 mg, 0.125 mmol) and a stir-bar was added 0.25 mL of a stock solution of $[\text{Ir}(\text{COD})\text{Cl}]_2$ (3.4 mg, 0.0050 mmol) and LiOTf (1.6 mg, 0.010 mmol) in 4.000 mL of 1,4-dioxane ($[\text{Ir}] = [\text{LiOTf}] = 0.0025 \text{ M}$). The vials were sealed under N_2 with a cap containing a PTFE septum and, once all the material had dissolved, were removed from the glovebox and were placed in a temperature-controlled aluminum heating block set at 110 °C. A vial was removed from the heating block every 20 min (0.33 – 1.66 h) followed by rapid cooling in an ice bath, removal of the solvent under reduced pressure, and dissolution into CDCl_3 . The consumption of substrate **4-2a** and the appearance of the product **4-3a** were quantified by integration of the alkene resonances of the ^1H NMR spectrum relative to 1,4-bis(trifluoromethyl)benzene as an internal standard.

Determination of reaction order in 4-L2 for $[\text{Ir}(\text{COD})\text{Cl}]_2$ -catalyzed hydroamination (Figure 4-3). To five screw-capped vials containing **4-2a** (41 mg, 0.125 mmol) and a stir-bar was added 0.25 mL of a stock solution of $[\text{Ir}(\text{COD})\text{Cl}]_2$ (12.7 mg, 0.0189 mmol) and **4-L2** (33.8 mg, 0.113 mmol) in 1.512 mL of 1,4-dioxane ($[\text{Ir}] = 0.025 \text{ M}$; $[\text{4-L2}] = 3[\text{Ir}]$). The vials were sealed under N_2 with a cap containing a PTFE septum and, once all the material had dissolved, were removed from the glovebox and were placed in a temperature-controlled aluminum heating block set at 65 °C. A vial was removed from the heating block every 1.5-2 h (up to 8 h) followed by rapid cooling in an ice bath, removal of the solvent under reduced pressure, and dissolution into CDCl_3 . The consumption of substrate **4-2a** and the appearance of the product **4-3a** were quantified by

integration of the alkene resonances of the ^1H NMR spectrum relative to 1,4-bis(trifluoromethyl)benzene as an internal standard. Pseudo-first order rate constants were obtained by plotting $\ln[\mathbf{4-2a}]_t$ vs. time (in all cases these gave linear plots). The k_{obs} values obtained in these experiments were plotted versus $[\mathbf{4-L2}]$ to determine the reaction order in added phosphine ligand at 65 °C (Figure S2). According to Figure 4-3, an inverse-order in $\mathbf{4-L2}$ was determined at 65 °C. Given that when 2.5 mol% $[\text{Ir}(\text{COD})\text{Cl}]_2$ was used at 110 °C the reaction rates were difficult to measure reproducibly, the reaction order in $\mathbf{4-L2}$ was determined using 0.5 mol% $[\text{Ir}(\text{COD})\text{Cl}]_2$ to be zero-order with varied $[\mathbf{4-L2}]$ (Figure 4-3).

Representative procedure for the determination of the rate of reaction (k_{obs}) for the hydroamination of $\mathbf{4-2a}$ with $[\text{Ir}(\text{COD})\text{Cl}]_2$ (Figure 4-4a). To eight screw-capped vials containing $\mathbf{4-2a}$ (41 mg, 0.125 mmol) and a stir-bar was added 0.25 mL of a stock solution of $[\text{Ir}(\text{COD})\text{Cl}]_2$ (7.1 mg, 0.011 mmol) in 4.227 mL of 1,4-dioxane ($[\text{Ir}] = 0.005 \text{ M}$). The vials were sealed under N_2 with a cap containing a PTFE septum and, once all the material had dissolved, were removed from the glovebox and were placed in a temperature-controlled aluminum heating block set at 110 °C. A vial was removed from the heating block every 20 min (0.33 – 2.33 h) followed by rapid cooling in an ice bath, removal of the solvent under reduced pressure, and dissolution into CDCl_3 . The consumption of substrate $\mathbf{4-2a}$ and the appearance of the product $\mathbf{4-3a}$ were quantified by integration of the alkene resonances of the ^1H NMR spectrum relative to 1,4-bis(trifluoromethyl)benzene as an internal standard. Rate constants (k_{obs}) were obtained through plots of $\ln[\mathbf{4-2a}]_t$ versus time (Figure 4-4a).

Determination of reaction order in catalyst for $[\text{Ir}(\text{COD})\text{Cl}]_2$ -catalyzed hydroamination (Figure 4-4b). Pseudo-first order rate constants were obtained by plotting $\ln[\mathbf{4-2a}]_t$ vs. time (in all cases these gave linear plots) for a series of experiments with varied $[\text{Ir}]$ (0.001 – 0.00475 M). The k_{obs} values obtained in these experiments were plotted versus $[\text{Ir}]$ to determine the reaction order in catalyst (Figure 4-4b).

Determination of reaction order in substrate ($\mathbf{4-2a}$) for $[\text{Ir}(\text{COD})\text{Cl}]_2$ -catalyzed hydroamination (Figure 4-4c). Pseudo-first order rate constants were obtained by plotting $\ln[\mathbf{4-2a}]_t$ vs. time (in all cases these gave linear plots) for a series of experiments with varied $[\mathbf{4-2a}]$ (0.02 – 0.15 M). The k_{obs} values obtained in these

experiments were plotted vs. [4-2a] to determine the reaction order in substrate (4-2a) (Figure 4-4c).

General procedure for the Hammett study with *para*-substituted arylamine substrates (Figure 4-5). To five screw-capped vials containing substrate (4-4a – 4-4e) (0.125 mmol) and a stir-bar was added 0.25 mL of a stock solution of [Ir(COD)Cl]₂ in 1,4-dioxane ([Ir] = 0.005 M). The vials were sealed under N₂ with a cap containing a PTFE septum and, once all the material had dissolved, were removed from the glovebox and were placed in a temperature-controlled aluminum heating block set at 110 °C. A vial was removed from the heating block every 20 min (0.33 – 1.66 h) followed by rapid cooling in an ice bath, removal of the solvent under reduced pressure, and dissolution into CDCl₃. The consumption of substrate (4-4a – 4-4e) and the appearance of the product (4-5a – 4-5e) were quantified by integration of the alkene resonances of the ¹H NMR spectrum relative to 1,4-bis(trifluoromethyl)benzene as an internal standard. Rate constants (*k*_{obs}) were obtained through plots of ln[4-4a – 4-4e]_t versus time (in all cases gave linear plots). A plot of log(*k*_{obsX}/*k*_{obsH}) versus σ_p generated a linear plot and a ρ value of -2.4(2) (Figure 4-5).

Determination of kinetic isotope effect (KIE) for [Ir(COD)Cl]₂-catalyzed hydroamination of 4-2a (Figure 4-6). Using the general procedure, pseudo-first order rate constants were obtained by plotting ln[4-2a]_t vs. time (or ln[4-2a-*d*₁]_t vs. time); in all cases these gave linear plots. The *k*_{obs} values obtained in these experiments were used to determine the H/D KIE (Figure 4-6).

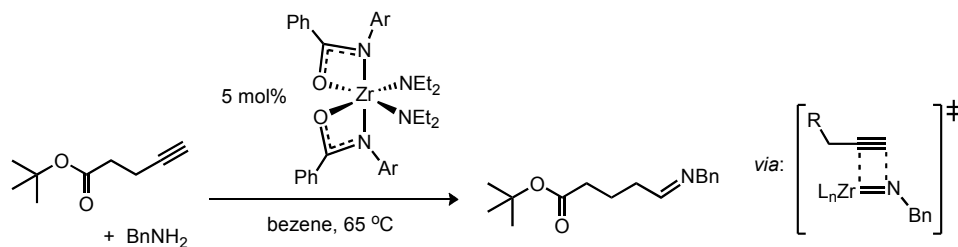
General procedure for the determination of activation parameters for the hydroamination of 4-2a employing [Ir(COD)Cl]₂ as a precatalyst (Figure 4-7). To five screw-capped vials containing 4-2a (0.125 mmol) and a stir-bar was added 0.25 mL of a stock solution of [Ir(COD)Cl]₂ in 1,4-dioxane ([Ir] = 0.005 M). The vials were sealed under N₂ with a cap containing a PTFE septum and, once all the material had dissolved, were removed from the glovebox and were placed in a temperature-controlled aluminum heating block set at desired temperature (90-130 °C). A vial was removed from the heating block every 20 min (0.33 – 1.66 h) followed by rapid cooling in an ice bath, removal of the solvent under reduced pressure, and dissolution into CDCl₃. The consumption of substrate 4-2a and the appearance of the product 4-3a were quantified by

integration of the alkene resonances of the ^1H NMR spectrum relative to 1,4-bis(trifluoromethyl)benzene as an internal standard. Pseudo-first order rate constants were obtained by plotting $\ln[\mathbf{4-2a}]_t$ vs. time (in all cases these gave linear plots). The k_{obs} values obtained in these experiments were used in Eyring and Arrhenius plots to determine the activation parameters for the hydroamination of $\mathbf{4-2a}$ with $[\text{Ir}(\text{COD})\text{Cl}]_2$ (Figure 4-7).

Chapter 5 – Gold-Catalyzed Intermolecular Hydroamination of Internal Alkynes with Dialkylamines: Scope and Mechanistic Studies

5.1 Introduction

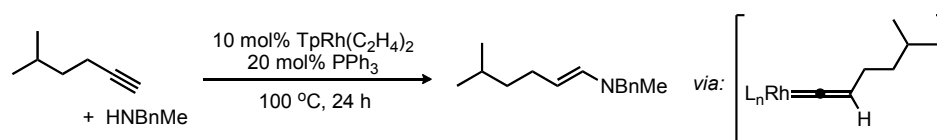
The intermolecular hydroamination of alkynes^[5a, 58a, 58d, 58o] with primary and secondary alkylamines represents an appealing method for the synthesis of highly functionalized imine or enamine products that are poised for further synthetic manipulations.^[85] However, the lack of general methods for mediating these transformations has rendered this strategy underutilized in synthesis. The use of Ti- and Zr-based catalysts for the addition of primary alkylamines to both terminal and internal alkynes is well documented in the hydroamination literature.^[86] However, the substrate scope displayed by such catalysts is often limited due to the intermediacy of Zr-imido species that can only be accessed from primary amine substrates. Such Zr-imido complexes affect alkyne hydroamination by way of a cycloaddition pathway, as represented in Scheme 5-1. As such, these catalysts exhibit characteristically poor performance for dialkylamine and internal alkyne pairings.^[86a, 86b]



Scheme 5-1. A representative example of the Zr-mediated hydroamination of terminal alkynes with primary amines proceeding through a Zr-imido intermediate (Ar = 2,6-diisopropylphenyl).

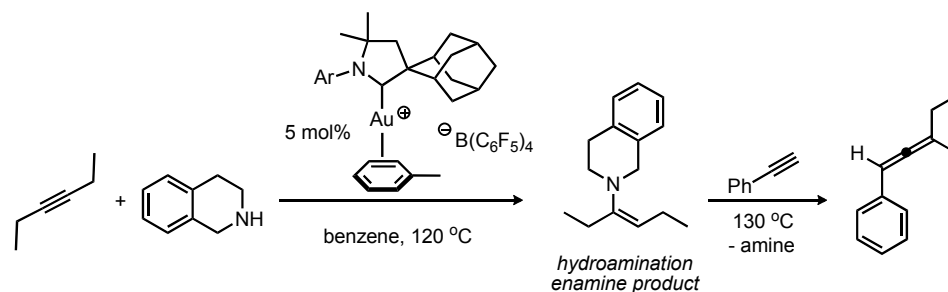
Although progress has been made for late metal-mediated intermolecular additions of anilines, amides, sulfonamides, substituted hydrazines, and carbamates to alkynes,^[87] the identification of catalysts capable of promoting the addition of more basic alkylamines to alkynes has proven to be significantly more challenging. In fact, the intermolecular metal-mediated addition of secondary alkylamines to alkynes is limited to only two systems. Using TpRh(C₂H₄)₂/PPh₃ (Tp = trispyrazolylborate) as a catalyst

mixture, exclusive anti-Markovnikov regioselectivity was observed for the hydroamination of terminal alkynes with a limited selection of primary and secondary alkylamines.^[88] Subsequent reduction of these linear imine and enamine products provided access to saturated secondary and tertiary amine products. However, attempts to expand the scope of this reaction to include internal alkynes were unsuccessful. In order to provide a rationale for this observation, it was proposed that the intermediacy of a rhodium-vinylidene species represented a crucial intermediate in this catalysis, thereby precluding the use of internal alkynes (Scheme 5-2).



Scheme 5-2. TpRh/PPh₃-mediated hydroamination of terminal alkynes with primary and secondary alkylamines proceeding through a proposed rhodium-vinylidene intermediate (Tp = trispyrazolylborate).

There has only been one catalyst system reported that is capable of the hydroamination of internal alkynes with secondary alkylamines. Employing a cationic gold complex featuring a CAAC ancillary ligand (CAAC = cyclic(alkyl)(amino)carbene),^[89] the addition of Et₂NH and 1,2,3,4-tetrahydroisoquinoline to diphenylacetylene, 3-hexyne, and 1-phenyl-1-propyne has been reported, where in the latter example negligible regioselectivity was observed.^[90] These initial hydroamination reactions were used to access reactive enamine intermediates that were capable of further reactivity in the synthesis of allenes from two alkynes and a sacrificial amine (Scheme 5-3).^[90a] In this regard, the intermolecular addition of dialkylamines to a range of internal alkynes featuring a diverse substrate scope and with controlled regioselectivity represents an unmet challenge in hydroamination catalysis.



Scheme 5-3. Au-mediated synthesis of allenes by intermediate hydroamination of internal alkynes with secondary alkylamines (Ar = 2,6-diisopropylphenyl).

In this context, the content of Chapter 5 describes the use of a P,N-ligand to support a gold complex as a state-of-the-art pre-catalyst for the hydroamination of symmetrical and unsymmetrical internal alkynes with a variety of secondary dialkylamines with controlled regioselectivity. Furthermore, preliminary kinetic and stoichiometric investigations into the mechanism of this reaction will be discussed.

5.2 Results and Discussion

5.2.1 Catalyst Optimization Studies: Ligand, Solvent, and Salt Effects

Inspired by the seminal work of Bertrand and co-workers in this field,^[89-90] the pursuit of a general catalyst for the hydroamination of a range of functionalized dialkylamines with internal alkynes was undertaken. Studies were initiated by evaluating a series of P,N-substituted phenylene ligands developed in the Stradiotto laboratory,^[20a, 24] as well as other ligand motifs that have been employed successfully in Au-mediated hydroamination reactions, for the addition of morpholine to diphenylacetylene. The test reaction conditions selected for this initial catalyst screen employed 5 mol% Au(SMe₂)Cl, 5 mol% LiB(C₆F₅)₄•2.5OEt₂, and 6 mol% ligand at 110 °C in 1,4-dioxane for 1 h; the conversion of diphenylacetylene to the corresponding enamine was determined on the basis of GC data relative to dodecane as an internal standard against a calibration curve (Figure 5-1).

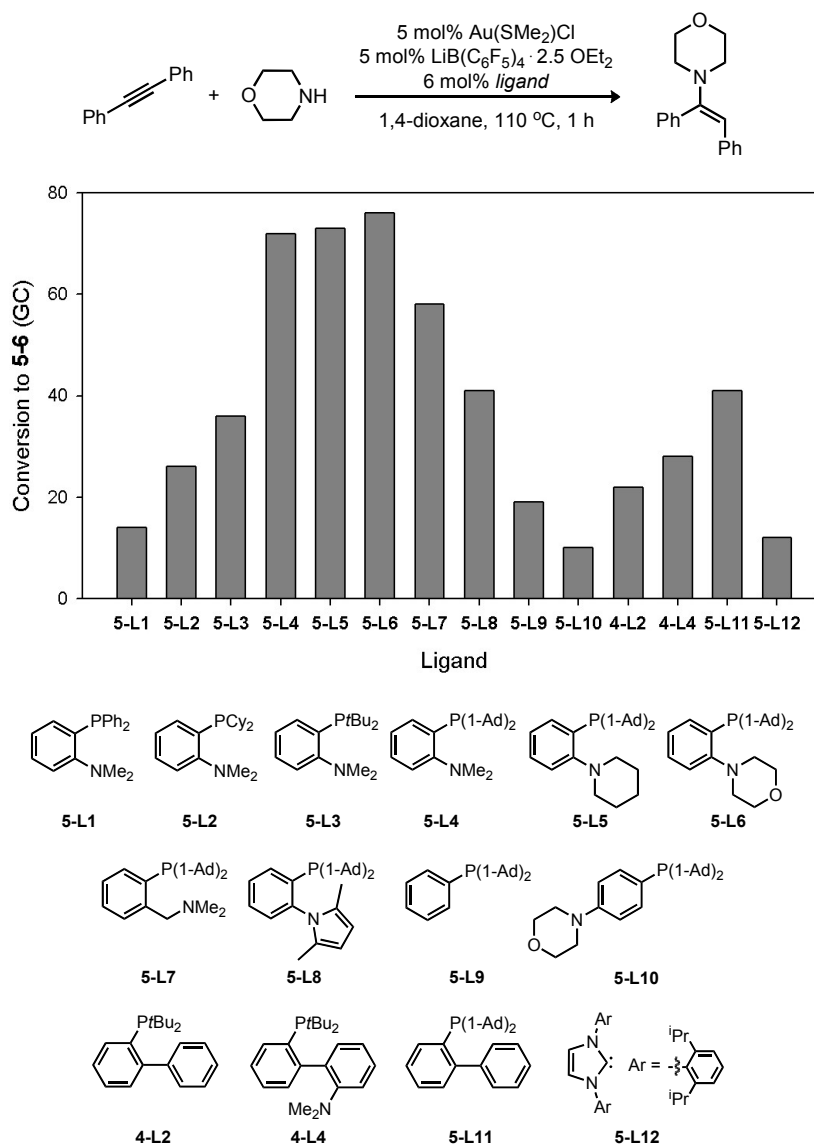


Figure 5-1. Ligand screen for the Au-catalyzed hydroamination of diphenylacetylene with morpholine. Conditions: alkyne:amine:(Me₂S)AuCl:L:LiB(C₆F₅)₄•2.5OEt₂ = 1:1:0.05:0.06:0.05 (0.3 mmol of alkyne) in 0.3 mL of 1,4-dioxane at 110 °C for 1 h. Yield of enamine determined by GC analysis.

Although P,N-ligands with Ph, Cy, or *t*Bu substituted phosphines provided modest conversions, those featuring a bulky, electron rich di(1-adamantyl)phosphino group and an *ortho*-dialkylamino donor (**5-L4**, **5-L5**, or **5-L6**) provided the highest yields of the desired enamine product. Replacement of the *ortho*-amine for a benzylic amine (**5-L7**), lowering the basicity of the nitrogen (**5-L8**), removing the pendant nitrogen moiety (**5-L9**), or positioning the nitrogen donor in the *para*-position (**5-L10**) were all deleterious to catalyst activity. In combination, these results suggest that the *ortho*-amine fragment in **5-**

L4, **5-L5**, and **5-L6** may play a direct role in the observed hydroamination catalysis.^[91] Alternatively, using the ligands *t*Bu-JohnPhos (**4-L2**), *t*Bu-DavePhos (**4-L4**), P(Ad)₂(*o*-biphenyl) (**5-L11**) or IPr (**5-L12**) gave comparatively poor results. The test reaction also proved to be highly sensitive to the nature of the chloride-abstracting metal salt, whereby AgB(C₆F₅)₄ provided superior conversions versus more commonly used activators in Au-catalysis, such as triflate and triflimide salts (Figure 5-2). Furthermore, when employing [(**5-L6**)AuCl] (**5-1**) as a pre-catalyst, toluene or 1,4-dioxane could be used interchangeably as the reaction solvent, whereas the use of chlorinated solvents such as 1,2-dichloroethane (DCE) or highly polar solvents such as *N,N*-dimethylacetamide (DMA), dimethylsulfoxide (DMSO), or *N,N*-dimethylformamide (DMF) inhibited the Au-mediated hydroamination reaction.

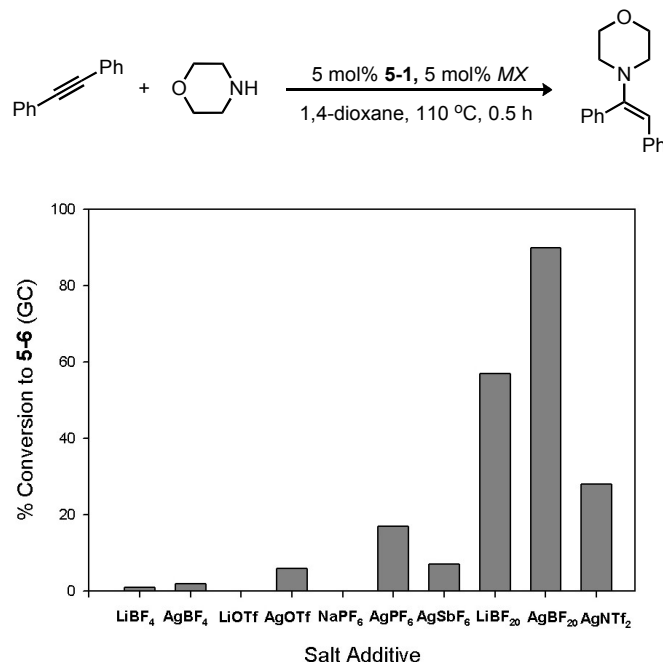


Figure 5-2. Salt effects for the Au-catalyzed hydroamination of diphenylacetylene with morpholine. Conditions: alkyne:amine:[(**L6**)AuCl]:M⁺X⁻ = 1:1:0.05:0.05 (0.3 mmol of alkyne) in 0.3 mL of dioxane at 110 °C for 0.5 h. Yield of enamine determined by GC analysis (BF₂₀ = B(C₆F₅)₄).

Monitoring the initial reaction kinetics for the test reaction using pre-formed complexes **5-1**, [(**5-L11**)AuCl] (**5-2**), and [(**5-L12**)AuCl] (**5-3**) in the presence of AgB(C₆F₅)₄ demonstrated that the discrepancy between the performance of these ligands, under the test conditions selected, is a consequence of the higher initial rates of reaction

that are achieved when using **5-1**, rather than differences in catalyst lifetime (Figure 5-3). As such, catalytic mixtures of **5-1** and $\text{AgB}(\text{C}_6\text{F}_5)_4$ in toluene or 1,4-dioxane were employed for all subsequent catalytic studies.

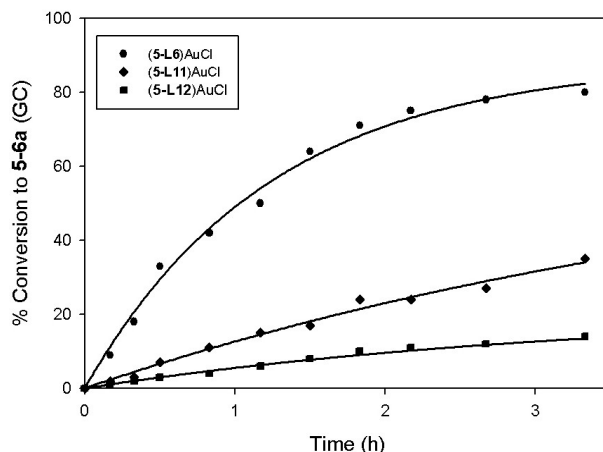


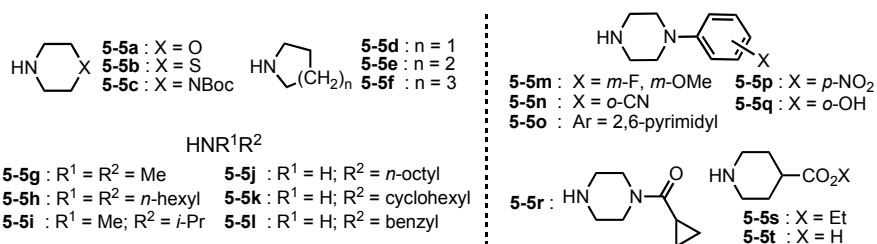
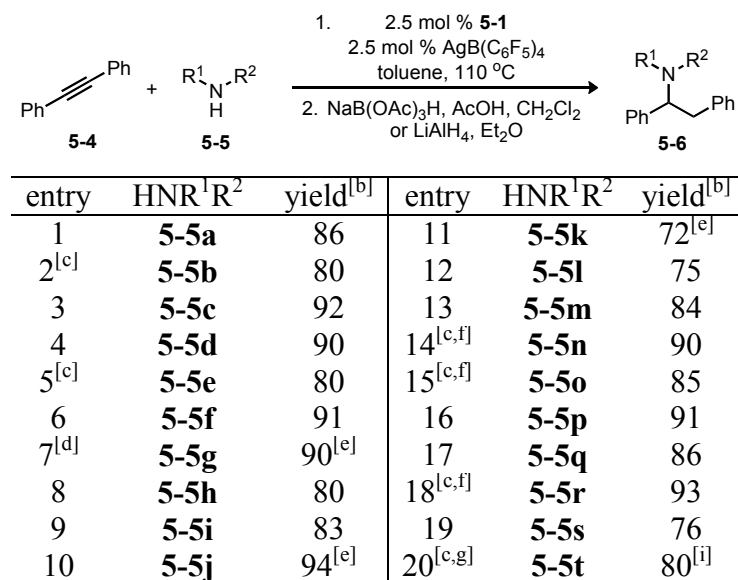
Figure 5-3. Comparison of the initial rates of reaction for the Au-catalyzed hydroamination of diphenylacetylene with morpholine using **5-1** (top), **5-2** (middle), and **5-3** (bottom).

5.2.2 Substrate Scope for the Au-Catalyzed Addition of Dialkylamines to Internal Alkynes

The scope of the hydroamination of diphenylacetylene with a diversity of functionalized dialkylamines, as well as primary alkylamines, using catalytic mixtures of **5-1** and $\text{AgB}(\text{C}_6\text{F}_4)_5$ was explored (Table 5-1). To simplify isolation and purification, the enamine or imine products were isolated as the corresponding amines after *in situ* reduction with $\text{NaB}(\text{OAc})_3\text{H}/\text{AcOH}$ or LiAlH_4 , respectively. The addition of cyclic secondary alkylamines containing ether, sulfide, or N-Boc linkages (entries 1-3), as well as those based on five, six, and seven membered rings (entries 4-6), proceeded in excellent yields. Acyclic primary and secondary alkylamines, in particular dimethylamine, were also suitable substrates for the addition to diphenylacetylene (entries 7-12); however, attempts to use more bulky dialkylamines such as $(i\text{-Pr})_2\text{NH}$ proved unsuccessful. Given the ubiquity of 1-arylpiperazines in biologically active pharmaceuticals,^[92] the development of efficient methods for their incorporation into organic molecules is of significant interest. The **5-1**/ $\text{AgB}(\text{C}_6\text{F}_5)_4$ -mediated

hydroamination of diphenylacetylene with 1-arylpiperazines featuring halide, ether, nitrile, nitro, hydroxy, and cyclopropylamide functional groups, as well as a 2,6-pyrimidyl substituted piperazine, proceeded with excellent isolated yields (entries 13-18). Furthermore, dialkylamine substrates containing alcohol or carboxylic acid groups were also readily added to the alkyne without observable side-products arising from hydrophenoxylation or hydrocarboxylation (entries 17 and 20).^[93]

Table 5-1. Gold-Catalyzed Hydroamination of Diphenylacetylene (**5-4**) with Primary and Secondary Amines^[a]



^[a]Conditions. **5-4:5-5:5-1:AgB(C₆F₅)₄** = 1:1.1:0.025:0.025 (0.8 mmol of amine) in 0.8 mL of toluene at 110 °C for 16 h. ^[b] Isolated yield of reduction product. ^[c] 5 mol % **5-1** and 5 mol % AgB(C₆F₅)₄ used. ^[d] In THF/1,4-dioxane (3:2) at 90 °C for 16 h. ^[e] GC yield relative to dodecane as an internal standard. ^[f] Reaction time = 24 h. ^[g] In 1,4-dioxane ([alkyne] = 0.5 mM). ^[h] ¹H NMR yield relative to 1,3,5-trimethoxybenzene as an internal standard. ^[i] Isolated as the enamine hydrolysis product.

The hydroamination of unsymmetrically substituted internal alkynes (**5-7**) with dialkylamines also proceeded in good to excellent yields with moderate to excellent

regioselectivities (Table 5-2). Prior to reduction of the **5-8/5-9** enamine product mixtures, the regioselectivity of the reaction was determined by integration of the enamine vinyl hydrogens relative to 1,3,5-trimethoxybenzene as an internal standard (^1H NMR; Figure 5-4). Using the aryl-alkyl alkyne **5-7a** and morpholine **5-5a**, a 4:1 mixture of enamine products **5-8a:5-9a** was observed (entry 1). The regiochemistry could be improved by substitution of the phenyl ring with either electron-donating or –withdrawing groups. For instance, *p*-OMe substitution of the aryl ring promoted exclusive formation of **5-8b** (entry 2) and, conversely, *p*-CN substitution promoted a reversal of regiochemistry favoring the enamine product **5-9c** (entry 3). This trend was further exploited in the hydroamination of **5-7d** – **5-7f**. Using the parent phenyl substrate **5-7d**, enamine products **5-8d:5-9d** were observed in a 3:1 ratio (entry 4); however, *p*-OMe substitution (**5-7e**) resulted in a drastic change in regiochemistry to favor **5-8e** in a 75% yield with an 18:1 ratio (entry 5). When employing the acyclic amine **5-5i** in the hydroamination of alkyne **5-7e**, the enamine products were formed with 4:1 regioselectivity (entry 6). In contrast to the benzyl-substituted alkyne **5-7c**, the hydroamination of the electron-poor alkyne **5-7f** with **5-5a** did not proceed (entry 7). However, the use of an electron-deficient pyridyl-substituted alkyne proceeded with complete regioselectivity in an 80% yield (entry 8). These results show that the electronic nature of the alkyne significantly guides the regioselectivity of this catalysis.

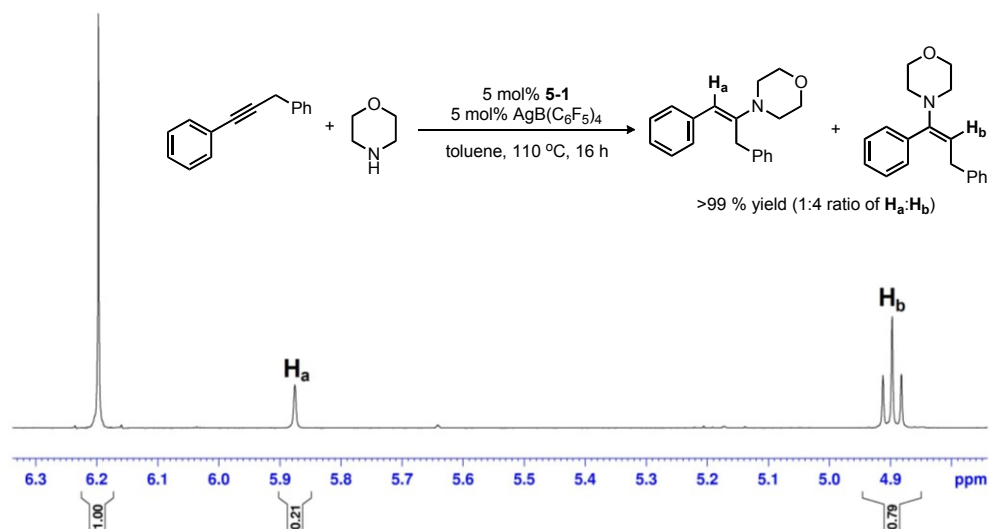
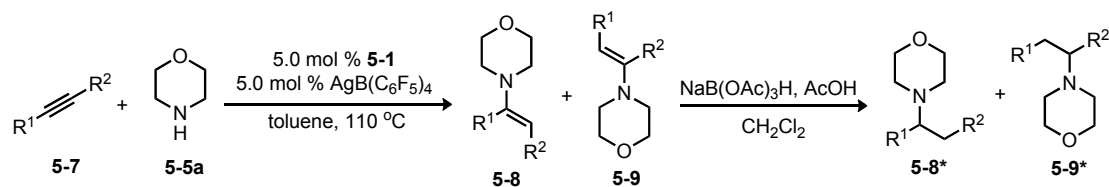


Figure 5-4. Representative example for determining regioselectivity by relative integration of enamine signals against an internal standard by ^1H NMR. (δ 6.2 ppm = 1,3,5-trimethoxybenzene)

Table 5-2. Gold-Catalyzed Hydroamination of Internal Alkynes with Morpholine (**5-5a**) and other secondary alkylamines^[a]



entry	alkyne	yield ^[b]	selectivity ^[c]
1	X = H (5-7a)	86	4:1
2	X = OMe (5-7b)	88	>20:1
3	X = CN (5-7c)	76	1:19
4	X = H (5-7d)	86 ^[d]	3:1
5	X = OMe (5-7e)	75	18:1
6 ^[e]	X = OMe (5-7e)	83 ^[d]	4:1
7	X = CN (5-7f)	n.r.	-
8		80 ^[d]	1:>20
9 ^[f]		90 ^[d]	2:1 ^[g]
10		73	>20:1
11 ^[h]		88 ^[d]	>20:1
12		79	3:1
13 ^[h]		76	5:1

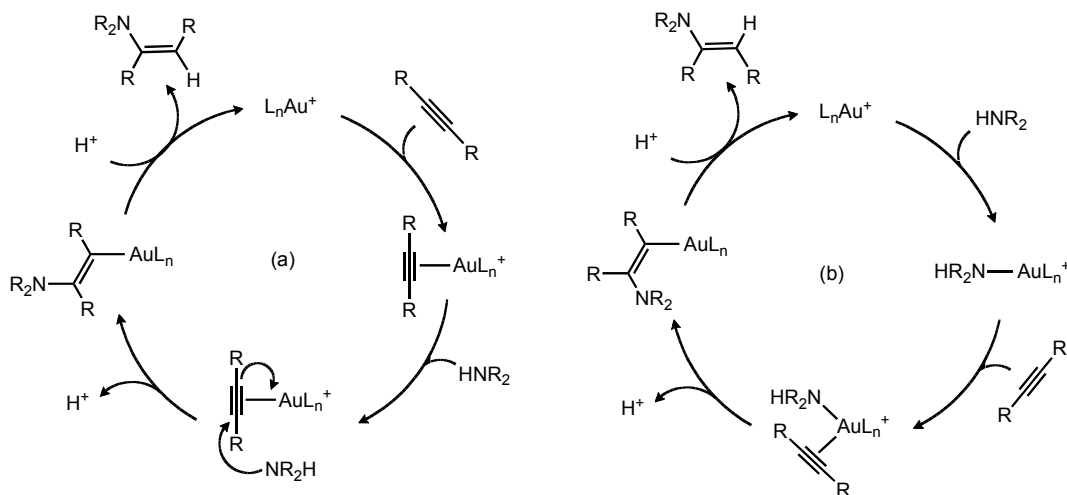
^[a] Conditions. **5-7:5-5a:5-1:AgB(C₆F₅)₄** = 1:1.1:0.025:0.025 (0.8 mmol of amine) in 0.8 mL of toluene at 110 °C for 16 h. ^[b] Isolated yield of combined enamine reduction products **5-8*** and **5-9***. ^[c] Ratio of enamine products **5-8:5-9** determined by ¹H NMR relative to 1,3,5-trimethoxybenzene prior to reduction. ^[d] ¹H NMR yield of enamine relative to 1,3,5-trimethoxybenzene. ^[e] Using amine **5-5i**. ^[f] 2.5 mol % **5-1** and 2.5 mol % AgB(C₆F₅)₄. ^[g] Ratio of an olefin isomerization product to the expected hydroamination product. ^[h] Using amine **5-5o**.

Further evidence of the functional group tolerance exhibited by this catalyst system was achieved via the hydroamination of alkynes possessing a phthalimide-protected amine or a silyl-protected alcohol with amine substrates **5-5a** or **5-5o**, which proceeded regioselectively in good yields (entries 10-13). Not only does this study represent the first observation of the regioselective hydroamination of internal alkynes

with dialkylamines, but it also provides qualitative information pertaining to the mechanism of this transformation (see Section 5.2.3.3).

5.2.3 Mechanistic Studies

Although empirical information pertaining to Au-catalyzed hydroamination reactions is sparse, competing mechanisms based on amine nucleophilic attack or alkyne insertion are generally proposed to rationalize the addition of nitrogen nucleophiles to unsaturated C–C multiple bonds (Scheme 5-4).^[94] The most commonly proposed mechanism for the addition of weakly basic nitrogen nucleophiles to unsaturated C–C bonds involves initial coordination of the C–C multiple bond to a cationic gold center, which activates the substrate towards nucleophilic attack by the amine. Subsequent protonolysis of the gold-vinyl (or alkyl) intermediate facilitates the release of the hydroamination product and a catalytically active Au species (Scheme 5-4a).^[68e, 95] Alternatively, qualitative investigations into the hydroamination of alkynes and allenes with more basic arylamines and ammonia, respectively, have provided convincing insight into reaction pathways involving insertion of the unsaturated C–C multiple bond into an unobserved Au-amide by way of a tri-coordinated [(ligand)Au(amine)(alkyne)] complex (Scheme 5-4b).^[96]

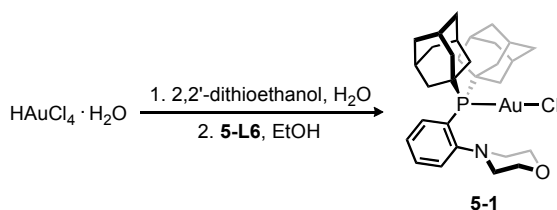


Scheme 5-4. Competing mechanistic pathways for the Au-catalyzed hydroamination of internal alkynes with dialkylamines based on (a) nucleophilic attack and (b) alkyne insertion mechanisms.

On the basis of these reports, two competing mechanisms involving either nucleophilic attack of the dialkylamine on a Au-coordinated alkyne or insertion of the alkyne into a Au-amido complex could be envisioned for the Au-mediated hydroamination reactions discussed in Section 5.2.2. As such, a combined stoichiometric and kinetic analysis of this transformation was conducted with the intent of revealing the key factors that contribute to the effectiveness of this catalyst system, with a particular emphasis on understanding the origin of the rate-accelerating benefits when employing a P,N-ligand framework.

5.2.3.1 Stoichiometric reactions of **5-1**/ $\text{AgB}(\text{C}_6\text{F}_5)_4$ with 3-hexyne and morpholine

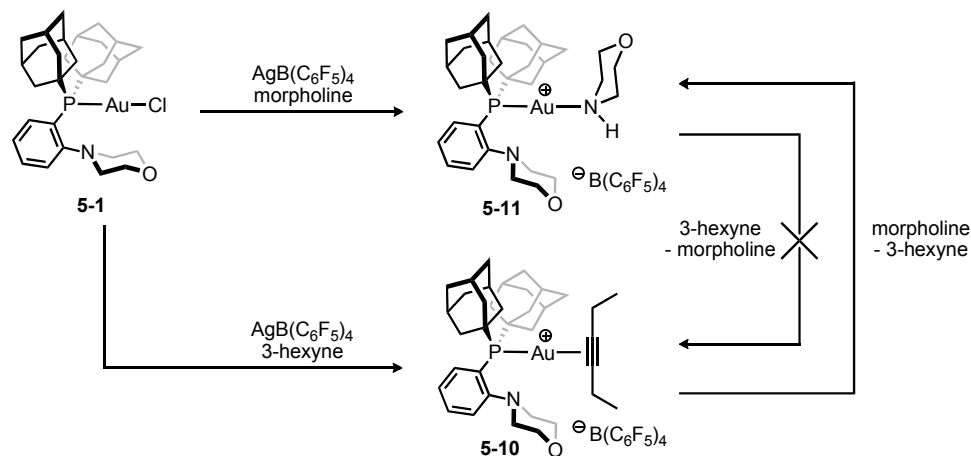
In order to gain insight into the nature of the catalytically active species for the Au-catalyzed alkyne hydroamination with dialkylamines, preliminary stoichiometric and crystallographic experiments were conducted. The precursory compound (**5-L6**)AuCl (**5-1**) was prepared in an 87% isolated yield from the reaction of *in situ* reduced $\text{HAuCl}_4 \cdot \text{H}_2\text{O}$ with 1 equiv. **5-L6** in a EtOH/ H_2O solvent co-mixture (Scheme 5-5). The structure of **5-1** was determined initially on the basis of NMR spectroscopic data, and subsequently was confirmed by use of single-crystal X-ray diffraction techniques (Figure 5-5). The structural features in **5-1** are consistent with monodentate coordination of the di(1-adamantyl)phosphino group in **5-L6** to Au with a linear P-Au-Cl dihedral angle of 175.6° , as is commonly observed in related monodentate phosphine gold-chloride complexes.^[97] The most notable feature in the crystal structure of **5-1** is that the morpholino fragment of **5-L6** remains uncoordinated.



Scheme 5-5. Synthesis of **5-1**.

The reaction of equimolar amounts of **5-1** and $\text{AgB}(\text{C}_6\text{F}_5)_4$ in the presence of 3-hexyne (1 equiv.) produced the cationic alkyne complex $[(\text{5-L6})\text{Au}(3\text{-hexyne})]^+\text{B}(\text{C}_6\text{F}_5)_4^-$

(**5-10**). Although the isolation of **5-10** in analytically pure form has been thwarted by the apparent instability of this complex in solution and upon workup, the ^1H and ^{13}C NMR characterization data obtained *in situ* are consistent with the target complex. Upon treatment of *in situ* generated **5-10** with 1 equiv. of morpholine (**5-5a**), the alkyne was readily displaced to form a new species, which was subsequently identified as the isolable and crystallographically characterized amine adduct $[(\mathbf{5-L6})\text{Au}(\text{morpholine})]^+\text{B}(\text{C}_6\text{F}_5)_4^-$ (**5-11**) (Figure 5-5). Notably, treatment of **5-11** with excess 3-hexyne did not regenerate **5-10**, which may suggest the intermediacy of **5-11** in catalysis (Scheme 5-6). Indeed, using **5-11** as a pre-catalyst afforded comparable activity to that of **5-1**/ $\text{AgB}(\text{C}_6\text{F}_5)_4$ mixtures for the hydroamination of diphenylacetylene with morpholine.



Scheme 5-6. Stoichiometric reactions of **5-1** with morpholine and 3-hexyne.

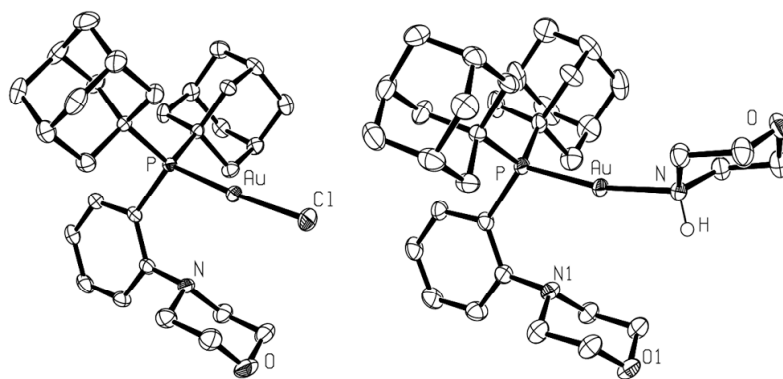


Figure 5-5. ORTEP diagram for **5-1** (left) and **5-11** (right), shown with 50% displacement ellipsoids; selected hydrogen atoms and the $B(C_6F_5)_4$ anion in **5-11** have been removed for clarity. Selected metrical parameters in **5-1**: Au-P 2.2554(5) Å; Au-Cl 2.3128(5) Å; P-Au-Cl 175.611(19)°. Selected metrical parameters in **5-11**: Au-P 2.2658(4) Å; Au-N 2.1143(12) Å; P-Au-N 168.70(3)°.

5.2.3.2 Kinetic Investigations

Kinetic studies were performed to define the hydroamination reaction pathway and to better understand the influence of [catalyst], [amine], and [alkyne] on the sequence of reaction events. Experiments were conducted on the **5-11**-mediated hydroamination of diphenylacetylene by morpholine. The empirical rate law was derived by systematically varying the concentrations of **5-11**, diphenylacetylene, and morpholine at 110 °C in toluene. Experiments carried out by varying [**5-11**] over the range 2.3 to 15 mM exhibited a linear trend when plotted against the measured rate constant (k_{obs}), indicating a first-order dependence of rate on catalyst concentration (Figure 5-6a). By varying [diphenylacetylene (**5-4**)] over the range 0.76-1.6 M, a first-order trend was also observed in the plot of [**5-4**] versus observed rate constant (Figure 5-6b). Conversely, varied morpholine concentration over a range of 0.65 to 1.6 M revealed a zero-order dependence in a plot of [morpholine (**5-5a**)] versus the observed rate constant (Figure 5-6c). As a result, the empirical rate law for the reaction on the basis of the preliminary data is described by the equation: $rate = k_{obs}[5-11]^1[5-4]^1[5-5a]^0$, where [catalyst (**5-11**)] and [diphenylacetylene (**5-4**)] are both first-order, and [morpholine (**5-5a**)] is zero-order.

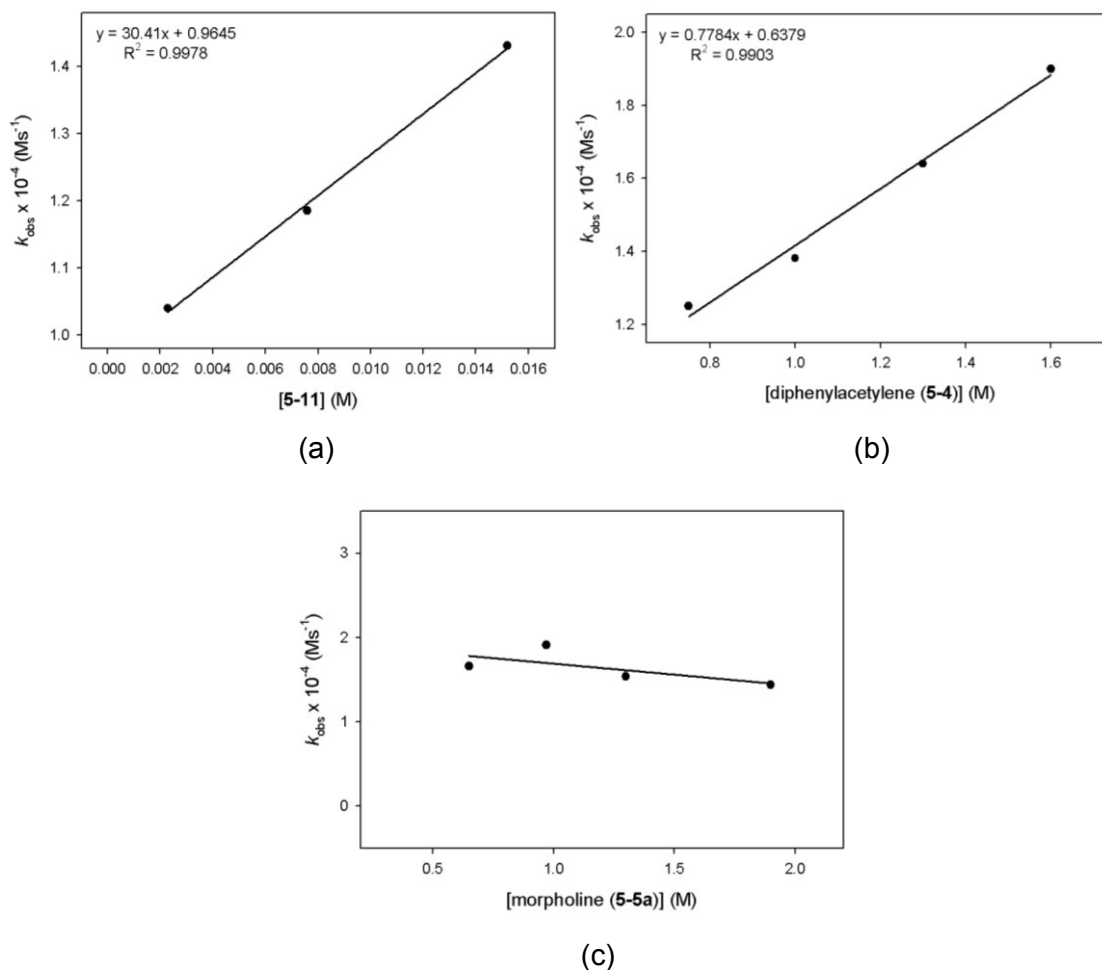


Figure 5-6. (a) Relationship between k_{obs} and the **[5-11]**. The reactions were conducted at the following concentrations: **[5-11]** = 2.3×10^{-3} M to 1.5×10^{-2} M, **[5-4]** = 7.6×10^{-1} M, and **[5-5a]** = 7.6×10^{-1} M. (b) Relationship between k_{obs} and the **[diphenylacetylene (5-4)]**. The reactions were conducted at the following concentrations: **[5-1]** = $[\text{AgB}(\text{C}_6\text{F}_5)_4]$ = 7.5×10^{-3} M, **[5-4]** = 7.5×10^{-1} M to 1.6 M, and **[5-5a]** = 7.5×10^{-1} M. (c) Relationship between k_{obs} and the **[5-5a]**. The reactions were conducted at the following concentrations: **[5-1]** = $[\text{AgB}(\text{C}_6\text{F}_5)_4]$ = 5.0×10^{-3} M, **[5-4]** = 6.5×10^{-1} M, and **[5-5a]** = 6.5×10^{-1} M to 1.9 M.

Activation parameters for the conversion of **5-4** and **5-5a** to **5-6** mediated by **5-1/AgB(C₆F₅)₄** were obtained by measuring the rate of reaction over the temperature range of 90 to 130 °C. The data were plotted according to the Eyring and Arrhenius equations to afford values of $\Delta H^\ddagger = +25(2)$ kcal/mol, $\Delta S^\ddagger = -11(3)$ e.u., and $E_a = +26(1)$ kcal/mol, with the negative ΔS^\ddagger suggesting a rather organized transition state and the large ΔH^\ddagger being consistent with a strong Au-substrate interaction imposing a greater barrier to the turnover-limiting step (Figure 5-7).

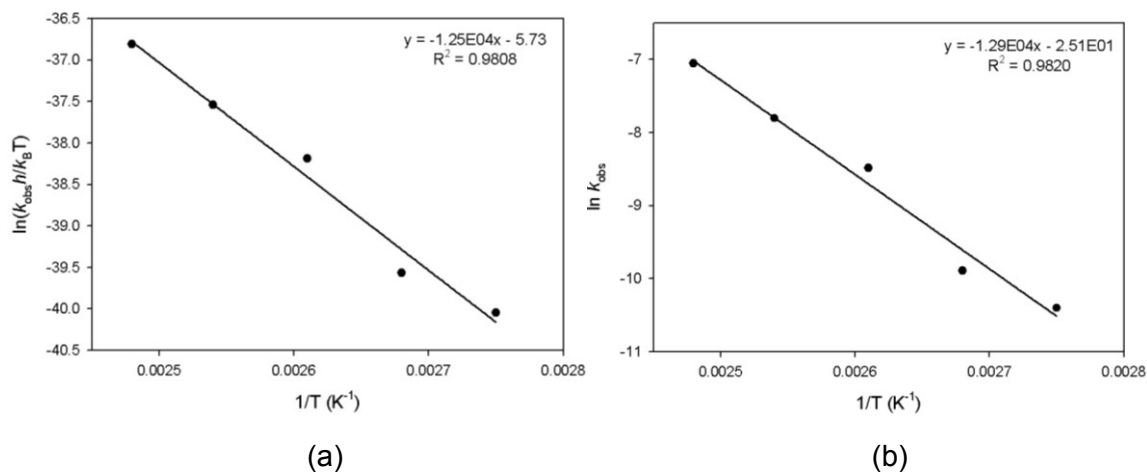


Figure 5-7. (a) Eyring plot for the hydroamination of diphenylacetylene with morpholine catalyzed by **5-1**/ $\text{AgB}(\text{C}_6\text{F}_5)_4$. The reactions were conducted in toluene over a temperature range of 90–130 °C at the following concentrations: $[\mathbf{5-4}] = [\mathbf{5-5a}] = 7.2 \times 10^{-1}$ M and $[\mathbf{5-1}] = [\text{AgB}(\text{C}_6\text{F}_5)_4] = 5.0 \times 10^{-3}$ M. (b) Arrhenius plot for the hydroamination of diphenylacetylene with morpholine catalyzed by **5-1**/ $\text{AgB}(\text{C}_6\text{F}_5)_4$. The reactions were conducted in toluene over a temperature range of 90–130 °C at the following concentrations: $[\mathbf{5-4}] = [\mathbf{5-5a}] = 7.2 \times 10^{-1}$ M and $[\mathbf{5-1}] = [\text{AgB}(\text{C}_6\text{F}_5)_4] = 7.2 \times 10^{-3}$ M.

Using morpholine that was selectively deuterated at the N-H bond, a $k_{\text{H}}/k_{\text{D}}$ kinetic isotope effect of 1.5(1) was measured (Figure 5-8). The magnitude of this value suggests that the proton derived from the amine is likely not involved in a turnover-limiting protonation event. Rather, a secondary kinetic isotope effect or a reversible proton transfer leading to an equilibrium isotope effect, which translates into different rates of rate-limiting alkyne insertion, seem more plausible (see Section 5.2.3.3).

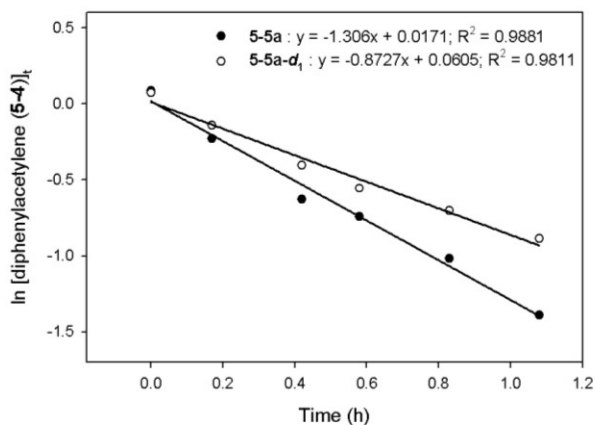
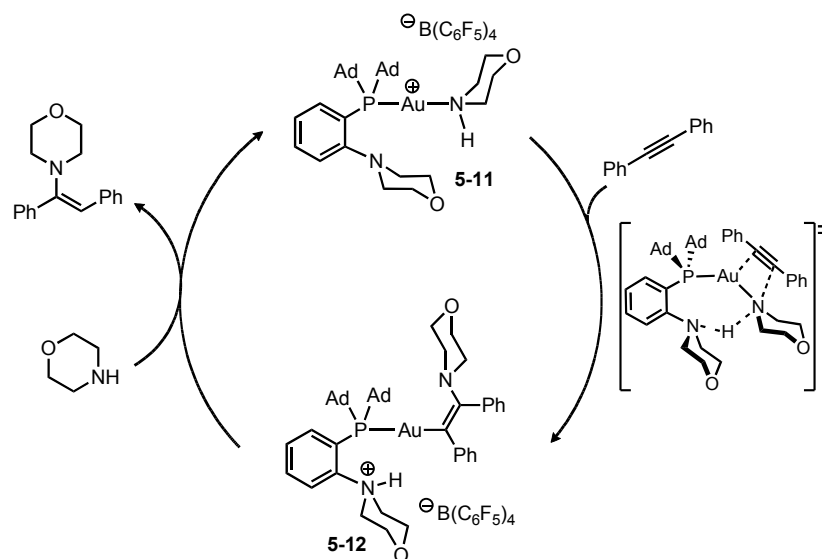


Figure 5-8. H/D kinetic isotope effect for the **5-1**/ $\text{AgB}(\text{C}_6\text{F}_5)_4$ -catalyzed hydroamination of diphenylacetylene with morpholine. The reactions were conducted at the following concentrations: $[\mathbf{5-5a}/\mathbf{5-5a-d}_1] = 1.1 \text{ M}$, $[\mathbf{5-4}] = 1.1 \text{ M}$, and $[\mathbf{5-1}] = [\text{AgB}(\text{C}_6\text{F}_5)_4] = 1.1 \times 10^{-2} \text{ M}$.

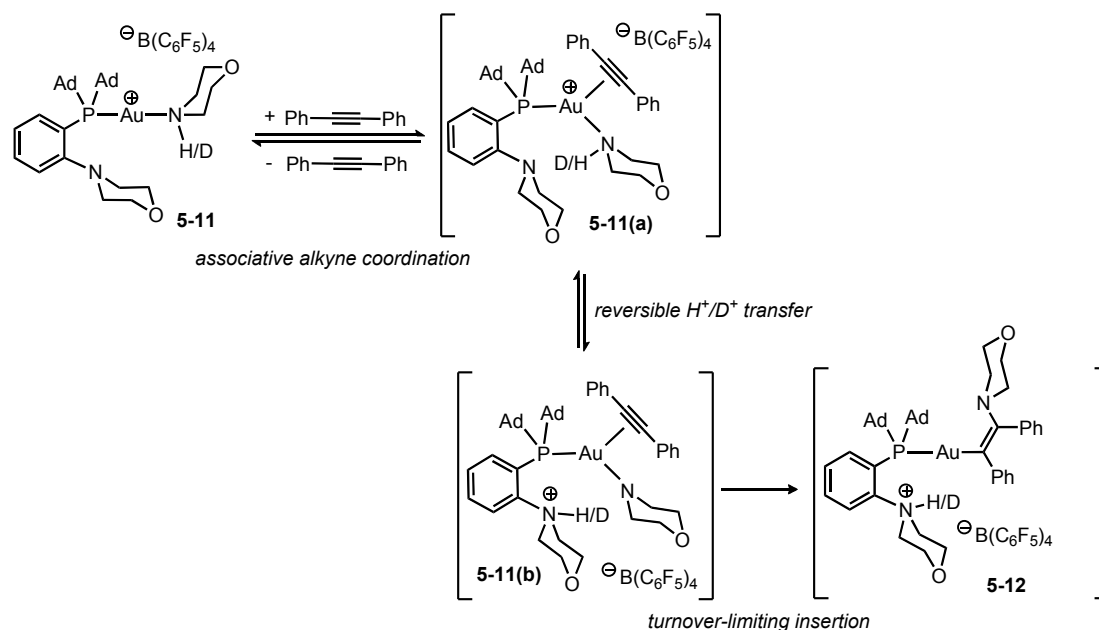
5.2.3.3 Mechanistic Discussion

Collectively, the kinetics, deuterium labeling, stoichiometric studies, and moderate to excellent degree of regioselectivity are most consistent with an alkyne insertion pathway. A plausible inner-sphere mechanism might involve associative coordination of the alkyne to **5-11** concomitant with reversible proton-transfer followed by turnover-limiting insertion of the alkyne to generate a vinyl-gold intermediate (**5-12**).^[98] Subsequent proto-deauration would liberate the enamine product and, when in the presence of excess morpholine (**5-5a**), regenerate **5-11**. Similar insertion mechanisms have been proposed for gold-catalyzed additions of arylamines to allenes and ammonia to alkynes.^[96] In light of the rate-accelerating effects^[96] achieved when employing a P,N-ligand such as **5-L6**, the pendant nitrogen donor is envisioned to participate in catalysis by facilitating one or more mechanistically relevant proton-transfer steps (Scheme 5-7).



Scheme 5-7. Proposed mechanism for the **5-11**-mediated hydroamination of diphenylacetylene with morpholine.

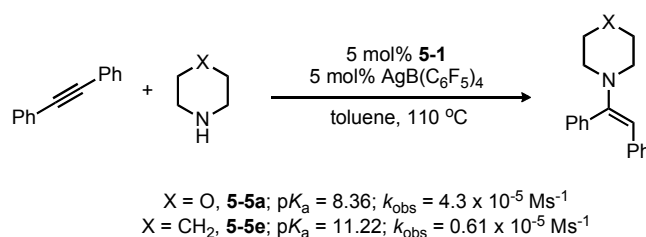
This mechanistic proposal is consistent with the empirically derived rate law, whereby both [**5-11**] and [diphenylacetylene (**5-4**)] would be expected to exhibit a first-order dependence on the rate of reaction and a zero-order dependence on [morpholine (**5-5a**)] would be expected, given that the proto-deauration event occurs following the turnover-limiting insertion. Attempts to observe the proposed gold-vinyl species **5-12** by monitoring the catalytic reaction through ^1H and ^{31}P NMR methods were unsuccessful. Furthermore, attempts to trap out **5-12** via net $\text{HB}(\text{C}_6\text{F}_5)_4$ extrusion by treatment of mixtures of **5-11** and diphenylacetylene with the bases $\text{NaN}(\text{SiMe}_3)_3$, K_2CO_3 , or $n\text{BuLi}$ resulted in complex reaction mixtures from which no pure material could be isolated. Protonolysis of the gold-vinyl bond in **5-12** could be envisioned to occur either intramolecularly by the ligand-bound ammonium proton derived from the initial morpholine substrate molecule, or intermolecularly by an incoming morpholine substrate. Attempts to provide insight into this process by use of crossover experiments employing **5-5e/5-5a- d_1** mixtures would be thwarted by immediate H/D scrambling of the substrate molecules.



Scheme 5-8. Proposed series of transformations leading up to turnover-limiting alkyne insertion.

A more detailed explanation for the proposed series of transformations that are traversed from **5-11** to **5-12** is depicted in Scheme 5-8. Reversible associative coordination of the alkyne to **5-11** could generate the tri-coordinated cationic $[(\mathbf{5-L6})\text{Au}(\mathbf{5-4})(\mathbf{5-5a})]^{\oplus}$ species (**5-11(a)**), which could orient the Au-bound substrate morpholine N-H bond towards the morpholino donor group of the P,N-ligand **5-L6** to develop an energetically favorable hydrogen bonding interaction. Subsequent reversible proton transfer would produce the transient gold-amido complex **5-11(b)**, which would be poised to undergo turnover-limiting insertion of the coordinated alkyne to generate the postulated gold-vinyl species **5-12**. It can be argued that the proposal of a reversible proton transfer directly preceding a turnover-limiting insertion event is entirely consistent with the measured H/D kinetic isotope effect of 1.5(1). The equilibrium between **5-11(a)** and **5-11(b)** would inherently control the overall concentration of $[\mathbf{5-11(b)}]$ and thus the overall rate of reaction. In conducting the catalysis with morpholine- d_1 (**5-5a-d₁**), the proton transfer equilibrium between **5-11(a)-d₁** and **5-11(b)-d₁** will be altered, thereby lowering the overall $[\mathbf{5-11(b)-d_1}]$. This equilibrium isotope effect will be manifested in decreased reaction rates for the deuterated substrate, giving rise to the observed $k_{\text{H}}/k_{\text{D}}$ of 1.5. Furthermore, if proton transfer between the P,N-ligand morpholino group and Au-coordinated morpholine substrate does represent a mechanistically important process,

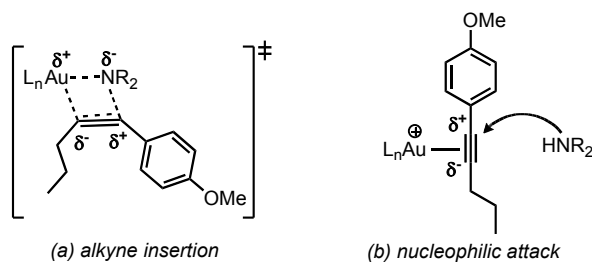
then the relative pK_a values of the amine substrate should also have a direct influence on the proposed equilibrium and thus the observed reaction rates. Using the amine substrates morpholine (**5-5a**) and piperidine (**5-5e**), which have comparable steric environments and significantly different pK_a values (pK_a (in H_2O) = 8.36 (**5-5a**) and 11.22 (**5-5e**) for the corresponding ammonium salts),^[99] considerably different reaction rates were measured ($k_{obs} = 4.3 \times 10^{-5} \text{ Ms}^{-1}$ (**5-5a**); $k_{obs} = 0.61 \times 10^{-5} \text{ Ms}^{-1}$ (**5-5e**)) (Scheme 5-9). The observation that decreased reaction rates are measured for the more basic amine substrate **5-5e** is consistent with an impeded proton transfer step proposed in Scheme 5-8. Although the reaction sequence described in Scheme 5-8 depicts the formation of discrete reaction intermediates, a more likely scenario would involve concerted processes that feature proton transfer concomitant with alkyne insertion to form intermediates of the type **5-12**.



Scheme 5-9. Comparison of reaction rates (k_{obs}) for amines with varied pK_a values in the hydroamination of diphenylacetylene catalyzed by **5-1**/ $AgB(C_6F_5)_4$ (pK_a values presented are for the corresponding ammonium salts).

Further information regarding the mechanism of this transformation can be ascertained from the qualitative regioselectivity trends observed in the hydroamination of unsymmetrical internal alkynes (Table 5-2). The moderate to excellent regioselectivity that is achieved when using catalytic mixtures of **5-1**/ $AgB(C_6F_5)_4$ for the hydroamination of internal alkynes with dialkylamines provides further evidence for an alkyne insertion mechanism, in that the interplay of electronic and non-bonding repulsion in the four-membered insertive transition state can be viewed as being responsible for the observed regioselectivity. The orientation of the alkyne with respect to the $Au-NR_2$ bond should be expected to stabilize the electrophilic metal center in the transition state by positioning the alkyne carbon with greater electron density in line with Au (Scheme 5-10a). In contrast, the observed regioselectivity may also be rationalized by selective nucleophilic attack of the amine on the more electron-deficient carbon of the Au-coordinated alkyne

(Scheme 5-10b). However, the observation that exclusive > 95% selectivity is only observed for several of the internal alkynes surveyed suggests that, in conjunction with the electronic effects, the steric profile of the unsymmetrical internal alkynes must also play a meaningful role in the observed regioselectivities.



Scheme 5-10. Two potential rationales for the regioselectivity observed in the hydroamination of unsymmetrical alkynes based on the two competing mechanisms of (a) alkyne insertion and (b) amine nucleophilic attack.

An alternative mechanism that is also consistent with the empirical rate law involves turnover-limiting associative displacement of a Au-coordinated amine with the alkyne followed by nucleophilic attack of the amine on the Au-coordinated alkyne, as in Scheme 5-4a. While such a mechanism cannot be unambiguously refuted based on the available data, the stoichiometric reactions involving amine and alkyne (Scheme 5-6) would appear to cast doubt on the viability of such a mechanism. Given the mechanistic complexities of Au-mediated transformations,^[94] further experimentation is needed in order to elucidate the origin of high catalytic activity when employing **5-L6** and related ligands.

5.3 Conclusions

The catalytic, gold-mediated, intermolecular hydroamination of a wide range of internal alkynes by dialkylamines has been explored in terms of scope and mechanism. In conjunction with an appropriately selected chloride-abstracting metal salt ($\text{AgB}(\text{C}_6\text{F}_5)_4$), a gold complex (**5-1**) featuring a P,N-ligand (**5-L6**) has been identified as a highly effective pre-catalyst for this transformation that has significantly extended the substrate scope and synthetic utility of metal-mediated alkyne hydroamination. In particular, this catalyst has

been shown to be very effective for the addition of a range of functionalized dialkylamines to internal alkynes. Furthermore, the hydroamination of unsymmetrical internal alkynes with dialkylamines has been achieved with synthetically useful regioselectivities. A preliminary stoichiometric and kinetic analysis of this system was conducted to provide insight into the operative mechanism, with particular attention given to the origin of the rate-accelerating benefits of employing a P,N-ligand architecture. Collectively, the results of these studies are most consistent with an alkyne insertion mechanism. A potential mechanistic scenario would involve associative coordination of the alkyne to a cationic gold-amine complex, followed by reversible proton transfer concomitant with turnover-limiting insertion of the alkyne into the Au-amide bond to generate a vinyl-gold intermediate. Subsequent proto-deauration of this species would liberate the enamine product and regenerate the catalytically active cationic Au species. Turnover-limiting insertion following a reversible proton transfer is consistent with the measured H/D kinetic isotope effect as well as the observation that more basic amine substrates have reduced rates of catalysis. Given the limited number of catalysts that have proven capable of promoting the intermolecular addition of dialkylamines to internal alkynes, in particular with regards to the regioselective addition of amines to unsymmetrical internal alkynes, the catalytic and mechanistic findings discussed herein represent an important contribution toward expanding the synthetic utility of metal-mediated alkyne hydroamination reactions. The studies conducted in Chapter 5 represent a preliminary account of substrate scope and mechanistic studies for the **5-1**/AgB(C₆F₅)₄-mediated hydroamination of internal alkynes with dialkylamines; the focus of further investigations is outlined in Chapter 6 (see Section 6.4)

5.4 Experimental Section

5.4.1 General Considerations

Stoichiometric organometallic reactions and all catalysis were conducted in the absence of oxygen and water under an atmosphere of dinitrogen, either by use of standard Schlenk methods or within an mBraun glovebox apparatus, utilizing glassware that was oven-dried (130 °C) and evacuated while hot prior to use, whereas the work-up and isolation of the products from the catalytic reactions were conducted on the bench-top

using standard techniques. 1,4-Dioxane (Aldrich) was dried over Na/benzophenone followed by distillation under an atmosphere of dinitrogen. Toluene was deoxygenated by sparging with dinitrogen followed by passage through a double column solvent purification system purchased from mBraun Inc. 1,2-Dimethoxyethane (DME), 1,2-dichloroethane (DCE), dimethylformamide (DMF), dimethylsulfoxide (DMSO), acetonitrile (MeCN), and dimethylacetamide (DMA) were deoxygenated by sparging with dinitrogen gas followed by storage over activated 4 Å molecular sieves for 48 h prior to use. Chloroform-*d*₁ (Cambridge Isotopes) was used as received. All solvents used within the glovebox were stored over activated 4 Å molecular sieves. H₂AuCl₄·H₂O (Strem), IPr (Strem), *t*Bu-JohnPhos (Aldrich), *t*Bu-Davephos (Strem), LiBF₄ (Aldrich), AgBF₄ (Strem), LiOTf (Aldrich), AgOTf (Aldrich), NaPF₆ (Aldrich), AgPF₆ (Strem), AgSbF₆ (Strem), AgNTf₂ (Aldrich), and LiB(C₆F₅)₄·2.5 Et₂O (Boulder Scientific) were evacuated under reduced pressure for 24 h prior to use. Au(SMe₂)Cl,^[100] AgB(C₆F₅)₄,^[101] IPrAuCl,^[102] **L1-L3**,^[20a] **L4**, **L9**, **L10**,^[24a] **L5-L8**,^[24b] and **L13**^[103] were prepared according to literature procedures. All other reagents were used as received. ¹H and ¹³C NMR characterization data were collected at 300 K on a Bruker AV-500 spectrometer operating at 500.1 and 125.8 MHz (respectively) with chemical shifts reported in parts per million downfield of SiMe₄. GC data were obtained on a Shimadzu GC-2014 equipped with a SGE BP-5 30m. 0.25 mm I.D. column. GC yields were quantified by using a calibration curve relative to dodecane as an internal standard. Mass spectrometric data were acquired by Mr. Xiao Feng (Mass Spectrometry Laboratory, Dalhousie University) and elemental analysis data were obtained from Midwest Microlab, Indianapolis, Indiana.

5.4.2 Synthetic Details and Characterization Data

Synthesis of 5-1. 2,2'-Thiodiethanol (0.435 mL, 4.34 mmol) was added dropwise to a magnetically stirred solution of H₂AuCl₄·H₂O (0.492 g, 1.45 mmol) in H₂O (1.5 mL) over the course of 0.5 h, which caused the reaction mixture to turn from a yellow-orange color to colorless. Following this addition, solid **5-L6** (0.671 g, 1.45 mmol) was added all at once followed by EtOH (4.5 mL). The mixture was stirred at ambient temperature for 3 h. At this time, the reaction mixture was filtered and the resulting solid was washed with

methanol (4 x 2 mL). **5-1** was then retrieved as an analytically pure white solid (0.877 g, 1.26 mmol, 87 %). Anal Calcd for C₃₀H₄₂AuClNOP: C 51.77; H 6.08; N 2.01. Found: C 51.71; H 6.09; N 2.11. ¹H NMR (CD₂Cl₂): δ 7.80 (m, 1H, Ar-CH), 7.63-7.59 (m, 2H, Ar-CH), 7.34 (m, 1H, Ar-CH), 4.66 (dt, *J* = 11.0, 3.0 Hz, 2H, morpholino), 3.74 (dd, *J* = 11.5, 3.0 Hz, 2H, morpholino), 3.06 (dt, *J* = 12.0, 3.0 Hz, 2H, morpholino), 2.67 (br. d, *J* = 11.0 Hz, 2H, morpholino), 2.26-2.17 (m, 6H, adamantyl), 2.15-2.06 (m, 6H, adamantyl), 2.01-1.94 (m, 6H, adamantyl), 1.72-1.64 (m, 12H, adamantyl); ¹³C{¹H} NMR (CD₂Cl₂): δ 149.2 (d, *J* = 12.6 Hz, Ar-quat.), 125.3 (Ar-CH), 122.7 (Ar-CH), 117.0 (d, *J* = 12.6 Hz, Ar-CH), 115.0 (d, *J* = 7.8 Hz, Ar-CH), 55.8 (morpholino), 44.8 (morpholino), 32.3 (adamantyl-CH₂), 26.3 (adamantyl-CH₂), 18.8 (d, *J* = 10.3 Hz, adamantyl-CH); ³¹P{¹H} NMR (CD₂Cl₂): δ 52.0. Crystals suitable for X-ray crystallographic analysis were grown from vapor diffusion of diethyl ether into a concentrated solution of **5-1** in dichloromethane.

Synthesis of 5-2. 2,2'-Thiodiethanol (0.156 mL, 1.56 mmol) was added dropwise to a magnetically stirred solution of HAuCl₄•H₂O (0.177 g, 0.521 mmol) in H₂O (1 mL) over the course of 0.5 h, which caused the reaction mixture to turn from a yellow-orange color to colorless. Following this addition, solid **5-L11** (0.237 g, 0.521 mmol) was added all at once followed by EtOH (3 mL). The mixture was stirred at ambient temperature for 3 h. At this time, the reaction mixture was filtered and resulting solid was washed with methanol (4 x 2 mL). **5-2** was then isolated as analytically pure white solid (0.294 g, 0.428 mmol, 82 %). Anal Calcd for C₃₂H₃₉AuClP: C 55.94; H 5.72. Found: C 55.69; H 5.58. ¹H NMR (CD₂Cl₂): δ 7.94 (m, 1H, Ar-CH), 7.59-7.50 (m, 3H, Ar-CH), 7.45-7.39 (m, 2H, Ar-CH), 7.31 (m, 1H, Ar-CH), 7.20-7.14 (m, 2H, Ar-CH), 2.28-2.21 (m, 6H, adamantyl), 2.19-2.11 (m, 6H, adamantyl), 2.09-1.99 (m, 6H, adamantyl), 1.79-1.67 (m, 12H, adamantyl); ¹³C{¹H} NMR (CD₂Cl₂): δ 151.1 (d, *J* = 13.8 Hz, Ar-quat.), 143.6 (Ar-quat.), 135.2 (Ar-CH), 133.9 (d, *J* = 7.5 Hz, Ar-CH), 130.8 (Ar-CH), 129.9 (Ar-CH), 128.9 (Ar-CH), 128.4 (Ar-CH), 126.9 (d, *J* = 6.3 Hz, Ar-CH), 42.7 (adamantyl-CH), 36.8 (adamantyl-CH₂), 29.3 (adamantyl-CH₂); ³¹P{¹H} NMR (CD₂Cl₂): δ 61.7.

Synthesis of 5-10. To a magnetically stirred solution of **5-1** (0.016 g, 0.022 mmol) and 3-hexyne (8 μL, 0.067 mmol) in CH₂Cl₂ (1 mL) was added solid AgB(C₆F₅)₄ (0.021 g, 0.026 mmol) which caused the immediate formation of an off-white precipitate. After 1

h of magnetic stirring, ^{31}P NMR of the reaction mixture showed quantitative consumption of **5-1** and the formation of a new species. Although we have thus far not been able to isolate **5-10** in analytically pure form due to the apparent instability of this complex in solution and upon workup, ^1H and ^{13}C NMR characterization data obtained *in situ* are consistent with the target complex. ^1H NMR (CD_2Cl_2): δ 7.88 (m, 1H, Ar-CH), 7.78-7.74 (m, 2H, Ar-CH), 7.55 (m, 1H, Ar-CH), 4.15-4.06 (m, 4H, morpholino), 3.30-3.21 (m, 2H, morpholino), 2.89 (br q, $^3J_{\text{HH}} = 7.0$ Hz, 4H, CH_2), 2.73-2.66 (m, 2H, morpholino), 2.24-2.16 (m, 6H, adamantyl), 2.11-2.01 (m, 12H, adamantyl), 1.83-1.75 (m, 6H, adamantyl), 1.73-1.67 (m, 6H, adamantyl), 1.47 (br t, $^3J_{\text{HH}} = 7.4$ Hz, 6H, CH_3); $^{13}\text{C}\{^1\text{H}\}$ NMR (CD_2Cl_2): δ 157.5 (Ar-quat.), 135.9 (Ar-CH), 134.0 (Ar-CH), 127.4 (d, $J_{\text{PC}} = 28.5$ Hz, Ar-CH), 126.9 (d, $J_{\text{PC}} = 18.5$ Hz, Ar-CH), 96.3 (d, $J_{\text{PC}} = 47.0$ Hz, alkyne-quat.), 67.5 (morpholino), 55.6 (morpholino), 42.4 (adamantyl- CH_2), 36.0 (adamantyl- CH_2), 28.7 (d, $J_{\text{PC}} = 11.3$ Hz, Ad-CH), 17.9 (CH_2), 14.8 (CH_3); $^{31}\text{P}\{^1\text{H}\}$ NMR (CD_2Cl_2): δ 58.1.

Synthesis of 5-11. To a magnetically stirred solution of **5-1** (0.031 g, 0.044 mmol) and morpholine (8 μL , 0.088 mmol) in CH_2Cl_2 (2 mL) was added solid $\text{AgB}(\text{C}_6\text{F}_5)_4$ (0.035 g, 0.044 mmol) which caused the immediate formation of an off-white precipitate. After 0.5 h of stirring, ^{31}P NMR of the reaction mixture showed quantitative consumption of **5-1** and the formation of a new species. The reaction mixture was filtered through Celite followed by removal of the solvent and other volatile components under vacuum. The crude material was washed with Et_2O (2 x 2 mL) followed by drying *in vacuo* to afford **5-11** as an analytically pure white solid (0.055 g, 0.039 mmol, 89 %). Anal Calcd for $\text{C}_{58}\text{H}_{51}\text{AuBF}_{20}\text{N}_2\text{O}_2\text{P}$: C 48.83; H 3.60; N 1.96. Found: C 49.13; H 3.47; N 1.95. ^1H NMR (CD_2Cl_2): δ 7.85 (m, 1H, Ar-CH), 7.73 (m, 1H, Ar-CH), 7.66 (m, 1H, Ar-CH), 7.48 (m, 1H, Ar-CH), 4.30-4.20 (m, 2H, morpholine(a)), 4.14 (br s, 1H, NH), 4.11-4.05 (m, 2H, morpholine(b)), 4.04-3.95 (m, 2H, morpholine(a)), 3.86 (dt, $J = 2.5, 11.0$ Hz, 2H, morpholine(b)), 3.68-3.57 (m, 2H, morpholine(a)), 3.50-3.40 (m, 2H, morpholine(a)), 3.22 (dt, $J = 2.5, 11.0$ Hz, 2H, morpholine(b)), 2.69 (d, $J = 12.0$ Hz, 2H, morpholine(b)), 2.31-2.18 (m, 6H, adamantyl), 2.16-1.99 (m, 12H, adamantyl), 1.85-1.74 (m, 6H, adamantyl), 1.73-1.62 (m, 6H, adamantyl); $^{13}\text{C}\{^1\text{H}\}$ NMR (CD_2Cl_2): δ 158.1 (Ar-quat.), 135.7 (Ar-CH), 134.2 (Ar-CH), 127.5 (d, $J = 5.0$ Hz, Ar-CH), 126.6 (d, $J = 7.5$ Hz, Ar-CH), 68.3 (morpholine(b)), 67.2 (morpholine(a)), 54.8 (morpholine(b)), 51.9

(morpholine(a)), 43.2 (adamantyl-CH₂), 36.6 (adamantyl-CH₂), 29.2 (d, $J = 9.8$ Hz, adamantyl-CH); ³¹P{¹H} NMR (CD₂Cl₂): δ 51.5. Crystals suitable for X-ray crystallographic analysis were grown from vapor diffusion of diethyl ether into a concentrated solution of **5-11** in dichloromethane.

General procedure for the Au-catalyzed intermolecular hydroamination of alkynes with secondary alkylamines (Tables 5-1 and 5-2). To a screw-capped vial containing **5-1** (14 mg, 0.020 mmol), AgB(C₆F₅)₄ (16 mg, 0.020 mmol), the alkyne (0.8 mmol) and a stir-bar was added 0.8 mL of toluene followed by the amine (0.96 mmol). The vial was sealed under N₂ with a cap containing a PTFE septum, was removed from the glovebox and was placed in a temperature-controlled aluminum-heating block set to 110 °C. After 16 h of magnetic stirring, the vial was removed from the heating block and was cooled to ambient temperature followed by removal of the solvent and other volatile components *in vacuo*. For unsymmetrically substituted alkynes (Table 5-2), the regioselectivity was determined before reduction by integration of the vinyl-hydrogens of each enamine relative to 1,3,5-trimethoxybenzene as an internal standard (¹H NMR). The residue was dissolved with CH₂Cl₂ (5 mL) and was quantitatively transferred to a screw-capped vial containing sodium triacetoxyborohydride (339 mg, 1.6 mmol) followed by the addition of acetic acid (0.092 mL, 1.6 mmol). The suspension was then stirred at ambient temperature for 16-24h. The reaction was quenched by the addition of 1M NaOH (aq) (3 mL). The phases were separated and the aqueous layer extracted with two further portions of CH₂Cl₂. The combined organic phases were dried over Na₂SO₄ and filtered. After removal of the solvent, the resulting tertiary amine products were purified by column chromatography on silica gel. Structural assignments of the tertiary amine products were made on the basis 1D and 2D NMR techniques.

Table 5-1, Entry 1. The indicated compound was purified by flash chromatography on silica gel (CH₂Cl₂:MeOH:NH₄OH = 1000:10:1) in a 86 % yield (184 mg) as an off-white solid. ¹H NMR (CDCl₃): δ 7.29-7.20 (m, 3H), 7.19-7.10 (m, 5H), 6.99-6.95 (m, 2H), 3.77-3.71 (m, 4H), 3.51 (dd, $J = 5.0, 9.5$ Hz, 1H), 3.37 (dd, $J = 5.0, 13.0$ Hz, 1H), 2.92 (dd, $J = 9.5, 13.0$ Hz, 1H), 2.64-2.54 (m, 2H), 2.53-2.46 (m, 2H);

$^{13}\text{C}\{^1\text{H}\}$ NMR (CDCl_3): δ 139.6, 139.2, 129.4, 128.7, 127.9, 127.1, 125.8, 72.3, 67.2, 51.3, 39.2. HRMS (ESI/[M+H] $^+$) calcd. for $\text{C}_{18}\text{H}_{22}\text{NO}$: 268.1696. Found: 268.1694.

Table 5-1, Entry 2. The indicated compound was purified by flash chromatography on silica gel (hexanes:EtOAc = 20:1 \rightarrow 10:1) in a 80 % yield (182 mg) as a white solid. ^1H NMR (CDCl_3): δ 7.34-7.14 (m, 8H), 7.13-7.08 (m, 2H), 3.77 (dd, J = 5.0, 5.0 Hz, 1H), 3.31 (dd, J = 10.0, 10.0 Hz, 1H), 3.06 (dd, J = 10.0, 10.0 Hz, 1H), 2.92-2.85 (m, 2H), 2.79-2.63 (m, 6H); $^{13}\text{C}\{^1\text{H}\}$ NMR (CDCl_3): δ 139.7, 138.8, 129.2, 128.6, 127.9, 127.8, 127.1, 125.8, 72.0, 52.1, 38.1, 28.2. HRMS (ESI/[M+H] $^+$) calcd. for $\text{C}_{18}\text{H}_{22}\text{NS}$: 284.1467. Found: 284.1475.

Table 5-1, Entry 3. The indicated compound was purified by flash chromatography on silica gel (hexanes:EtOAc = 5:1) in a 92 % yield (271 mg) as a white solid. ^1H NMR (CDCl_3): δ 7.31-7.22 (m, 3H), 7.20-7.11 (m, 5H), 7.03-6.99 (m, 2H), 3.62 (dd, J = 10.0, 5.0 Hz, 1H), 3.49-3.39 (m, 4H), 3.35 (dd, J = 15.0, 5.0 Hz, 1H), 2.99 (dd, J = 10.0, 10.0 Hz, 1H), 2.47 (br s, 4H), 1.46 (s, 9H); $^{13}\text{C}\{^1\text{H}\}$ NMR (CDCl_3): δ 154.7, 139.3, 139.2, 129.3, 128.7, 127.9, 127.1, 125.8, 79.4, 71.8, 50.2, 44.3, 39.2, 28.4. HRMS (ESI/[M+H] $^+$) calcd. for $\text{C}_{23}\text{H}_{31}\text{N}_2\text{O}_2$: 367.2380. Found: 367.2381.

Table 5-1, Entry 4. The indicated compound was purified by flash chromatography on silica gel (CH_2Cl_2 :MeOH: NH_4OH = 500:10:1 \rightarrow 200:10:1) in a 90 % yield (180 mg) as a light yellow oil. ^1H NMR (CDCl_3): δ 7.25-7.08 (m, 8H), 6.90-6.86 (m, 2H), 3.40 (dd, J = 4.2, 12.9 Hz, 1H), 3.34 (dd, J = 4.4, 10.1 Hz, 1H), 2.95 (dd, J = 10.0, 12.6 Hz, 1H), 2.75-2.62 (m, 2H), 2.55-2.42 (m, 2H), 1.91-1.71 (m, 4H); $^{13}\text{C}\{^1\text{H}\}$ NMR (CDCl_3): δ 142.5, 139.3, 129.7, 128.5, 128.1, 128.0, 127.1, 125.9, 73.6, 53.3, 43.1, 23.5. HRMS (ESI/[M+H] $^+$) calcd. for $\text{C}_{18}\text{H}_{22}\text{N}$: 252.1747. Found: 252.1742.

Table 5-1, Entry 5. The indicated compound was purified by flash chromatography on silica gel (hexanes:EtOAc = 5:1) in a 80 % yield (167 mg) as a colorless oil. ^1H NMR (CDCl_3): δ 7.31-7.10 (m, 8H), 7.07-7.02 (m, 2H), 3.64 (dd, J = 10.0, 5.0 Hz, 1H), 3.56 (dd, J = 10.0, 5.0 Hz, 1H), 3.05 (dd, J = 10.0, 10.0 Hz, 1H), 2.57-2.36 (m, 4H), 1.68-1.53 (m, 4H), 1.45-1.35 (m, 2H); $^{13}\text{C}\{^1\text{H}\}$ NMR (CDCl_3): δ 140.0, 139.4, 129.3, 128.9, 127.8, 127.6, 126.8, 125.6, 72.8, 51.4, 39.2, 26.4, 24.6. HRMS (ESI/[M+H] $^+$) calcd. for $\text{C}_{19}\text{H}_{24}\text{N}$: 266.1903. Found: 266.1914.

Table 5-1, Entry 6. The indicated compound was purified by flash chromatography on silica gel (CH₂Cl₂:MeOH:NH₄OH = 200:10:1) in a 91 % yield (203 mg) as a waxy yellow solid. ¹H NMR (CDCl₃): δ 7.32-7.20 (m, 7H), 7.18-7.13 (m, 1H), 7.12-7.09 (m, 2H), 3.94 (dd, *J* = 6.0, 8.0 Hz, 1H), 3.33 (dd, *J* = 6.0, 13.5 Hz, 1H), 3.03 (dd, *J* = 8.5, 13.5 Hz, 1H), 2.83-2.77 (m, 2H), 2.69-2.62 (m, 2H), 1.67-1.55 (m, 8H); ¹³C{¹H} NMR (CDCl₃): δ 141.2, 140.3, 129.3, 128.5, 127.8, 127.7, 126.6, 125.6, 70.7, 52.1, 39.4, 29.2, 26.9. HRMS (ESI/[M+H]⁺) calcd. for C₂₀H₂₆N: 280.2060. Found: 280.2059.

Table 5-1, Entry 7. The indicated compound was obtained in a 90 % GC yield based on relative integration to dodecane as an internal standard. ¹H NMR (CDCl₃): δ 7.41-7.34 (m, 5H), 7.09-7.04 (m, 2H), 6.95 (m, 1H), 6.83-6.68 (m, 2H), 5.57 (s, 1H), 2.75 (s, 6H); ¹³C{¹H} NMR (CDCl₃): δ 151.9, 139.7, 138.1, 130.7, 129.1, 129.0, 128.5, 128.1, 123.9, 104.2, 41.4.

Table 5-1, Entry 8. The indicated compound was purified by flash chromatography on silica gel (hexanes:EtOAc = 20:1) in a 80 % yield (235 mg) as a colorless oil. ¹H NMR (CDCl₃): δ 7.32-7.08 (m, 10H), 3.99 (dd, *J* = 5.0, 5.0 Hz, 1H), 3.28 (dd, *J* = 15.0, 5.0 Hz, 1H), 3.04 (dd, *J* = 15.0, 5.0 Hz, 1H), 2.66-2.57 (m, 2H), 2.36-2.29 (m, 2H), 1.51-1.41 (m, 4H), 1.37-1.19 (m, 12H), 0.93 (t, *J* = 5.0 Hz, 6H); ¹³C{¹H} NMR (CDCl₃): δ 140.7, 140.6, 129.3, 128.8, 127.9, 127.6, 126.6, 125.6, 66.2, 50.1, 38.5, 31.8, 27.9, 27.1, 22.7, 14.1. HRMS (ESI/[M+H]⁺) calcd. for C₂₆H₄₀N: 366.3155. Found: 366.3169.

Table 5-1, Entry 9. The indicated compound was purified by flash chromatography on silica gel (hexanes:EtOAc = 5:1) in a 83 % yield (167 mg) as a colorless oil. ¹H NMR (CDCl₃): δ 7.26-7.09 (m, 8H), 6.94-6.90 (m, 2H), 3.76 (dd, *J* = 5.0, 15.0 Hz, 1H), 3.39 (dd, *J* = 15.0, 5.0 Hz, 1H), 3.05 (sept, *J* = 5.0 Hz, 1H), 3.86 (dd, *J* = 15.0, 10.0 Hz, 1H), 2.33 (s, 3H), 1.04 (d, *J* = 5.0 Hz, 3H), 0.96 (d, *J* = 5.0 Hz, 3H); ¹³C{¹H} NMR (CDCl₃): δ 142.3, 139.8, 129.4, 128.5, 127.8, 127.7, 126.2, 125.5, 69.3, 49.5, 40.9, 32.1, 19.6, 16.6. HRMS (ESI/[M+H]⁺) calcd. for C₁₈H₂₄N: 254.1903. Found: 254.1909.

Table 5-1, Entry 10. The indicated compound was obtained in a 84 % GC yield relative to dodecane as an internal standard. Diagnostic characterization data obtained

from crude material: ^1H NMR (CDCl_3): δ 7.86-7.78 (m, 2H), 7.42-7.37 (m, 4H), 7.35-7.28 (m, 4H), 4.18 (s, 2H), 3.61 (t, $J = 7.4$ Hz, 2H), 1.80 (pentet, $J = 7.4$ Hz, 2H), 1.43-1.25 (m, 10H), 0.95 (t, $J = 7.1$ Hz, 3H); $^{13}\text{C}\{^1\text{H}\}$ NMR (CDCl_3): δ 165.9, 140.7, 136.6, 129.5, 128.8, 128.3, 128.2, 127.2, 126.4, 52.5, 35.1, 32.0, 31.2, 29.6, 29.4, 27.8, 22.8, 14.2.

Table 5-1, Entry 11. The indicated compound was obtained in a 72 % GC yield relative to dodecane as an internal standard. Diagnostic characterization data obtained from crude material: ^1H NMR (CDCl_3): δ 7.83-7.78 (m, 2H), 7.46-7.29 (m, 8H), 4.16 (s, 2H), 3.65 (septet, $J = 5.1$ Hz, 1H), 1.90-1.82 (m, 2H), 1.78-1.66 (m, 6H), 1.42-1.30 (m, 2H); $^{13}\text{C}\{^1\text{H}\}$ NMR (CDCl_3): δ 163.7, 141.3, 137.5, 132.1, 130.1-127.4 (5 Ar-CH), 60.7, 35.4, 34.3, 26.2, 25.2.

Table 5-1, Entry 12. The indicated compound was purified by flash chromatography on silica gel (hexanes:EtOAc = 5:1) in a 75 % yield (172 mg) as a colorless oil. ^1H NMR (CDCl_3): δ 7.45-7.25 (m, 11H), 7.20-7.16 (m, 4H), 3.95 (dd, $J = 5.0, 10.0$ Hz, 1H), 3.73 (d, $J = 10.0$ Hz, 1H), 3.53 (d, $J = 10.0$ Hz, 1H), 3.00 (m, 2H), 1.84 (br s, 1H); $^{13}\text{C}\{^1\text{H}\}$ NMR (CDCl_3): δ 143.7, 140.4, 138.8, 129.3, 128.3, 128.2, 127.9, 127.4, 127.1, 126.7, 126.3, 63.6, 51.3, 42.3. HRMS (ESI/[M+H] $^+$) calcd. for $\text{C}_{21}\text{H}_{22}\text{N}$: 288.1747. Found: 288.1746.

Table 5-1, Entry 13. The indicated compound was purified by flash chromatography on silica gel (hexanes:EtOAc = 10:1) in a 84 % yield (260 mg) as a white solid. ^1H NMR (CDCl_3): δ 7.32-7.12 (m, 8H), 7.04-7.00 (m, 2H), 6.26-6.20 (m, 2H), 6.15 (m, 1H), 3.79 (s, 3H), 3.63 (dd, $J = 10.0, 5.0$ Hz, 1H), 3.41 (dd, $J = 10.0, 5.0$ Hz, 1H), 3.21 (m, 4H), 3.00 (dd, $J = 15.0, 10.0$ Hz, 1H), 2.73-2.63 (m, 4H); $^{13}\text{C}\{^1\text{H}\}$ NMR (CDCl_3): δ 165.7, 163.7, 161.6 (d, $J = 12.6$ Hz), 153.4 (d, $J = 12.6$ Hz), 139.6 (d, $J = 25.2$ Hz), 129.6, 128.9, 128.1, 127.4, 126.0, 97.6, 95.6 (d, $J = 25.2$ Hz), 92.2 (d, $J = 25.2$ Hz), 72.1, 55.6, 50.5, 49.0, 39.6. HRMS (ESI/[M+H] $^+$) calcd. for $\text{C}_{25}\text{H}_{28}\text{FN}_2\text{O}$: 391.2180. Found: 391.2185.

Table 5-1, Entry 14. The indicated compound was purified by flash chromatography on silica gel (hexanes:EtOAc = 5:1) in a 90 % yield (264 mg) as a white solid. ^1H NMR (CDCl_3): δ 7.57 (dd, $J = 2.0, 7.5$ Hz, 1H), 7.50 (m, 1H), 7.31-7.22 (m, 3H), 7.21-7.11 (m, 5H), 7.04-6.99 (m, 4H), 3.66 (dd, $J = 5.5, 9.0$ Hz, 1H), 3.41 (dd, $J = 5.5,$

13.0 Hz, 1H), 3.31-3.21 (m, 4H), 2.99 (dd, $J = 9.5, 13.5$ Hz, 1H), 2.83-2.70 (m, 4H); $^{13}\text{C}\{^1\text{H}\}$ NMR (CDCl_3): δ 155.7, 139.6, 139.3, 134.4, 133.7, 129.4, 128.7, 128.0, 127.9, 127.1, 125.8, 121.5, 118.5, 118.4, 105.7, 72.0, 51.8, 50.5, 39.3. HRMS (ESI/[M+H]⁺) calcd. for $\text{C}_{25}\text{H}_{26}\text{N}_3$: 368.2121. Found: 368.2108.

Table 5-1, Entry 15. The indicated compound was purified by flash chromatography on silica gel (CH_2Cl_2 :MeOH = 50:1) in a 85 % yield (234 mg) as a white solid. ^1H NMR (CDCl_3): δ 8.79-8.73 (m, 2H), 7.78-7.55 (m, 8H), 7.52-7.45 (m, 2H), 6.96-6.90 (m, 1H), 4.37-4.24 (m, 4H), 4.11 (m, 1H), 3.86 (m, 1H), 3.48 (m, 1H), 3.10-3.00 (m, 4H); $^{13}\text{C}\{^1\text{H}\}$ NMR (CDCl_3): δ 157.6, 139.4, 129.4, 128.8, 127.9, 127.8, 127.1, 125.8, 109.6, 71.9, 50.3, 43.9, 39.2. HRMS (ESI/[M+H]⁺) calcd. for $\text{C}_{22}\text{H}_{25}\text{N}_4$: 345.2074. Found: 345.2062.

Table 5-1, Entry 16. The indicated compound was purified by flash chromatography on silica gel (CH_2Cl_2 :MeOH = 30:1) in a 91 % yield (281 mg) as a yellow solid. ^1H NMR (CDCl_3): δ 8.16-8.11 (m, 2H), 7.32-7.23 (m, 3H), 7.22-7.13 (m, 5H), 7.05-7.00 (m, 2H), 6.83-6.78 (m, 2H), 3.66 (dd, $J = 6.0, 9.0$ Hz, 1H), 3.48-3.42 (m, 4H), 3.39 (dd, $J = 5.5, 14.0$ Hz, 1H), 3.01 (dd, $J = 9.0, 13.0$ Hz, 1H), 2.72-2.64 (m, 4H); $^{13}\text{C}\{^1\text{H}\}$ NMR (CDCl_3): δ 154.8, 139.1, 139.0, 138.3, 129.3, 128.6, 128.0, 127.9, 127.3, 125.9, 112.4, 71.7, 49.9, 47.2, 39.2. HRMS (ESI/[M+H]⁺) calcd. for $\text{C}_{24}\text{H}_{26}\text{N}_3\text{O}_2$: 388.2020. Found: 388.2010.

Table 5-1, Entry 17. The indicated compound was purified by flash chromatography on silica gel (CH_2Cl_2 :MeOH = 50:1) in a 86 % yield (250 mg) as an off-white solid. ^1H NMR (CDCl_3): δ 7.35-7.26 (m, 3H), 7.24-7.13 (m, 6H), 7.13-7.08 (m, 1H), 7.07-7.02 (m, 2H), 6.97 (dd, $J = 1.5, 8.0$ Hz, 1H), 6.90 (dt, $J = 1.5, 7.5$ Hz, 1H), 3.70 (dd, $J = 5.5, 9.5$ Hz, 1H), 3.41 (dd, $J = 5.5, 13.0$ Hz, 1H), 3.05 (dd, $J = 9.5, 13.0$ Hz, 1H), 3.00-2.89 (m, 4H), 2.72 (br s, 4H); $^{13}\text{C}\{^1\text{H}\}$ NMR (CDCl_3): δ 151.5, 139.3, 139.2, 139.0, 129.3, 128.7, 127.9, 127.8, 127.2, 126.4, 125.8, 121.4, 119.9, 113.9, 71.9, 52.9, 51.0, 39.3. HRMS (ESI/[M+H]⁺) calcd. for $\text{C}_{24}\text{H}_{27}\text{N}_2\text{O}$: 359.2118. Found: 359.2119.

Table 5-1, Entry 18. The indicated compound was purified by flash chromatography on silica gel (hexanes:EtOAc = 2:1) in a 93 % yield (246 mg) as a colorless oil. ^1H NMR (CDCl_3): δ 7.33-7.23 (m, 3H), 7.21-7.12 (m, 5H), 7.05-6.99 (m, 2H), 3.78-3.61 (m, 5H), 3.37 (dd, $J = 5.5, 13.5$ Hz, 1H), 3.00 (dd, $J = 9.0, 13.0$ Hz, 1H),

2.61-2.47 (m, 4H), 1.71 (m, 1H), 0.98 (m, 2H), 0.75 (m, 2H); $^{13}\text{C}\{^1\text{H}\}$ NMR (CDCl_3): δ 171.7, 139.3, 139.2, 129.3, 128.7, 127.9, 127.8, 127.2, 125.9, 71.7, 53.4, 50.8, 49.9, 45.7, 42.3, 39.2, 10.8, 7.3. HRMS (ESI/[M+H] $^+$) calcd. for $\text{C}_{22}\text{H}_{27}\text{N}_2\text{O}$: 335.2118. Found: 335.2116.

Table 5-1, Entry 19. The indicated compound was purified by flash chromatography on silica gel (hexanes:EtOAc = 5:1) in a 76 % yield (207 mg) as a colorless oil. ^1H NMR (CDCl_3): δ 7.32-7.11 (m, 8H), 7.07-7.02 (m, 2H), 4.15 (q, J = 7.0 Hz, 2H), 3.66 (dd, J = 7.0, 7.0 Hz, 1H), 3.35 (dd, J = 7.0, 13.5 Hz, 1H), 3.09-2.95 (m, 3H), 2.22 (m, 1H), 2.14 (m, 1H), 2.02-1.69 (m, 5H), 1.27 (t, J = 7.0 Hz, 3H); $^{13}\text{C}\{^1\text{H}\}$ NMR (CDCl_3): δ 175.2, 139.7, 139.4, 129.3, 128.7, 127.8, 127.7, 126.9, 125.7, 71.7, 60.1, 51.1, 48.5, 41.4, 31.1, 28.6, 28.5, 14.2. HRMS (ESI/[M+H] $^+$) calcd. for $\text{C}_{22}\text{H}_{28}\text{NO}_2$: 338.2115. Found: 338.2108.

Table 5-1, Entry 20. In order to most accurately reflect the yield of this reaction, given the difficulty in isolating pure material after reduction, the enamine compound was isolated as the corresponding hydrolysis ketone product in an 80 % yield. Prior to hydrolysis, $^1\text{H}/^{13}\text{C}\{^1\text{H}\}$ NMR analysis of the crude reaction mixture indicated the following diagnostic signals for the enamine product. ^1H NMR (dioxane- d_8): δ 10.54 (br s, 1H), 7.57 (m, 1H), 7.38 (m, 1H), 7.33-7.27 (m, 3H), 7.01-6.94 (m, 2H), 6.87 (m, 1H), 6.78-6.77 (m, 2H), 5.66 (s, 1H), 3.35-3.27 (m, 2H), 2.64-2.55 (m, 2H), 2.43 (m, 1H), 1.95-1.86 (m, 2H), 1.79-1.70 (m, 2H); $^{13}\text{C}\{^1\text{H}\}$ NMR (dioxane- d_8): δ 177.0, 152.2, 139.9, 138.7, 131.1, 129.3, 129.2, 128.9, 128.4, 124.8, 106.7, 49.3, 41.6, 29.2.

Table 5-2, Entry 1. The indicated compounds were purified by flash chromatography on silica gel (CH_2Cl_2 :MeOH: NH_4OH = 1000:10:1) in a combined 86 % yield (194 mg) as colorless oils (major – 157 mg; minor – 36 mg). ^1H NMR analysis of the reaction mixture prior to reduction indicated a product ratio of 4:1. **major** - ^1H NMR (CDCl_3): δ 7.45-7.39 (m, 2H), 7.37-7.29 (m, 5H), 7.26-7.21 (m, 1H), 7.20-7.14 (m, 2H), 3.79-3.70 (m, 4H), 3.36 (dd, J = 5.0, 9.0 Hz, 1H), 2.57-2.41 (m, 6H), 2.32 (m, 1H), 2.09 (m, 1H); $^{13}\text{C}\{^1\text{H}\}$ NMR (CDCl_3): δ 142.1, 139.8, 128.7, 128.3, 128.2, 128.1, 127.2, 125.7, 69.7, 67.2, 50.8, 34.1, 32.3. HRMS (ESI/[M+H] $^+$) calcd. for $\text{C}_{19}\text{H}_{24}\text{NO}$: 282.1852. Found: 282.1870. **minor** - ^1H NMR (CDCl_3): δ 7.33-7.26 (m, 4H), 7.24-7.13 (m, 6H), 3.70-3.63 (m, 4H), 3.01 (pent, J = 7.0 Hz, 1H), 2.93 (dd, J = 7.0, 12.5 Hz, 2H), 2.72-2.65

(m, 4H), 2.57 (dd, $J = 6.5, 13.5$ Hz, 2H); $^{13}\text{C}\{^1\text{H}\}$ NMR (CDCl_3): δ 140.7, 129.1, 128.1, 125.7, 68.5, 67.4, 49.0, 35.8. HRMS (ESI/[M+H] $^+$) calcd. for $\text{C}_{19}\text{H}_{24}\text{NO}$: 282.1852. Found: 282.1867.

Table 5-2, Entry 2. The identity of the regioisomer was determined by ^1H NMR of the crude enamine product before reduction. The indicated compound was purified by flash chromatography on silica gel (CH_2Cl_2 :MeOH: $\text{NH}_4\text{OH} = 1000:10:1$) in a 88 % yield (219 mg) as a light orange oil. ^1H NMR analysis of the reaction mixture prior to reduction indicated a product ratio of >20:1. ^1H NMR (CDCl_3): δ 7.33-7.27 (m, 2H), 7.24-7.19 (m, 3H), 7.17-7.13 (m, 2H), 6.96-6.92 (m, 2H), 3.87 (s, 3H), 3.76-3.66 (m, 4H), 3.29 (dd, $J = 5.5, 9.0$ Hz, 1H), 2.54-2.39 (m, 6H), 2.27 (m, 1H), 2.03 (m, 1H); $^{13}\text{C}\{^1\text{H}\}$ NMR (CDCl_3): δ 158.8, 142.3, 131.8, 129.8, 128.4, 128.3, 125.8, 113.6, 69.1, 67.3, 55.3, 50.9, 34.3, 32.6. HRMS (ESI/[M+H] $^+$) calcd. for $\text{C}_{20}\text{H}_{26}\text{NO}_2$: 312.1958. Found: 312.1942.

Table 5-2, Entry 3. The identity of the regioisomer was determined by ^1H NMR of the crude enamine product before reduction. The indicated compound was purified by flash chromatography on silica gel (CH_2Cl_2 :MeOH: $\text{NH}_4\text{OH} = 1000:10:1$) in a 76 % yield (188 mg) as a beige solid. ^1H NMR analysis of the reaction mixture prior to reduction indicated a product ratio of 1:19. ^1H NMR (CDCl_3): δ 7.57-7.52 (m, 2H), 7.33-7.28 (m, 2H), 7.26-7.19 (m, 3H), 7.18-7.14 (m, 2H), 3.70-3.61 (m, 4H), 3.03 (dd, $J = 5.5, 13.5$ Hz, 1H), 2.97 (m, 1H), 2.88 (dd, $J = 8.5, 14.0$ Hz, 1H), 2.77-2.70 (m, 2H), 2.67-2.57 (m, 3H), 2.50 (dd, $J = 8.5, 13.5$ Hz, 1H); $^{13}\text{C}\{^1\text{H}\}$ NMR (CDCl_3): δ 146.6, 140.0, 131.9, 129.9, 129.1, 128.5, 126.2, 119.2, 109.6, 68.5, 67.4, 48.9, 36.1, 35.6. HRMS (ESI/[M+H] $^+$) calcd. for $\text{C}_{20}\text{H}_{23}\text{N}_2\text{O}$: 307.1805. Found: 307.1798.

Table 5-2, Entry 4. The indicated compounds were observed in a combined 86 % ^1H NMR yield in a 3:1 ratio relative to 1,3,5-trimethoxybenzene as an internal standard. *major* – ^1H NMR (toluene- d_8): δ 7.39-7.35 (m, 2H), 7.26-7.23 (m, 1H), 7.22-7.18 (m, 2H), 4.59 (t, $J = 7.0$ Hz, 1H), 3.55-3.50 (m, 4H), 2.58-2.54 (m, 4H), 2.04 (q, $J = 7.0$ Hz, 2H), 1.40 (sextet, $J = 7.0$ Hz, 2H), 0.87 (t, $J = 7.5$ Hz, 3H); $^{13}\text{C}\{^1\text{H}\}$ NMR (toluene- d_8): δ 128.4, 127.5, 126.5, 104.5, 65.4, 48.7, 29.1, 23.1, 12.2. *minor* – ^1H NMR (toluene- d_8): δ 7.22-7.18 (m, 2H), 7.15-7.10 (m, 3H), 5.51 (s, 1H), 3.49-3.45 (m, 4H), 2.53-2.49 (m, 4H), 2.31-2.26 (m, 2H), 1.51 (sextet, $J = 7.5$ Hz, 2H), 0.87 (t, $J = 7.5$ Hz, 3H); $^{13}\text{C}\{^1\text{H}\}$ NMR (toluene- d_8): δ 126.6, 126.5, 126.0, 103.9, 65.3, 47.1, 27.7, 20.4, 12.3.

Table 5-2, Entry 5. The identity of the regioisomer was determined by ^1H NMR of the crude enamine product before reduction. The indicated compound was purified by flash chromatography on silica gel ($\text{CH}_2\text{Cl}_2:\text{MeOH}:\text{NH}_4\text{OH} = 1000:10:1$) in a 75 % yield (158 mg) as a faint yellow oil. ^1H NMR analysis of the reaction mixture prior to reduction indicated a product ratio of 18:1. ^1H NMR (CDCl_3): δ 7.19-7.15 (m, 2H), 6.91-6.87 (m, 2H), 3.84 (s, 3H), 3.74-3.67 (m, 4H), 3.21 (dd, $J = 4.6, 9.7$ Hz, 1H), 2.55-2.45 (m, 2H), 2.44-2.37 (m, 2H), 1.90 (m, 1H), 1.70 (m, 1H), 1.36-1.21 (m, 2H), 1.19-0.99 (m, 2H), 0.85 (t, $J = 7.4$ Hz, 3H); $^{13}\text{C}\{^1\text{H}\}$ NMR (CDCl_3): δ 158.7, 132.3, 129.6, 113.4, 70.1, 67.2, 55.2, 51.1, 32.2, 28.5, 22.8 14.0. HRMS (ESI/[M+H] $^+$) calcd. for $\text{C}_{16}\text{H}_{26}\text{NO}_2$: 264.1958. Found: 264.1940.

Table 5-2, Entry 6. The indicated compounds were observed in a combined 83 % ^1H NMR yield in a 4:1 ratio relative to 1,3,5-trimethoxybenzene as an internal standard. *major* - ^1H NMR (CDCl_3): δ 7.26-7.22 (m, 2H), 6.93-6.89 (m, 2H), 4.45 (t, $J = 7.2$ Hz, 1H), 3.86 (s, 3H), 3.18 (pentet, $J = 6.7$ Hz, 1H), 2.54 (s, 3H), 1.91 (m, 2H), 1.35 (m, 2H), 0.96 (d, $J = 6.9$ Hz, 6H), 0.86 (t, $J = 7.4$ Hz, 3H); $^{13}\text{C}\{^1\text{H}\}$ NMR (CDCl_3): δ 159.1, 149.1, 132.0, 131.0, 113.6, 105.2, 55.7, 49.1, 31.1, 30.8, 25.1, 18.8, 14.2. *minor* - ^1H NMR (CDCl_3): δ 7.12-7.08 (m, 2H), 6.99-6.96 (m, 2H), 5.32 (s, 1H), 3.90 (s, 3H), 3.17 (m, 1H), 2.59 (s, 3H), 1.45 (m, 2H), 1.14 (d, $J = 7.4$ Hz, 6H), 0.96 (t, $J = 7.1$ Hz, 3H), 0.91 (t, $J = 7.6$ Hz, 2H); $^{13}\text{C}\{^1\text{H}\}$ NMR (CDCl_3): δ 156.8, 149.7, 133.7, 130.0, 113.9, 102.2, 55.6, 47.6, 30.5, 30.4, 22.9, 19.7, 14.5.

Table 2, Entry 8. The indicated compound was observed in an 80 % ^1H NMR yield in a 1:>20 ratio relative to 1,3,5-trimethoxybenzene as an internal standard. ^1H NMR (CDCl_3): δ 8.48 (m, 1H), 7.52 (dt, $J = 7.5, 1.8$ Hz, 1H), 7.06 (dt, $J = 7.9, 1.1$ Hz, 1H), 6.92 (m, 1H), 5.52 (s, 1H), 3.80-3.76 (m, 4H), 3.09-3.05 (m, 4H), 2.79-2.74 (m, 2H), 1.61-1.52 (m, 2H), 0.98 (t, $J = 7.2$ Hz, 3H); $^{13}\text{C}\{^1\text{H}\}$ NMR (CDCl_3): δ 161.6, 158.6, 148.8, 135.8, 123.1, 118.7, 103.2, 67.0, 47.8, 29.7, 22.0, 14.2.

Table 5-2, Entry 9. The indicated compounds were observed in a combined 90 % ^1H NMR yield in a 2:1 ratio of the olefin isomerization product (major) to the expected hydroamination product (minor) relative to 1,3,5-trimethoxybenzene as an internal standard. *major* - ^1H NMR (toluene- d_8): δ 4.42 (q, $J = 6.8$ Hz, 1H), 3.56-3.52 (m, 4H), 2.55-2.49 (m, 4H), 2.10-2.02 (m, 2H), 1.65 (d, $J = 7.4$ Hz, 3H), 1.46 (sextet, $J = 7.4$ Hz,

2H), 0.92 (t, $J = 7.5$ Hz, 3H); $^{13}\text{C}\{^1\text{H}\}$ NMR (toluene- d_8): δ 97.4, 65.9, 48.5, 28.3, 20.4, 12.7, 11.6. *minor* – ^1H NMR (toluene- d_8): δ 4.31 (t, $J = 7.4$ Hz, 1H), 3.56-3.52 (m, 4H), 2.55-2.49 (m, 4H), 2.10-2.02 (m, 4H), 1.04 (t, $J = 7.5$ Hz, 3H), 1.00 (t, $J = 7.5$ Hz, 3H); $^{13}\text{C}\{^1\text{H}\}$ NMR (toluene- d_8): δ 104.9, 65.8, 48.3, 19.9, 19.7, 14.7, 12.4.

Table 5-2, Entry 10. The indicated compound was purified by flash chromatography on silica gel ($\text{CH}_2\text{Cl}_2:\text{MeOH}:\text{NH}_4\text{OH} = 1000:10:1$) in a 73 % yield (212 mg) as an off-white solid. ^1H NMR analysis of the reaction mixture prior to reduction indicated a product ratio of $>20:1$. ^1H NMR (CDCl_3): δ 7.87-7.82 (m, 2H), 7.76-7.71 (m, 2H), 7.35-7.20 (m, 5H), 3.72-3.64 (m, 6H), 3.29 (dd, $J = 5.0, 9.0$ Hz, 1H), 2.51-2.34 (m, 4H), 1.98 (m, 1H), 1.78 (m, 1H), 1.62 (m, 1H), 1.49 (m, 1H); $^{13}\text{C}\{^1\text{H}\}$ NMR (CDCl_3): δ 168.3, 139.7, 133.9, 132.1, 128.5, 128.2, 127.3, 123.1, 69.9, 67.2, 50.9, 37.9, 29.6, 25.4. HRMS (ESI/ $[\text{M}+\text{H}]^+$) calcd. for $\text{C}_{22}\text{H}_{25}\text{N}_2\text{O}_3$: 365.1860. Found: 365.1861.

Table 2, Entry 11. The indicated compound was observed in an 88 % ^1H NMR yield in a $>20:1$ ratio relative to 1,3,5-trimethoxybenzene as an internal standard. ^1H NMR (CDCl_3): δ 8.28 (d, $J = 4.8$ Hz, 2H), 7.79 (dd, $J = 5.4, 3.2$ Hz, 2H), 7.69 (dd, $J = 5.5, 3.0$ Hz, 2H), 7.29-7.25 (m, 3H), 7.21-7.16 (m, 2H), 6.46 (t, $J = 4.7$ Hz, 1H), 4.62 (t, $J = 7.6$ Hz, 1H), 3.81-3.74 (m, 4H), 3.66 (t, $J = 7.0$ Hz, 2H), 2.81-2.75 (m, 4H), 2.35 (m, 2H); $^{13}\text{C}\{^1\text{H}\}$ NMR (CDCl_3): δ 168.1, 161.6, 157.7, 151.6, 137.0, 133.6, 132.0, 129.4, 128.0, 127.4, 122.9, 109.8, 101.6, 48.8, 43.6, 38.6, 27.4.

Table 5-2, Entry 12. The identity of the regioisomers was determined by ^1H NMR of the crude enamine product before reduction. The indicated compounds were purified by flash chromatography on silica gel (hexanes:EtOAc = 10:1 \rightarrow 5:1) in a combined 79 % yield (229 mg) as colorless oils (major – 176 mg; minor – 53 mg). ^1H NMR analysis of the reaction mixture prior to reduction indicated a product ratio of 3:1. *major* – ^1H NMR (CDCl_3): δ 7.36-7.24 (m, 5H), 3.73-3.68 (m, 4H), 3.58-3.53 (m, 2H), 3.23 (dd, $J = 5.0, 9.5$ Hz, 1H), 2.53-2.44 (m, 2H), 2.43-2.35 (m, 2H), 1.93 (m, 1H), 1.72 (m, 1H), 1.57-1.42 (m, 2H), 1.26-1.06 (m, 2H), 0.88 (s, 9H), 0.03 (m, 6H); $^{13}\text{C}\{^1\text{H}\}$ NMR (CDCl_3): δ 140.7, 128.6, 128.1, 127.0, 70.6, 67.3, 63.0, 51.2, 32.9, 32.3, 25.9, 22.4, 18.3, -5.3. HRMS (ESI/ $[\text{M}+\text{H}]^+$) calcd. for $\text{C}_{21}\text{H}_{38}\text{NO}_2\text{Si}$: 364.2666. Found: 364.2671. *minor* – ^1H NMR (CDCl_3): δ 7.33-7.27 (m, 2H), 7.23-7.16 (m, 3H), 3.77-3.68 (m, 4H), 3.60-3.54 (m, 2H), 3.00 (dd, $J = 4.5, 13.0$ Hz, 1H), 2.75-2.69 (m, 2H), 2.64 (m, 1H), 2.59-2.53 (m,

2H), 2.39 (dd, $J = 8.5, 13.0$ Hz, 1H), 1.69 (m, 1H), 1.54-1.37 (m, 3H), 0.89 (s, 9H), 0.04 (m, 6H). $^{13}\text{C}\{^1\text{H}\}$ NMR (CDCl_3): δ 140.9, 129.2, 128.2, 125.7, 67.5, 66.3, 63.1, 48.7, 35.5, 29.9, 26.1, 25.9, 18.3, -5.3. HRMS (ESI/[M+H]⁺) calcd. for $\text{C}_{21}\text{H}_{38}\text{NO}_2\text{Si}$: 364.2666. Found: 364.2675.

Table 2, Entry 13. The indicated compounds were observed in a combined 76 % ^1H NMR yield in a 5:1 ratio relative to 1,3,5-trimethoxybenzene as an internal standard. *major* - ^1H NMR (CDCl_3): δ 8.32 (d, $J = 4.9$ Hz, 2H), 7.40-7.37 (m, 2H), 7.30-7.26 (m, 1H), 7.22-7.18 (m, 2H), 6.49 (t, $J = 4.6$ Hz, 1H), 4.69 (t, $J = 7.4$ Hz, 1H), 3.87-3.80 (m, 4H), 3.58 (t, $J = 6.5$ Hz, 2H), 2.84-2.79 (m, 4H), 2.05 (m, 2H), 1.59 (m, 2H), 0.89 (s, 9H), 0.04 (s, 6H); $^{13}\text{C}\{^1\text{H}\}$ NMR (CDCl_3): δ 162.2, 158.1, 150.0, 138.4, 130.1, 128.4, 127.9, 110.3, 106.8, 63.2, 49.8, 44.3, 34.9, 28.9, 26.4, 25.1, -4.9.

Representative procedure for the determination of the rate constants (k_{obs}) for the hydroamination of 5-4 with 5-5 catalyzed by 5-1/AgB(C₆F₅)₄. To six screw-capped vials containing 5-1 (4.3 mg, 0.0030 mmol) and a stir-bar was added 0.100 mL of a stock solution of dodecane (34 μL , 0.15 mmol) in toluene and 0.500 mL of a stock solution of diphenylacetylene (54 mg, 0.30 mmol) in toluene followed by morpholine (26 μL , 0.3 mmol). The vials were sealed under N_2 with a cap containing a PTFE septum, removed from the glovebox, and were placed in a temperature-controlled aluminum heating block set at 110 °C. At a given sample time, a vial was removed from the heating block followed by rapid cooling in an ice bath. The conversion of diphenylacetylene to the enamine product was quantified by GC analysis of the crude reaction mixture relative to dodecane as an internal standard using a calibration curve. The resulting concentration versus time data were corrected for the starting concentration of organic reagents based on an initial GC run at time-zero before heating. Pseudo-first order rate constants were obtained by plotting $\ln[5-4]_t$ vs. time (in all cases these gave linear plots; $R^2 > 0.98$).

Determination of reaction order in catalyst for 5-11-catalyzed hydroamination (Figure 5-6a). Pseudo-first order rate constants were obtained by plotting $\ln[\text{diphenylacetylene}(5-4)]_t$ vs. time (in all cases these gave linear plots) for a series of experiments with varied [5-11] (0.0023 – 0.015 M). The k_{obs} values obtained in

these experiments were plotted versus [5-11] to determine the reaction order in catalyst (Figure 5-6a).

Determination of reaction order in diphenylacetylene (5-4) for the 5-11/AgB(C₆F₅)₄-catalyzed hydroamination (Figure 5-6a). Pseudo-first order rate constants were obtained by plotting $\ln[\text{diphenylacetylene(5-4)}]_t$ vs. time (in all cases these gave linear plots) for a series of experiments with varied [diphenylacetylene (5-4)] (0.75 – 1.6 M). The k_{obs} values obtained in these experiments were plotted versus [diphenylacetylene (5-4)] to determine the reaction order in alkyne (Figure 5-6b).

Determination of reaction order in morpholine (5-5a) for the 5-11/AgB(C₆F₅)₄-catalyzed hydroamination (Figure 5-6c). Pseudo-first order rate constants were obtained by plotting $\ln[\text{diphenylacetylene(5-4)}]_t$ vs. time (in all cases these gave linear plots) for a series of experiments with varied [morpholine (5-5a)] (0.65 – 1.9 mM). The k_{obs} values obtained in these experiments were plotted versus [morpholine (5-5a)] to determine the reaction order in amine (Figure 5-6c).

General procedure for the determination of activation parameters for the hydroamination of 5-4 with 5-5a employing 5-1/AgB(C₆F₅)₄ (Figure 5-7). To six screw-capped vials containing 5-1 (2.1 mg, 0.0030 mmol), AgB(C₆F₅)₄ (2.4 mg, 0.0030 mmol) and a stir-bar was added 0.300 mL of a stock solution of dodecane (34 μL , 0.15 mmol) in toluene and 0.300 mL of a stock solution of diphenylacetylene (54 mg, 0.3 mmol) in toluene followed by morpholine (26 μL , 0.3 mmol). The vials were sealed under N₂ with a cap containing a PTFE septum, removed from the glovebox, and were placed in a temperature-controlled aluminum heating block set at desired temperature (90-130 °C). At a given sample time, a vial was removed from the heating block followed by rapid cooling in an ice bath. The conversion of diphenylacetylene to the enamine product was quantified by GC analysis of the crude reaction mixture relative to dodecane as an internal standard using a calibration curve. The resulting concentration versus time data were corrected for the starting concentration of organic reagents based on an initial GC run at time-zero before heating. Pseudo-first order rate constants were obtained by plotting $\ln[\text{alkyne (5-4)}]_t$ vs. time (in all cases these gave linear plots; $R^2 > 0.98$). The k_{obs} values obtained in these experiments were used in Eyring and Arrhenius analyses (Figure 5-7) and values of ΔH^\ddagger , ΔS^\ddagger , and E_a were calculated.

Determination of kinetic isotope effect (KIE) for 5-1/AgB(C₆F₅)₄-catalyzed hydroamination of 5-4 and 5-5a (Figure 5-8). Using the general procedure, pseudo-first order rate constants were obtained by plotting $\ln[\text{diphenylacetylene (5-4)}]_t$ vs. time; in all cases these gave linear plots. The k_{obs} values obtained in these experiments were used to determine the H/D KIE (Figure 5-8).

5.4.3 Crystallographic Solution and refinement Details

Crystallographic data collection, solution, and refinement for all structures were conducted by Drs. Robert McDonald and Michael Ferguson, X-Ray Crystallography Laboratory, University of Alberta. Selected crystallographic data are located in tabulated form at the end of this chapter; the ORTEP diagrams featured in the text were prepared by use of ORTEP-3 for Windows version 1.074.^[32]

Crystallographic characterization of 5-1 and 5-11. Crystallographic data for **5-1** and **5-11** were obtained at 173(±2) K on a Bruker D8/APEX II CCD diffractometer using graphite-monochromated Mo K α ($\lambda = 0.71073 \text{ \AA}$) radiation, employing samples that were mounted in inert oil and transferred to a cold gas stream on the diffractometer. Programs for diffractometer operation, data collection, data reduction, and absorption correction were supplied by Bruker. For **5-1** the structure was solved by use of direct methods, while for **5-11** the structure was solved by using a Patterson search/structure expansion. Refinements were carried out by use of full-matrix least-squares procedures (on F^2) with $R1$ based on $F_o^2 \geq 2\sigma(F_o^2)$ and $wR2$ based on $F_o^2 \geq -3\sigma(F_o^2)$. Anisotropic displacement parameters were employed throughout for the non-hydrogen atoms. All hydrogen atoms were added at calculated positions and refined by use of a riding model employing isotropic displacement parameters based on the isotropic displacement parameter of the attached atom.

Table 5.3. Crystallographic Data for **5-1** and **5-11**.

	5-1	5-11
empirical formula	C ₃₁ H ₄₄ AuCINOP	C ₅₈ H ₅₁ AuBF ₂₀ N ₂ O ₂ P
formula weight	780.96	1426.75
crystal dimensions (mm)	0.55 x 0.20 x 0.15	0.51 x 0.48 x 0.42
crystal system	orthorhombic	triclinic
space group	<i>Pna</i> 2 ₁	<i>P</i> (-1)
<i>a</i> (Å)	19.9341 (6)	12.6170 (9)
<i>b</i> (Å)	10.8494 (3)	12.7549 (10)
<i>c</i> (Å)	13.9902 (15)	18.2237 (14)
α (deg)	90	88.5121 (8)
β (deg)	90	72.5456 (7)
γ (deg)	90	80.7996 (8)
<i>V</i> (Å ³)	3025.70 (15)	2760.9 (4)
<i>Z</i>	4	2
ρ_{calcd} (g cm ⁻³)	1.714	1.716
μ (mm ⁻¹)	5.206	2.807
range of transmission	0.5149 – 0.1626	0.3852 – 0.3280
2 θ limit (deg)	55.02	55.16
index ranges	-25 ≤ <i>h</i> ≤ 25 -14 ≤ <i>k</i> ≤ 14 -18 ≤ <i>l</i> ≤ 18	-16 ≤ <i>h</i> ≤ 16 -16 ≤ <i>k</i> ≤ 16 -23 ≤ <i>l</i> ≤ 23
total data collected	25086	24447
independent reflections	6786	12622
<i>R</i> _{int}	0.0130	0.0092
observed reflections	6639	12290
data/restraints/params	6786 / 0 / 343	12622 / 0 / 766
goodness-of-fit	1.043	1.073
<i>R</i> ₁ [<i>F</i> _o ² ≥ 2σ(<i>F</i> _o ²)]	0.0128	0.0154
<i>wR</i> ₂ [<i>F</i> _o ² ≥ -3σ(<i>F</i> _o ²)]	0.0332	0.0411

Chapter 6 – Conclusions

6.1 Chapter 2

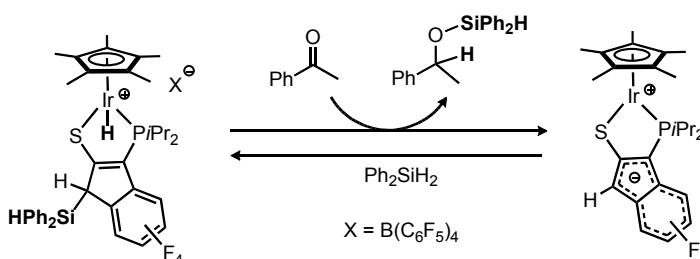
6.1.1 Summary

The synthesis and divergent reactivity of new coordinately unsaturated cationic and zwitterionic Cp*Ir complexes supported by κ^2 -3-PiPr₂-2-S-indene was reported in Chapter 2. Treatment of 0.5 equiv [Cp*IrCl₂]₂ with 1/3-PiPr₂-2-StBu-indene afforded Cp*Ir(Cl)(κ^2 -3-PiPr₂-2-S-indene) **2-1**. Addition of AgOTf or LiB(C₆F₅)₄·2.5OEt₂ to **2-1** gave coordinately unsaturated [Cp*Ir(κ^2 -3-PiPr₂-2-S-indene)]⁺X⁻ (X = OTf, **2-2**; X = B(C₆F₅)₄, **2-3**), which represent rare examples of isolable coordinately unsaturated [Cp*Ir(κ^2 -P,S)]⁺X⁻ complexes. Exposure of **2-2** to CO afforded **2-4**, while treatment of **2-3** with PMe₃ generated **2-5**. Treatment of **2-1** with K₂CO₃ in CH₃CN allowed for the isolation of the unusual acetonitrile adduct **2-7**, in which the CH₃CN bridges the Lewis acidic Cp*Ir and Lewis basic indenide fragments of the targeted coordinately unsaturated zwitterion Cp*Ir(κ^2 -3-PiPr₂-2-S-indenide) **2-6**. In contrast to the formation of **2-4**, exposure of **2-7** to CO did not afford the corresponding CO-adduct; instead, a clean 1:1 mixture of (κ^2 -3-PiPr₂-2-S-indene)Ir(CO)₂ **2-8** and 1,2,3,4-tetramethylfulvene was generated. Treatment of **2-2** with Ph₂SiH₂ resulted in the net loss of Ph₂Si(OTf)H to give Cp*Ir(H)(κ^2 -3-PiPr₂-2-S-indene) **2-9**. In contrast, treatment of **2-3** with Ph₂SiH₂ or PhSiH₃ proceeded via H-Si addition across Ir-S to give the corresponding [Cp*Ir(H)(κ^2 -3-PiPr₂-2-S(SiHPhX)-indene)]⁺B(C₆F₅)₄⁻ complexes **2-10** (X = Ph) or **2-11** (X = H), which feature a newly established S-Si linkage. Compound **2-10** was observed to effect net C-O bond cleavage in diethyl ether with net loss of Ph₂Si(OEt)H, affording [Cp*Ir(H)(κ^2 -3-PiPr₂-2-SEt-indene)]⁺B(C₆F₅)₄⁻ **2-12**. Furthermore, **2-10** proved capable of transferring Ph₂SiH₂ to acetophenone, with concomitant regeneration of **2-3**; however, **2-2** and **2-3** did not prove to be effective ketone hydrosilylation catalysts. Treatment of 1/3-PiPr₂-2-StBu-indene with 0.5 equiv [Cp*RhCl₂]₂ gave Cp*Rh(Cl)(κ^2 -3-PiPr₂-2-S-indene) **2-13** in 94% yield. Combination of **2-13** and LiB(C₆F₅)₄·2.5Et₂O produced the coordinately unsaturated cation [Cp*Rh(κ^2 -3-PiPr₂-2-S-indene)]⁺ B(C₆F₅)₄⁻ **2-14**, which was transformed into [Cp*Rh(H)(κ^2 -3-PiPr₂-2-S(SiHPh₂)-indene)]⁺B(C₆F₅)₄⁻ **2-15** via net

H-Si addition of Ph_2SiH_2 to Rh-S. Unlike **2-2** and **2-3**, complex **2-14** was shown to be an effective catalyst for ketone hydrosilylation. Treatment of **2-7** with Ph_2SiH_2 resulted in the loss of CH_3CN , along with the formation $\text{Cp}^*\text{Ir}(\text{H})(\kappa^2\text{-3-}P\text{iPr}_2\text{-2-}S\text{-}(1\text{-diphenylsilylindene}))$ **2-16** as a mixture of diastereomers. The formation of **2-16** corresponds to heterolytic H-Si bond activation, involving net addition of H^- and Ph_2HSi^+ fragments to Ir and indenide in the unobserved zwitterion **2-6**. Collectively, these results demonstrate the versatility of donor-functionalized indene ancillary ligands in allowing for the selection of divergent metal-ligand cooperativity pathways (simply by ancillary ligand deprotonation) in the activation of small molecule substrates.

6.1.2 Future Directions

Despite having successfully illustrated the potential of **2-10** and **2-15** to transfer net H^- and SiPh_2H^+ (derived from H-Si addition of Ph_2SiH_2 across the Rh/Ir-thiolate linkage) to acetophenone in a stoichiometric and catalytic fashion, respectively, similar reactivity from **2-16** has yet to be observed. Although the metal-ligand cooperative activation of Ph_2SiH_2 by the putative zwitterion **2-6** proceeds to afford the $\text{M}^{\wedge}\text{X}'$ derived product **2-16**, this species is reluctant to deliver the activated silane to ketones, presumably due to the increased Si-C bond strength (versus the Si-S in **2-10**). A potential ligand modification that might help to facilitate this transfer, resulting in the more facile regeneration of **2-6**, could involve the installation of electron-withdrawing groups on C4 through C7 on the indenide backbone in **2-6**. This would render the Si-C_{indenyl} linkage in the analogous silane activation product (i.e. **2-16**) more labile due to the increased stability of the resulting indenide anion formed upon heterolytic Si-C cleavage, and thus more susceptible to dissociation and transfer to ketone substrates (Scheme 6-1).



Scheme 6-1. Postulated application of a fluorinated $\text{Cp}^*\text{M}(\kappa^2\text{-}P,S\text{-indene-F}_4)$ ($\text{M}=\text{Ir, Rh}$) complex in the $\text{M}^{\wedge}\text{X}'$ derived organosilane activation with transfer to ketones substrates.

6.2 Chapter 3

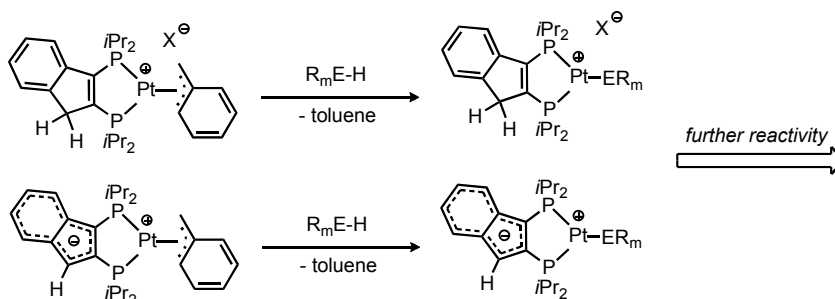
6.2.1 Summary

Chapter 3 described the preparation of neutral and cationic (κ^2 -3-*PiPr*₂-2-*StBu*-indene)Pt(benzyl) complexes, as well as structurally related zwitterions in which the formally cationic metal fragment was counterbalanced by an indenide or borate fragment that was contained within the ancillary ligand backbone. Treatment of (COD)Pt(η^1 -benzyl)Cl with 1/3-*PiPr*₂-2-*StBu*-indene provided the neutral (κ^2 -3-*PiPr*₂-2-*StBu*-indene)Pt(η^1 -benzyl)Cl complex **3-1**. Dehydrohalogenation of **3-1** with NaN(SiMe₃)₂ provided access to the zwitterionic complex (κ^2 -3-*PiPr*₂-2-*StBu*-indenide)Pt(η^3 -benzyl) **3-2**. Treatment of **3-2** with DMAP afforded the adduct **3-3**. Notably, both **3-2** and **3-3** exhibited relatively broad ¹H NMR features, which may be attributable to slow inversion at sulfur, and/or η^1 - η^3 dynamics of the coordinated benzyl ligand. The indenide-based zwitterion **3-2** was used in the preparation of alternative cationic and zwitterionic (κ^2 -*P,S*)Pt(η^3 -benzyl) complexes, whereby treatment of **3-2** with B(C₆F₅)₃ afforded the borate-based zwitterion **3-4** and addition of H(OEt)₂B(C₆F₅)₄ to **3-2** produced the cationic complex **3-5**. Although the reactivity of zwitterionic and cationic complexes **3-2** and **3-5** with E-H containing substrates was rather complex and uninformative, treatment of **3-4** with Ph₂SiH₂ provided access to [(κ^2 -3-*PiPr*₂-2-*StBu*-(1-diphenylsilylindene))Pt(η^3 -benzyl)]⁺HB(C₆F₅)₃⁻ **3-6** where the indenide coordinated B(C₆F₅)₃ group in **3-4** had been replaced by a diphenylsilyl-group.

6.2.2 Future Directions

In monitoring the reactivity of the zwitterionic (**2-2** and **2-4**) and cationic (**2-5**) (κ^2 -*P,S*)Pt(η^3 -benzyl) complexes with E-H containing substrates, the Pt-CH₂Ph linkage remained unreacted in all cases. Given the *trans* disposition of the sulfur and benzyl ligands in all of the crystallographically characterized (κ^2 -*P,S*)Pt(η^1/η^3 -benzyl) complexes, it could be rationalized that replacement of the ligand sulfur donor fragment with a more *trans*-labilizing dialkylphosphine would, in conjunction with affording a more electron-rich Pt center, encourage heightened reactivity of cationic and zwitterionic Pt-benzyl complexes towards E-H oxidative addition/C-H reductive elimination reaction

sequences (Scheme 6-2). The development of bis(phosphino)-indene ligands towards this goal is currently underway in the Stradiotto research group.



Scheme 6-2. Proposed development of cationic and zwitterionic (κ^2 -*P,P*)Pt(η^3 -benzyl) complexes for E-H σ -bond activation studies.

6.3 Chapter 4

6.3.1 Summary

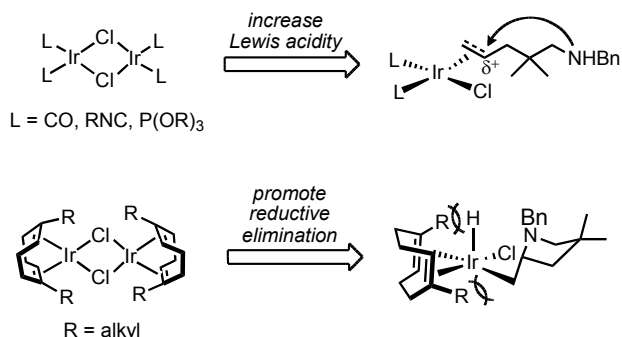
The identification, substrate scope, and mechanism of the $[\text{Ir}(\text{COD})\text{Cl}]_2$ -mediated cyclohydroamination of primary as well as secondary alkyl- or arylamines to unactivated olefins was discussed in Chapter 4. Catalyst optimization studies examining the cyclization of *N*-benzyl-2,2-diphenylpent-4-en-1-amine (**4-2a**) to the corresponding pyrrolidine (**4-3a**) revealed that for reactions conducted at 110 °C neither the addition of salts (*Nn*Bu₄Cl, LiOTf, AgBF₄, or LiB(C₆F₅)₄·2.5OEt₂) nor phosphine co-ligands served to enhance the catalytic performance of $[\text{Ir}(\text{COD})\text{Cl}]_2$. In this regard, the rate of intramolecular hydroamination of **4-2a** employing $[\text{Ir}(\text{COD})\text{Cl}]_2$ /**4-L2** (**4-L2** = 2-(di-*t*-butylphosphino)biphenyl) catalyst mixtures exhibited an inverse-order dependence on **4-L2** at 65 °C, and a zero-order rate dependence on **4-L2** at 110 °C. However, the use of 5 mol% HNEt₃Cl as a co-catalyst was required in order to promote the cyclization of primary amine substrates. Kinetic analysis of the hydroamination of **4-2a** revealed that the reaction rate displays first order dependence on the concentration of Ir and inverse order dependence with respect to both substrate (**4-2a**) and product (**4-3a**) concentrations; a primary kinetic isotope effect ($k_{\text{H}}/k_{\text{D}} = 3.4(3)$) was also observed. Eyring and Arrhenius analyses for the cyclization of **4-2a** to **4-3a** afforded $\Delta H^\ddagger = 20.9(3)$ kcal mol⁻¹, $\Delta S^\ddagger = -23.1(8)$ e.u., and $E_{\text{a}} = 21.6(3)$ kcal mol⁻¹, while a Hammett study of related arylamine

substrates revealed that increased electron density at nitrogen encourages hydroamination ($\rho = -2.4$). Plausible mechanisms involving either activation of the olefin or the amine functionality could be envisioned and were scrutinized computationally. An energetically demanding oxidative addition of the amine N–H bond to the Ir center precludes the latter mechanism and instead initial activation of the olefin bond prevailed. Notably, such an olefin activation mechanism had not previously been documented for Ir-catalyzed alkene hydroamination. The proposed operative mechanistic scenario involves: (1) smooth and reversible nucleophilic attack of the amine unit on the metal-coordinated C=C double bond to afford a zwitterionic intermediate; (2) Ir–C bond protonolysis via stepwise proton transfer from the ammonium unit to the metal and ensuing reductive elimination; and (3) associative cycloamine removal by new substrate molecule. The computational analysis indicated that reductive elimination involving a highly reactive and thus difficult to observe Ir–hydrido intermediate, and passing through a highly organized transition state structure, is turnover limiting and consistent with the measured thermodynamic parameters. The assessed effective barrier for cyclohydroamination of a prototypical secondary alkylamine agrees well with empirically determined Eyring parameters.

6.3.2 Future Directions

Using the mechanistic information ascertained in this study, the development of alternative Ir-based catalysts to address the current limitations of this system represents an attractive target. The design or application of alternative ligands to promote more readily one or more of the key mechanistic steps, in particular the turnover-limiting reductive elimination, would be ideal. Replacement of the diene ligand in $[\text{Ir}(\text{COD})\text{Cl}]_2$ with alternative π -acid ligands (i.e. CO, isonitriles, or phosphites) may promote a more electrophilic metal center thus promoting a situation where the alkene is more activated towards nucleophilic attack of the pendant amine. Alternatively, the development of diene ligands that feature substitution of the olefin hydrogens with more sterically-demanding groups may enhance catalyst performance by lowering the barrier to turnover-limiting C–H reductive elimination (Scheme 6-3). Studies directed towards understanding further the underlying mechanistic steps of this transformation will continue to play an important

role in the rational pursuit of increasingly more effective Ir catalysts for the intramolecular alkene hydroamination reaction.



Scheme 6-3. Alternative ligands that may enhance catalyst performance by either adjusting the Lewis acidity of the metal center (top) or promoting C-H reductive elimination (bottom).

6.4 Chapter 5

6.4.1 Summary

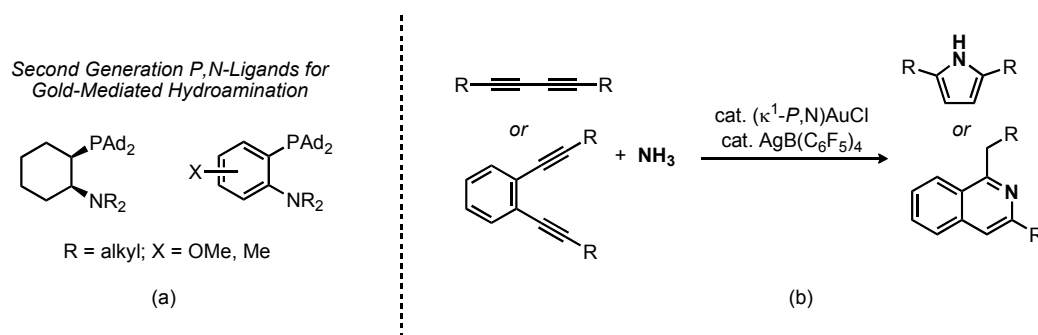
The use of a P,N-ligand (**5-L6**) to support the gold complex **5-1** as a state-of-the-art pre-catalyst for the hydroamination of symmetrical and unsymmetrical internal alkynes with a variety of secondary dialkylamines containing a diverse range of functional groups with controlled regioselectivity was the focus of Chapter 5. Catalyst optimization studies examining the addition of morpholine (**5-5a**) to diphenylacetylene (**5-4**) revealed significant rate-accelerating effects when employing ligands possessing sterically demanding di(1-adamantyl)phosphino and *ortho*-amino groups, as well as AgB(C₆F₅)₄ as a chloride-abstraction reagent. In this regard, the rate of morpholine addition to diphenylacetylene when employing catalytic mixtures of **5-1**/AgB(C₆F₅)₄ was found to be superior to the rates observed when using alternative biaryl (**5-L11**) or carbene (**5-L12**) ligands. The reaction of **5-1** and AgB(C₆F₅)₄ (1:1) in the presence of 3-hexyne (1 equiv.) produced the cationic alkyne complex [(**5-L6**)Au(3-hexyne)]⁺B(C₆F₅)₄⁻ (**5-10**). Upon treatment with 1 equiv. of morpholine (**5-5a**), the alkyne was displaced to form the catalytically active amine adduct [(**5-L6**)Au(morpholine)]⁺B(C₆F₅)₄⁻ (**5-11**). Kinetic analysis of the hydroamination of **5-4** with **5-5a** revealed that the reaction rate displays first order dependence on both the concentration of catalyst (**5-11**) and diphenylacetylene

(**5-4**), as well as a zero-order dependence on morpholine (**5-5a**) concentration, to give the empirical rate law equation: $\text{rate} = k_{\text{obs}}[\mathbf{5-11}]^1[\mathbf{5-4}]^1[\mathbf{5-5a}]^0$. Eyring and Arrhenius analyses for the addition of **5-5a** to **5-4** afforded $\Delta H^\ddagger = 25(2)$ kcal mol⁻¹, $\Delta S^\ddagger = -11(3)$ e.u., and $E_a = 26(1)$ kcal mol⁻¹, while a relatively small kinetic isotope effect of 1.5(1) was measured. Collectively the kinetic and stoichiometric studies, when coupled with the high degree of regioselectivity observed, are most consistent with an inner-sphere mechanism involving insertion of the alkyne into a Au–N bond. In light of the rate-accelerating effects achieved when employing a P,N-ligand such as **5-L6**, it is suggested that the pendant nitrogen donor may participate in catalysis by facilitating one or more mechanistically relevant proton-transfer steps; however, further experimentation is needed in order to elucidate the origin of high catalytic activity when employing **5-L6** and related ligands.

6.4.2 Future Directions

This preliminary catalytic and mechanistic account of the (κ^1 -P,N)Au-mediated hydroamination of internal alkynes with dialkylamines has provided an opportunity to develop further this reaction through expanded substrate scope and ligand design. The continued extension of the reaction scope to include a more diverse selection of unsymmetrical alkynes possessing varied electronic and steric properties could provide more detailed insight into the factors that control the regiochemistry of this reaction, as well as provide further support for an insertion mechanism. In order to provide further support for the proposed alkyne insertion mechanism, a more thorough kinetic analysis of this system should be executed. By conducting the kinetic measurements using the initial rates method under more dilute reaction conditions with a more broad range of initial catalyst and substrate concentrations, the subtleties of the reaction with respect to reaction order and saturation kinetics could be evaluated. Using the proposed mechanism outlined in Chapter 5 (see Section 5.2.3.3), it could be envisioned that at low initial amine concentrations a first-order dependence in amine would be observed. Moreover, at high initial alkyne concentrations the potential for a switch from a first-order rate dependence to zero-order rate dependence may be observed; such phenomena would be consistent with saturation kinetics.^[81]

In conjunction with a computational collaboration, further experimentation will be required before metal-ligand bifunctional catalysis can be unequivocally proposed. However, using this current hypothesis, the development of alternative P,N-ligands that may facilitate this proton transfer more effectively is a worthwhile pursuit. For instance, the basicity of the *ortho*-morpholino moiety in **5-L6** is weakened due to the mesomeric withdrawal of electron-density by the aryl-backbone of the ligand. The nitrogen donor could be rendered more electron-rich by either selective substitution of the ligand aryl backbone with electron-donating groups (i.e. OMe or Me groups) or by replacement of the aryl ring for a saturated cyclohexyl backbone (Scheme 6-4a). By increasing the basicity of the ligand nitrogen fragment, the proposed equilibrium between **5-11(a)** and **5-11(b)** (see Chapter 5, Scheme 5-8) should be more biased towards **5-11(b)** thereby increasing the concentration of the Au-amido species prior to turnover-limiting alkyne insertion. Through an intimate understanding of the electronic influences of the P,N-ligand on catalytic behavior, it is anticipated that this catalyst system could be effectively ‘tuned’ for task-specific hydroamination reactions, in particular for the efficient synthesis of pyrroles and isoquinolines via the hydroamination of diynes with ammonia (Scheme 6-4b).



Scheme 6-4. (a) Second generation ligands for Au-mediated hydroamination. (b) Proposed development of ammonia hydroamination reactions for the synthesis of pyrroles and isoquinolines.

References

- [1] a) V. Gewin, *Nature* **2006**, *440*, 378; b) B. M. Trost, *Acc. Chem. Res.* **2002**, *35*, 695; c) B. M. Trost, *Angew. Chem. Int. Ed.* **1995**, *34*, 259.
- [2] a) J. I. van der Vlugt, *Chem. Soc. Rev.* **2010**, *39*, 2302; b) R. H. Crabtree, *Chem. Rev.* **2010**, *110*, 575; c) L. Kollár, *Modern Carbonylation Methods*, Wiley-VCH, Weinheim, **2008**; d) W. S. Knowles, R. Noyori, *Acc. Chem. Res.* **2007**, *40*, 1238; e) G. J. Domski, J. M. Rose, G. W. Coates, A. D. Bolig, M. Brookhart, *Prog. Polym. Sci.* **2007**, *32*, 30; f) R. H. Grubbs, *Handbook of Metathesis*, Wiley-VCH, Weinheim, **2003**; g) J. A. Gladysz, *Chem. Rev.* **2000**, *100*, 1167.
- [3] P. B. Kettler, *Org. Process Res. Dev.* **2003**, *7*, 342.
- [4] a) G. J. Kubas, *Adv. Inorg. Chem.* **2004**, *56*, 127; b) K. J. Haack, S. Hashiguchi, A. Fujii, T. Ikariya, R. Noyori, *Angew. Chem. Int. Ed.* **1997**, *36*, 285; c) A. L. Casalnuovo, J. C. Calabrese, D. Milstein, *J. Am. Chem. Soc.* **1988**, *110*, 6738.
- [5] a) J. F. Hartwig, *Organotransition Metal Chemistry*, University Science Books, Sausalito, CA, **2010**; b) R. H. Crabtree, *The Organometallic Chemistry of the Transition Metals*, John Wiley and Sons, Hoboken, NJ, **2005**.
- [6] a) D. A. Colby, R. G. Bergman, J. A. Ellman, *Chem. Rev.* **2010**, *110*, 624; b) R. Dietiker, P. Chen, *Angew. Chem. Int. Ed.* **2004**, *43*, 5513; c) A. J. Chalk, J. F. Harrod, *J. Am. Chem. Soc.* **1965**, *87*, 16.
- [7] a) A. M. Johns, M. Utsunomiya, C. D. Incarvito, J. F. Hartwig, *J. Am. Chem. Soc.* **2006**, *128*, 1828; b) J. Takaya, J. F. Hartwig, *J. Am. Chem. Soc.* **2005**, *127*, 5756.
- [8] a) R. Noyori, *Angew. Chem. Int. Ed.* **2002**, *41*, 2008; b) W. S. Knowles, *Angew. Chem. Int. Ed.* **2002**, *41*, 1999.
- [9] a) R. R. Schrock, *Angew. Chem. Int. Ed.* **2006**, *45*, 3748; b) R. H. Grubbs, *Angew. Chem. Int. Ed.* **2006**, *45*, 3760; c) Y. Chauvin, *Angew. Chem. Int. Ed.* **2006**, *45*, 3740.
- [10] D. S. Surry, S. L. Buchwald, *Angew. Chem. Int. Ed.* **2008**, *47*, 6338.
- [11] A. Fürstner, P. W. Davies, *Angew. Chem. Int. Ed.* **2007**, *46*, 3410.
- [12] a) D. Benito-Garagorri, K. Kirchner, *Acc. Chem. Res.* **2008**, *41*, 201; b) M. E. van der Boom, D. Milstein, *Chem. Rev.* **2003**, *103*, 1759.

- [13] a) S. J. Roseblade, A. Pfaltz, *Acc. Chem. Res.* **2007**, *40*, 1402; b) P. Braunstein, *Chem. Rev.* **2006**, *106*, 134.
- [14] a) P. Braunstein, F. Naud, *Angew. Chem. Int. Ed.* **2001**, *40*, 680; b) C. S. Slone, D. A. Weinberger, C. A. Mirkin, *Prog. Inorg. Chem.* **1999**, *48*, 233.
- [15] a) R. Crabtree, *Acc. Chem. Res.* **1979**, *12*, 331; b) R. R. Schrock, J. A. Osborn, *J. Am. Chem. Soc.* **1976**, *98*, 2134; c) R. R. Schrock, J. A. Osborn, *J. Am. Chem. Soc.* **1976**, *98*, 2143.
- [16] a) M. G. Schrems, E. Neumann, A. Pfaltz, *Angew. Chem. Int. Ed.* **2007**, *46*, 8274; b) S. Bell, B. Wustenberg, S. Kaiser, F. Menges, T. Netscher, A. Pfaltz, *Science* **2006**, *311*, 642.
- [17] A. Macchioni, *Chem. Rev.* **2005**, *105*, 2039.
- [18] S. P. Smidt, N. Zimmermann, M. Studer, A. Pfaltz, *Chem. Eur. J.* **2004**, *10*, 4685.
- [19] M. Stradiotto, K. D. Hesp, R. J. Lundgren, *Angew. Chem. Int. Ed.* **2010**, *49*, 494.
- [20] a) R. J. Lundgren, M. Stradiotto, *Chem. Eur. J.* **2008**, *14*, 10388; b) R. J. Lundgren, M. A. Rankin, R. McDonald, G. Schatte, M. Stradiotto, *Angew. Chem. Int. Ed.* **2007**, *46*, 4732; c) J. Cipot, R. McDonald, M. J. Ferguson, G. Schatte, M. Stradiotto, *Organometallics* **2007**, *26*, 594; d) J. Cipot, R. McDonald, M. Stradiotto, *Chem. Commun.* **2005**, 4932.
- [21] M. Stradiotto, J. Cipot, R. McDonald, *J. Am. Chem. Soc.* **2003**, *125*, 5618.
- [22] J. Cipot, C. M. Vogels, R. McDonald, S. A. Westcott, M. Stradiotto, *Organometallics* **2006**, *25*, 5965.
- [23] a) M. A. Rankin, G. Schatte, R. McDonald, M. Stradiotto, *Organometallics* **2008**, *27*, 6286; b) M. A. Rankin, D. F. MacLean, R. Schatte, R. McDonald, M. Stradiotto, *J. Am. Chem. Soc.* **2007**, *129*, 15855; c) M. A. Rankin, G. Schatte, R. McDonald, M. Stradiotto, *J. Am. Chem. Soc.* **2007**, *129*, 6390; d) M. A. Rankin, R. McDonald, M. J. Ferguson, M. Stradiotto, *Organometallics* **2005**, *24*, 4981; e) M. A. Rankin, R. McDonald, M. J. Ferguson, M. Stradiotto, *Angew. Chem. Int. Ed.* **2005**, *44*, 3603.
- [24] a) R. J. Lundgren, A. Sapping-Kumankumah, M. Stradiotto, *Chem. Eur. J.* **2010**, *16*, 1983; b) R. J. Lundgren, B. D. Peters, P. G. Alsabeh, M. Stradiotto, *Angew. Chem. Int. Ed.* **2010**, *49*, 4071.

- [25] H. Grützmacher, *Angew. Chem. Int. Ed.* **2008**, *47*, 1814.
- [26] a) P. L. Holland, R. A. Andersen, R. G. Bergman, *Comments Inorg. Chem.* **1999**, *21*, 115; b) R. G. Bergman, *Polyhedron* **1995**, *14*, 3227; c) K. G. Caulton, *New J. Chem.* **1994**, *18*, 25; d) M. D. Fryzuk, C. D. Montgomery, *Coord. Chem. Rev.* **1989**, *95*, 1; e) H. E. Bryndza, W. Tam, *Chem. Rev.* **1988**, *88*, 1163; f) T. B. Gunnoe, *Eur. J. Inorg. Chem.* **2007**, 1185; g) J. R. Fulton, A. W. Holland, D. J. Fox, R. G. Bergman, *Acc. Chem. Res.* **2002**, *35*, 44.
- [27] a) T. Ikariya, K. Murata, R. Noyori, *Org. Biomol. Chem.* **2006**, *4*, 393; b) M. Ito, T. Ikariya, *Chem. Commun.* **2007**, 5134; c) T. Ikariya, A. J. Blacker, *Acc. Chem. Res.* **2007**, *40*, 1300; d) S. E. Clapham, A. Hadzovic, R. H. Morris, *Coord. Chem. Rev.* **2004**, *248*, 2201.
- [28] a) E. Khaskin, M. A. Iron, L. J. W. Shimon, J. Zhang, D. Milstein, *J. Am. Chem. Soc.* **2010**, *132*, 8542; b) A. D. Phillips, G. Laurencyzy, R. Scopelliti, P. J. Dyson, *Organometallics* **2007**, *26*, 1120; c) C. Gunanathan, Y. Ben-David, D. Milstein, *Science* **2007**, *317*, 790; d) E. Ben-Ari, G. Leitus, L. J. W. Shimon, D. Milstein, *J. Am. Chem. Soc.* **2006**, *128*, 15390; e) J. Zhang, G. Leitus, Y. Ben-David, D. Milstein, *J. Am. Chem. Soc.* **2005**, *127*, 10840; f) C. E. Radzewich, M. P. Coles, R. F. Jordan, *J. Am. Chem. Soc.* **1998**, *120*, 9384.
- [29] a) S. R. Klei, T. D. Tilley, R. G. Bergman, *J. Am. Chem. Soc.* **2000**, *122*, 1816; b) S. R. Klei, T. D. Tilley, R. G. Bergman, *Organometallics* **2001**, *20*, 3220; c) B. A. Arndtsen, R. G. Bergman, *Science* **1995**, *270*, 1970; d) B. A. Arndtsen, R. G. Bergman, T. A. Mobley, T. H. Peterson, *Acc. Chem. Res.* **1995**, *28*, 154.
- [30] J. K. Liu, X. F. Wu, J. A. Iggo, J. L. Xiao, *Coord. Chem. Rev.* **2008**, *252*, 782.
- [31] a) D. P. Klein, G. M. Kloster, R. G. Bergman, *J. Am. Chem. Soc.* **1990**, *112*, 2022; b) Y. Ohki, M. Sakamoto, K. Tatsumi, *J. Am. Chem. Soc.* **2008**, *130*, 11610.
- [32] L. J. Farrugia, *J. Appl. Crystallogr.* **1997**, *30*, 565.
- [33] M. Gorol, H. W. Roesky, M. Noltemeyer, H. G. Schmidt, *Eur. J. Inorg. Chem.* **2005**, 4840.
- [34] a) M. R. Ringenberg, S. L. Kokatam, Z. M. Heiden, T. B. Rauchfuss, *J. Am. Chem. Soc.* **2008**, *130*, 788; b) S. Arita, T. Koike, Y. Kayaki, T. Ikariya, *Organometallics* **2008**, *27*, 2795; c) K. Mashima, T. Abe, K. Tani, *Chem. Lett.* **1998**, 1201; d) D. B. Grotjahn, T. L. Groy, *J. Am. Chem. Soc.* **1994**, *116*, 6969.
- [35] D. M. Tellers, J. C. M. Ritter, R. G. Bergman, *Inorg. Chem.* **1999**, *38*, 4810.

- [36] a) X. J. Wang, H. Y. Chen, X. W. Li, *Organometallics* **2007**, *26*, 4684; b) F. L. Taw, A. H. Mueller, R. G. Bergman, M. Brookhart, *J. Am. Chem. Soc.* **2003**, *125*, 9808; c) F. L. Taw, P. S. White, R. G. Bergman, M. Brookhart, *J. Am. Chem. Soc.* **2002**, *124*, 4192; d) C. S. Chin, D. Chong, B. Lee, H. Jeong, G. Won, Y. Do, Y. J. Park, *Organometallics* **2000**, *19*, 638.
- [37] H. Hashimoto, H. Tobita, H. Ogino, *Organometallics* **1993**, *12*, 2182.
- [38] D. S. Glueck, R. G. Bergman, *Organometallics* **1990**, *9*, 2862.
- [39] A. Ienco, M. J. Calhorda, J. Reinhold, F. Reineri, C. Bianchini, M. Peruzzini, F. Vizza, C. Mealli, *J. Am. Chem. Soc.* **2004**, *126*, 11954.
- [40] R. C. Linck, R. J. Pafford, T. B. Rauchfuss, *J. Am. Chem. Soc.* **2001**, *123*, 8856.
- [41] D. J. Parks, J. M. Blackwell, W. E. Piers, *J. Org. Chem.* **2000**, *65*, 3090.
- [42] a) K. A. Nolin, J. R. Krumper, M. D. Pluth, R. G. Bergman, F. D. Toste, *J. Am. Chem. Soc.* **2007**, *129*, 14684; b) J. J. Kennedy-Smith, K. A. Nolin, H. P. Gunterman, F. D. Toste, *J. Am. Chem. Soc.* **2003**, *125*, 4056.
- [43] K. Hartke, A. Schillingpindur, *Liebigs Ann. Chem.* **1984**, 552.
- [44] a) H. D. Flack, G. Bernardinelli, *J. Appl. Cryst.* **2000**, *33*, 1143; b) H. D. Flack, G. Bernardinelli, *Acta Crystallogr.* **1999**, *55*, 908.
- [45] a) B. M. Boardman, J. M. Valderrama, F. Munoz, G. Wu, G. C. Bazan, R. Rojas, *Organometallics* **2008**, *27*, 1671; b) J. H. Cho, G. P. A. Yap, C. G. Riordan, *Inorg. Chem.* **2007**, *46*, 11308; c) Y. F. Chen, C. Sui-Seng, D. Zargarian, *Angew. Chem. Int. Ed.* **2005**, *44*, 7721; d) Y. F. Chen, G. Wu, G. C. Bazan, *Angew. Chem. Int. Ed.* **2005**, *44*, 1108; e) H. Y. Kwon, S. Y. Lee, B. Y. Lee, D. M. Shin, Y. K. Chung, *Dalton Trans.* **2004**, 921; f) C. B. Shim, Y. H. Kim, B. Y. Lee, Y. Dong, H. Yun, *Organometallics* **2003**, *22*, 4272.
- [46] a) R. van de Coevering, M. Kuil, A. P. Alferys, T. Visser, M. Lutz, A. L. Spek, R. Gebbink, G. van Koten, *Organometallics* **2005**, *24*, 6147; b) C. C. Lu, J. C. Peters, *J. Am. Chem. Soc.* **2004**, *126*, 15818; c) C. C. Lu, J. C. Peters, *J. Am. Chem. Soc.* **2002**, *124*, 5272; d) R. van de Coevering, M. Kuil, R. Gebbink, G. van Koten, *Chem. Commun.* **2002**, 1636.
- [47] a) E. Khaskin, P. Y. Zavalij, A. N. Vedernikov, *Angew. Chem. Int. Ed.* **2007**, *46*, 6309; b) C. M. Thomas, J. C. Peters, *Organometallics* **2005**, *24*, 5858; c) J. C. Thomas, J. C. Peters, *J. Am. Chem. Soc.* **2003**, *125*, 8870; d) J. C. Thomas, J. C.

- Peters, *J. Am. Chem. Soc.* **2001**, *123*, 5100; e) T. Marx, L. Wesemann, S. Dehnen, *Organometallics* **2000**, *19*, 4653.
- [48] R. J. Lundgren, M. A. Rankin, R. McDonald, M. Stradiotto, *Organometallics* **2008**, *27*, 254.
- [49] N. Oberbeckmann-Winter, P. Braunstein, R. Welter, *Organometallics* **2004**, *23*, 6311.
- [50] a) R. Malacea, L. Routaboul, E. Manoury, J. C. Daran, R. Poli, *J. Organomet. Chem.* **2008**, *693*, 1469; b) R. Romeo, L. Monsu' Scolaro, M. R. Plutino, A. Romeo, F. Nicolo', A. Del Zotto, *Eur. J. Inorg. Chem.* **2002**, 629.
- [51] a) E. Hauptman, P. J. Fagan, W. Marshall, *Organometallics* **1999**, *18*, 2061; b) M. Bressan, A. Morvillo, *J. Organomet. Chem.* **1986**, *304*, 267; c) L. E. Crascall, S. A. Litster, A. D. Redhouse, J. L. Spencer, *J. Organomet. Chem.* **1990**, *394*, C35.
- [52] K. Izod, *Coord. Chem. Rev.* **2002**, *227*, 153.
- [53] A. Sonoda, P. M. Bailey, P. M. Maitlis, *Dalton Trans.* **1979**, 346.
- [54] a) P. J. Shapiro, P. J. Sinnema, P. Perrotin, P. H. M. Budzelaar, H. Weihe, B. Twamley, R. A. Zehnder, J. J. Nairn, *Chem. Eur. J.* **2007**, *13*, 6212; b) M. Bochmann, S. J. Lancaster, O. B. Robinson, *Chem. Commun.* **1995**, 2081.
- [55] a) J. C. Wasilke, Z. J. A. Komon, X. H. Bu, G. C. Bazan, *Organometallics* **2004**, *23*, 4174; b) T. F. Wang, C. C. Hwu, C. W. Tsai, Y. S. Wen, *Dalton Trans.* **1998**, 2091.
- [56] M. Janka, G. K. Anderson, N. P. Rath, *Organometallics* **2000**, *19*, 5071.
- [57] P. Jutzi, C. Müller, A. Stämmler, H. G. Stämmler, *Organometallics* **2000**, *19*, 1442.
- [58] a) T. E. Müller, K. C. Hultsch, M. Yus, F. Foubelo, M. Tada, *Chem. Rev.* **2008**, *108*, 3795; b) J. F. Hartwig, *Nature* **2008**, *455*, 314; c) R. A. Widenhofer, *Chem. Eur. J.* **2008**, *14*, 5382; d) R. Severin, S. Doye, *Chem. Soc. Rev.* **2007**, *36*, 1407; e) A. R. Chianese, S. J. Lee, M. R. Gagne, *Angew. Chem. Int. Ed.* **2007**, *46*, 4042; f) I. Aillaud, J. Collin, J. Hannedouche, E. Schulz, *Dalton Trans.* **2007**, 5105; g) R. A. Widenhofer, X. Q. Han, *Eur. J. Org. Chem.* **2006**, 4555; h) K. C. Hultsch, *Adv. Synth. Catal.* **2005**, *347*, 367; i) K. C. Hultsch, *Org. Biomol. Chem.* **2005**, *3*, 1819; j) F. Alonso, I. P. Beletskaya, M. Yus, *Chem. Rev.* **2004**, *104*, 3079; k) J. F. Hartwig, *Pure Appl. Chem.* **2004**, *76*, 507; l) P. W. Roesky, T. E. Müller, *Angew.*

- Chem. Int. Ed.* **2003**, *42*, 2708; m) F. Pohlki, S. Doye, *Chem. Soc. Rev.* **2003**, *32*, 104; n) M. Nobis, B. Drießen-Holscher, *Angew. Chem. Int. Ed.* **2001**, *40*, 3983; o) T. E. Müller, M. Beller, *Chem. Rev.* **1998**, *98*, 675.
- [59] A. M. Johns, N. Sakai, A. Ridder, J. F. Hartwig, *J. Am. Chem. Soc.* **2006**, *128*, 9306.
- [60] Z. B. Zhang, S. D. Lee, R. A. Widenhoefer, *J. Am. Chem. Soc.* **2009**, *131*, 5372.
- [61] a) S. Hong, A. M. Kawaoka, T. J. Marks, *J. Am. Chem. Soc.* **2003**, *125*, 15878; b) B. M. Trost, W. P. Tang, *J. Am. Chem. Soc.* **2003**, *125*, 8744; c) G. A. Molander, E. D. Dowdy, S. K. Pack, *J. Org. Chem.* **2001**, *66*, 4344; d) D. O'Hagan, *Nat. Prod. Rep.* **2000**, *17*, 435; e) V. M. Arredondo, S. Tian, F. E. McDonald, T. J. Marks, *J. Am. Chem. Soc.* **1999**, *121*, 3633.
- [62] a) H. F. Yuen, T. J. Marks, *Organometallics* **2009**, *28*, 2423; b) E. L. Lu, W. Gan, Y. F. Chen, *Organometallics* **2009**, *28*, 2318; c) J. Hannedouche, I. Aillaud, J. Collin, E. Schulz, A. Trifonov, *Chem. Commun.* **2008**, 3552; d) G. F. Zi, L. Xiang, H. B. Song, *Organometallics* **2008**, *27*, 1242; e) B. D. Stubbert, T. J. Marks, *J. Am. Chem. Soc.* **2007**, *129*, 4253; f) B. D. Stubbert, T. J. Marks, *J. Am. Chem. Soc.* **2007**, *129*, 6149; g) D. V. Vitanova, F. Hampel, K. C. Hultzs, *J. Organomet. Chem.* **2007**, *692*, 4690; h) M. Rastätter, A. Zulys, P. W. Roesky, *Chem. Eur. J.* **2007**, *13*, 3606; i) D. Riegert, J. Collin, J. C. Daran, T. Fillebeen, E. Schulz, D. Lyubov, G. Fukin, A. Trifonov, *Eur. J. Inorg. Chem.* **2007**, 1159; j) X. H. Yu, T. J. Marks, *Organometallics* **2007**, *26*, 365; k) M. Rastätter, A. Zulys, P. W. Roesky, *Chem. Commun.* **2006**, 874; l) D. V. Gribkov, K. C. Hultzs, F. Hampel, *J. Am. Chem. Soc.* **2006**, *128*, 3748; m) S. Bambirra, H. Tsurugi, D. van Leusen, B. Hessen, *Dalton Trans.* **2006**, 1157; n) K. C. Hultzs, D. V. Gribkov, F. Hampel, *J. Organomet. Chem.* **2005**, *690*, 4441; o) H. Kim, P. H. Lee, T. Livinghouse, *Chem. Commun.* **2005**, 5205; p) J. Y. Kim, T. Livinghouse, *Org. Lett.* **2005**, *7*, 4391; q) F. Lauterwasser, P. G. Hayes, S. Bräse, W. E. Piers, L. L. Schafer, *Organometallics* **2004**, *23*, 2234; r) S. Hong, T. J. Marks, *Acc. Chem. Res.* **2004**, *37*, 673.
- [63] a) W. Zhang, J. B. Werness, W. P. Tang, *Tetrahedron* **2009**, *65*, 3090; b) M. R. Crimmin, M. Arrowsmith, A. G. M. Barrett, I. J. Casely, M. S. Hill, P. A. Procopiou, *J. Am. Chem. Soc.* **2009**, *131*, 9670; c) M. Arrowsmith, M. S. Hill, G. Kociok-Köhn, *Organometallics* **2009**, *28*, 1730; d) S. Datta, M. T. Gamer, H. W. Roesky, *Organometallics* **2008**, *27*, 1207; e) P. H. Martinez, K. C. Hultzs, F. Hampel, *Chem. Commun.* **2006**, 2221.
- [64] a) A. V. Lee, M. Sajitz, L. L. Schafer, *Synthesis* **2009**, 97; b) B. Lian, T. P. Spaniol, P. Horrillo-Martinez, K. C. Hultzs, J. Okuda, *Eur. J. Inorg. Chem.* **2009**, 429; c) J. Cho, T. K. Hollis, T. R. Helgert, E. J. Valente, *Chem. Commun.* **2008**, 5001; d) L. Xiang, H. B. Song, G. F. Zi, *Eur. J. Inorg. Chem.* **2008**, 1135; e)

- S. Majumder, A. L. Odom, *Organometallics* **2008**, *27*, 1174; f) M. C. Wood, D. C. Leitch, C. S. Yeung, J. A. Kozak, L. L. Schafer, *Angew. Chem. Int. Ed.* **2007**, *46*, 354; g) A. V. Lee, L. L. Schafer, *Eur. J. Inorg. Chem.* **2007**, 2243; h) A. L. Gott, A. J. Clarke, G. J. Clarkson, P. Scott, *Organometallics* **2007**, *26*, 1729; i) C. Müller, C. Loos, N. Schulenberg, S. Doye, *Eur. J. Org. Chem.* **2006**, 2499; j) D. A. Watson, M. Chiu, R. G. Bergman, *Organometallics* **2006**, *25*, 4731; k) P. D. Knight, I. Munslow, P. N. O'Shaughnessy, P. Scott, *Chem. Commun.* **2004**, 894.
- [65] a) L. Ackermann, L. T. Kaspar, A. Althammer, *Org. Biomol. Chem.* **2007**, *5*, 1975; b) B. Schlummer, J. F. Hartwig, *Org. Lett.* **2002**, *4*, 1471.
- [66] K. Komeyama, T. Morimoto, K. Takaki, *Angew. Chem. Int. Ed.* **2006**, *45*, 2938.
- [67] a) B. M. Cochran, F. E. Michael, *J. Am. Chem. Soc.* **2008**, *130*, 2786; b) B. M. Cochran, F. E. Michael, *Org. Lett.* **2008**, *10*, 329; c) F. E. Michael, B. M. Cochran, *J. Am. Chem. Soc.* **2006**, *128*, 4246.
- [68] a) J. Zhang, C.-G. Yang, C. He, *J. Am. Chem. Soc.* **2006**, *128*, 1798; b) C. F. Bender, R. A. Widenhoefer, *Chem. Commun.* **2006**, 4143; c) C. F. Bender, R. A. Widenhoefer, *Org. Lett.* **2006**, *8*, 5303; d) X. Y. Liu, C. H. Li, C. M. Che, *Org. Lett.* **2006**, *8*, 2707; e) X. Q. Han, R. A. Widenhoefer, *Angew. Chem. Int. Ed.* **2006**, *45*, 1747.
- [69] a) X. Shen, S. L. Buchwald, *Angew. Chem. Int. Ed.* **2010**, *49*, 564; b) Z. Liu, J. F. Hartwig, *J. Am. Chem. Soc.* **2008**, *130*, 1570; c) E. B. Bauer, G. T. S. Andavan, T. K. Hollis, R. J. Rubio, J. Cho, G. R. Kuchenbeiser, T. R. Helgert, C. S. Letko, F. S. Tham, *Org. Lett.* **2008**, *10*, 1175.
- [70] H. Ohmiya, T. Moriya, M. Sawamura, *Org. Lett.* **2009**, *11*, 2145.
- [71] a) C. F. Bender, W. B. Hudson, R. A. Widenhoefer, *Organometallics* **2008**, *27*, 2356; b) C. F. Bender, R. A. Widenhoefer, *J. Am. Chem. Soc.* **2005**, *127*, 1070.
- [72] a) R. Dorta, *Iridium Complexes in Organic Synthesis*, Wiley-VCH, Weinheim, **2009**; b) J. R. Zhou, J. F. Hartwig, *J. Am. Chem. Soc.* **2008**, *130*, 12220; c) R. Dorta, P. Egli, F. Zürcher, A. Togni, *J. Am. Chem. Soc.* **1997**, *119*, 10857.
- [73] a) L. D. Field, B. A. Messerle, K. Q. Vuong, P. Turner, *Dalton Trans.* **2009**, 3599; b) D. Ebrahimi, D. F. Kennedy, B. A. Messerle, D. B. Hibbert, *Analyst* **2008**, 817; c) S. Burling, L. D. Field, B. A. Messerle, S. L. Rumble, *Organometallics* **2007**, *26*, 4335; d) R. Y. Lai, K. Surekha, A. Hayashi, F. Ozawa, Y. H. Liu, S. M. Peng, S. T. Liu, *Organometallics* **2007**, *26*, 1062; e) X. W. Li, A. R. Chianese, T. Vogel, R. H. Crabtree, *Org. Lett.* **2005**, *7*, 5437.

- [74] K. D. Hesp, D. Wechsler, J. Cipot, A. Myers, R. McDonald, M. J. Ferguson, G. Schatte, M. Stradiotto, *Organometallics* **2007**, *26*, 5430.
- [75] a) C. F. Bender, R. A. Widenhoefer, *Chem. Commun.* **2008**, 2741; b) J. Penzien, R. Q. Su, T. E. Müller, *J. Mol. Cat. A.* **2002**, *182*, 489; c) T. E. Müller, M. Berger, M. Grosche, E. Herdtweck, F. P. Schmidtchen, *Organometallics* **2001**, *20*, 4384.
- [76] G. Kovács, G. Ujaque, A. Lledós, *J. Am. Chem. Soc.* **2008**, *130*, 853.
- [77] a) N. Sakai, A. Ridder, J. F. Hartwig, *J. Am. Chem. Soc.* **2006**, *128*, 8134; b) J. Pawlas, Y. Nakao, M. Kawatsura, J. F. Hartwig, *J. Am. Chem. Soc.* **2002**, *124*, 3669; c) L. K. Vo, D. A. Singleton, *Org. Lett.* **2004**, *6*, 2469; d) U. Nettekoven, J. F. Hartwig, *J. Am. Chem. Soc.* **2002**, *124*, 1166.
- [78] J. L. McBee, A. T. Bell, T. D. Tilley, *J. Am. Chem. Soc.* **2008**, *130*, 16562.
- [79] a) C. Leighton-Munro, S. A. Delp, N. M. Alsop, E. D. Blue, T. B. Gunnoe, *Chem. Commun.* **2008**, 111; b) C. Leighton-Munro, S. A. Delp, E. D. Blue, T. B. Gunnoe, *Organometallics* **2007**, *26*, 1483.
- [80] E. Genin, S. Antoniotti, V. Michelet, J. P. Genêt, *Angew. Chem. Int. Ed.* **2005**, *44*, 4949.
- [81] E. V. Anslyn, D. A. Dougherty, *Modern Physical Organic Chemistry*, 1st ed., University Science Books, Sausalito, **2006**.
- [82] M. Green, T. A. Kuc, S. H. Taylor, *Chem. Commun.* **1970**, 1553.
- [83] P. R. Auburn, P. B. Mackenzie, B. Bosnich, *J. Am. Chem. Soc.* **1985**, *107*, 2033.
- [84] M. Dochnahl, J. W. Pissarek, S. Blechert, K. Löhnwitz, P. W. Roesky, *Chem. Commun.* **2006**, 3405.
- [85] a) S. Mukherjee, J. W. Yang, S. Hoffmann, B. List, *Chem. Rev.* **2007**, *107*, 5471; b) S. Kobayashi, H. Ishitani, *Chem. Rev.* **1999**, *99*, 1069; c) Z. Rappoport, *The Chemistry of Enamines*, John Wiley & Sons Ltd., West Sussex, **1994**.
- [86] a) D. C. Leitch, P. R. Payne, C. R. Dunbar, L. L. Schafer, *J. Am. Chem. Soc.* **2009**, *131*, 18246; b) Z. Zhang, D. C. Leitch, M. Lu, B. O. Patrick, L. L. Schafer, *Chem. Eur. J.* **2007**, *13*, 2012; c) A. Heutling, F. Pohlki, S. Doye, *Chem. Eur. J.* **2004**, *10*, 3059; d) L. Ackermann, *Organometallics* **2003**, *22*, 4367; e) A. Tillack, I. G. Castro, C. G. Hartung, M. Beller, *Angew. Chem. Int. Ed.* **2002**, *41*, 2541; f) P. J. Walsh, A. M. Baranger, R. G. Bergman, *J. Am. Chem. Soc.* **1992**, *114*, 1708.

- [87] a) D.-M. Cui, J.-Z. Zheng, L.-Y. Yang, C. Zhang, *Synlett* **2010**, 5, 809; b) H. Duan, S. Sengupta, J. L. Peteron, N. G. Akhmedov, X. Shi, *J. Am. Chem. Soc.* **2009**, 131, 12100; c) A. Leyva, A. Corma, *Adv. Synth. Catal.* **2009**, 351, 2876; d) S. L. Dabb, B. A. Messerle, *Dalton Trans.* **2008**, 6368; e) J. W. Sun, S. A. Kozmin, *Angew. Chem. Int. Ed.* **2006**, 45, 4991; f) T. Shimada, Y. Yamamoto, *J. Am. Chem. Soc.* **2002**, 124, 12670; g) C. G. Hartung, A. Tillack, H. Trauthwein, M. Beller, *J. Org. Chem.* **2001**, 66, 6339.
- [88] Y. Fukumoto, H. Asai, M. Shimizu, N. Chatani, *J. Am. Chem. Soc.* **2007**, 129, 13792.
- [89] V. Lavallo, G. D. Frey, S. Kousar, B. Donnadieu, G. Bertrand, *Proc. Nat. Acad. Sci.* **2007**, 104, 13569.
- [90] a) X. M. Zeng, G. D. Frey, S. Kousar, G. Bertrand, *Chem. Eur. J.* **2009**, 15, 3056; b) X. M. Zeng, G. D. Frey, R. Kinjo, B. Donnadieu, G. Bertrand, *J. Am. Chem. Soc.* **2009**, 131, 8690.
- [91] N. Nishina, Y. Yamamoto, *Tetrahedron* **2009**, 65, 1799.
- [92] a) S. Caccia, *Curr. Drug Metab.* **2007**, 8, 612; b) M. L. López-Rodríguez, M. J. Morcillo, E. Fernández, M. L. Rosado, L. Pardo, K. J. Schaper, *J. Med. Chem.* **2001**, 44, 198.
- [93] a) M. R. Kuram, M. Bhanuchandra, A. K. Sahoo, *J. Org. Chem.* **2010**, 75, 2247; b) B. M. Trost, W. Brieden, K. H. Baringhaus, *Angew. Chem. Int. Ed.* **1992**, 31, 1335; c) Z. B. Huo, N. T. Patil, T. A. Jin, N. K. Pahadi, Y. Yamamoto, *Adv. Synth. Catal.* **2007**, 349, 680.
- [94] A. S. K. Hashmi, *Angew. Chem. Int. Ed.* **2010**, 49, 5232.
- [95] a) R. E. Kinder, Z. Zhang, R. A. Widenhoefer, *Org. Lett.* **2008**, 10, 3157; b) Z. B. Zhang, C. Liu, R. E. Kinder, X. Q. Han, H. Qian, R. A. Widenhoefer, *J. Am. Chem. Soc.* **2006**, 128, 9066.
- [96] a) V. Lavallo, G. D. Frey, B. Donnadieu, M. Soleilhavoup, G. Bertrand, *Angew. Chem. Int. Ed.* **2008**, 47, 5224; b) N. Nishina, Y. Yamamoto, *Angew. Chem. Int. Ed.* **2006**, 45, 3314; c) E. Mizushima, T. Hayashi, M. Tanaka, *Org. Lett.* **2003**, 5, 3349.
- [97] P. Pérez-Galan, N. Delpont, E. Herrero-Gómez, F. Maseras, A. M. Echavarren, *Chem. Eur. J.* **2010**, 16, 5324.

- [98] a) A. S. K. Hashmi, T. D. Ramamurthi, F. Rominger, *Adv. Synth. Catal.* **2010**, 352, 971; b) A. S. K. Hashmi, A. M. Schuster, F. Rominger, *Angew. Chem. Int. Ed.* **2009**, 48, 8247.
- [99] H. K. Hall, *J. Am. Chem. Soc.* **1957**, 79, 5441.
- [100] R. Uson, A. Laguna, *Organomet. Synth.* **1986**, 3, 322.
- [101] M. Kuprat, M. Lehmann, A. Schulz, A. Villinger, *Organometallics* **2010**, 29, 1421.
- [102] P. de Fremont, N. M. Scott, E. D. Stevens, S. P. Nolan, *Organometallics* **2005**, 24, 2411.
- [103] A. Aranyos, D. W. Old, A. Kiyomori, J. P. Wolfe, J. P. Sadighi, S. L. Buchwald, *J. Am. Chem. Soc.* **1999**, 121, 4369.